

University of Alberta

**CHEMICAL KINETIC BASED SIMULATION FOR AN HCCI ENGINE AND
ITS COMBUSTION**

by 

Paitoon Kongsereparp

A thesis submitted to the Faculty of Graduate Studies and Research in partial
fulfillment of the requirements for the degree **Doctor of Philosophy**

in

Department of Mechanical Engineering

Edmonton, Alberta
Spring 2008



Library and
Archives Canada

Published Heritage
Branch

395 Wellington Street
Ottawa ON K1A 0N4
Canada

Bibliothèque et
Archives Canada

Direction du
Patrimoine de l'édition

395, rue Wellington
Ottawa ON K1A 0N4
Canada

Your file *Votre référence*
ISBN: 978-0-494-45547-0
Our file *Notre référence*
ISBN: 978-0-494-45547-0

NOTICE:

The author has granted a non-exclusive license allowing Library and Archives Canada to reproduce, publish, archive, preserve, conserve, communicate to the public by telecommunication or on the Internet, loan, distribute and sell theses worldwide, for commercial or non-commercial purposes, in microform, paper, electronic and/or any other formats.

The author retains copyright ownership and moral rights in this thesis. Neither the thesis nor substantial extracts from it may be printed or otherwise reproduced without the author's permission.

AVIS:

L'auteur a accordé une licence non exclusive permettant à la Bibliothèque et Archives Canada de reproduire, publier, archiver, sauvegarder, conserver, transmettre au public par télécommunication ou par l'Internet, prêter, distribuer et vendre des thèses partout dans le monde, à des fins commerciales ou autres, sur support microforme, papier, électronique et/ou autres formats.

L'auteur conserve la propriété du droit d'auteur et des droits moraux qui protègent cette thèse. Ni la thèse ni des extraits substantiels de celle-ci ne doivent être imprimés ou autrement reproduits sans son autorisation.

In compliance with the Canadian Privacy Act some supporting forms may have been removed from this thesis.

While these forms may be included in the document page count, their removal does not represent any loss of content from the thesis.

Conformément à la loi canadienne sur la protection de la vie privée, quelques formulaires secondaires ont été enlevés de cette thèse.

Bien que ces formulaires aient inclus dans la pagination, il n'y aura aucun contenu manquant.


Canada

University of Alberta

Library Release Form

Name of Author: Paitoon Kongsereeparp

Title of Thesis: Chemical Kinetic Based Simulation for an HCCI Engine
and its Combustion

Degree: Doctor of Philosophy

Year this Degree Granted: 2008

Permission is hereby granted to the University of Alberta Library to reproduce single copies of this thesis and to lend or sell such copies for private, scholarly or scientific research purposes only.

The author reserves all other publication and other rights in association with the copyright in the thesis, and except as herein before provided, neither the thesis nor any substantial portion thereof may be printed or otherwise reproduced in any material form whatsoever without the author's prior written permission.

.....
Paitoon Kongsereeparp
4-9 Mechanical Engineering Building
Edmonton, Alberta, Canada, T6G 2G8

Date:.....
January 31, 2008

ABSTRACT

Operating an engine with homogeneous charge compression ignition (HCCI) technique is a promising technique to lower NO_x emissions of engines while achieving high efficiency. Nevertheless, applications for HCCI are still limited due to the absence of a definite means to control ignition timing. Ignition in an HCCI engine depends on an array of parameters such as fuel type, mixture composition and intake conditions, (i.e., controlling an HCCI engine can only be done through the adjustment of these parameters). For this reason, it is important to understand the mechanism by which these parameters affect HCCI combustion in order to develop feasible control parameters.

This dissertation focuses on a computational investigation of the possible control parameters for an HCCI engine. The study was conducted for two fuels with a wide octane number (ON) range: natural gas, (extremely high ON fuel), and n-heptane, (extremely low ON fuel). The study also covers four different engine operating modes of varying intake pressure and engine speed.

The aim is to: 1) unveil the mechanism by which various parameters affect HCCI combustion; and 2) identify the most feasible parameter for ignition timing control. The models developed are a chemical kinetics based HCCI engine model with zero-dimensional, single zone combustion and with quasi-dimensional, multi-zone combustion. Several techniques have been introduced to enhance the efficiency, accuracy and reliability of multi-zone HCCI engine modeling, including: 1) novel solutions to calculate properties at intake valve closure;

2) improvements to heat transfer modeling, and 3) a segregating solver technique that reduces computational effort. The developed model is applied to investigate the effects on HCCI combustion of adjusting mixture composition variables, such as %reformer gas.

The mechanisms by which various mixture compositions affect HCCI combustion fall into three classes: thermodynamic properties, mixture reactivity, and combustion chamber environmental effects. Study results show that the dominant factor affecting HCCI ignition timing differs with base fuel and operating condition. With both high ON and low ON fuels, blending controlled amounts of reformer gas into the base fuel provides a means to control HCCI ignition timing, (and thus optimize efficiency), over a range of speed/load operating conditions.

ACKNOWLEDGEMENT

The experience during the last four years has been absolutely wonderful. I truly appreciate everyone who has supported me both directly and indirectly.

Firstly, I would like to acknowledge the unconditional support of my parents, Mr. Viroj and Mrs. Chotika Kongsereeparp, throughout my academic studies. Their enthusiasm for encouraging my pursuits in life has been extremely important to me. Without their love, I would not even dream of this day.

I owe Dr. M David Checkel a great deal. He has always been supportive. To me, he is an excellent engineer, teacher, and supervisor. Personally, I will never forget his invitation to celebrate Christmas at his home, which was also my first Christmas celebration in Edmonton. His guidance, advice and encouragement have been truly terrific.

Many thanks to the professors of the Department of Mechanical Engineering at the University of Alberta. Their enthusiasm for teaching and research provided me with the necessary academic foundation to complete my studies. I will always remember my time in the Department with great fondness.

Finally, I also owe a great deal of gratitude to many people, such as my brothers (Paiboon and Paikij Kongsereeparp), my coffee buddy/friend and his family (Glen and Liusa Thomas), my colleagues (Vahid Hosseini and Dan Hanford), and TSA friends. Without their support, it would have been ten times more difficult to be here.

ABBREVIATIONS & NOMENCLATURES

AFR	Air fuel ratio
ATAC	Active thermo atmospheric combustion
CD	Combustion duration
CFD	Computational fluid dynamics
CHM	Chalmer mechanism
CI	Compression ignition
CNG	Compressed natural gas
CR	Compression ratio
EGR	Exhaust gas recirculation
EVC	Exhaust valve closed
EVO	Exhaust valve opened
FVV	Fully variable valve control
GA	Genetic algorithm
GHG	Green house gas
HCCI	Homogeneous charge compression ignition
HRR	Heat release rate
IC	Internal combustion
IMEP	Indicated mean effective pressure
IVC	Intake valve closed
IVO	Intake valve opened
MZM	Multi zone model
NG	Natural gas
NVH	Noise, vibration and harshness
Nu	Nusselt number
ON	Octane Number
PDF	Power density function
PM	Particular matter
Pr	Prandtl number
Re	Reynolds number

RG	Reformer gas
RPM	Revolution per minute
SFC	Specific fuel consumption
SOC	Start of main combustion
SI	Spark ignition
SMZM	Segregated multi-zone model
SZM	Single zone model
$\%EGR$	EGR fraction
A	Arrhenius coefficient
A_C	Curtain area
A_E	Effective flow area
A_i	Intake effective flow area
A_e	Exhaust effective flow area
A_{total}	Total area of a system surrounding
A_R	Reference area
B	Bore diameter
$C(i,j)$	Covariance function of the two sets (i and j) of data
C_{pk}^0	Specific heat constant
C_D	Drag coefficient
D_v	Valve diameter
D_{jk}	Binary diffusion coefficient
E	Activating energy
EGR	Exhaust Gas Recirculation
F	Troe factor
F/A	Fuel-air ratio
G	Gibb's free energy
H_k^0	Absolute enthalpy of the k^{th} species
H_f	Enthalpy of formation
K_C	Equilibrium constant based on species concentration
K_P	Equilibrium constant based on pressure

K_T	The factor for setting temperature variation at IVC
$[M]$	Molar concentration of species M
L	Characteristic length
L_v	Valve lift
MW_i	Molecular weight of the i^{th} species
N	Engine speed (rpm)
N_S	Total number of species
N_E	Number of opening channels
N_Z	Number of zones
P	In-cylinder pressure
P_{exh}	Exhaust pressure
P_{int}	Intake manifold pressure
Q	Total heat transfer into/out of a system (in-cylinder chamber)
Q_k	Heat transfer into/out of the k^{th} zone
R	Ratio of connecting rod length to crank radius
$R(i,j)$	Correlation coefficient of the two sets (i and j) of data
R_{ave}	Average ideal gas constant on mass basis
$R_{ave,k}$	Average ideal gas constant on mass basis of the k^{th} zone
R_k	Average ideal gas constant on mass basis of the k^{th} zone
R_u	Universal ideal gas constant on molar basis
RG	Reformer Gas
S_k^0	Absolute entropy of the k^{th} species
SOC	Start of main combustion
T	In-cylinder temperature
T_{cool}	Cooling temperature
T_{int}	Temperature of mixtures in an intake manifold
T_k	Mixture temperature of the k^{th} zone
T_w	Wall temperature
U	Total internal energy inside a combustion chamber
U_k	Internal energy inside the k^{th} zone
V^+	Positive valence

V	Negative valence
V_{IVC}	In-cylinder volume at IVC
V_{EVC}	In-cylinder volume at EVC
V_c	Clearance volume
V_{cyl}	In-cylinder volume
V_k	Volume of the k^{th} zone
V_1	Volume of the 1 st zone
W_i	Molecular weight of the i^{th} species
X_k	Mole fraction of the k^{th} species
Y_i	Mass fraction of the i^{th} species
$Y_{k,i}$	Mass fraction of the i^{th} species in the k^{th} zone
Z_{rot}	Rotational relaxation collision number at 298K
a_{nk}	NASA coefficient of the k^{th} species ($n = 1, 2, 3, \dots$)
\bar{c}_p	Average specific heat constant at constant pressure (on mass basis)
\bar{c}_v	Average specific heat constant at constant volume (on mass basis)
$c_{v,i}$	Specific heat constant of the i^{th} species
$(dP/d\theta)_{max}$	Maximum rate of pressure rise (bar/CA)
f	Internal residual fraction
f_k	Internal residual fraction in the k^{th} zone
h_c	Convection heat transfer coefficient
h_{actual}	Actual convection heat transfer coefficient
$h_{woschni}$	Convection heat transfer calculated from Woschni correlation
h_i	Enthalpy of the i^{th} species
h_{uni}	Enthalpy of the uniform mixtures
h_{int}	Enthalpy of the intake mixtures
k	Ratio of specific heat
k_B	Boltzmann constant
k_{fi}	Forward rate constant of i^{th} reaction
k_{ri}	Reverse rate constant of i^{th} reaction

k_0	Forward rate constant of i^{th} reaction at high pressure region
k_∞	Forward rate constant of i^{th} reaction at low pressure region
k_f	Conductive heat constant
m_{EGR}	The amount of external exhaust gas recirculation
m_{RG}	The amount of reformer gas
m_{cyl}	Mass inside a cylinder
m_{fuel}	The amount of fuel
m_i	Total mass of the i^{th} species
m_{int}	Total amount of intake mass
\dot{m}_j	Mass flow rate through the j^{th} opening channel
m_k	The amount of mass inside the k^{th} zone
$m_{k,i}$	The amount of mass of the i^{th} species in the k^{th} zone
m_1	The amount of mass inside the 1 st zone
n	Total number of moles
p	Partial pressure
p_T	Upstream pressure
p_0	Downstream pressure
r_c	Compression ratio
<i>stoich</i>	Stoichiometric
t	Time measured reference to IVC ($t @ IVC = 0$ sec)
u_i	Total internal energy of the i^{th} species
$u_{i,k}$	Total internal energy of the i^{th} species in the k^{th} zone
v	Characteristic velocity
v^*	Characteristic velocity for heat transfer across zone boundaries
v_{EVC}	Specific volume (volume per mass ratio) at EVC
v_{IVC}	Specific volume (volume per mass ratio) at IVC
v_{mot}	Motoring characteristic velocity
v_{comb}	Combustion characteristic velocity
x_r	Residual fraction
$[x_k]$	Molar concentration of the k^{th} species

α	Polarizability
ε	Emissivity
ρ	Mixture density
ε/k_B	Lennard-Jones potential wall depth
η_k	Single component viscosities of the k^{th} species
λ	Average Gas thermal conductivity
λ_k	Gaseous thermal conductivity of the k^{th} species
λ_{lar}	Laminar gas thermal conductivity of the mixtures
λ_{tur}	Turbulent gas thermal conductivity of the mixtures
σ	Lennard-Jones collision diameter
σ_k	Lennard-Jones collision diameter of the k^{th} species
τ	Inverse of a characteristic time scale of relative temperature rise
μ	Gas dynamic viscosity
μ_{lar}	Laminar gas dynamic viscosity
μ_{tur}	Turbulent gas dynamic viscosity
μ_D	Dipole moment
ν'_{ki}	Stoichiometric coefficient of the k^{th} species (reactant) in the i^{th} reaction
ν''_{ki}	Stoichiometric coefficient of the k^{th} species (product) in the i^{th} reaction
ω	Relaxation factor
$\dot{\omega}_k$	Rate of production of the k^{th} species
$\dot{\omega}_{k,i}$	Contribution of the i^{th} reaction to the rate of production of the k^{th} species
θ	Crank angle position
ϕ	Equivalent ratio
γ	Ratio of specific heat
$\Omega^{(2,2)*}$	Collision integral parameter

TABLE OF CONTENTS

1	INTRODUCTION	1
1.1	HCCI COMBUSTION.....	2
1.1.1	<i>HCCI Combustion Principle.....</i>	2
1.1.2	<i>Main Advantages of HCCI Combustion</i>	3
1.1.3	<i>Main Disadvantages of HCCI Combustion</i>	4
1.2	RESEARCH ON HCCI ENGINES.....	5
1.2.1	<i>Compression Ratio (CR).....</i>	5
1.2.2	<i>Intake conditions.....</i>	6
1.2.3	<i>Using external/internal exhaust gas recirculation (EGR)</i>	7
1.2.4	<i>Blending different octane rating fuels.....</i>	8
1.3	THESIS QUESTIONS	10
1.4	CHEMICAL KINETIC RELATED HCCI MODELING.....	11
1.4.1.	<i>Semi-chemical kinetic based model</i>	12
1.4.2.	<i>Single zone chemical kinetic based combustion Model</i>	13
1.4.3.	<i>Multi-Zone chemical kinetic based Combustion Model.....</i>	14
1.4.4.	<i>Chemical kinetic model integrated with 3D CFD.....</i>	15
1.5	MODEL SELECTION.....	15
1.6	LIMITATIONS AND UNCERTAINTIES OF CURRENT MULTI ZONE MODELS.....	16
1.7	OBJECTIVES OF THIS WORK	18
1.8	MODEL DEVELOPED	19
1.9	OUTLINE OF THE DISSERTATION	19
2	CHEMICAL KINETIC CALCULATION AND MECHANISM OPTIMIZATION.....	21
2.1	THERMODYNAMIC PROPERTIES CALCULATION	22
2.2	CHEMICAL KINETICS CALCULATION.....	23
2.2.1.	<i>Rate of Change of Particular Species:.....</i>	24
2.2.2.	<i>Chemical Equilibrium Constant</i>	25
2.2.3.	<i>Chemical Kinetic Coefficients:</i>	26
2.2.4.	<i>Pressure-Dependent Reactions.....</i>	27
2.3	SHOCK TUBE CALCULATION AND MECHANISM VALIDATION.....	30
2.3.1.	<i>Zero-dimensional Shock tube Calculation.....</i>	30
2.3.2.	<i>Performance of the Methane and Heptane Mechanism.....</i>	31

2.4	REACTION PATH OF HEPTANE COMBUSTION	32
2.4.1.	<i>First Stage Auto-Ignition or "Cool Flame"</i>	35
2.4.2.	<i>Second stage auto-ignition or "main combustion"</i>	40
2.5	SENSITIVITY ANALYSIS OF INFLUENTIAL REACTIONS.....	44
2.6	GENETIC ALGORITHM OPTIMIZATION.....	46
2.5.1.	<i>Genetic Algorithm</i>	47
2.5.2.	<i>Objective Function and Optimization Results</i>	50
2.5.3.	<i>Performance of Optimized Mechanism</i>	52
2.7	SUMMARY.....	59
3	SINGLE ZONE HCCI MODEL	60
3.1.	MAIN ASSUMPTIONS OF THE MODEL	61
3.2.	GOVERNING EQUATIONS FOR THE CLOSED SYSTEM (PERIOD FROM IVC TO EVO)	62
3.2.1.	<i>Equation for In-Cylinder Pressure</i>	62
3.2.2.	<i>Equation for In-Cylinder Volume</i>	63
3.2.3.	<i>Equation for Species Concentrations</i>	63
3.2.4.	<i>Equation for Mixture Temperature</i>	64
3.2.5.	<i>Equation for Mass Conservation</i>	65
3.2.6.	<i>Initial condition Setup – Mixing Phenomena Modeling</i>	65
3.3.	HEAT TRANSFER CALCULATION.....	68
3.3.1.	<i>Convection Heat Transfer</i>	68
3.3.2.	<i>Radiation Heat Transfer</i>	70
3.3.3.	<i>Effective Wall Temperature Correlation</i>	72
3.4.	GAS EXCHANGE SUB-MODELING	76
3.5.	CHEMCOMB SINGLE ZONE HCCI MODEL	80
3.5.1.	<i>Required Inputs</i>	81
3.5.2.	<i>Solver</i>	86
3.6.	MODEL PERFORMANCE.....	87
3.6.1.	<i>Experimental Set-up</i>	88
3.6.2.	<i>Model Validation Based on Pressure Trace</i>	89
3.6.3.	<i>Model Performance in Capturing the Start of Main Combustion</i>	91
3.7.	SUMMARY.....	93
4	MULTI ZONE HCCI MODEL.....	94
4.1.	MAIN ASSUMPTIONS OF THE MODEL	95
4.2.	ZONE CONFIGURATION	96

4.3.	INHOMOGENEITY SCHEME	98
4.4.	TRANSPORT PROPERTIES CALCULATION.....	102
4.5.	CALCULATIONS FOR THE CLOSED SYSTEM INTERVAL	106
4.5.1.	<i>Governing equations of a full multi zone model</i>	106
4.5.2.	<i>Heat transfer</i>	109
4.6.	SEGREGATION SOLVER.....	112
4.5.1.	<i>Evaluating volume change rate of each zone:</i>	113
4.5.2.	<i>Adjusting pressure and volume of each zone:</i>	114
4.7.	TECHNIQUE TO SMOOTH PRESSURE TRACE	116
4.8.	CHEMCOMB MULTI ZONE HCCI MODEL	117
4.9.	MODEL PERFORMANCE	123
4.9.1.	<i>Model performance in capturing in-cylinder pressure history</i>	123
4.9.2.	<i>Model performance in capturing important engine parameters</i>	126
4.10.	SUMMARY.....	132
 5 THE EFFECTS OF CHANGING MIXTURE COMPOSITION PARAMETERS ON HEPTANE- AND METHANE-HCCI COMBUSTION		134
5.1	MEASURES OF IN-CYLINDER ENVIRONMENT, THERMODYNAMIC AND CHEMISTRY PROPERTIES WITH CHANGING MIXTURES	135
5.2	EQUIVALENCE RATIO EFFECTS ON HCCI COMBUSTION	137
5.3	REFORMER GAS EFFECTS ON HCCI COMBUSTION.....	143
5.4	EXTERNAL EGR EFFECTS ON HCCI COMBUSTION	149
5.5	INTERNAL EGR EFFECTS ON HCCI COMBUSTION	156
5.6	ENGINE CONTROL AT DIFFERENT OPERATING MODES.....	159
5.7	CONTROL PERSPECTIVE	165
5.8	SUMMARY.....	168
 6 SUMMARY AND FUTURE WORK.....		170
6.1.	SUMMARY OF MODEL DEVELOPMENT	170
6.2.	SUMMARY OF MODEL APPLICATION.....	172
6.3.	FUTURE WORK	173
 REFERENCES.....		176
 APPENDIX A.....		186

APPENDIX B	187
B.1. CONVERSION OF UNITS REGARDING MOLE, MASS AND CONCENTRATION	187
B.2. MIXTURE AVERAGE PROPERTIES	188
APPENDIX C	189
APPENDIX D	195

TABLE OF FIGURES

FIGURE 2-1 : EXAMPLE OF THERMODYNAMIC COEFFICIENT DATA INPUT [105].....	23
FIGURE 2-2 : EXAMPLE OF CHEMICAL KINETIC DATA INPUT.....	29
FIGURE 2-3: SHOCK TUBE DIAGRAM.....	30
FIGURE 2-4: PERFORMANCE OF GRI MECH ON SHOCK-TUBE IGNITION DELAY [105].....	33
FIGURE 2-5 : PERFORMANCE OF CHM MECH ON SHOCK-TUBE IGNITION DELAY [116]	33
FIGURE 2-6 : VALIDATION OF ORIGINAL CHALMERS MECHANISM ON AN HCCI ENGINE FUELLED WITH HEPTANE/RG MIXTURES.....	34
FIGURE 2-7: VALIDATION OF CHM MODEL FOR HEPTANE COMBUSTION VIA COMPARISON WITH PRESSURE TRACE FROM ENGINE EXPERIMENTS.....	34
FIGURE 2-8: VOLUMETRIC HEAT RELEASE WITH PRODUCTION/CONSUMPTION OF SELECTED SPECIES DURING 1ST STAGE AUTO-IGNITION (COOL FLAME), CHM MODEL	36
FIGURE 2-9: MAJOR REACTIONS THAT INVOLVE H ₂ O, CHM MODEL	36
FIGURE 2-10: MAJOR REACTIONS THAT INVOLVE CO, CHM MODEL	37
FIGURE 2-11 : MAJOR REACTIONS (TOP 9) THAT INVOLVE OH RADICALS, CHM MODEL.....	38
FIGURE 2-12 : MAJOR REACTIONS (TOP7) THAT INVOLVE CH ₂ O RADICALS, CHM MODEL	39
FIGURE 2-13 : MAJOR REACTIONS (TOP7) THAT INVOLVE C ₅ H ₁₁ CO RADICALS DURING FIRST STAGE COMBUSTION, CHM MODEL.....	39
FIGURE 2-14 : MAJOR REACTIONS (TOP 4) THAT INVOLVE H ₂ O ₂ DURING FIRST STAGE COMBUSTION, CHM MODEL.....	40
FIGURE 2-15 : VOLUMETRIC HEAT RELEASE WITH PRODUCTION/ CONSUMPTION OF SELECTED SPECIES DURING MAIN STAGE COMBUSTION, CHM MODEL	41
FIGURE 2-16 : KEY REACTIONS INVOLVING CO ₂ RADICALS, CHM MODEL	42
FIGURE 2-17 : KEY REACTIONS INVOLVING H ₂ O SPECIES, CHM MODEL	42
FIGURE 2-18 : KEY REACTIONS INVOLVING OH RADICALS, CHM MODEL	43
FIGURE 2-19 : KEY REACTIONS INVOLVING H ₂ O ₂ RADICALS, CHM MODEL.....	43
FIGURE 2-20 : SENSITIVITY ANALYSIS OF PRE-EXPONENTIAL COEFFICIENTS OF INFLUENTIAL REACTIONS	45
FIGURE 2-21 : SENSITIVITY ANALYSIS OF TEMPERATURE DEPENDENT PARAMETERS (β) OF THE SELECTED INFLUENTIAL REACTIONS.....	46
FIGURE 2-22 : SCHEMATIC DIAGRAM ILLUSTRATING THE THREE INHERITED CHILDREN IN GENETIC ALGORITHM (FROM [131])	48
FIGURE 2-23 : GENETIC ALGORITHM FLOW CHART.....	49
FIGURE 2-24 : PERFORMANCE OF A MODIFIED CHALMER MECHANISM ON SHOCK-TUBE IGNITION DELAY PREDICTION AT DIFFERENT INITIAL PRESSURES.....	53

FIGURE 2-25 : PERFORMANCE OF A MODIFIED CHALMER MECHANISM ON SHOCK-TUBE IGNITION DELAY PREDICTION AT DIFFERENT MIXTURE COMPOSITIONS	53
FIGURE 2-26 : COMPARISON OF COMPRESSION PRESSURE TRACES OF A 700 RPM HCCI ENGINE OPERATING WITH 0.8 EQUIVALENCE RATIO HEPTANE/AIR MIXTURES, 40% EGR, 1 BAR INTAKE PRESSURE AND 100°C INTAKE TEMPERATURE	55
FIGURE 2-27 : COMPARISON OF COMPRESSION PRESSURE TRACES OF A 700 RPM HCCI ENGINE OPERATING WITH 0.65 EQUIVALENCE RATIO HEPTANE/AIR MIXTURES, 30%EGR, 1BAR INTAKE PRESSURE AND 100°C INTAKE TEMPERATURE	56
FIGURE 2-28 : COMPARISON OF COMPRESSION PRESSURE TRACES OF A 800 RPM HCCI ENGINE OPERATING WITH 0.47 EQUIVALENCE RATIO HEPTANE/AIR MIXTURES, 40% EGR, 1.5 BAR INTAKE PRESSURE AND 115°C INTAKE TEMPERATURE	57
FIGURE 2-29 : OVERALL PERFORMANCE OF ORIGINAL CHM IN PREDICTING SOC OF N-HEPTANE HCCI ENGINE WITH RG BLEND AMOUNT VARYING FROM 0% TO 25% OF FUEL	58
FIGURE 2-30 : OVERALL PERFORMANCE OF A GA-OPTIMIZED CHALMER MECHANISM IN PREDICTING SOC OF N-HEPTANE HCCI ENGINE WITH RG BLEND AMOUNT VARYING FROM 0% TO 25% ..	58
FIGURE 3-1: SCHEMATIC OF A SINGLE ZONE MODEL	61
FIGURE 3-2: THE SCHEMATIC OF MIXTURES AT INTAKE VALVE OPENED (A)	66
FIGURE 3-3 : SIMULATION RESULTS OF A CNG-HCCI ENGINE, USING THE ORIGINAL SINGLE ZONE MODEL WITH DIFFERENT STARTING POINTS	67
FIGURE 3-4 : CONTRIBUTION OF ENGINE KNOCK TO WALL TEMPERATURE (DETERMINED BY TRIAL AND ERROR BASED ON EXPERIMENTAL DATA).....	74
FIGURE 3-5 : THE PERFORMANCE OF THE MODEL WITH AND WITHOUT WALL TEMPERATURE CORRELATION (USING A METHANE FUELLED HCCI ENGINE).....	75
FIGURE 3-6 : DISCHARGE COEFFICIENTS FOR INTAKE AND EXHAUST PROCESS (FROM [72]).....	78
FIGURE 3-7: REGRESSION ANALYSIS OF FUEL-, RG- AND AIR- MASS FLOWS OF A METHANE FUELLED HCCI ENGINE.....	78
FIGURE 3-8 : REGRESSION ANALYSIS OF FUEL-, RG- AND AIR- MASS FLOWS OF A HEPTANE FUELLED HCCI ENGINE.....	79
FIGURE 3-9 : EXAMPLE OF IN-CYLINDER PRESSURE DURING GAS EXCHANGING PROCESS	79
FIGURE 3-10: MAIN STRUCTURE OF SINGLE ZONE CALCULATION IN CHEMCOMB (THE NAMES IN THE CHART REFERRED TO APPENDIX C)	80
FIGURE 3-11 : EXAMPLE OF AN INPUT FILE FOR A SINGLE ZONE MODEL - OPTION 1 (SPECIFIES CONDITIONS AT IVC)	83
FIGURE 3-12 : EXAMPLE OF AN INPUT FILE FOR A SINGLE ZONE MODEL - OPTION 2 (SPECIFIES THE AMOUNT OF MASS FLOW INTO AN ENGINE)	84
FIGURE 3-13 : EXAMPLE OF AN INPUT FILE FOR A SINGLE ZONE MODEL - OPTION 3	85
FIGURE 3-14: SCHEMATIC DIAGRAM OF AN EXPERIMENTAL SET-UP [146].....	89

FIGURE 3-15 : COMPARISON OF PRESSURE HISTORIES FROM A METHANE-FUELLED HCCI ENGINE OPERATING WITH TWO DIFFERENT CONDITIONS.....	90
FIGURE 3-16 : COMPARISON IN PRESSURE HISTORIES OF AN N-HEPTANE-FUELLED HCCI ENGINE OPERATING WITH TWO DIFFERENT CONDITIONS.....	91
FIGURE 3-17 : COMPARISON BETWEEN SIMULATED AND EXPERIMENTAL SOC OF A CNG HCCI ENGINE THROUGH A REGRESSION ANALYSIS.....	92
FIGURE 3-18 : COMPARISON BETWEEN SIMULATED AND EXPERIMENTAL SOC OF A HEPTANE HCCI ENGINE THROUGH A REGRESSION ANALYSIS.....	92
FIGURE 4-1 : DEVELOPMENT OF ZONE CONFIGURATION.....	96
FIGURE 4-2 : EFFECTS OF ZONE NUMBERS ON PRESSURE TRACE AND COMPUTATION TIME	97
FIGURE 4-3 : PATTERN OF IN-CYLINDER TEMPERATURE AND INTERNAL RESIDUAL DISTRIBUTION AT IVC. BOTH RESIDUAL AND TEMPERATURE ARE ASSUMED HIGHER AT THE CYLINDER ‘CORE’ REGION.....	98
FIGURE 4-4 : MOTION OF FLUIDS IN CYLINDER DURING GAS INTAKE PROCESS	99
FIGURE 4-5 : A FLOW CHART FOR SETTING MASS AND TEMPERATURE DISTRIBUTION.....	99
FIGURE 4-6 : CONFIGURATION OF VOLUME DISTRIBUTION AT IVC	101
FIGURE 4-7 : EXAMPLE OF INPUT TABLE FOR TRANSPORT PROPERTY COEFFICIENTS	103
FIGURE 4-8: SCHEMATIC OF HEAT TRANSFER	110
FIGURE 4-9: CORRECTING FACTOR TO HEAT TRANSFER MODELING FOR ENGINE KNOCK.....	112
FIGURE 4-10 : AN ALGORITHM FOR SEGREGATING A MZM	114
FIGURE 4-11 : A COMPARISON OF REQUIRED COMPUTATIONAL TIME WHEN USING FULLY COUPLING AND SEGREGATED SOLVERS (ON A 2.2GHZ DUAL-CORE PROCESSOR, AMD OPTERON PC WITH 2.6GB RAM)	116
FIGURE 4-12: COMPARISON BETWEEN RAW AND FILTERED PRESSURE TRACES	116
FIGURE 4-13 : EFFECTS OF SEGREGATING TIME STEP TO HCCI PRESSURE TRACE OF A METHANE ENGINE.....	119
FIGURE 4-14 : MAIN STRUCTURE OF MINGLE ZONE CALCULATION IN CHEMCOMB (THE NAMES IN THE CHART REFERRED TO APPENDIX C)	119
FIGURE 4-15: EXAMPLE OF AN INPUT FILE FOR A SINGLE ZONE MODEL OPTION 1	120
FIGURE 4-16: EXAMPLE OF AN INPUT FILE FOR A SINGLE ZONE MODEL OPTION 2	121
FIGURE 4-17: EXAMPLE OF AN INPUT FILE FOR A SINGLE ZONE MODEL OPTION 3	122
FIGURE 4-18 : COMPARISON OF PRESSURE HISTORIES FROM A METHANE FUELLED HCCI ENGINE OPERATING WITH TWO DIFFERENT CONDITIONS.....	124
FIGURE 4-19 : COMPARISON OF PRESSURE HISTORIES FROM N-HEPTANE FUELLED HCCI ENGINE OPERATING WITH TWO DIFFERENT CONDITIONS.....	124
FIGURE 4-20 : PREDICTION OF THE START OF MAIN COMBUSTION FROM A CNG ENGINE	127
FIGURE 4-21 : PREDICTION OF THE START OF MAIN COMBUSTION FROM A HEPTANE ENGINE	127

FIGURE 4-22 : EXAMPLE OF EXPERIMENTAL FLUCTUATIONS CAPTURED BY A MODEL (THE FIVE CASES WERE PERFORMED IN A 470 RPM CNG-HCCI ENGINE WITH $\phi \sim 0.37$, %EGR $\sim 5\%$, $T_{INT} = 413.15K$ AND $P_{INT} = 0.92$ BARS).....	128
FIGURE 4-23 : EXAMPLE OF MZM PERFORMANCE ON SOME ENGINE PARAMETERS FROM A CNG ENGINE.....	129
FIGURE 4-24 : EXAMPLE OF MZM PERFORMANCE ON SOME ENGINE PARAMETERS FROM A HEPTANE ENGINE.....	129
FIGURE 4-25 : PERFORMANCE OF MZM ON CAPTURING THE TRENDS OF PRESSURE RELATED PARAMETERS OF A CNG ENGINE	130
FIGURE 4-26 : PERFORMANCE OF MZM ON CAPTURING THE TRENDS OF PRESSURE RELATED PARAMETERS OF A HEPTANE ENGINE	130
FIGURE 4-27 : PERFORMANCE OF MZM ON CAPTURING THE TRENDS OF ENGINE PERFORMANCE PARAMETERS OF A CNG ENGINE	131
FIGURE 4-28 : PERFORMANCE OF MZM ON CAPTURING THE TRENDS OF ENGINE PERFORMANCE PARAMETERS OF A HEPTANE ENGINE	131
FIGURE 5-1 : TIMING OF H_2O_2 AND OH CONCENTRATION CHANGES AT THE TIME OF CNG IGNITION	137
FIGURE 5-2 : PRESSURE HISTORIES FROM A CNG ENGINE OPERATING WITH DIFFERENT ϕ MIXTURES	138
FIGURE 5-3 : PRESSURE HISTORIES FROM A HEPTANE ENGINE OPERATING WITH DIFFERENT ϕ MIXTURES	138
FIGURE 5-4 : WALL- AND IVC- TEMPERATURES OF A CNG ENGINE WITH VARIOUS ϕ MIXTURES ..	140
FIGURE 5-5 : WALL- AND IVC- TEMPERATURES OF A HEPTANE ENGINE WITH VARIOUS ϕ MIXTURES	140
FIGURE 5-6 : VARIATION OF SPECIFIC HEAT RATIO, K, IN A CNG-FUELED ENGINE WITH DIFFERENT ϕ . (THESE K VALUES ARE WEIGHTED AVERAGE OF MULTIPLE ZONES WITH VARIABLE COMPOSITIONS, CAUSING NON-SMOOTH BEHAVIOUR AS ZONES REACT)	141
FIGURE 5-7 : VARIATION OF SPECIFIC HEAT RATIO, K, IN A HEPTANE-FUELED ENGINE WITH DIFFERENT ϕ	141
FIGURE 5-8 : RATE OF TEMPERATURE RISE, $DT/DT@T$, FOR CNG-FUELED HCCI WITH VARIOUS FUEL FRACTIONS	142
FIGURE 5-9 : RATE OF TEMPERATURE RISE, $DT/DT@T$, FOR HEPTANE-FUELED HCCI WITH VARIOUS FUEL FRACTIONS	143
FIGURE 5-10 : PRESSURE HISTORIES FROM A CNG ENGINE WITH RG ADDITION	144
FIGURE 5-11 : PRESSURE HISTORIES FROM A HEPTANE ENGINE WITH RG ADDITION	144
FIGURE 5-12 : WALL- AND IVC- TEMPERATURES OF A CNG ENGINE WITH RG ADDITION.....	146
FIGURE 5-13 : WALL- AND IVC- TEMPERATURES OF A HEPTANE ENGINE WITH RG ADDITION.....	146

FIGURE 5-14 : VARIATION OF SPECIFIC HEAT RATIO, K, IN A CNG-FUELED ENGINE WITH VARYING RG FRACTIONS.....	147
FIGURE 5-15 : VARIATION OF SPECIFIC HEAT RATIO, K, IN A HEPTANE-FUELED ENGINE WITH VARYING RG FRACTIONS	147
FIGURE 5-16 : RATE OF TEMPERATURE RISE, $dT/dT@T$, FOR CNG-FUELED HCCI WITH RG ADDITION	148
FIGURE 5-17 : RATE OF TEMPERATURE RISE, $dT/dT@T$, FOR HEPTANE-FUELED HCCI WITH RG ADDITION	148
FIGURE 5-18 : CNG-HCCI PRESSURE TRACES OF AN ENGINE OPERATING WITH DIFFERENT %EGR	150
FIGURE 5-19 : HEPTANE-HCCI PRESSURE TRACES OF AN ENGINE OPERATING WITH DIFFERENT %EGR	150
FIGURE 5-20 : EFFECTS OF EXTERNAL EGR TO WALL- AND IVC- TEMPERATURES INSIDE A CNG ENGINE.....	151
FIGURE 5-21 : EFFECTS OF EXTERNAL EGR ON WALL- AND IVC- TEMPERATURES INSIDE A HEPTANE ENGINE.....	152
FIGURE 5-22 : A COMPARISON OF RATIO OF SPECIFIC HEAT BETWEEN FRESH CHARGES AND EXHAUSTS USING DIFFERENT ϕ CNG MIXTURES.....	152
FIGURE 5-23 : THERMODYNAMIC (K) EFFECTS OF EXTERNAL EGR ADDITION TO CNG HCCI.....	153
FIGURE 5-24 : THERMODYNAMIC (K) EFFECTS OF EXTERNAL EGR ADDITION TO HEPTANE HCCI.	154
FIGURE 5-25 : RATE OF TEMPERATURE RISE FOR CNG-FUELED HCCI WITH VARIOUS EGR FRACTIONS	155
FIGURE 5-26 : RATE OF TEMPERATURE RISE FOR HEPTANE-FUELED HCCI WITH VARIOUS EGR FRACTIONS	155
FIGURE 5-27 : INTAKE AND EXHAUST VALVE PROFILES.....	156
FIGURE 5-28 : PRESSURE TRACES OF A METHANE HCCI ENGINE OPERATING WITH DIFFERENT HOT EGR LEVELS	157
FIGURE 5-29 : PRESSURE TRACES OF A METHANE HCCI ENGINE OPERATING WITH DIFFERENT HOT EGR LEVELS	157
FIGURE 5-30 : EFFECTS OF EXTERNAL EGR TO WALL- AND IVC- TEMPERATURES INSIDE A HEPTANE ENGINE.....	158
FIGURE 5-31 : EFFECTS OF EXTERNAL EGR TO WALL- AND IVC- TEMPERATURES INSIDE A HEPTANE ENGINE.....	158
FIGURE 5-32 : EFFECTS OF CHANGING EQUIVALENT RATIO UNDER DIFFERENT OPERATING MODES IN A HEPTANE ENGINE, (A) METHANE HCCI ENGINE AND (B) HEPTANE HCCI ENGINE	162
FIGURE 5-33 : EFFECTS OF CHANGING $3H_2-1CO$ RG UNDER DIFFERENT OPERATING,.....	163

FIGURE 5-34 : EFFECTS OF CHANGING % EXTERNAL EGR UNDER DIFFERENT OPERATING, (A) METHANE HCCI ENGINE AND (B) HEPTANE HCCI ENGINE	164
FIGURE 5-35 : PRESSURE HISTORIES OF A SUPERCHARGED CNG ENGINE OPERATING AT TWO DIFFERENT SPEEDS	165
FIGURE 6-1 : THE EXAMPLE OF PERFORMANCE MAP THAT CAN BE FILLED IN BY THE DEVELOPED MODELS	174

TABLE OF TABLES

TABLE 2-1 : PARAMETERS USED IN EQUATION 2.27	28
TABLE 2-2 : SHOCK TUBE IGNITION DELAY INITIAL CONDITIONS FOR GA OPTIMIZATION	51
TABLE 2-3 : SZM INITIAL CONDITIONS FOR GA OPTIMIZATION.....	51
TABLE 2-4: MODIFIED COEFFICIENTS FOR A HEPTANE MECHANISM	51
TABLE 3-1: CORRELATIONS AND CONSTANTS FOR WOSCHNI HEAT TRANSFER CALCULATION	70
TABLE 3-2 : PARAMETERS FOR CALCULATING EMISSIVITIES OF H ₂ O AND CO ₂	72
TABLE 3-3 : INITIAL CONDITIONS FOR PERFORMANCE TESTING OF SZM WITH EFFECTIVE WALL CORRELATION	75
TABLE 3-4 : ENGINE SPECIFICATION. (NOTE THE FIRST COMPRESSION RATIO IS FOR A CNG-HCCI ENGINE, AND THE SECOND IS FOR AN N-HEPTANE-HCCI ENGINE).	88
TABLE 4-1 : COEFFICIENTS FOR CALCULATING COLLISION INTEGRAL AND ASSOCIATED PARAMETERS [110]	104
TABLE 4-2 : RELATED PARAMETERS FOR CALCULATING TRANSLATIONAL, ROTATIONAL AND VIBRATIONAL CONTRIBUTIONS TO THERMAL CONDUCTIVITY OF AN INDIVIDUAL SPECIES	105

PAPERS RELATED TO THE THESIS

This section lists the papers that are related to the model developed in this thesis. The papers were written by either the author or the author's colleague (Vahid Hosseini) with the author's supervisor (Dr. M David Checkel).

1. Model development:

Kongsereeparp P, Kashani B and Checkel MD. (2005). A stand-alone multi-zone model for combustion in HCCI engines. Proceedings of ICEF 05. ICEF2005-1241 in Fall Technical Conference of the ASME Internal Combustion Engine Division. Ottawa, Canada.

Kongsereeparp P and Checkel MD. (2007). Novel Method of Setting Initial Conditions for Multi-zone HCCI Combustion Modeling. SAE Paper, 2007-01-0674.

2. Application of a model to study HCCI combustion

Kongsereeparp P and Checkel MD. (2006). Investigating the Effects of Reformed Fuel Blending in a Natural Gas-HCCI Engine Using a Multi-Zone Model. CI/CS Spring Technical Meeting. Waterloo, Canada.

Kongsereeparp P and Checkel MD. (2007). Investigating the Effects of Reformed Fuel Blending in a Methane- or n-Heptane-HCCI Engine Using a Multi-Zone Model. SAE Paper, 2007-01-0205

Kongsereeparp P and Checkel MD. (2007). Influence of Reformer Gas Replacement and its Composition on CNG- and Heptane-HCCI Combustion Using a Single Zone Combustion Model. CI/CS Spring Technical Meeting. Banff, Canada.

Kongsereeparp P and Checkel MD. (2007). Ignition Mechanism of n-Heptane/Air Mixtures in an HCCI Combustion Engine. CI/CS Spring Technical Meeting. Banff, Canada.

Kongsereparp P and Checkel MD. (2008). Study of Reformer Gas Effects on n-Heptane HCCI - Combustion Using a Chemical Kinetic Mechanism Optimized by Genetic Algorithm. Accepted for SAE World Congress, SAE 2008-01-0039

Kongsereparp P and Checkel MD. (2008). Environmental, Thermodynamic and Chemical Factor Effects on Heptane- and Methane-fuelled HCCI Combustion with Various Mixture Compositions. Accepted for SAE World Congress, SAE 2008-01-0038

Hosseini V and Checkel MD. (2007). Combustion timing control of Heptane-fueled HCCI by reformer gas: experiments and chemical kinetic modeling. CI/CS Spring Technical Meeting. Banff, Canada

Hosseini V and Checkel MD. (2008). Reformer Gas Composition Effect on HCCI Combustion of n-Heptane, iso-Octane. Accepted for SAE World Congress, SAE 2008-01-0049

Hosseini V. (2008). Reformer Gas Application in HCCI Combustion Engine. PhD thesis, submitted to the Department of Mechanical Engineering, the University of Alberta

1 INTRODUCTION

An internal combustion engine is the most common technology to power vehicles. In addition, it is also a main power generator for some industries, such as small-scale electricity production. However, the use of internal combustion engines leads to some serious problems regarding environmental degradation and consumption of fossil energy. Unpleasant by-products from such engines include green house gas (GHG) emissions and unwanted pollutants such as nitrogen oxides (NO_x), carbonmonoxide (CO), hydrocarbon (HC), particulate matter (PM), sulfurdioxides (SO_2) etc. These engine by-products are of special concern to the world community and, consequently, several stringent regulations have been applied to engine design. Fossil fuel depletion is another major global concern that affects the viability of internal combustion engines.

To overcome the above problems (i.e., to reduce emissions and the use of fossil fuels), one might suggest a renewable energy alternative or new vehicle technology such as hydrogen fuel cells or electric motors. However, costs, on-board storage and current availability of infrastructure limit the possibility of using those techniques in automobiles in the near-term. Additionally, overall life-cycle emissions of some alternative fuels might not be less than conventional fuels [1]. Since using another energy source to drive a vehicle does not seem competitive within the next decade, a more feasible short-term solution is to develop a fossil-fuel-based engine that is highly efficient. Having high efficiency means that these engines would use less energy and, consequently, produce less greenhouse gas products.

With conventional Otto (gasoline or Spark Ignition) and Diesel (Compression Ignition) engines, it is difficult to reduce some toxic emissions, especially NO_x . Such toxic emissions normally occur in high temperature regions of flame fronts (both propagating and diffusive flames) where the mixture compositions are close to stoichiometric. These production of NO_x requires running engines at less-than

optimum efficiency and use of significant aftertreatment system which as a result reduces the overall efficiency of the engine. Additionally, in terms of efficiency, the Otto engine has a limitation of using high compression ratio due to engine knock.

Searching through literature, one of the most prominent techniques to enhance engine efficiency while reducing NO_x emissions is to operate an engine with HCCI technology. The definition of HCCI and its concept are explained below.

1.1 HCCI Combustion

HCCI is an abbreviation for “Homogeneous Charge Compression Ignition”, which is an alternative way to operate an internal combustion engine. This technique can also be referred to by different names such as ATAC (Active Thermo Atmospheric Combustion) [2-5], CAI (Controlled Auto-Ignition) [6, 7], PCCI (Premixed Charge Compression Ignition), PREDIC (Premixed lean Diesel Combustion) [8], CIHC (Compression Ignited Homogenous Charge) [9], and MK (Modulated Kinetic) [10, 11].

1.1.1 HCCI Combustion Principle

The principle of HCCI can be viewed as a hybrid between spark ignition (SI) and compression ignition (CI) engines. Like the concept of SI engines, premixed mixtures are first charged into a cylinder. However, instead of using a spark plug to control ignition timing, the mixtures ignite by autoignition due to compression, as in CI engines. Based on the autoignition by compression, the combustion of an HCCI engine is mainly controlled by the chemical and thermodynamic properties of the mixtures and is first initiated by several hot auto-igniting spots at the core regions where temperature is higher than the other regions [12, 13]. Since HCCI combustion is controlled mainly by chemical kinetics [14], only certain combinations of mixture and engine operating parameters will produce good combustion (without partial burning or engine knock)._HCCI combustion is

critically dependent on such varied parameters as fuel ignition quality, equivalence ratio, intake temperature, compression ratio, coolant temperature, engine speed and residual fraction.

Before continuing the discussion on HCCI combustion, it is worthwhile to define engine knock in an HCCI. In a spark ignition engine, knock occurs when the compressed, unburned mixtures beyond the flame front spontaneously auto-ignite, generating pressure waves across the combustion chamber. These rapidly echoing pressure waves are characteristic of engine knock and the knock severity is proportional to the fraction of mixture which auto-ignites. In an HCCI engine, the normal combustion process involves chemical auto-ignition of the entire mixture over a short period of time and, if that period becomes too short, excessively rapid pressure rise can generate knock pressure waves. Therefore, for a particular HCCI engine, knock can be defined by a maximum-rate-of-pressure-rise threshold. For this study, engine knock was experimentally defined as pressure rise rate exceeding 8 bar/CA.

Although the first letter in HCCI stands for 'Homogeneous', in a real engine mixtures are not absolutely homogeneous. In fact, if everything is truly uniform throughout a combustion chamber until the combustion takes place, the engine would tend to operate with severe knock since all heat would release at one time. In a real HCCI engine, stratification of mixture composition and temperature across a combustion chamber before combustion is expected and may be the most significant reason for having a finite combustion duration [16-18]. This stratification is likely to be caused by heat dissipation to the walls and non-perfect mixing during early compression [17, 19, 20]. A good discussion on the effects of inhomogeneity can be found in [21-23].

1.1.2 Main Advantages of HCCI Combustion

The principle of HCCI combustion engines leads to several advantages over conventional Otto and Diesel engines. Compared to an Otto engine, HCCI allows

the engine to operate with greater compression ratio, resulting in greater efficiency. Additionally, the fact that HCCI can operate with wide open throttle operation at part load provides higher efficiency [24]. The absence of spark ignition and early developing flame growth reduces the cyclic variation [25]. In comparison with conventional diesel engines, the absence of locally stoichiometric regions lowers the peak combustion temperature of an HCCI engine, which substantially reduces NO_x emissions [26, 27] as well as reducing heat dissipation (enhancing engine efficiency).

In addition to having high compression ratio and less heat dissipation through the wall, the fast combustion rate is also favorable to HCCI engine efficiency if the combustion can be controlled to take place at the appropriate time. Finally, the possibility to operate a wide open throttle engine with very high EGR leads to a better efficiency.

1.1.3 Main Disadvantages of HCCI Combustion

Although HCCI is very promising to provide an internal combustion engine with a better efficiency and lower NO_x emissions, there are three big challenges that the HCCI technique must overcome. One is the difficulty in controlling ignition timing. Combustion in an HCCI engine absolutely relies on the chemical reactivity of the mixtures in the thermo active environment. In other words, there is no external way to specify the ignition timing such that the engine operates normally and gains its maximum performance. This leads to the second challenge of using HCCI to power an IC engine: the limited operating range. Changing the operating conditions such as engine speed and load could result in knocking or misfiring. When knock occurs, the efficiency is significantly dropped and the engine has unacceptable levels of noise, vibrations and harshness (NVH). Another technical problem of an engine operating with HCCI technique is cold-start as acceptable combustion only takes place when the environment provides exactly enough energy to stimulate auto-ignition of mixtures [28]. Therefore,

another operating mode such as SI is required to start the engine, causing another technical difficulty in controlling good combustion during the transient mode.

It can be concluded that HCCI is a valuable concept that can be used to solve problems of internal combustion engines, provided that all the problems are economically solved. Operating an engine with HCCI can provide a gain in engine efficiency up to 20% [17] while keeping some emissions, such as NO_x, below legal limits.

1.2 Research on HCCI Engines

Since it was introduced by Onishi in 1978 [5] under the name of ATAC (Active Thermo Atmospheric Combustion), HCCI has been intensively researched in order to overcome its limitations as discussed in 1.1.3. Several techniques have been examined both experimentally and numerically that can be organized into four main categories: compression ratio, intake conditions, EGR, and fuel blends.

1.2.1 Compression Ratio (CR)

An HCCI engine normally operates with highly diluted mixtures in order to slow down the combustion rate. Therefore a higher compression ratio is often found in an HCCI engine. Compression ratio selection is bracketed by auto-ignitibility of mixtures at the end of compression (lower limit) and engine knock (upper limit). In other words, the selected compression ratio must be high enough to oxidize the mixtures but not so high that engine knock occurs. Selecting CR is one major problem for a combined SI/HCCI engine in which too high CR leads to engine knock in SI operating mode while too low CR impede auto-ignition during HCCI mode.

A higher CR can partially offset the requirement of a heating system at the intake manifold since high CR increases temperature at the end of compression [29]. Some research on varying CR HCCI engines has already been done by [29, 30].

As combustion temperature increases with CR, leading to more complete combustion, NO_x emissions are greater while CO and HC are reduced. A mechanically adjustable compression ratio from to was already achieved by Haraldsson et al [31].

1.2.2 Intake conditions

As ignition in an HCCI engine relies on the chemical kinetic reactions that depend exponentially on temperature, initial temperature can greatly influence the combustion behavior (possibly the most influential controllable parameter) [32, 33]. Higher temperature leads to advanced ignition timing, shorter ignition delay, faster heat release rate [7, 34], improved combustion efficiency (especially when the mixtures are highly diluted during low load operations) [35] and widened operating range of an engine fuelled with high octane rating fuels [14, 36]. Despite all the advantages, using an intake heating system to control a real HCCI engine suffers from several liabilities. Costs, energy use and complications of adding a heating system are the first concern. Next, volumetric efficiency is significantly reduced by high intake temperature as the density of intake charge is greatly reduced. Additionally, NO_x emissions slightly increase when using hotter intakes as the maximum heat release and combustion rate are being enhanced [34]. More importantly, adjusting intake temperature in order to control HCCI combustion is not feasible on a fast engine operating under various conditions due to its slow response, although some efforts have been tried to achieve faster intake temperature adjustment by varying the blend of two streams of hot and cold air [37].

Another controllable intake parameter is intake pressure which can be either reduced by throttling the intake or raised by a super charging system. While reducing engine efficiency, throttling the intake of an HCCI engine can provide more stable combustion, decrease CO emissions and increase exhaust temperature at idle operations since it allows the engine to operate with less dilution [38, 39]. Increasing intake pressure was mostly used to enhance engine power output,

(HCCI operation at IMEP up to 16 bar [40]), with the benefit of widening engine operating range, higher combustion efficiency and lower CO and HC emissions [41-43]. Nevertheless, some difficulties have arisen when increasing intake pressure. Firstly, back pressure must be greater than intake pressure in order to recirculate exhaust back to the intake system [44]. The turbine used in a turbo-charging system needs to be smaller with a greater pressure ratio due to low exhaust temperature that causes high density and slow flow rate [43]. Additionally, the pumping loss in a turbocharged HCCI engine is high. Finally, since some energy in the exhaust is used to operate a turbine, the exhaust temperature could be significantly reduced, causing a slow CO-HC conversion rate in a catalytic converter (or a light-off temperature problem) [45].

1.2.3 Using external/internal exhaust gas recirculation (EGR)

Since it has faster combustion compared to conventional SI and DI engines, an HCCI engine can tolerate greater amounts of exhaust gas recirculation (EGR) and, therefore, gains a greater advantage from EGR. In fact, an HCCI engine requires high levels of EGR to slow down the combustion rate and reduce maximum pressure at some operating points [30, 46]. EGR can be classified into two categories: 1) external EGR and 2) internal EGR. The external EGR (or cold EGR) is the combustion gas that is directly recirculated back to the intake system and blended with fresh intake fuel/air mixtures. The combustion products remaining in a combustion chamber from the previous operating cycle are known as internal EGR (or hot EGR). Depending on the type of EGR, the effects of recycled exhaust on HCCI combustion behavior can be summarized into the following five categories [46]:

- Charge heating effects – advance ignition timing, increase combustion stability, shorten combustion duration and enhance heat release rate, (strongest for internal EGR).
- Dilution effects – reduce combustion rate and therefore provide smoother and quieter operation, (both internal and external EGR).

- Thermodynamic properties change effects – retard ignition timing [45] and extend combustion duration due to a lower ratio of specific heats, (both internal and external EGR).
- Chemical properties change effects – retard ignition timing (both internal and external EGR).
- Stratification effects – extend burn duration (both internal and external EGR).

To conclude, external EGR was found to retard start of main combustion (SOC), prolong combustion duration, reduce combustion rate and diminish NO_x emissions [45, 47] due to dilution, thermodynamic, chemical, and stratification effects. Hot (internal) EGR shares four common effects (dilution, thermodynamic, chemical and stratification) with external EGR [48]. However, as the additional heating effect with hot EGR has a significant influence on HCCI combustion characteristics [49], the influences of hot EGR on SOC, combustion duration, combustion rate and NO_x emissions are less significant compared to those obtained from cold EGR. Meanwhile, combustion stability is improved [50, 51]. The possible amount of EGR applied is limited by power output requirement and dilution effects which cause unstable combustion, misfiring and high HC-CO emissions.

1.2.4 Blending different octane rating fuels

It is arguable that auto-ignitibility of mixtures used in an HCCI engine should be defined as a function of octane number (ON), temperature history and other factors [52-54]. However, the ON alone is still a good and easy approximation of the auto-ignitibility of fuel mixtures in an HCCI engine. Mixtures of higher octane rating fuels are more difficult to auto-ignite. As the ignition timing of HCCI engines depends on auto-ignition, variable blends between two different octane fuels can significantly change HCCI combustion behavior and engine performance. Blending different octane rating fuels can be summarized in two approaches: 1) blends between two base fuels such as heptane-octane blends and

2) mixtures of base fuel with reformer gas additives. Both approaches can influence HCCI combustion enough that they can potentially be used for ignition timing control as discussed by several researchers [55-58].

The previous studies showed that at a given intake temperature, mixtures of lower ON fuels require lower intake temperature [54, 59] and could achieve a wider operation range [56, 60]. However, using low ON fuels could lead to early ignition and therefore is applicable only to low compression ratio engines, thus reducing efficiency. Using high ON fuels retards SOC, decreases combustion efficiency, increases HC/CO emissions [58], decreases NO_x emissions and requires hotter intake mixtures or greater compression ratio. Several attempts have been tried to control fuel (ON) qualities by blending two different fuels such as diesel-gasoline [42, 61], heptane-ethanol [43, 62], DME-MRG [63], DME-methanol [64], DME-methane [65], gasoline-hydrogen and natural gas-hydrogen [29, 66].

Blends with reformed fuels have also shown significant effects on HCCI combustion and, therefore, have been demonstrated as a feasible means for HCCI combustion timing control [29]. Blending hydrogen with compressed natural gas (CNG) can advance combustion timing, thus decreasing the high inlet temperature required and extending the lean-mixture operating range [29, 67, 68]. Hosseini and Checkel [69] concluded that adding RG to diesel-like fuels retards ignition timing and lengthens the combustion period. Two effects of RG on HCCI combustion have been studied: 1. temperature changes due to the changed thermal properties of the mixture and 2. auto-ignition chemistry changes due to the changed chemical kinetic properties of the mixture [70]. The relative importance of the two factors varies depending on the base fuel chemistry. An understanding of which factor dominates is important in designing an appropriate HCCI control strategy.

Among the HCCI combustion control techniques discussed above, (sections 1.2.1 to 1.2.4), varying fuel composition as a key parameter to control HCCI

combustion in an engine is promising due to the great advantage of having the flexibility to control the engines on a cycle-by-cycle basis. Changing composition includes altering air-to-fuel ratio (AFR), varying the blend of two different octane number (ON) fuels and using external/internal exhaust gas recirculation (EGR). Although several studies have already reported the effects of altering such parameters on different fuels over a wide range of operation, the reasons behind those effects have not been yet investigated in great detail except for external EGR [71].

Changes in combustion behavior in a slow engine operating with low exhaust temperature can be attributed to the following three different factors: 1. temperature changes due to the changed thermal properties of the mixture; 2. auto-ignition chemistry changes due to the changed chemical kinetic properties of the mixture; and 3. environmental changes due to changed operating conditions. The relative importance of the three factors varies depending on the base fuel chemistry. Understanding which factor dominates is important in designing and justifying an appropriate HCCI control strategy. In addition, in order to select a viable control method, sensitivity of HCCI combustion to each control parameter must be compared. It must be noted that the best HCCI control technique could vary depending on the octane qualities of base fuels and engine conditions as well as operating modes.

1.3 Thesis Questions

HCCI combustion is sensitive to a complex array of operating variables including fuel octane quality, mixture dilution, intake manifold conditions, engine speed and compression ratio. Changing those parameters alters the combustion in an HCCI engine due to 1) mixture properties difference and 2) variation in in-cylinder conditions such as IVC conditions and wall temperature. This study is intended to investigate the effects of changing mixture composition on HCCI combustion in order to gain a better understanding and therefore be able to

identify suitable methods to control an HCCI engine. The answers to the following questions are therefore required:

1. How do various composition-change methods (changing ϕ , RG, %cool EGR or % hot EGR) rank in their effects on HCCI combustion?
2. How do the changes of in-cylinder environment affect HCCI combustion?
3. How do the changes of mixture thermodynamics affect HCCI combustion?
4. How do the changes of mixture chemistry affect HCCI combustion?
5. What are the effects of changing mixture composition at different operating modes (high/low speed, low/high intake pressure)?

Engine modeling was chosen to conduct this study and answer the addressed questions for several reasons. Firstly, the costs and expenses involved. Numerical simulation does not have any extra costs other than the software license and labor to build and simulate a model. Additionally, it is much simpler to use a proper model, once it is validated, to conduct a parametric study of an HCCI engine. It is very difficult to perform a parametric study on an actual engine primarily because of the difficulty in having only one parameter change while keeping the others constant in an actual engine. Another reason is to prevent engine damage that would occur from severe engine knock due to improper conditions. The most important reason why a numerical study is favorable is the crucial information that can only be directly obtained from a simulation such as thermodynamic properties and chemical kinetic process. Aside from the above reasons, which are directly related to this study, a good model is also very useful in designing and developing an engine with less experimental work. Having said that, data from experiments is very important to test and validate the model during the early stage of modeling development.

1.4 Chemical kinetic related HCCI Modeling

Several techniques have been developed to model HCCI combustion, which can be summarized into two main categories. One is a chemical-kinetic based model

and the other is a semi-chemical based model. The chemical-kinetic based model is defined as a model that uses chemical kinetics of mixtures to describe the auto-ignition of HCCI combustion. The chemical-kinetic based model can be further categorized into 1) Single zone combustion model, 2) Multi-zone combustion model, and 3) CFD-kinetic coupled model. Unlike chemical-kinetic based model, the semi-chemical kinetic based model is built based on critical values from chemical kinetic combustion of the mixtures; however, it does not include sufficient detail of chemical kinetic mechanism, (i.e., the number of reactions incorporated in the model is less than or equal to two). The semi-chemical kinetic based model includes temperature threshold, knock integrated approach and Global Arrhenius rate of the integrated reaction threshold.

1.4.1. Semi-chemical kinetic based model

There are three well-known approaches to model start of combustion in an HCCI engine: temperature threshold, knock integrated and integrated global Arrhenius rate threshold.

Temperature threshold: The model uses an isentropic or polytropic process to model in-cylinder pressure and temperature during compression. The start of combustion is assumed to be the point when the mixture's temperature exceeds a critical value. The Wiebe function [15, 72] is used to model this combustion process. The model was found to be inaccurate in some operating conditions [73] since temperature is not the only trigger for combustion initiation. Other effects such as different chemical interactions, reactant concentrations and wall temperature can significantly change the combustion-initiation temperature. Considering these facts, this method could possibly provide accurate predictions of the start of main combustion if enormous data base that accounts for every possible cases were created.

Knock integrated approach: Like the temperature threshold model, the in-cylinder pressure during compression and expansion are calculated based on an

isentropic assumption. The point where the main combustion starts is found from a knock integrated model introduced by Livengood et al [74] and developed by a series of researchers [75, 76]. This model has been developed based on the fact that combustion in an HCCI engine begins with auto-ignition which is similar to engine knock. A great deal of effort has been applied to improve the model for control applications.

Global Arrhenius rate of the integrated reaction threshold: This approach was intended to overcome the limitation of not considering reactant concentration in the preceding two approaches. To set the point where combustion initiates, the model considers only a single global reaction whose reaction rate is expressed by an Arrhenius reaction rate. Combustion is said to occur once the reaction rate exceeds a threshold which is found empirically based on the experiment.

Due to the absence of chemical reaction detail, a semi-chemical kinetic based model cannot accurately predict the start of combustion unless proper validations and parameter tunings were done. In addition, the predictions should be made within a validating range. Nevertheless, computational time required for these models is marginal so the trade-off between computational time and accuracy makes these models suitable and feasible for control application.

1.4.2. Single zone chemical kinetic based combustion Model

The idea of a single-zone model (SZM) is that all properties inside the combustion chamber are considered to be uniform and the heat transfer between the working fluid and the chamber wall is calculated globally using some correlation such as Woschni [77]. Many HCCI studies have used this method [32, 78-84]. For example, Goldsborough [82] used a SZM to study the HCCI technique in a high compression ratio engine fuelled with hydrogen and natural gas. The findings of these studies show that the start of the main combustion could be predicted accurately by a single zone model, provided that appropriate initial conditions were assigned and heat transfer during compression was

properly estimated. However, not considering the temperature gradient developed during compression in this model and neglecting boundary layer zones leads to an over-prediction of the peak pressure, peak temperature and NO_x emission. In addition, a single zone model can not accurately predict combustion duration (CD), heat release rate (HRR) and the rate of pressure change since the model inherently predicts that all of the mixture ignites at one time [18, 85].

1.4.3. Multi-Zone chemical kinetic based Combustion Model

A multi-zone model is used to overcome the limitations of a single zone model by accounting for the spatial inhomogeneity, especially between core regions and boundaries. Instead of considering the space inside a combustion chamber as one big volume, it is divided into several small volumes (zones or cells). The number of zones and zone configurations have been varied depending on a compromise between accuracy and computational efforts. Several studies have already been done on a MZM [18-20, 23, 70, 86-91]. Using a MZM, combustion duration, peak pressure, heat release curve and formation of NO_x emissions can be accurately predicted since the temperature gradient between zones ensures that the mixture is not all ignited at one time. The remaining limitation on parametric prediction from a multi-zone model was the emissions of unburnt products such as hydrocarbons and carbon monoxide [4]; however, the introduction of zones representing crevices significantly improved the performance of the model on predicting HC and CO emissions [92].

The major challenge of using an MZM is initial condition estimation, (i.e., the values across a combustion chamber needs to be specified). For this matter, several attempts have been used, such as computational fluid dynamic (CFD) [19, 20, 89, 90] and probability density function (PDF) [93, 94].

1.4.4. Chemical kinetic model integrated with 3D CFD

If highly detailed chemical kinetic modeling can be integrated with a CFD simulation providing accurate initial and boundary conditions, the coupled CFD-chemical kinetic model would provide the most accurate results as it continuously captures the consequences from both chemical reactions and mixture circulation inside a combustion chamber. This leads to the remarkable advantage of this model in capturing the effects of mixture movement (especially turbulence) and engine geometry on HCCI combustion. Both 2D [95, 96] and 3D [21, 97, 98] CFD models have already been integrated with chemical kinetic models to model HCCI combustion behaviors.

Although such model shows promising results in explaining some features of HCCI combustion, especially the effects of turbulence and some emissions, there are some limits to this approach. Highly detail chemical kinetic mechanisms need to be reduced for use in the model as the computational demands are already extensive. Further, excessive computational time makes it difficult to conduct parametric studies investigating the sensitivity of HCCI combustion to a wide range of controllable parameters. Finally, due to a great deal of computational time, processor speed and memory required, the simulation cannot be handled by a personal computer, limiting the flexibility of using the model.

1.5 Model Selection

The intents of this study, which are to:

- 1) understand physical phenomena inside a combustion chamber and
- 2) perform a sensitivity analysis for design and control purposes,

limit the choice of models that can be used. As they only provide the accurate information on ignition timing for a pre-calibrated range of conditions, the semi-chemical based models are not suitable to this study. Full three dimensional flow codes that include turbulent flow, mixing, heat transfer and chemistry are too

computationally intensive and would limit the amount of modeling which can be done. In addition, although the importance of turbulence is still inconclusive, there are indications that turbulent fluctuations have only limited effects on the key outcomes of HCCI combustion. For example, the cycle-to-cycle variations are generally smaller than conventional spark ignition engines. Unlike traditional internal combustion engines where the combustion characteristic greatly depend on flame front development, the combustion characteristic of a homogeneous charge compression ignition (HCCI) engine is mainly governed by the chemistry of the mixtures.

These considerations lead to a compromise approach where flow codes might be used to assess the distributions and in-homogeneity levels of temperature and mixtures in the cylinder using relatively coarse time steps during the intake and early compression process. Once compression temperature is high enough to consider chemical reaction, a multi-zone chemical kinetic model can be used (with appropriately short time steps) to examine the ignition and combustion phenomena. This describes the multi-zone modeling approach used in this work.

1.6 Limitations and uncertainties of current multi zone models

Several artificial factors inherent in model calculations can influence the predictions obtained from a chemical kinetic based model. The first factor is the chemical kinetic mechanism. This is obviously the main concern in any chemical-kinetic based models since the ignition point and combustion behaviors greatly depend on the kinetic mechanism of the mixtures. The uncertainty of chemical kinetic mechanisms can be seen through the fact that there is no single mechanism that can generally be applied to all conditions. All mechanisms in use for fuels more complex than H_2 are inherently reduced mechanisms and the only solution is to optimize the mechanism for particular operating conditions.

Another uncertainty in models arises from heat transfer sub-modeling. Heat transfer is one of the most critical aspects for HCCI combustion since the ignition timing greatly depends on the in-cylinder temperature history. The most popular heat transfer model for an HCCI engine is to use a Woschni correlation [77] with one constant wall temperature for every testing case, although some studies have shown significant effects of different wall temperatures both experimentally and numerically [99]. Changes in wall temperature due to operating conditions are currently accounted for by adjusting the heat transfer coefficient accordingly to operations and engines. Another problem of using the Woschni coefficient to model HCCI combustion is that Woschni does not include the effects of engine knock. (The discussions on the importance of engine knock to heat dissipation and the necessity of having knock effects in heat transfer sub modeling of an HCCI engine can be found in Section 4.5.2). Finally, although the importance of turbulence to HCCI combustion is still controversial, (discussions on turbulence effects can be found in [21, 100]), it could significantly affect in-cylinder spatial heat transfer during compression and expansion process, influencing mixture inhomogeneity [101, 102]. Therefore, an inclusion of turbulence affecting heat transfer between zones across a combustion chamber is needed [103, 104].

A decision of the number of zones is also critical, which could range from a small number (such as two, [86]) to a large number (such as thirty, [91]). Setting initial conditions and their distribution across the multiple zones is a major problem of using a chemical kinetic based model. It is thought that proper initial conditions with a sufficient numbers of zones can provide an accurate prediction to HCCI engines and, therefore, CFD has been introduced to evaluate properties at an initial point (intake valve closed, IVC). Although promising results can be obtained from a CFD-MZM sequential model [19, 89], the complication and computational time required limit the use of the model in a large-scale parametric study. This leads to the need for simpler and more effective methods to set conditions at IVC.

To enhance the predictive ability and utility of the model, the above addressed limitations need to be overcome, leading to the first objective of this study which is to build a reliable, stand-alone MZM model that can be executed on regular personal computers within a reasonable time scale.

1.7 Objectives of this work

Several objectives were set for the model being developed to be able to answer the addressed question in Section 1.3. The first group of objectives is aimed at developing a reliably predictive model that can simulate and explain the behavior of an HCCI engine over a range of controllable parameters without any arbitrary adjustment. The sub-objectives in this first group are:

- To improve the heat transfer model by including radiation heat transfer and variable wall temperature,
- To sequentially combine a one-dimensional isentropic flow model with an HCCI combustion model in order to evaluate the parameters at IVC,
- To generate the property inhomogeneity distributions based on realistic physics and ideal gas theory for use in multi-zone combustion model and
- To make the model solve fast enough to be used.

Using a model proven capable of simulating the phenomena inside a combustion chamber, the following objectives need to be achieved in order to answer the addressed questions:

- To determine the dominant effects of changing mixture compositions on HCCI combustion and HCCI engine parameters
- To observe the effects of varying mixture compositions on HCCI combustion at different operating modes

- To pre-determine the best technique to control ignition timing of a HCCI engine based on the sensitivity of HCCI engine characteristics to controllable variables and response time.

1.8 Model developed

This section provides the overall picture of the model that has been developed. The details can be found in Chapters 2, 3 and 4.

The chemical-kinetics based modeling was constructed in MATLAB and converted to a stand-alone executable file (.exe), named CHEMCOMB, as mentioned in [18]. The Simulation Option in CHEMCOMB offers four different models to investigate HCCI engines. Those models are 1) zero-dimensional shock tube ignition delay calculation, 2) a genetic algorithm model to optimize reaction parameters, 3) a single zone HCCI engine model and 4) a multi zone HCCI engine model. Additionally, there are two solving options for the multi-zone model: 1) a full coupling (or sequential) solver and 2) a segregating solver. In addition to the four models, the CHEMCOMB package offers a tool to perform sensitivity analysis of a chemical kinetic mechanism and of engine performance.

1.9 Outline of the Dissertation

This study is divided into three parts: 1) development of the chemical kinetics calculation and mechanism selection, 2) HCCI engine model development and 3) sensitivity and performance studies of an HCCI engine operating with different controllable parameters. The content of this thesis is organized into six chapters.

Chapter 2 – reviews some important calculations of thermodynamic properties and chemical kinetics. A zero-dimensional shock tube model was developed in order to verify and optimize the chemical kinetic mechanisms to be used in an actual engine simulation.

Chapter 3 – integrates chemical kinetic and thermodynamic properties (used to evaluate thermodynamic states of mixtures inside a combustion chamber) to an engine simulation, forming a single zone combustion model. The engine simulation includes in-cylinder volume change due to piston movement, one-dimensional, isentropic flow to model gas exchanging and heat transfer model.

Chapter 4 – develops the multi zone model, including the inhomogeneity across a combustion chamber. In addition to a new set of governing equations to model phenomena from IVC to EVO, the initial conditions of each zone are also systematically specified.

Chapter 5 – studies the effects of varying different aspects of mixture composition, based on the model developed in Chapter 4. Mixture compositions are altered by changing the equivalence ratio, the amount of reformer gas replacement of base fuel, the external EGR fraction and the internal EGR fraction. The effects on HCCI combustion were also observed and preliminary indications of optimum control strategy are developed.

Chapter 6 – summarizes the study and suggests the area of possible future work.

2 Chemical Kinetic Calculation and Mechanism Optimization

The intent of this chapter is to lay out the basic theory of chemical kinetics used in both single zone and multi zone combustion models and to prepare valid mechanisms for methane/air and n-heptane/air mixtures. This chapter first reviews the thermodynamic properties estimation using NASA coefficients and the Arrhenius chemical kinetic calculation. These two basic calculations are then used to model a zero dimensional shock tube calculation in order to confirm the chemical kinetic calculation and validate the mechanisms for both methane and heptane oxidation. The GRI mech 3.0 mechanism [105] was selected for natural gas while the heptane mechanism was adopted from Chalmers University [106]. Although the validation on shock tube showed promising results for both selected mechanisms, the preliminary study on a single zone combustion model, (discussed in Chapter 3), suggested that improvement was required for a better quantitative prediction of a heptane fuelled HCCI engine, especially when some part of the fuel was replaced by simulated reformer gas (75% H_2 -25% CO). As the mechanism was already well structured [17], the performance could be enhanced by changing only the parameters of some influential reactions identified by an investigation on auto-ignition processes together with sensitivity analysis. As widely used by others, a genetic algorithm was selected to optimize Arrhenius parameters of the addressed reactions [107-109].

Instead of using an MKS (Metre-Kilogram-Second) unit system, all calculations in this study are based on the CGS (Centimetre-Gram-Second) unit system in which the unit of length is centimeter, the unit of mass is gram and the unit of time is second [110]. The CGS unit system is commonly used in chemistry, primarily because of the scale of some parameters such as gas concentration. The conversion between the CGS unit system and the SI system can be found in Appendix A.

2.1 Thermodynamic Properties Calculation

Thermodynamic properties of the mixtures are required in order to evaluate the condition inside a cylinder and to calculate an equilibrium constant of a particular reaction. Thermodynamic properties are represented by a 6th order NASA polynomial (requiring a set of 7 coefficients) [105, 111]. For each species, two sets of coefficients are needed (one for low temperature and the other for high temperature). The point that separates the low temperature interval from the high temperature interval is normally at 1000K unless specified otherwise. An example of input information for thermodynamic calculations can be found in Figure 2-1 which describes oxygen gas, (O₂). The first line describes the chemical species by a name (O2), by the combustion, (O 2), indicating two oxygen atoms and by phase (G) indicating gas. The next two numbers, (200, 3500), give the minimum temperature and maximum temperature (in Kelvin) for the property correlations. The final number on the first line, (1000), indicates the break point between low temperature and high temperature correlation equations. The next 7 numbers are the coefficients for the estimation at high temperature while the last 7 numbers are for low temperature values. The calculation of basic properties is given by Equations (2.1), (2.2) and (2.3).

$$\frac{C_{pk}^0}{R_u} = a_{1k} + a_{2k}T + a_{3k}T^2 + a_{4k}T^3 + a_{5k}T^4 \quad (2.1)$$

$$\frac{H_k^0}{R_u T} = a_{1k} + \frac{a_{2k}}{2}T + \frac{a_{3k}}{3}T^2 + \frac{a_{4k}}{4}T^3 + \frac{a_{5k}}{5}T^4 + \frac{a_{6k}}{6} \quad (2.2)$$

$$\frac{S_k^0}{R_u} = a_{1k} \ln T + \sum_{n=2}^N \frac{a_{nk} T^{(n-1)}}{(n-1)} + a_{N+2,k} \quad (2.3)$$

```

O2      O 2      G 200.000 3500.000 1000.000 1
3.28253784E+00 1.48308754E-03-7.57966669E-07 2.09470555E-10-2.16717794E-14 2
-1.08845772E+03 5.45323129E+00 3.78245636E+00-2.99673416E-03 9.84730201E-06 3
-9.68129509E-09 3.24372837E-12-1.06394356E+03 3.65767573E+00 4

```

Figure 2-1 : Example of Thermodynamic Coefficient Data Input [105]

Note that H_k^0 is an absolute enthalpy (see Equation 2.4) which is different from tabulated data in which the enthalpy of formation ($\Delta H_f(298K)$) is usually excluded.

$$H_k^0(T) = \Delta H_f(298K) + \int_{T=298}^T H(T) dT \quad (2.4)$$

2.2 Chemical Kinetics Calculation

Changes in mixture composition from reactants (before combustion) to products (after combustion) are caused by reactions between fuels and oxygen. Such reactions happen in a certain pattern from chain initiation \rightarrow chain propagation and chain branching \rightarrow chain termination [112]. This process takes place at an appropriate time for efficient engine operation for certain conditions (temperature, pressure and engine speed), depending on mixture composition. To describe the process of changing compositions, a chemical kinetics calculation is used. This section first describes the rate of change in molar concentration and mass fraction of a particular species. Such a calculation is associated with forward/reverse rate constants that are discussed in Sections 2.2.3 and 2.2.4. Note that the following discussion is based on CHEMKIN calculations and, therefore, much of the credit of this section (Section 2.2) is devoted to Kee et al, the authors of the CHEMKIN manual [110].

2.2.1. Rate of Change of Particular Species:

Changes in species concentration inside a closed system (in an engine, the system is closed between intake valve closed to exhaust valve opened) are due to chemical kinetics. Considering a reaction that is in the form:



the rate of change in molar concentration (so-called “chemical production rate”) of the k^{th} species due to the i^{th} reaction can be found from,

$$\dot{\omega}_{k,i} = (\nu''_{k,i} - \nu'_{k,i}) \left(k_{f,i} \prod_{k=1}^{N_s} [x_k]^{\nu'_{k,i}} - k_{r,i} \prod_{k=1}^K [x_k]^{\nu''_{k,i}} \right) \quad (2.12)$$

The example of molar concentration change can be demonstrated using the following equations. Consider the reaction,



At 1200 K, the forward and reverse reaction rate constants are equal to $1 \times 10^{14} \text{ cm}^3/(\text{mol}\cdot\text{S})$ and $6.3756 \times 10^{-7} \text{ cm}^3/(\text{mol}\cdot\text{S})$ respectively (calculation of reaction rates can be found in Section 2.4.3). Using Equation 2.12, the rate of change in molar concentration of [O] and [OH], (the unit is $\text{mol}/(\text{cm}^3\cdot\text{S})$), are:

$$\frac{d[\text{O}]}{dt} = (0 - 1) (1 \times 10^{14} [\text{O}][\text{H}_2] - 6.3756 \times 10^{-7} [\text{H}][\text{OH}]) \quad (2.13)$$

$$\frac{d[\text{OH}]}{dt} = (1 - 0) (1 \times 10^{14} [\text{O}][\text{H}_2] - 6.3756 \times 10^{-7} [\text{H}][\text{OH}]) \quad (2.14)$$

Summing all production/destruction rates of the k^{th} species (Equation 2.12) from every reaction, the total rate of chemical production of the k^{th} species can be found (Equation 2.15) as:

$$\dot{\omega}_k = \sum_{i=1}^R \dot{\omega}_{k,i} \quad (2.15)$$

When a third body is required to remove the energy to complete the recombination, the production rate must include the effects of the third body by adding one coefficient to Equation 2.12 as shown in Equation 2.16.

$$\dot{\omega}_{k,i} = \left(\sum \alpha [x_k] \right) (v''_{k,i} - v'_{k,i}) \left(k_{f,i} \prod_{k=1}^{N_S} [x_k]^{v''_{k,i}} - k_{r,i} \prod_{k=1}^K [x_k]^{v'_{k,i}} \right) \quad (2.16)$$

The unit of chemical rate of production is mol/(cm³-sec) which, in other words, is the rate of change in molar concentration. Applying Equation B.2 from Appendix B, the rate of mass fraction change due to chemical kinetics can be calculated as,

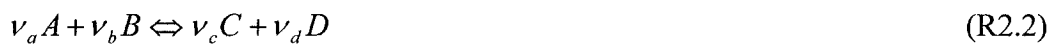
$$\frac{dY_k}{dt} = \frac{\dot{\omega}_k W_k}{\rho} \quad (2.17)$$

From Equations 2.14 and 2.15, it can be seen that the calculation involves forward/reverse rate constants. Sections 2.2.2 and 2.2.3 explain how to calculate those constants.

2.2.2. Chemical Equilibrium Constant

The chemical equilibrium constant is important as it is used to interpret reverse reaction rate constants in some cases (see Section 2.2.3). Based on thermodynamic theory, equilibrium state is defined as the state where the Gibb's free energy of the system is minimized [112, 113]. As a result, the derivative of Gibb's free at the equilibrium point is equal to zero and the equilibrium constant can be found.

Consider the reaction,



The chemical equilibrium constant for an ideal gas reaction can be written as [15, 113],

$$K_p = \frac{Y_c^{\nu_c} Y_c^{\nu_c}}{Y_c^{\nu_c} Y_c^{\nu_c}} \left(\frac{P}{P_0} \right)^{\Delta \nu} = \exp \left(- \frac{\Delta G^\circ}{R_U T} \right) \quad (2.18)$$

where,

$$\Delta \nu = \nu_c + \nu_d - \nu_a - \nu_b \quad (2.19)$$

and

$$\Delta G^\circ = \nu_c G_C^\circ + \nu_d G_D^\circ - \nu_a G_A^\circ - \nu_b G_B^\circ \quad (2.20)$$

Note that the “subscript P” of the term K_p indicates the equilibrium constant based on partial pressures of the species. To transform from partial pressure based equilibrium constant to concentration based equilibrium constant, multiplies Equation 2.16 by $R/T^{-\Delta \nu}$ [112] giving:

$$K_C = \exp \left(- \frac{\Delta G}{RT} \right) \times \left(\frac{R_U}{T^{-\Delta \nu}} \right) \quad (2.21)$$

2.2.3. Chemical Kinetic Coefficients:

The rates at which reactions progress can be calculated from the Arrhenius theory. The Arrhenius reaction rate is based on potential collisions of reacting species. The reactions proceed only when the level of molecular energy is greater than the activation energy. The energy of molecules is assumed to be purely kinetic, which depends on temperature. The reaction rate coefficient is given by,

$$k = A \times T^\beta \times \exp \left(\frac{-E}{R_u T} \right) \quad (2.22)$$

Equation 2.22 is applied to both forward and reverse reaction rate constants. However, most of the time, the reverse reaction rate constants (A , β and E) are not given. In this case, the reverse rate constants of the i^{th} reaction was calculated from the equilibrium constants as,

$$k_r = \frac{k_f}{K_C} \quad (2.23)$$

2.2.4. Pressure-Dependent Reactions

Third-body collision is required to trigger some particular reactions that only occur at low pressure, (i.e., at high enough pressure, those reactions can proceed by themselves),

- At low pressure : $A+B+M \rightleftharpoons C+M$
- Above some pressure limit : $A+B \rightleftharpoons C$

Therefore, the chemical rates of those reactions do not solely depend on temperature but also vary with pressure. Important reactions in this class are either unimolecular recombination fall-off reactions or chemically activated bimolecular reactions [110]. The chemical rate of unimolecular recombination reaction is faster at high pressure while chemically activated bimolecular reactions have decreasing chemical rates at higher pressure.

In order to calculate the reaction rates of those reactions, Arrhenius coefficients must be specified for both high and low pressure regions, using a simple Arrhenius formula (see Equations 2.24 and 2.25). The only problem arises at the fall-off region or transition region where special treatment is required.

$$k_0 = A_0 T^{\beta_0} \exp(-E/RT) \quad (2.24)$$

$$k_\infty = A_\infty T^{\beta_\infty} \exp(-E/R_U T) \quad (2.25)$$

From Equations 2.24 and 2.25, the chemical rate at any pressure can be fitted into the form of,

$$k = k_{\infty} \left(\frac{P_r}{1 + P_r} \right) F \quad (2.26)$$

where P_r is reduced pressure, which can be found from,

$$P_r = \frac{k_0[M]}{k_{\infty}} \quad (2.27)$$

F in Equation 2.26 is a fitting parameter, which can be calculated differently depending on the method selected. For the Lindemann form, F is set to unity. A more complex approach to calculating F is the SRI form by Stewart et al, [114] in [110], or the Troe form by Troe, [115] in [110]. Widely used in combustion chemistry, the Troe form was selected to calculate the parameter F in this study.

Parameters for calculating F using the Troe method are α , T^{***} , T^* , and T^{**} . These four parameters are used to estimate the other set of parameters c, n, d and F_{cent} (see calculation in Table 2-1). After obtaining c, n, d and F_{cent} , F can be calculated from,

$$\log F = \left[1 + \left[\frac{\log P_r + c}{n - d(\log P_r + c)} \right] \right] \log F_{cent} \quad (2.28)$$

Table 2-1 : Parameters Used in Equation 2.27

c	$= -0.4 - 0.67 \log F_{cent}$
n	$= 0.75 - 1.27 \log F_{cent}$
d	$= 0.14$
F_{cent}	$= (1 - \alpha) \exp(-T/T^{***}) + \alpha \exp(-T/T^*) + \exp(-T^{**}/T)$

Examples of the input data for chemical kinetic calculation are shown in Figure 2-2. The first reaction, $2\text{H}+\text{H}_2\text{O}\rightleftharpoons\text{H}_2+\text{H}_2\text{O}$, is an example of a normal reaction for which the forward and reverse rate constants are calculated by Equation 2.22 and 2.23, using Arrhenius parameters (A , β and E). As indicated at the end of the reaction, $A = 6.000\text{E}+19$, $\beta = -1.250$ and $E = 0.00$. The chemical production rate is given by Equation 2.12. The second reaction, $2\text{O}+\text{M}\rightleftharpoons\text{O}_2+\text{M}$, involves a third body species, so the chemical rate of production is calculated from Equation 2.16. (The α parameters in Equation 2.16 are indicated below the reaction line: i.e., α for $\text{H}_2 = 2.40$, α for $\text{H}_2\text{O} = 15.40$, α for $\text{CH}_4 = 2.00$, α for $\text{CO} = 1.75$, α for $\text{CO}_2 = 3.60$, α for $\text{C}_2\text{H}_6 = 3.00$ and α for $\text{AR} = 0.83$). The third sample reaction, $\text{H}+\text{CH}_2(+\text{M})\rightleftharpoons\text{CH}_3(+\text{M})$, is a pressure-dependent reaction. The Arrhenius parameter for k_0 is indicated after the reaction description, ($A = 6.000\text{E}+14$, $\beta = -1.250$ and $E = 0.00$), while the coefficients on the second line after the word "LOW/", ($A = 1.04\text{E}+26$, $\beta = -2.76$ and $E = 1600.00$) are for k_∞ . The Troe values, (α , T^{***} , T^* , and T^{**}), for rate constants in the fall-off region are given on the last line.

Once the chemical kinetics model was successfully built in MATLAB, the next step was to select the mechanisms to model combustion inside an HCCI engine. The well-known GRI mech 3.0 mechanism [105] was adopted to calculate methane/air combustion while the Chalmers University mechanism (CHM) [116] was used for heptane/air. Before applying the mechanisms in an engine simulation, their performance was tested on combustion data from a shock tube.

2H+H2O<=>H2+H2O	6.000E+19	-1.250	.00
!			
2O+M<=>O2+M	1.200E+17	-1.000	.00
H2/ 2.40/ H2O/15.40/ CH4/ 2.00/ CO/ 1.75/ CO2/ 3.60/ C2H6/ 3.00/ AR/ .83/			
!			
H+CH2(+M)<=>CH3(+M)	6.000E+14	.000	.00
LOW / 1.040E+26 -2.760 1600.00/			
TROE/ .5620 91.00 5836.00 8552.00/			

Figure 2-2 : Example of Chemical Kinetic Data Input

2.3 Shock Tube Calculation and Mechanism Validation

To validate the performance of the chemical kinetics mechanisms, zero dimensional shock-tube modeling was used. In this study, a shock tube in which ignition mechanism is driven by release of high pressure inert gas through a ruptured diaphragm was selected due to the availability in experimental data (see Figure 2-3). The ignition timing is defined as the time lag between the point when the shock wave reflects from the end of the shock tube and the mixture combustion.

2.3.1. Zero-dimensional Shock tube Calculation

The detailed calculation can be found in many publications, such as [117], and only the governing equations are included in this section, which are,

$$\frac{dT}{dt} = \frac{1}{\rho c_V} \sum_{i=1}^{N_S} (h_i \dot{\omega}_i \times W_i) + \frac{T}{c_V} \times \frac{dR_{ave}}{dT} \quad (2.29)$$

$$\frac{dP}{dt} = R_{ave} \times T \times \frac{d\rho}{dt} + \rho \times R_{ave} \times \frac{dT}{dt} \quad (2.30)$$

$$\frac{dY_i}{dt} = \frac{\dot{\omega}_i \times W_i}{\rho} \quad (2.31)$$



Figure 2-3: Shock Tube Diagram

2.3.2. Performance of the Methane and Heptane Mechanism

GRI mech 3.0 [105] was adopted to simulate a CNG fueled HCCI engine while the mechanism for heptane mixtures was a Chalmer mechanism (CHM) [116]. The performance of both mechanisms was validated by simulating ignition delay in a shock tube for the same conditions (initial pressure = 6 to 42 bar and $\phi = 0.5$ to 3) as the well known experimental data provided in [105, 116]. The purpose is not only to confirm the mechanisms themselves but also to ascertain the MATLAB chemical kinetic implementation. Various initial conditions were tested and plotted in Figure 2-4 (for methane auto-ignition) and Figure 2-5 (for heptane). It is notable that although the range of testing conditions for methane mixtures in a shock tube needs to be extrapolated to actual conditions inside the engine cylinder, the GRI mechanism has been proven suitable for simulating methane combustion in a HCCI engine as justified by several researchers [83, 118, 119]. Having said that, other mechanisms are being developed based on shock data under engine-like conditions and could potentially be used for engine simulation [120-122].

Good performance in predicting ignition delay in a shock tube was found with both GRI mech and CHM mechanisms over a wide range of initial conditions. This confirms that both our kinetic calculation and the mechanism were properly functional.

Although the CHM is capable of capturing shock tube ignition timing, our preliminary investigation predicting HCCI ignition showed that the mechanism can only qualitatively predict HCCI combustion when part of the fuel was replaced by 3H₂:1CO reformer gas (RG). Figure 2-6 shows the start of main combustion (SOC) timing validation of a single zone model (calculation found in Chapter 3) against experimental results from a heptane fuelled HCCI engine with varying RG blend fractions. In Figure 2-6, an alternative heptane mechanism from Patel et al (2004), named EVC mechanism, [123] was plotted as a comparison. The figure shows that model based on the EVC mechanism predicted a minimal

advance in SOC timing with increasing RG fuel replacement, (which was opposite to the trend observed in the engine); while the model using CHM predicted the expected behavior, (i.e., retarding SOC with increased RG fuel replacement). However, it under-estimated the quantitative effects from RG. Therefore, it would obviously be desirable to use experimental results to better optimize the chemical kinetic mechanism for both heptane and heptane-RG fuel mixtures. Before optimizing the reactions, it is important to explore the auto-ignition process of heptane/air mixtures in order to specify the important reactions that will be optimized.

2.4 Reaction Path of Heptane Combustion

This section describes the n-heptane auto-ignition process during the 1st and 2nd stages of combustion. Heptane HCCI combustion was investigated using a 700RPM CFR engine operating at part load ($\phi=0.4$) with 42%EGR under the operating conditions of 1.5 bar intake manifold pressure and 383K intake manifold temperature. The investigation was done using a single zone combustion model described in Chapter 3. The validation of the model to capture in-cylinder behavior was shown in Figure 2-7. Although this operating point seems to be at risk of severe knock operation due to early combustion, the maximum rate of pressure rise is approximately 8 bar/CA, meaning that only slight engine knock occurred.

The purpose of this analysis is to identify the important chemical processes, reactions and species that are responsible for the auto-ignition of pure-heptane-air mixtures. Understanding this process is important in order to identify the reactions to be optimized.

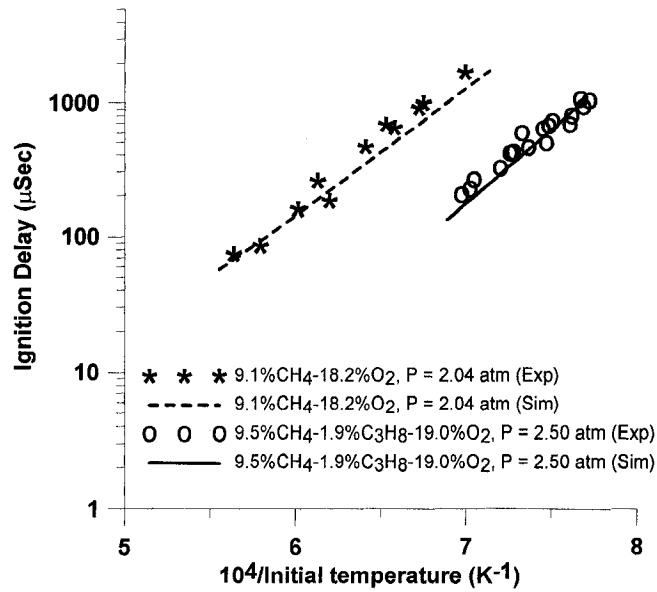


Figure 2-4: Performance of GRI mech on Shock-Tube Ignition Delay [105]

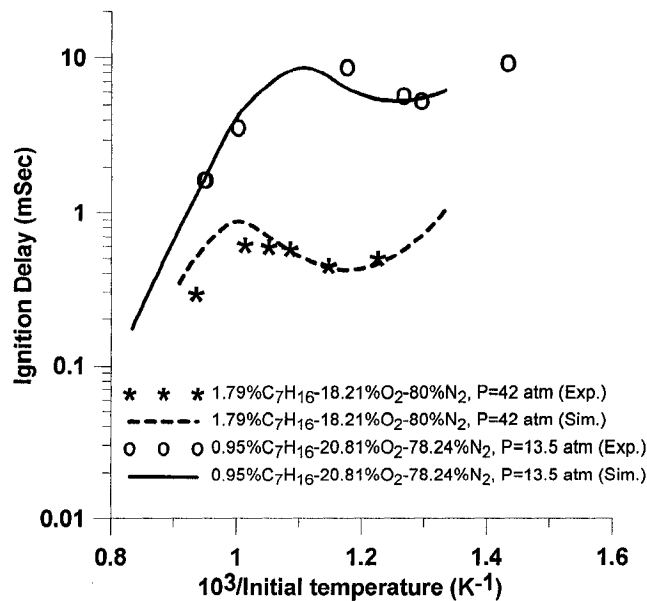


Figure 2-5 : Performance of CHM mech on shock-tube ignition delay [116]

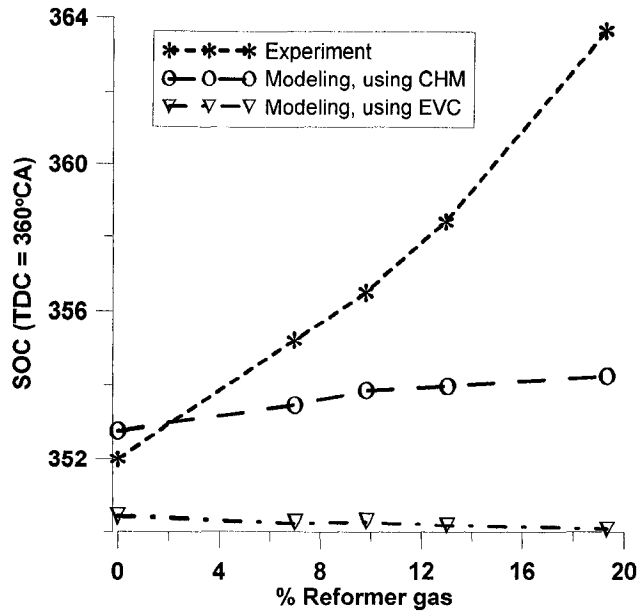


Figure 2-6 : Validation of original Chalmers mechanism on an HCCI engine fuelled with heptane/RG mixtures

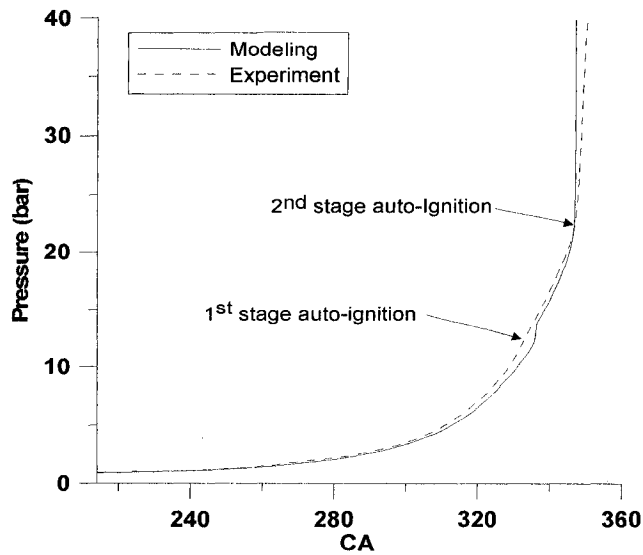


Figure 2-7: Validation of CHM model for heptane combustion via comparison with pressure trace from engine experiments

2.4.1. First Stage Auto-Ignition or "Cool Flame"

Figure 2-8 shows the heat release (negative values) associated with major reactions during the 1st stage auto-ignition (which occurs at approximately 335°CA in the modeled engine). The greatest heat release in the cool flame period is associated with H₂O and CO production. H₂O is mostly produced by the reactions R5, R6 and R142 (see Figure 2-9) while CO production mainly results from reactions R27 and R151 (see Figure 2-10). (Note that the reaction number is the same as the Chalmers University mechanism in [106]).



Based on these reaction equations, OH and CH₂O radicals are important to H₂O formation, while C₅H₁₁CO and HCO are key radicals associated with CO production. This raises interest in the history of these three radicals during the early auto-ignition period.

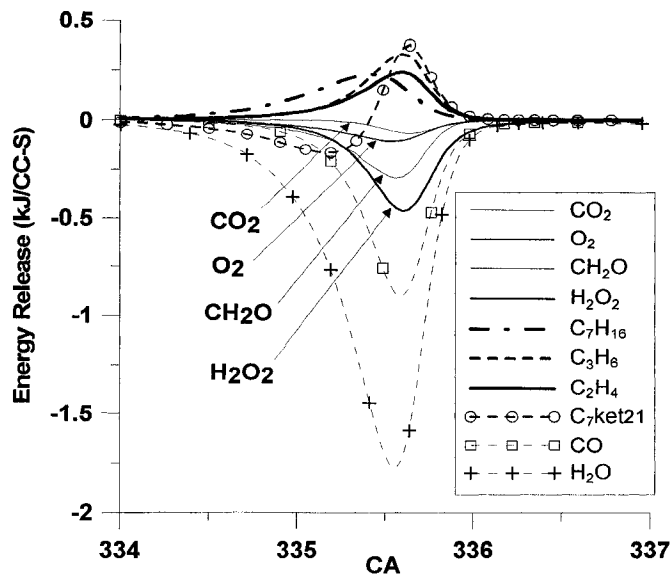


Figure 2-8: Volumetric heat release with production/consumption of selected species during 1st stage auto-ignition (cool flame), CHM model

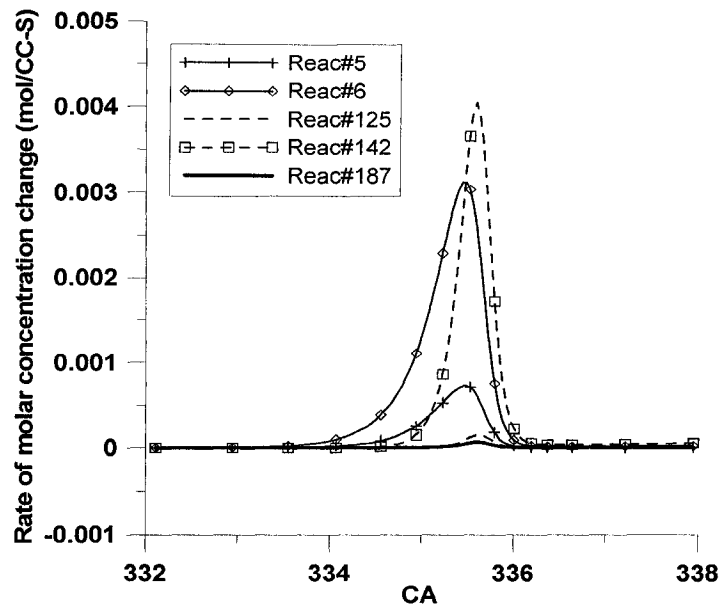


Figure 2-9: Major reactions that involve H₂O, CHM model

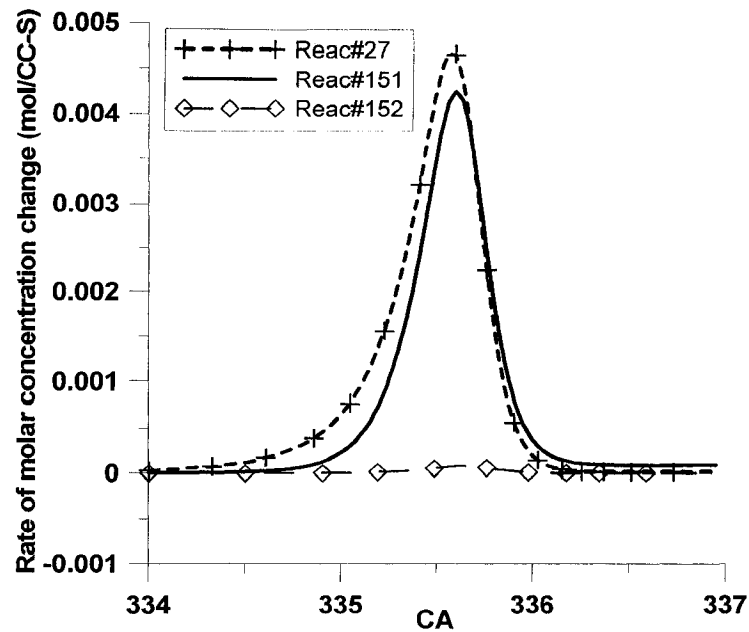


Figure 2-10: Major reactions that involve CO, CHM model

Figure 2-11 shows that OH is initially produced from C₇H₁₄O₂HO₂ decomposition via reaction R18. This reaction also produces ketone that further decomposes to additional OH radicals (reaction R19). One fate of the OH radicals produced is reaction with heptane (reaction R6), producing water and releasing some heat. As the temperature and the concentration of OH radicals surpass certain levels, reaction R142 provides a major path to produce H₂O and hence contribute to rapid temperature increase. Another important reaction consuming OH radicals is reaction R185. Although not significant in terms of heat release, R185 produces formaldehyde which contributes to reaction R142, the most prominent reaction forming H₂O and releasing heat. However, as Figure 2-12 shows, the major formaldehyde production route is via reaction R19.



Beyond raising in-cylinder temperature, the 1st stage or cool flame reactions also produce some influential radicals that lead to the 2nd stage or main auto-ignition. This radical production is probably more directly important than raising

temperature. Several radicals are produced in significant quantities and remain in the mixture after the cool flame period. For example, Figure 2-14 shows that production of peroxide radicals (H_2O_2) greatly exceeds consumption and peroxide is a major key to the main auto-ignition [13]. H_2O_2 radical production in the cool flame is mainly generated from HO_2 and collisions of HO_2 and CH_2O via reactions R122 and R143. The HO_2 radicals are produced by reactions R192 and R151.

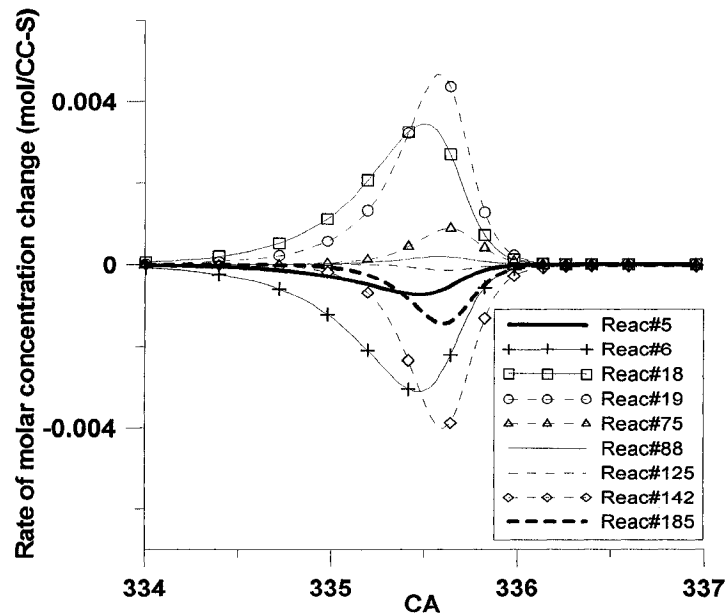
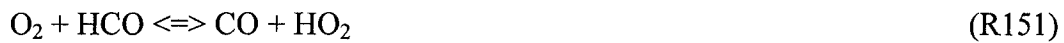


Figure 2-11 : Major reactions (Top 9) that involve OH radicals, CHM model

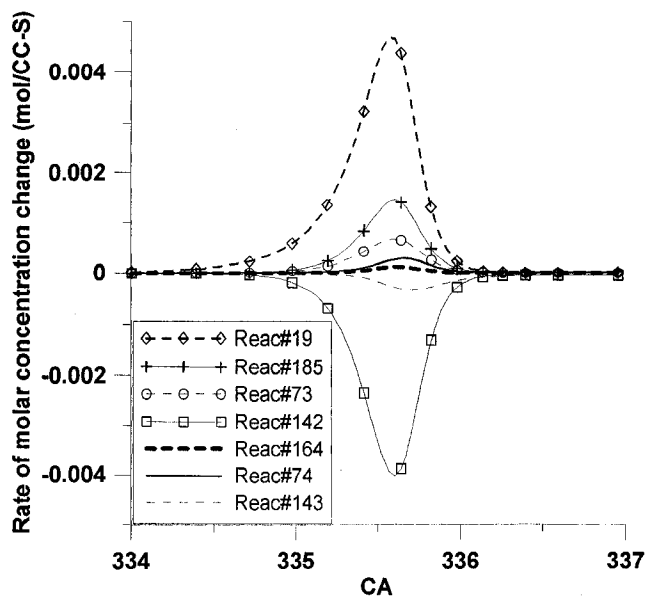


Figure 2-12 : Major reactions (Top7) that involve CH₂O radicals, CHM model

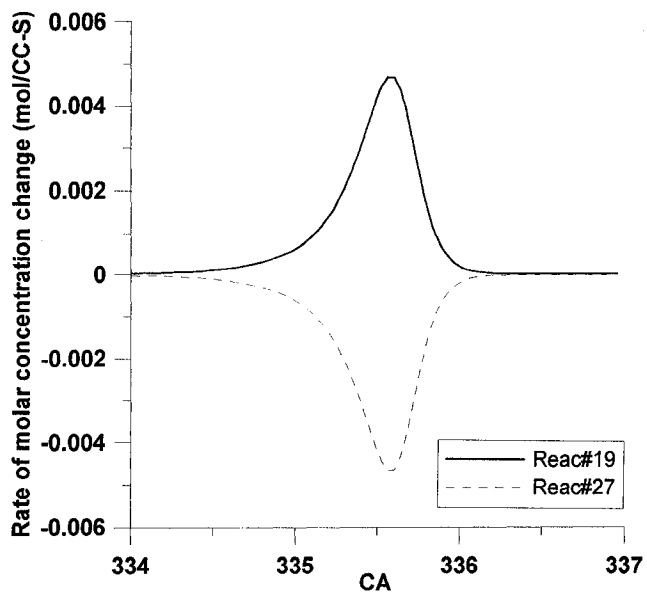


Figure 2-13 : Major reactions (Top7) that involve C₅H₁₁CO radicals during first stage combustion, CHM model

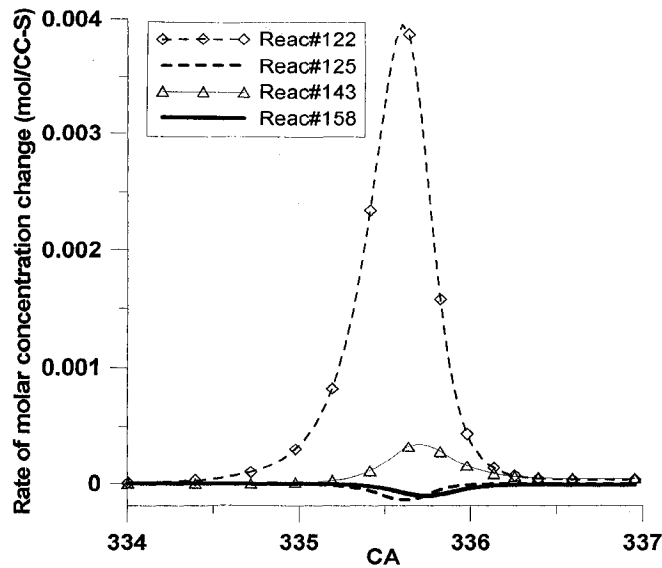


Figure 2-14 : Major reactions (Top 4) that involve H₂O₂ during first stage combustion, CHM model

2.4.2. Second stage auto-ignition or "main combustion"

At modeled engine conditions, the 2nd stage or main auto-ignition occurs at 347°CA. Figure 2-15 shows that heat release from CO₂ and H₂O formation is the major temperature driver during 2nd stage auto-ignition. CO₂ is mainly produced by reaction R97 (Figure 2-16) while reactions R142 and R110 produce most of the water during 2nd stage combustion (Figure 2-17). (Note that reaction R142 is also the key H₂O producing reaction during 1st stage combustion). These reactions involve hydroxyl radicals whose history is traced in Figure 2-18.



The most prolific reactions involving OH during main combustion are shown in Figure 2-18. OH production is mainly initiated by reactions involving HO₂ and H₂O₂, (R75 and R123). Of these two reactions, R123 is more important as it produces about twice as many OH radicals in the early, low-temperature period. The initial OH produced reacts with formaldehyde to form water (R142) resulting in some heat release that increases temperature. Consequently, some OH

production reactions, which have higher activation energy, (R102, R111 and R113), become more active and thus increase overall OH concentration. As the OH concentration level and temperature increase, R97 becomes the most important OH consumption reaction, producing CO₂ and thus the greatest heat release at main combustion (Figure 2-15).

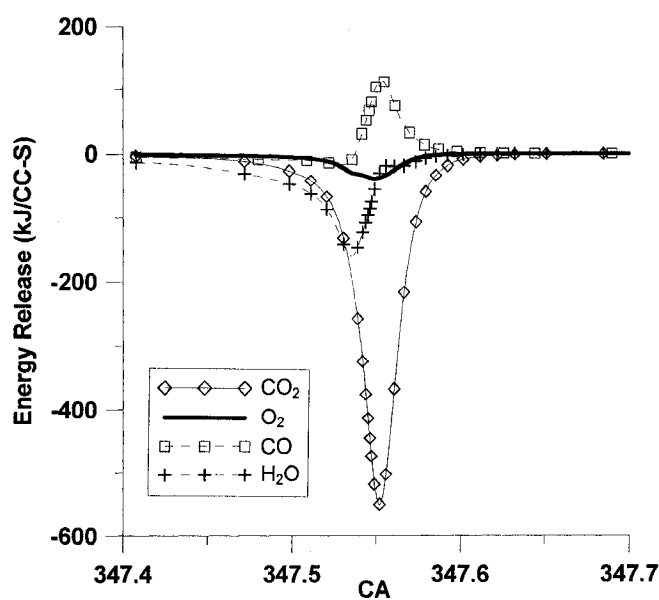
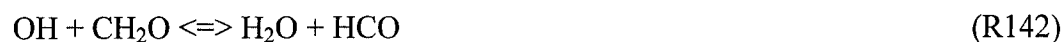


Figure 2-15 : Volumetric heat release with production/ consumption of selected species during main stage combustion, CHM model

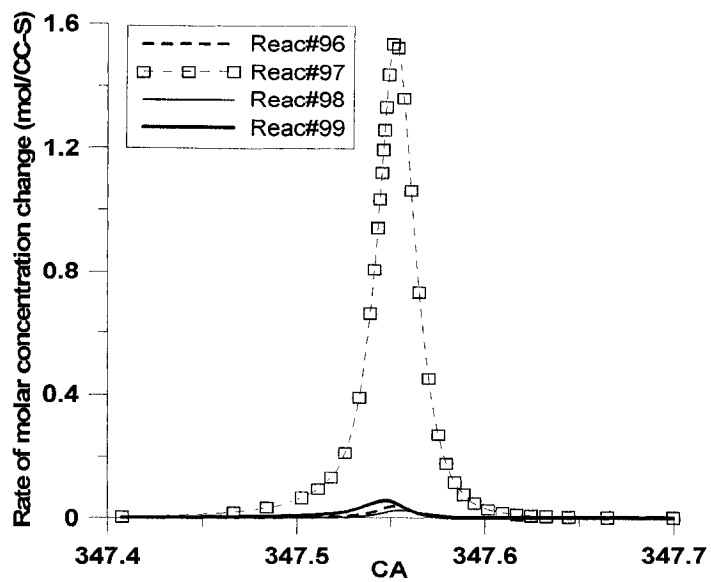


Figure 2-16 : Key reactions involving CO₂ radicals, CHM model

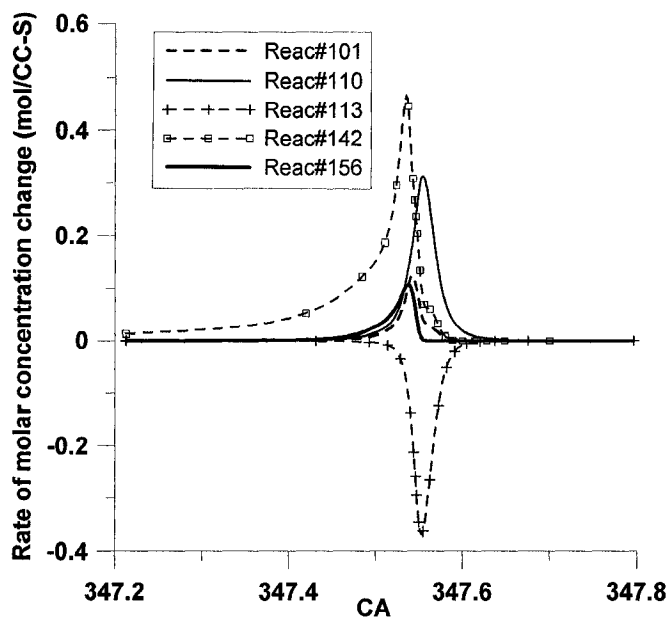


Figure 2-17 : Key reactions involving H₂O species, CHM model

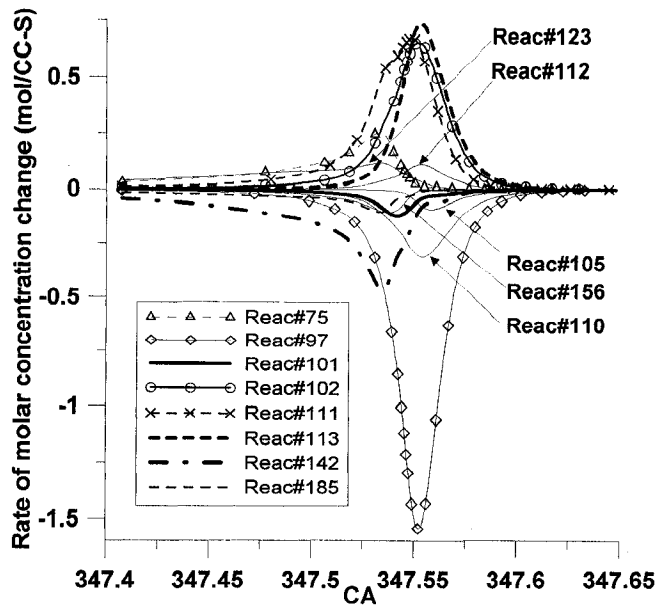


Figure 2-18 : Key reactions involving OH radicals, CHM model

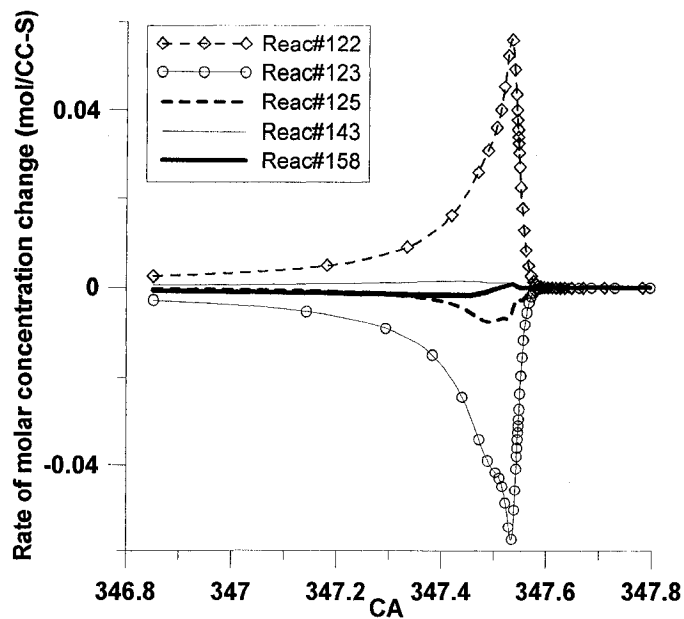


Figure 2-19 : Key reactions involving H₂O₂ radicals, CHM model

As reaction R123 is a key source of initial OH radicals for the main-stage reaction, the H₂O₂ radical is a key species contributing to the start of the 2nd stage ignition. Figure 2-19 shows that, just before the 2nd stage ignition, H₂O₂ is

produced mostly by reaction R122. After being formed by reactions R116 and R89, H₂O₂ radicals rapidly decompose by reaction R123 to produce OH radicals.



In general, it can be seen that H₂O and CO are the main components responsible for temperature rise during 1st stage combustion and the influential reactions include the reactions R5, R6, R18, R19. For the 2nd stage combustion, the main heat release is a result of H₂O and CO production which involves the reactions R97, R110 and R142.

2.5 Sensitivity Analysis of Influential Reactions

In addition to the auto-ignition process, finding the optimized reactions required a sensitivity analysis to be performed on the addressed influential reactions which, based on kinetic chain reactions of heptane-air mixtures, are the reactions **R5**, **R6**, **R18**, **R19**, **R27**, **R75**, **R97**, **R102**, **R110**, **R111**, **R122**, **R123**, **R125**, **R142**, **R143**, **R151**, **R185**, **R187** and **R192**. (Note that the underlined reactions are substantial to first stage combustion). A sensitivity analysis was measured via a relative difference between two calculated SOC (see Equation 2.32). One was calculated from original Arrhenius parameters while the other was obtained from the adjusted mechanism in which an Arrhenius parameter of each reaction was separately increased by a factor of two.

$$\text{Sensitivity}_i = \frac{\|SOC_{original} - SOC_{modified}\|}{SOC_{original}} \quad (2.32)$$

Figure 2-20 shows the sensitivity of SOC to the change in pre-exponential coefficient (A) of influential reactions. The figure suggests that the reactions R5, R6, R18, R19, R97, R102, R122, R123, R125, R142, R151 and R187 should be optimized. It is interesting to note that SOC is the most sensitive to H₂O production during cool flame. Doubling pre-exponential coefficients of three main

reactions for H₂O production (R5 R6 and R142) can change HCCI combustion from normal combustion to misfiring. The other important reaction to SOC is the main combustion triggering reaction, R123. Although the pre-exponential coefficients of the reactions R19 and R142 are also optimized, although sensitivity analysis shows relatively marginal effects as they are the most important reactions during 1st and 2nd stage combustion respectively. Therefore, the pre-exponential coefficients to optimize are of the reactions R5, R6, R18, R19, R29, R97, R102, R122, R123, R125, R142, R151 and R187.

The sensitivity of SOC to β in the influential reactions of the auto-ignition process is shown in Figure 2-21. The suggested optimization reactions are the reactions R6, R97 and R142. However, from observation, it was found that the reactions R290 and R272 are the 2nd and 3rd most sensitive reactions (not shown in the figure) to β and therefore should also be optimized.

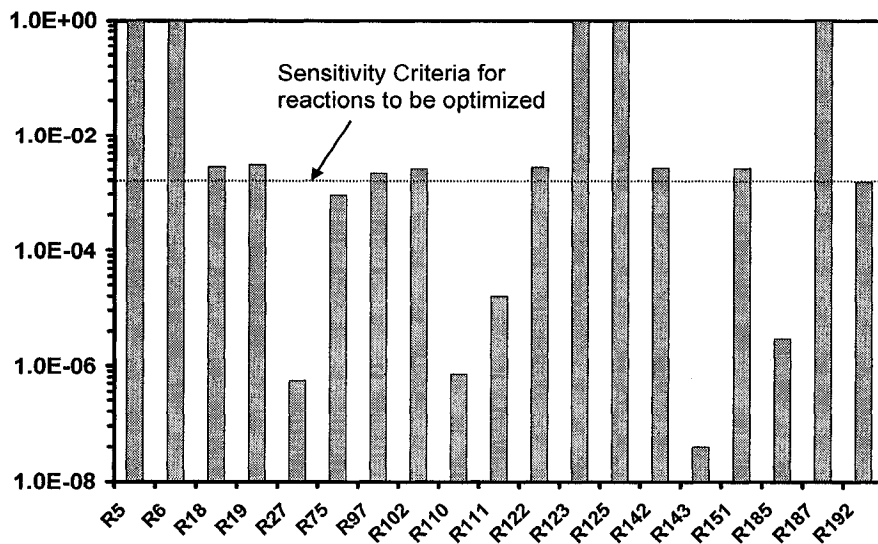


Figure 2-20 : Sensitivity analysis of pre-exponential coefficients of influential reactions

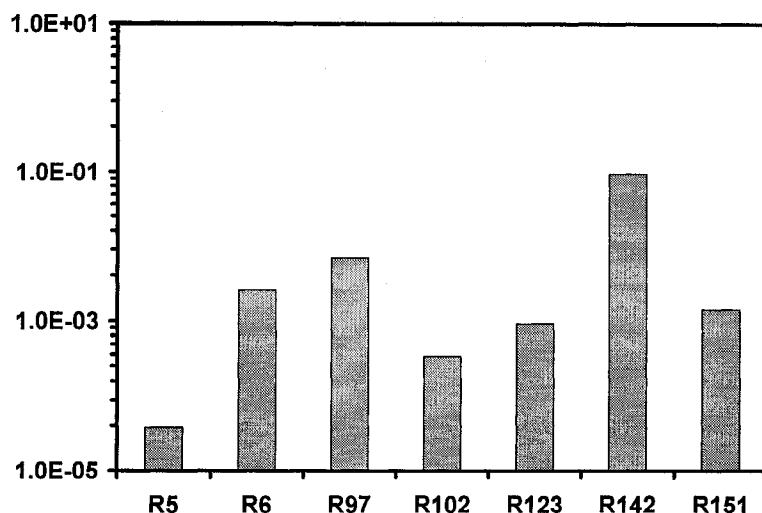


Figure 2-21 : Sensitivity analysis of temperature dependent parameters (β) of the selected influential reactions

2.6 Genetic Algorithm Optimization

In principle, several optimization techniques could be used to minimize the chemical kinetic simulation errors, (difference between simulation and experiment), by adjusting Arrhenius coefficients. Those include traditional gradient based methods using Hessian matrices [124], the objective function linearization technique [125], the solution mapping method [126], and stochastic methods such as Artificial Neural Network (ANN) [127] or Genetic Algorithm (GA) [107, 109, 128-130]. Practically, the complex structure of the problem and the limitations of computational time limit the suitability of gradient based methods and other non-stochastic methods experience several problems as reviewed by [109]. Among the stochastic methods, several studies have favored using GA [107, 109, 128-130] to optimize chemical kinetic mechanisms using either shock tube or HCCI engine data sets. The availability of a GA optimization toolbox in MATLAB [13] further favored use of GA since our chemical kinetic model is also MATLAB-based. (It is notable that some other MATLAB optimization toolbox, such as General Pattern Search, might be interesting for finding sets of optimum parameters. However, the other toolboxes considered do not appear to provide a computational or practical advantage for this problem as

the problem is highly nonlinear and the solution is ultimately extrapolated beyond the validation data sets. A GA optimization routine was developed and coupled with both single zone HCCI and zero-dimensional shock tube ignition models in order to optimize the heptane combustion mechanism.

2.5.1. Genetic Algorithm

Genetic Algorithm optimization is an evolutionary technique that allows researchers to tackle highly complex problems. The principle mimics evolutionary theory by producing generations of estimates in which the fittest individuals have a better chance to survive and pass their parameters, (genetics), to the next generation. The method starts with creating an initial population from possible values of parameters. For this case, reaction parameters were randomly assigned in the range +/-35% around the initial values. To create a new generation, three different methods are used: elitism, cross-over selection and mutation (see Figure 2-22). Elitism carries forward copies of best-fitness individuals into the new generation. Cross-over selection is the selective breeding approach which combines the attributes (genes) of two strong parents, (having less-than-elite fitness function values). Mutants are a random introduced population. When the modified parameters cause divergence, the program terminates that combination of parameters to prevent that set of genetics from propagating into the next generation. More detail on the working of genetic algorithm optimization can be found in [131].

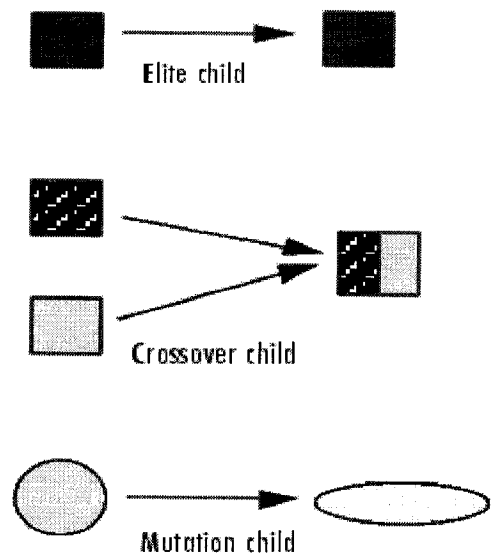


Figure 2-22 : Schematic diagram illustrating the three inherited children in Genetic Algorithm (from [131])

Population diversity and selective pressure are the key issues in forming a new generation from the three methods. An increase in a number of elite and cross-over selection children subdues population diversity but increases selective pressure, while more mutants enhance diversity but decrease selective pressure. The population number in each generation is another important parameter affecting the performance of GA. Greater population increases the chance of a more optimum solution but requires more computational efforts. For this study, preliminary trials showed that a population number of 15 for each generation was suitable. The cross over ratio (number of cross-over children / number of mutants) was set to 0.75 and the elite number was 2. At each generation, the selected parents were found from uniform selection, based on expectations and number of parents available.

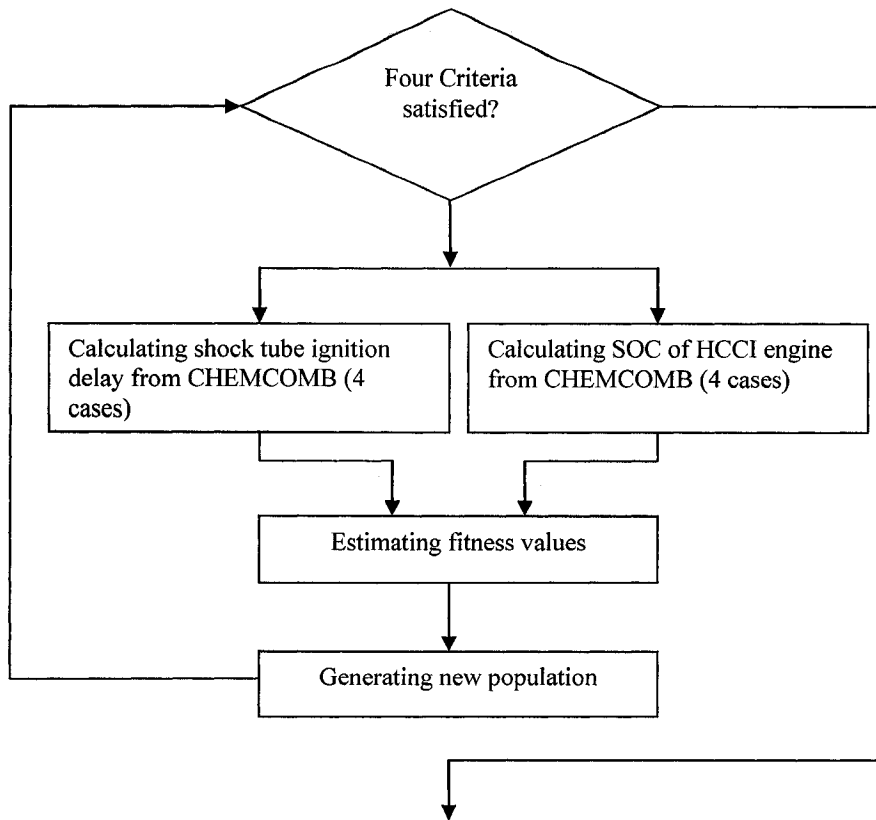


Figure 2-23 : Genetic Algorithm Flow Chart

The GA calculation ran until one of the following four criteria was exceeded:

- The number of generations exceeds 100.
- There is no improvement in the fitness function value for 50 consecutive generations.
- The computational time is longer than ~2 days.
- There is no improvement in the objective function for ~ 6 hours.

The integration of GA optimization to an auto-ignition single zone model (SZM) and shock tube model is shown in Figure 2-23. It is important to note that the performance of the GA might be further enhanced with proper parameters and selection strategy.

2.5.2. Objective Function and Optimization Results

The ultimate objective of this study is to find the set of chemical kinetic parameters that provides the most accurate simulation of the effects of H₂-CO reformer gas on heptane HCCI combustion. Ignition timing was selected as the key HCCI combustion characteristic to match since: 1) it is a single measurement achieved as a result of all the chemical reactions being considered, 2) it can be accurately measured both experimentally and in simulations, and 3) it can be calculated using a single zone model. The use of a SZM was indicated for GA optimization because the optimization process required more than a hundred runs to achieve the objective and this was not possible with currently available computer technology running a multi-zone model.

The optimization problem was a minimization of a negative inversion of relative errors from several cases (see Equation 2.33). The denominator includes 10⁻⁸ in order to prevent a “divided-by-zero” problem.

$$f = - \frac{1}{10^{-8} + \sum_{i=1}^{N_C} \left| \frac{SOC_i^{opt} - SOC_i^{tar}}{SOC_i^{target}} \right|} - \frac{1}{10^{-8} + \sum_{i=1}^{N_C} \left| \frac{FCT_i^{opt} - FCT_i^{tar}}{FCT_i^{tar}} \right|} - \frac{1}{10^{-8} + 0.1 \sum_{i=1}^{N_C} \left| \frac{ID_i^{opt} - ID_i^{tar}}{ID_i^{tar}} \right|} \quad (2.33)$$

N_C is the number of optimized cases used to optimize the mechanism, which was equal to 4 for the SZM and 6 for the shock tube model. The superscripts “opt” and “tar” indicate optimized and target values respectively. The initial conditions of six shock-tube cases are shown in Table 2-2. The conditions of those four different cases (with various RG fractions) for the SZM are summarized in Table 2-3. The port-fuel injection CFR engine (see Table 3-4 for the specification) was operating at 700 RPM at medium load conditions. After GA optimization using the GA-SZM coupled model, the optimized coefficients are shown in Table 2-4.

Table 2-2 : Shock tube ignition delay Initial conditions for GA optimization

Initial conditions (unit)		1	2	3
Pressure (bar)		13.5	13.5	13.5
Temperature (K)		1276	1026	909
Composition ratio	C ₇ H ₁₆	1	1	1
	O ₂	11	11	11
	N ₂	41.36	41.36	41.36
Initial conditions (unit)		4	5	6
Pressure (bar)		13.5	13.5	13.5
Temperature (K)		1187	998	772
Composition ratio	C ₇ H ₁₆	1	1	1
	O ₂	22	22	22
	N ₂	82.76	82.76	82.76

Table 2-3 : SZM Initial conditions for GA optimization

Fuel	Heptane					
Case	1	2	3	4	5	6
Equivalence ratio	0.46	0.47	0.46	0.46	0.46	0.46
Reformer Gas, % RG	0	4.9	10.3	15.4	25.1	30
Exhaust Recirc, % EGR	39.8	41.4	40.6	41.7	40.6	42
T Intake Manifold (K)	383	383	383	383	383	383
P intake manifold (bar)	0.153	0.153	0.153	0.153	0.153	0.153
P exhaust manifold (bar)	0.144	0.144	0.144	0.144	0.144	0.144

Table 2-4: Modified coefficients for a heptane mechanism based on Chalmer mechanism

Reaction	Original		Modified	
	A	B	A	B
5	8.6000E+09	1.100000	9.4375E+09	1.100000
6	4.8000E+09	1.300000	5.5350E+09	-0.028035
18	2.9650E+13	0.000000	3.7063E+13	0.000000
19	1.0000E+16	0.000000	7.8994E+15	0.000000
29	2.5000E+13	0.000000	2.6250E+13	0.000000
97	3.5100E+07	1.300000	2.0045E+07	1.365000
122	2.0000E+12	0.000000	1.3000E+12	0.000000
123	7.6000E+13	-0.370000	9.6255E+13	-0.370000
125	1.0000E+13	0.000000	1.6100E+13	0.000000
142	2.4300E+10	1.180000	2.0070E+10	0.490670
187	6.0200E+13	0.000000	3.5945E+13	0.000000
272	1.9300E+05	2.680000	1.9300E+05	3.618000

Although the optimized parameter set has been found through optimization against a limited number of experimental data points, the fact that these parameters can capture combustion behaviours of heptane-RG mixtures outside the referencing points, (as seen below and in Chapters 3 and 4), verifies the performance of the optimized mechanism for simulating heptane HCCI combustion without arbitrarily case-by-case adjustment of mechanism parameters.

2.5.3. Performance of Optimized Mechanism

The novelty and capability of original CHM and its well-defined structure must be emphasized, because it leads to generally accurate prediction of heptane/air auto-ignition for mixtures with no fuel reforming. Therefore, this section only verifies the capability of the modified (optimized) mechanism on predicting shock-tube ignition delay of pure heptane-air mixtures over a range of conditions. Although the modified mechanism was intended to capture in-situ behavior of HCCI combustion of heptane mixtures when blended with different RG fractions, it was mandatory to confirm that it could still predict auto ignition of pure heptane/air mixtures. The performance of the optimized mechanism was validated against the same shock-tube data as used to verify the original CHM mechanism [106]. This experimental set was originally from the work of Ciezki and Adomeit [132] with initial conditions ranging from initial pressure from 6 bar to 42 bar and ϕ from 0.5 to 2.

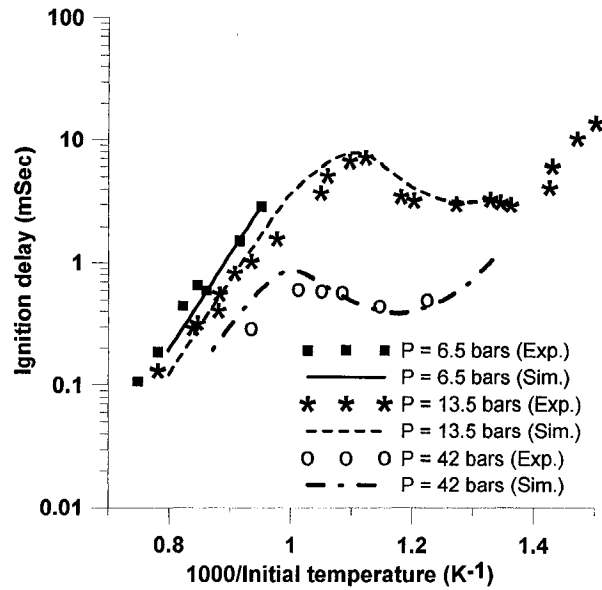


Figure 2-24 : Performance of a modified Chalmer mechanism on shock-tube ignition delay prediction at different initial pressures

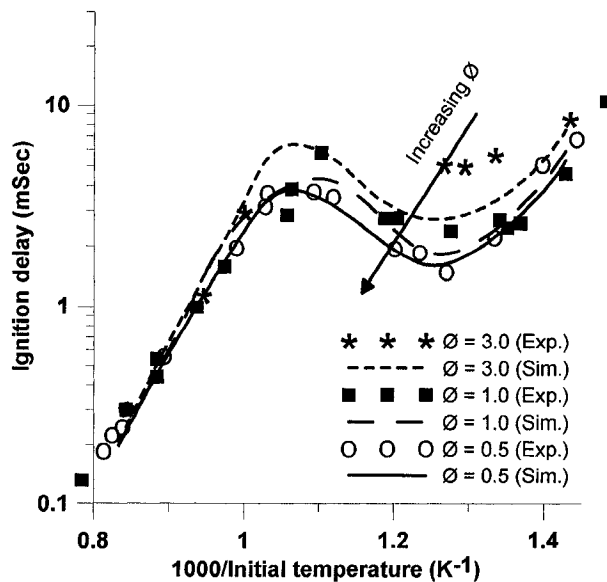


Figure 2-25 : Performance of a modified Chalmer mechanism on shock-tube ignition delay prediction at different mixture compositions

Figure 2-24 shows a fair agreement between simulation and experiments in a shock tube with various initial pressures. The trend of having shorter ignition delay for richer mixtures is captured by the model as shown in Figure 2-25. The

model predicted a slightly shorter ignition delay with 0.5 equivalence ratio but was still within the experimental variation of the shock tube values. It is notable that the dip in ignition delay due to the competition for H atoms between the chain branching- and the chain terminating- reactions occurring at certain temperatures can fairly well captured by the modified mechanism.

While matching shock tube ignition delay is a good test for mixture auto ignition, the real objective is to get a mechanism that can explain HCCI combustion of heptane-RG blends. Therefore, the validation of the mechanism on a practical HCCI engine when changing RG fractions is vital. This section validates the modified mechanism on an experimental HCCI engine with varied RG blend fraction at three different operating conditions (Figure 2-26 to Figure 2-28). The results obtained from the original mechanism were plotted to measure the improvement provided by the modified mechanism.

The modified mechanism generally performs well at predicting start of main combustion of different RG-heptane blends over a wide range of different operating conditions. Additionally, the mechanism gives a good estimation on the first stage combustion pressure rise as seen from the compression pressure match-up after the cool flame reactions. Considering any particular case, both original and modified mechanisms provide a good compression pressure prediction. However, the original mechanism suppressed the quantitative effects of additional RG additives, (i.e., retardation), predicting an early ignition especially when the mixtures are blended with more reformer gas. (Prediction excessively fast combustion after ignition is a well-known limitation of single zone models and is seen in every case. The SZM assumes lumped properties so all mixtures are burned in one time-step once the mixture ignites). Finally, it is notable that the modified mechanism slightly over-estimates the start of main combustion timing with 25%RG blending in the mixtures (see Figure 2-28).

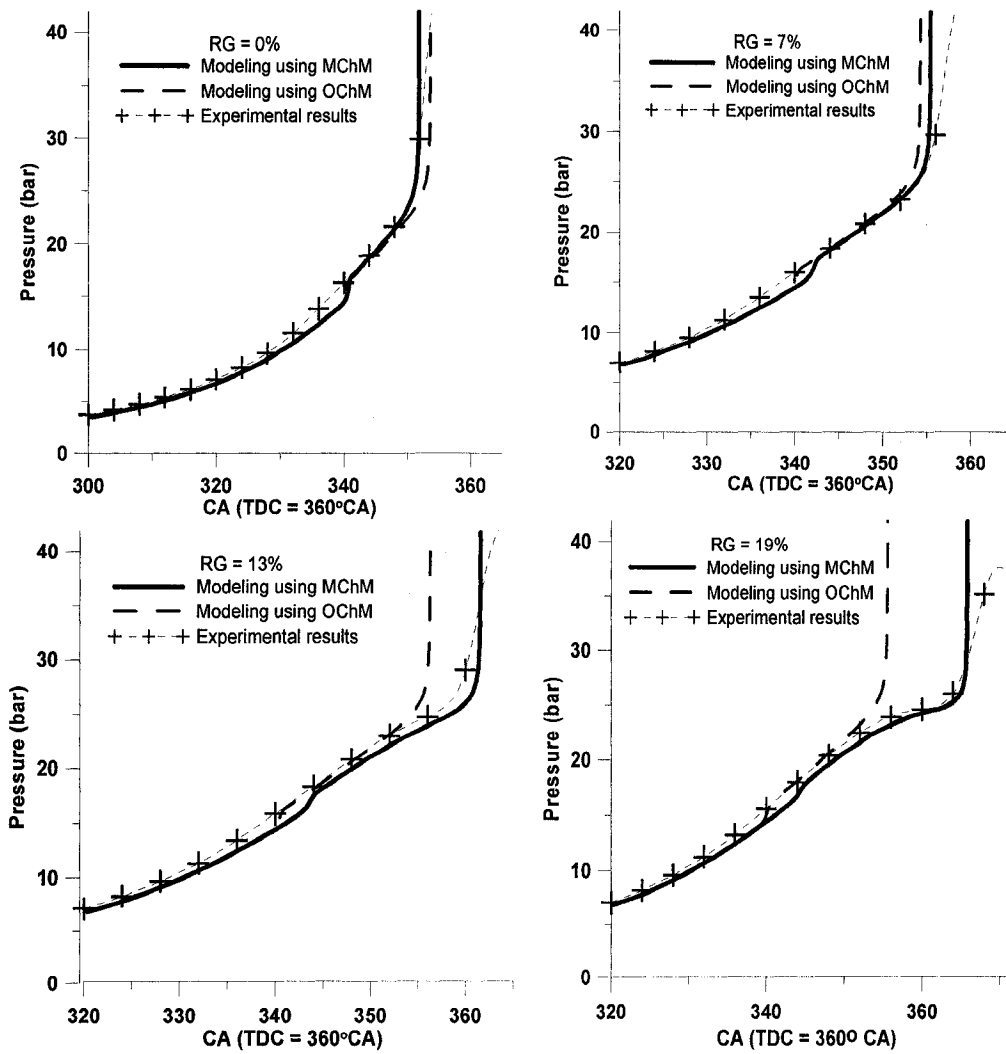


Figure 2-26 : Comparison of compression pressure traces of a 700 rpm HCCI engine operating with 0.8 equivalence ratio heptane/air mixtures, 40% EGR, 1 bar intake pressure and 100°C intake temperature

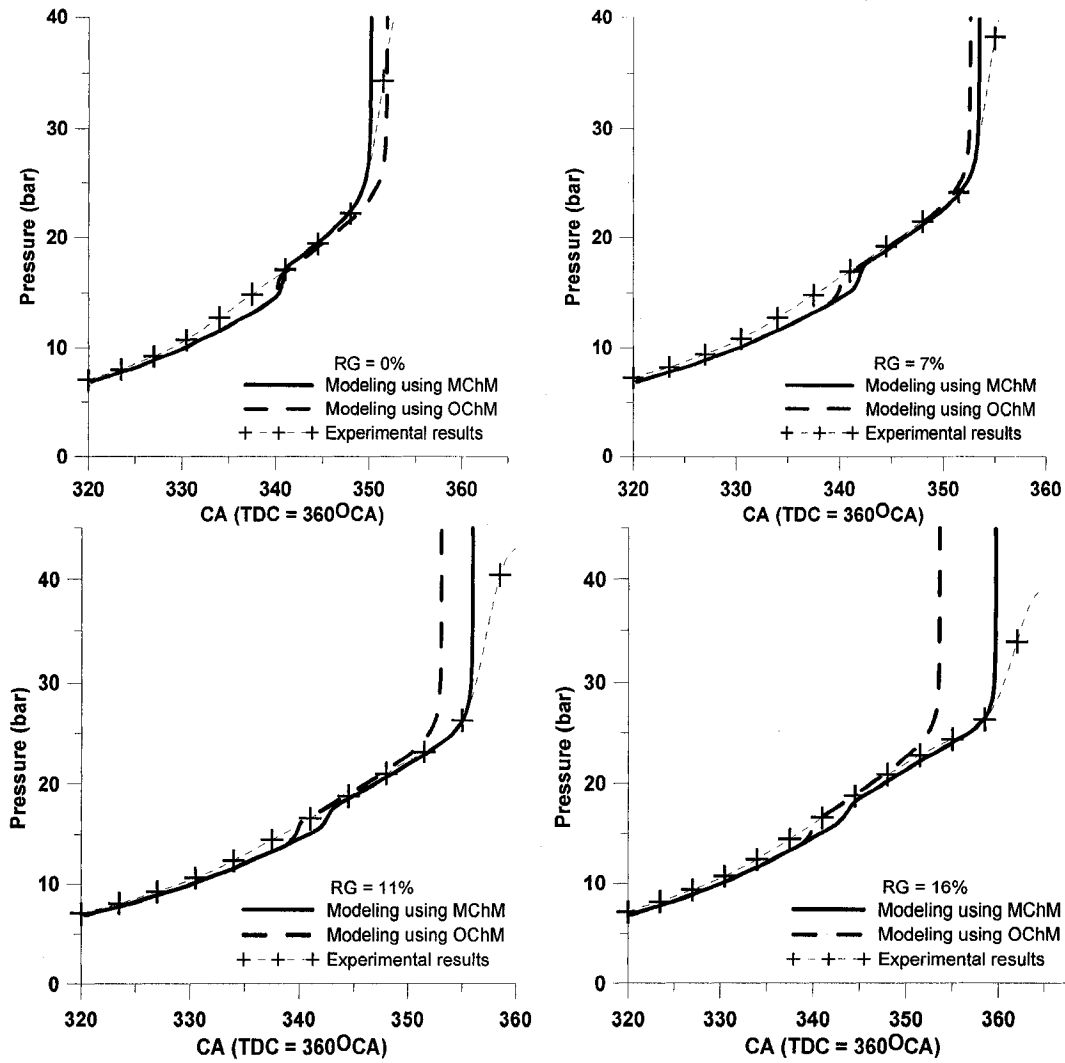


Figure 2-27 : Comparison of compression pressure traces of a 700 rpm HCCI engine operating with 0.65 equivalence ratio heptane/air mixtures, 30% EGR, 1bar intake pressure and 100°C intake temperature

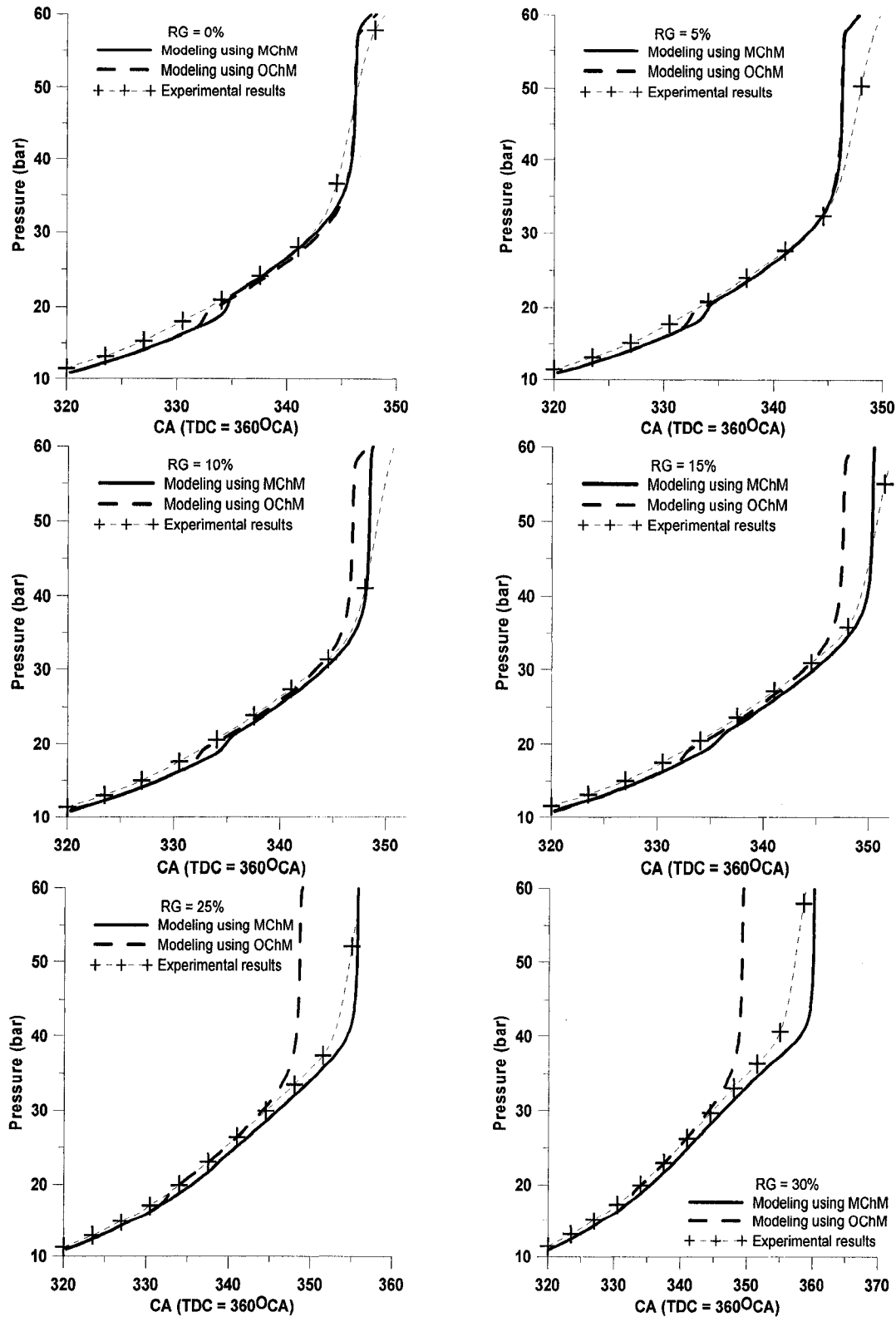


Figure 2-28 : Comparison of compression pressure traces of a 800 rpm HCCI engine operating with 0.47 equivalence ratio heptane/air mixtures, 40% EGR, 1.5 bar intake pressure and 115°C intake temperature

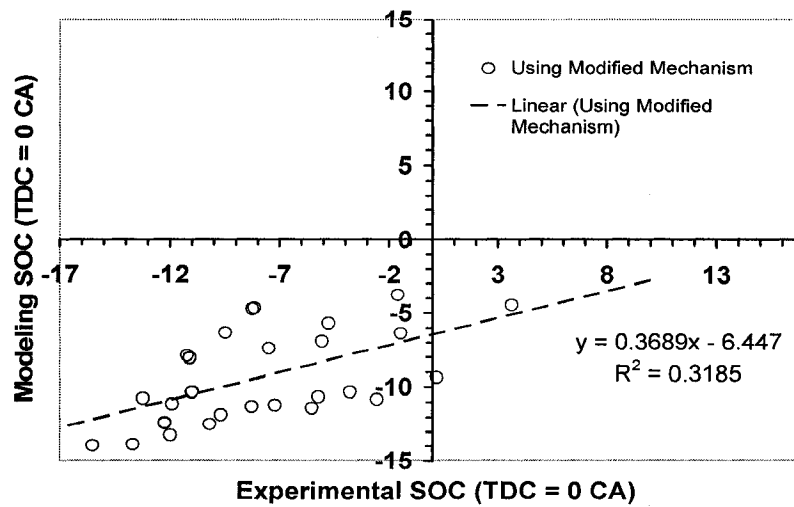


Figure 2-29 : Overall performance of original CHM in predicting SOC of n-heptane HCCI engine with RG blend amount varying from 0% to 25% of fuel

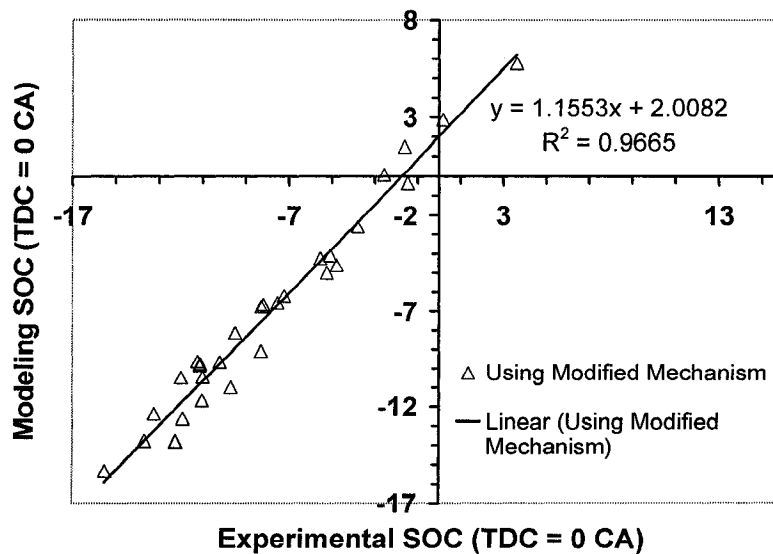


Figure 2-30 : Overall performance of a GA-optimized Chalmer mechanism in predicting SOC of n-heptane HCCI engine with RG blend amount varying from 0% to 25%

The overall performance of the mechanisms (both original and modified) on predicting SOC of a heptane fuelled HCCI engine was measured using regression analysis. For perfect performance, the slope of the best-fit linear regression relating those two variables would equal one and the y-intercept would be at the origin. The best-fit linear regressions for modified and original mechanisms have

been plotted in Figure 2-29 and Figure 2-30 respectively. The performance of the optimized mechanism is superior to that of the original mechanism in predicting SOC of a heptane engine operating with various RG fractions. (It must be emphasized again that the original CHM can accurately explain auto-ignition of heptane mixtures with no RG blending).

The capability of the GA-optimized mechanism to accurately simulate HCCI combustion timing for RG blend fractions up to 25% provides confidence for using the modified mechanism to explain chemical effects of RG on heptane HCCI combustion.

2.7 Summary

This chapter has reviewed basic thermodynamic property and chemical kinetic calculations as applied to a compression ignition model. The model developed was applied to simulate ignition delay in a shock tube in order to validate the selected mechanisms: GRI mech 3.0 [105] for methane/air combustion and Chalmers University mechanism [116] for heptane/air combustion. These two well-known mechanisms show very good performance in matching the ignition delay time in a pressure driven shock tube. Preliminary analysis showed problems when the Chalmers mechanism was applied to HCCI engines fueled with heptane/RG blends so a process was developed to systematically improve the mechanism. This involved studying auto-ignition to determine the most influential reactions and performing a sensitivity analysis to determine the most influential Arrhenius parameters. Without changing the basic reaction mechanism, a genetic algorithm optimization technique was combined with the chemical kinetics model to produce a better-optimized set of Arrhenius coefficients. The improved model has been validated with both shock tube and HCCI experimental data.

3 Single Zone HCCI Model

Inside a practical combustion engine, several phenomena are inter-related and need to be considered. Those phenomena include piston movement, heat dissipation to the cylinder wall, cylinder wall temperature, gas exchange processes and chemical reactions. To model a chemical based HCCI engine, the thermodynamic/chemical kinetic calculations (described in Chapter 2) must be integrated into an engine simulation. The engine simulation is commonly divided into two parts: the closed system part covers the compression, combustion and expansion, (with valves closed), and the open system part covers the intake and exhaust (with valves open).

This chapter first describes the main governing equations to calculate changes in variables during the closed system period based on volume changes due to the mechanical movement of a piston, the ideal gas relation and chemical kinetic calculations. The closed system interval from intake valve closed (IVC) to exhaust valve opened (EVO) includes the compression, combustion and expansion process. To start this calculation, the IVC conditions must be specified, including average in-cylinder pressure, volume of a combustion chamber, concentrations of each species, average temperature of the mixtures and the total mixture mass in the cylinder. Average properties at IVC (initial conditions of a combustion model) were found using two options: 1) manually specified or 2) a quasi 1D isentropic flow to calculate flow during intake. The last topics discussed are a brief code description, required inputs and the model performance.

3.1. Main Assumptions of the Model

The schematic of the single zone model is shown in Figure 3-1. The combustion chamber is a closed system and no blow-by has been considered. Changes in mixture properties and chemistry are assumed to be uniform throughout the combustion chamber, meaning that the cylinder charge has one bulk temperature, uniform thermodynamic properties and uniform concentration for each species. Temperature, pressure and mixture composition are related by the ideal gas law. Imperfectly stirred effects are considered by virtual enthalpy exchange between cooler intake gases and hotter, assumed-uniform residual mixtures (see Section 3.2.6). The un-burnt mixture is considered frozen below 500K for both engines. The heat transfer model includes simple convection and radiation, which will be discussed in Section 3.3. The composition of residual as well as external exhaust gas recirculation is assumed to be the complete combustion products, i.e., neglecting any dissociation and possible active radicals. This assumption is valid when the engine is operating with low engine speed and for conditions in which end-gas temperature is low, as was the case in this study.

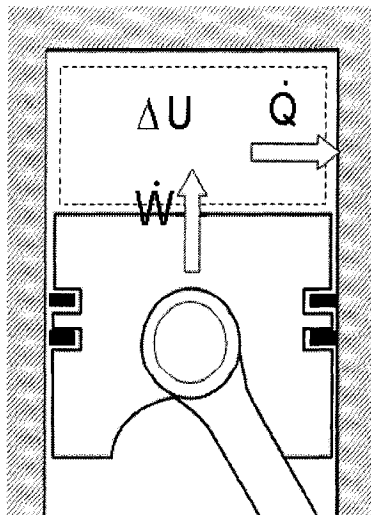


Figure 3-1: Schematic of a Single Zone model

3.2. Governing Equations for the Closed System (Period from IVC to EVO)

Three main parameters are needed to define the thermodynamic state of gases: pressure, temperature and gas composition. In this study, gas composition was described by mass fraction. These three descriptive parameters must be governed by either conservative- or constituent- equations. In addition, as the system inside a combustion chamber is constrained by piston movement, the governing equation of piston motion is required to describe volume change of a system. These four equations should ideally (without numerical errors) be sufficient to describe phenomena inside a combustion chamber, i.e., the amount of mass should automatically be conserved. Practically, numerical errors from machine precision can change the amount of mass which has been accumulated from one step to another. This requires an inclusion of mass conservation as the fifth governing equation.

This section describes the five equations that govern pressure, in-cylinder volume, mass fraction, temperature and total mass.

3.2.1. Equation for In-Cylinder Pressure

In-cylinder pressure is derived from an ideal gas equation (Equation 3.1) - a state equation that relates pressure, temperature and gas compositions. Its derivative (see Equation 3.2) was used to trace the in-cylinder pressure.

$$PV_{cyl} = nR_U T \quad (3.1)$$

$$\frac{dP}{dt} = \frac{1}{R_U} \frac{dR_U}{dt} - \frac{1}{V} \frac{dV_{cyl}}{dt} + \frac{1}{T} \frac{dT}{dt} \quad (3.2)$$

Note that the two derivatives (the rate of in-cylinder volume change and the rate of in-cylinder temperature change) are described in sub-Sections 3.2.2 and 3.2.3 respectively.

3.2.2. Equation for In-Cylinder Volume

Changing in-cylinder volume is governed by the mechanical movement of the piston which is calculated from the piston-crank geometry using the formula from Heywood [72] (see Equation 3.3). The rate of in-cylinder volume change is shown as a differential equation in Equation 3.4.

$$V_{cyl} = V_c \left[1 + \frac{1}{2}(r_c - 1) \left[R + 1 - \cos \theta - (R^2 - \sin^2 \theta)^{\frac{1}{2}} \right] \right] \quad (3.3)$$

$$\frac{dV_{cyl}}{dt} = V_c \left[\frac{1}{2}(r_c - 1) \left(\sin \theta \frac{d\theta}{dt} - \frac{1}{2}(R^2 - \sin^2 \theta)^{-\frac{1}{2}} (-\sin 2\theta) \frac{d\theta}{dt} \right) \right] \quad (3.4)$$

3.2.3. Equation for Species Concentrations

The chemical kinetic calculation as described in Chapter 2 is used to model the rate of change in mass fraction of each species and can be written as [83],

$$\frac{dY_k}{dt} = \frac{\dot{\omega}_k \times W_k}{\rho} + \sum_{j=1}^{N_E} \frac{\dot{m}_j}{m_{cyl}} (Y_{k,j} - Y_{k,cyl}) \quad (3.5)$$

Considering the interval between intake valve closure and the exhaust valve opening, the blow-by is neglected so the second term on the right hand side of Equation 3.5 is zero. The calculation of the chemical production rate for each species k can be found in Chapter 2 (Equation 2.17).

3.2.4. Equation for Mixture Temperature

The first law of thermodynamics, which balances internal energy changes with heat transfer to the wall and work done by the system, is used to model the rate of mixture temperature change (see Equation 3.6). Despite using the same principle (1st law of thermodynamics) as others [83, 133], the governing equation can appear in different forms for HCCI depending on the derivations and assumptions. The equation used is a dimensionless version of the energy conservation equations used in fluid mechanics models (neglecting energy transfers via convection and diffusion). Considering the classical first law equation,

$$\frac{dU}{dt} = \frac{dQ}{dt} - P \frac{dV_{cyl}}{dt} \quad (3.6)$$

The internal energy (the first term in Equation 3.6) is calculated as the sum of the internal energy of all species (Equation 3.7) with the derivative as shown in Equation 3.8.

$$U = \sum_{i=1}^{N_s} m_i u_i \quad (3.7)$$

$$\frac{dU}{dt} = \sum_{i=1}^{N_s} \left(m_i \frac{du_i}{dt} + u_i \frac{dm_i}{dt} \right) \quad (3.8)$$

The change in specific internal energy is calculated from Equation 3.9 while the change in mass of each species is derived from the chemical kinetic calculation (see Equation 3.10).

$$\frac{du_i}{dt} = c_{v,i} \frac{dT}{dt} \quad (3.9)$$

$$\frac{dm_i}{dt} = V_{cyl} \dot{\omega}_i W_i \quad (3.10)$$

Finally, substituting Equations 3.8, 3.9 and 3.10 back into Equation 3.6 yields,

$$\sum_{i=1}^{N_s} \left(m_i c_{v,i} \frac{dT}{dt} + u_i V_{cyl} \dot{\omega}_i W_i \right) = \frac{dQ}{dt} - P \frac{dV_{cyl}}{dt} \quad (3.11)$$

Rearranging Equation 3.11, the rate of temperature change is,

$$\frac{dT}{dt} = -\frac{1}{\rho c_v} \sum_{i=1}^{N_s} (u_i \dot{\omega}_i W_i) - \frac{R_U T \times \sum_{i=1}^{N_s} [x_i]}{m_{cyl} C_v} \frac{dV_{cyl}}{dt} + \frac{1}{m_{cyl} c_v} \frac{dQ}{dt} \quad (3.12)$$

3.2.5. Equation for Mass Conservation

Neglecting cylinder leakage and any blow-by, the model considered that the quantity of mass in the chamber remained constant over the period between IVC and EVO (Equation 3.13).

$$\frac{dm_{cyl}}{dt} = 0 \quad (3.13)$$

3.2.6. Initial condition Setup – Mixing Phenomena Modeling

With the five governing equations defined, the progress of compression, combustion and expansion can be calculated, provided that the initial conditions are known. Defining these initial conditions at the point of intake valve closure is one of the weak points of HCCI engine modeling. It is common to specify best-estimate initial conditions and then to arbitrarily adjust one parameter, (such as mixture temperature), until the simulation matches experimental values. As a means of improving single zone model performance, it was postulated that imperfectly stirred mixtures at the time of IVC could be affecting the compression process and the model should be adjusted to account for this.

Non-perfectly stirred mixtures (see Figure 3-2) have significant effects on HCCI combustion and could be a reason for some adjustments that have been made at IVC in existing models. To demonstrate this effect, the original single zone combustion model was used. If non-uniform mixtures do not have an impact on a

HCCI engine, changing the model starting points should result in the same pressure trace. (Note that chemical reactivity is assumed to be frozen in the early compression period when temperature is less than 500K). Figure 3-3 shows that varying the model starting points significantly affects modeled pressure traces. Starting a model at IVC (214°CA) gives the most difference in ignition timing and compression pressure. This disagreement seems to disappear as the model starting point moves toward the end of compression where the hotter residual and intake charge would be well blended. This result indicates that non-perfectly stirred mixture effects are not negligible.

In the model developed for this study, a method was created to consider the effects of non-perfectly stirred mixtures without an arbitrary adjustment by including an apparent enthalpy exchange from the ideally uniform residual mixtures (hotter) to the intake mixtures (colder). The rate of enthalpy transfer was estimated based on the enthalpy difference between ideally uniform residual and intake gas mixtures, in a straightforward heat transfer analogy (Equation 3.14-3.15).

$$\Delta h = h_{uni} - h_{int} \quad (3.14)$$

$$\Delta \dot{h} = \dot{h}_{uni} - \dot{h}_{int} = mc_p \frac{dT}{dt} - m_{int} c_{p,int} \frac{dT_{int}}{dt} \quad (3.15)$$

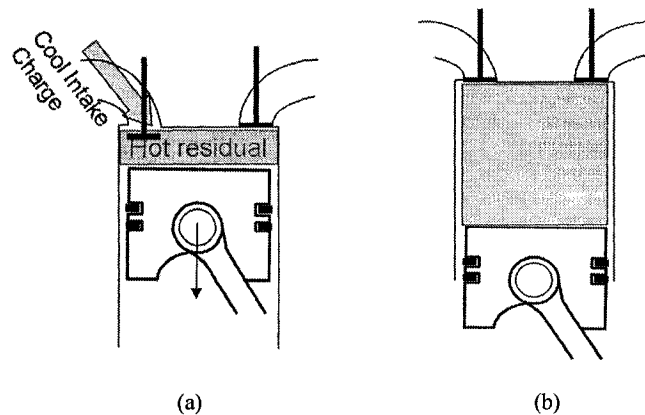


Figure 3-2: The schematic of mixtures at intake valve opened (a) and intake valve closed (b)

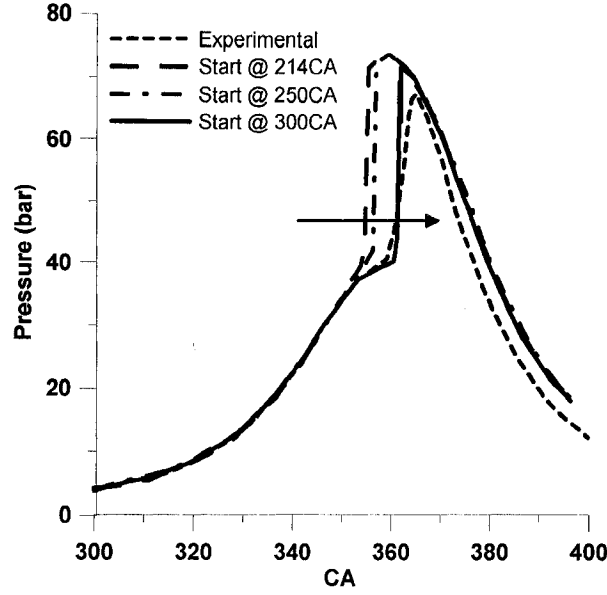


Figure 3-3 : Simulation results of a CNG-HCCI engine, using the original single zone model with different starting points

Note that the subscript “int” means “of intake mixtures”. Generally, the temperature calculated from the ideally uniform system, the so-called apparent temperature, is initially higher than the intake temperature. Therefore, the intake temperature increases relatively faster than the apparent temperature. The difference between these two rates of temperature rise can be modeled based on the difference between the apparent and intake temperatures. The temperature change rate of the intake mixture is calculated from,

$$\frac{dT_{int}}{dt} = \frac{m_{cyl} \bar{c}_p}{m_{int} \bar{c}_{p,int}} \times \frac{dT}{dt} + \tau(T - T_{int}) - \Gamma \left(\frac{m_{cyl} \bar{c}_p - m_{int} \bar{c}_{p,int}}{m_{int} \bar{c}_{p,int}} \right) \times \frac{dT}{dt} \quad (3.16)$$

where τ is the inverse of a characteristic time scale of relative temperature rise. This parameter indicates how fast the intake temperature changes relative to the apparent temperature change. Note that the last term is only needed to make the rate of intake temperature rise equal to the rate of apparent temperature rise when these two temperatures are equal, ($\Gamma = 0$ when $T_{uni} \neq T_{int}$, and $\Gamma = 1$ when $T_{uni} = T_{int}$). Therefore, this term will not be included in the new temperature governing equation (see Equation 3.17).

Finally, the rate of enthalpy transfer is treated as one of the heat transfers (dQ/dt) in the energy-balance governing equation. Therefore, Equation 3.12 which originally governs the energy balance for a SZM is replaced by Equation 3.17. The final governing equations for the modified SZM are therefore Equation 3.2, 3.4, 3.5, 3.11 and 3.17.

$$\frac{dT}{dt} = -\frac{1}{\rho c_v} \left(\sum u_i \dot{\omega}_i MW_i \right) - T \times \frac{\sum x_i R_i}{mc_v} \times \frac{dV}{dt} + \frac{1}{mc_v} \times \left(\frac{dQ}{dt} - \tau \times m_{\text{int}} \bar{c}_{p,\text{int}} (T - T_{\text{int}}) \right) \quad (3.17)$$

3.3. Heat Transfer Calculation

This section describes the model used to calculate the term dQ/dt in Equation 3.17. Most current engine models use the (modified) Woschni correlation with an assumed constant wall temperature, probably because of its simplicity. However, HCCI combustion is initiated by auto-ignition which is exponentially dependent on in-cylinder thermal conditions, so a more detailed calculation of heat transfer could potentially enhance the overall performance of any HCCI engine model. The additional details considered in the model developed for study are wall temperature which varies with operating conditions and radiation heat transfer. The heat transfer sub-modeling thus considers two main heat dissipations from the mixture to engine boundaries: heat convection and radiation.

3.3.1. Convection Heat Transfer

Given the assumption of having uniform properties across the combustion chamber, (i.e., a lumped zone with uniform bulk temperature, pressure and gas composition), no heat conduction is considered within the gaseous zone. In addition, convection due to fluid motion along the solid surface inside a combustion chamber (cylinder head, valves, cylinder walls and piston head) can be approximated using Equation 3.18 with a bulk temperature, which combines thermal conduction and convection using a single temperature difference.

$$\dot{q} = h_c A_{total} (T - T_w) \quad (3.18)$$

The parameter h_c is the heat-transfer coefficient which can be evaluated based on flow characteristics described by the dimensionless Nusselt (Nu), Reynolds (Re) and Prandtl (Pr) numbers. In general, the relation between these three dimensionless numbers is in the form of,

$$Nu = a \times Re^m \times Pr^n \quad (3.19)$$

The definitions of Nu, Re and Pr can be found in Equations 3.20 to 3.22.

$$Nu = \frac{h_c L}{k_f} \quad (3.20); \quad Re = \frac{\rho v L}{\mu} \quad (3.21); \quad Pr = \frac{c_p \mu}{k_f} \quad (3.22)$$

The values used for parameters a , m and n depends on the model selected. In this study, the Woschni correlation was adopted as in many other works. The Woschni correlation is widely used for engine research calculations (including HCCI) because it is based on key engine parameters affecting heat transfer including speed, cylinder dimensions and gas properties. As described in [134], the heat transfer coefficient can be calculated from Equation 3.23 with parameter values as shown in Table 3.1.

$$h = 0.00326 \times P^{0.8} \times \frac{(v_{mot} + v_{comb})^{0.8}}{B^{0.2} T^{0.53}} \quad (3.23)$$

Because the Woschni correlation was developed based on a diesel engine which has some different in-cylinder characteristics from our HCCI engine, (such as engine speed, diffusive flame growth, locally rich region and unburned gas composition), some modification is required to apply this correlation to HCCI engine modeling [17]. Although some researchers have reported that the Woschni correlation over-predicts heat transfer in a lean burn engine, our preliminary study has shown that the Woschni correlation actually under-predicted heat transfer in our engine: ($h_{actual}/h_{Woschni} = 2.26$). The ratio of actual-to-Woschni heat transfer coefficient was arrived at based on analysis of experimental

compression pressure traces. Note that the lower prediction in heat transfer from the Woschni correlation is due to the difference in our engine characteristics as mentioned earlier.

3.3.2. Radiation Heat Transfer

Although radiation from gases is negligible in many cases, having more EGR can significantly increase the emissivity inside a combustion chamber, especially during compression. In order to calculate the emissivity of gaseous mixtures, the effects of gas composition (especially “gray” gases such as CO₂, H₂O and CH₄), temperature and pressure on the emissivity were taken into account. As one simplification, CH₄ composition is treated as CO₂ when calculating emissivity since emissivity of CO₂ and CH₄ are of similar magnitude for most conditions (eg. T = 900 K to 5000 K and PL = 0.3 to 60.0 cm.atm per [135]). The CO₂ and H₂O emissivities [136] were calculated from,

$$\varepsilon_p = \frac{\varepsilon_p}{\varepsilon_0} \times \varepsilon_0 \quad (3.24)$$

Table 3-1: Correlations and constants for Woschni Heat transfer calculation

Parameters	v_{pis}	v_{mot}	v_{comb}
Correlations	$v_{pis} = \frac{2S \cdot rpm}{60}$	$v_{mot} = c_1'' v_{pis}$	$v_{comb} = c_2'' \frac{V_d T_{ig}}{P_{ig} V_{ig}} (P - P_{mot})$
Constant	compression	combustion/expansion	gas exchange process
c_1''	2.28	2.28	6.18
c_2''	0	0.00324	0

The $\varepsilon_p/\varepsilon_0$ ratio is the relative emissivity which depends on temperature, equivalent pressure (P_E), and a multiplication of partial pressure of gray gas to a path-length (L):

$$\frac{[(\varepsilon_p/\varepsilon_0) - 1]}{[(\varepsilon_p/\varepsilon_0) - 1]_{\max}} = f(pL) \quad (3.25)$$

Equation 3.26 is used to calculate $(\varepsilon_p/\varepsilon_0)_{\max}$ which appears in the denominator on the left hand side of Equation 3.25

$$\left(\frac{\varepsilon_p}{\varepsilon_0}\right)_{\max} = \frac{A \times P_E + B}{P_E + A + B - 1} \quad (3.26)$$

Parameters A , B and P_E are found from the following equations, depending on types of gas (as shown in Table 3-2).

The term $f(pL)$ appearing in Equation 3.25 is calculated from,

$$f(pL) = \exp\{-\xi(\lambda_{\max} - \lambda)^2\} \quad (3.27)$$

where ξ is a correcting factor, (equal to 0.5 for H₂O and 1.47 for CO₂) [136]. The position of the maxima (λ_{\max}) is assumed to depend on temperature only (Equation 3.28).

$$\lambda_{\max} = \log(13.2\tau^2) \quad (3.28)$$

Finally, the parameters λ and τ can be calculated from Equations 3.29 and 3.30. Note that p is a gray-gas partial pressure (bar) and L is a path-length (cm) and is calculated from $3.6V_{cyl}/A_{total}$.

Table 3-2 : Parameters for Calculating Emissivities of H₂O and CO₂**(Note that $\tau = 0.75$ when temperature is less than 750 K)**

	H ₂ O	CO ₂
<i>A</i>	$A = 1.888 - 2.053 \log \tau$	$A = 0.10\tau^{-1.45} + 1.0$
<i>B</i>	$B = 1.10\tau^{-1.4}$	$B = 0.23$
P_E	$P_E = P_T \left(1 + 4.9 \frac{P}{P_T} \sqrt{\frac{273}{T}} \right)$	$P_E = P_T \left(1 + 0.28 \frac{P}{P_T} \right)$

$$\lambda = \log pL \quad (3.29)$$

$$\tau = T/1000 \quad (3.30)$$

3.3.3. Effective Wall Temperature Correlation

Most numerical studies are currently based on the assumption of having the same wall temperature for all simulation cases. This is true only when the engine is operating at similar conditions, i.e., engine speed, engine load and engine knock. In contrast, operating an engine under various power levels and engine knock leads to different wall temperatures even when the coolant temperature is constant, (i.e., excessive heat remains in the system and heats up the cylinder wall). (Note that the current model overcomes this problem by arbitrarily adjusting some of the heat transfer model constants as shown in [17]).

Different wall temperatures can significantly affect combustion behaviors, especially in an HCCI engine in which combustion greatly relies on the auto-ignitibility of the mixtures in the active environment, i.e., thermal conditions inside a combustion chamber. The importance of wall temperature to an internal combustion engine was discussed in detail in [137].

To develop an HCCI engine model that can predict combustion behavior over a wide range of conditions, an accurate wall temperature model is vital. Several models have been proposed by other studies [138-140] to predict wall temperature. Most of these models are based on Finite Element Analysis (FEA) of the heat transfer between the material of an engine body and water jackets. Those calculations are, however, computationally expensive and require enormous data inputs (such as the engine body and water jacket dimensions) as well as assumptions. Combining FEA and chemical-based combustion models is very challenging since each of these modeling techniques requires significant computational resources.

A simpler but more productive way to model wall temperature of chemical-based engine modeling at various conditions is to use a well-defined correlation. Fischer [141] (in [142]) has proposed a correlation (see Equation 3.31) to estimate wall temperature based on coolant temperature, engine load and engine speed. Fischer's correlation was developed using a light-load diesel engine operating at normal conditions (no engine knock) which is somewhat comparable to the lean mixture compositions used in the HCCI engine. However, since an in-situ HCCI engine often operates under slightly (sometimes severely) knock conditions, use of the Fischer model would require an added term to include the extra heat loss associate with knock (see Equation 3.32).

$$T_{wall} (^{\circ}C) = T_{cool} (^{\circ}C) + (0.945 - 0.0078 \times T_{cool} (^{\circ}C)) \times \frac{N_s (rpm)}{60} + 4.2 \times imep (bar) \quad (3.31)$$

$$T_{wall} (^{\circ}C) = T_{cool} (^{\circ}C) + (0.945 - 0.0078 \times T_{cool} (^{\circ}C)) \times \frac{N_s (rpm)}{60} + 4.2 \times imep (bar) + Knock \ Term \quad (3.32)$$

Since engine knock severity of a specific engine with short combustion duration varies with the maximum rate of pressure rise, the knock term can be written as a function of the maximum rate of pressure rise. Based on available experimental data from a CFR engine, a function relating wall temperature rise to maximum

rate of pressure rise is proposed in Figure 3-4. This figure shows that changes in wall temperature due to engine knock become substantial when the engine knock is beyond a moderate level. This function could be slightly different from engine to engine depending on the engine geometry and cooling system. In addition, since the wall temperature modeling has been developed based on a single zone HCCI engine model with a specific heat transfer calculation (Section 3.3.1 and 3.3.2), the calculated wall temperature must be considered to be an “effective” wall temperature (not an actual wall temperature). Nevertheless, the combination of the effective wall temperature and heat transfer sub-modeling could be a more accurate representation of heat loss through the wall (than having fixed wall temperature)¹.

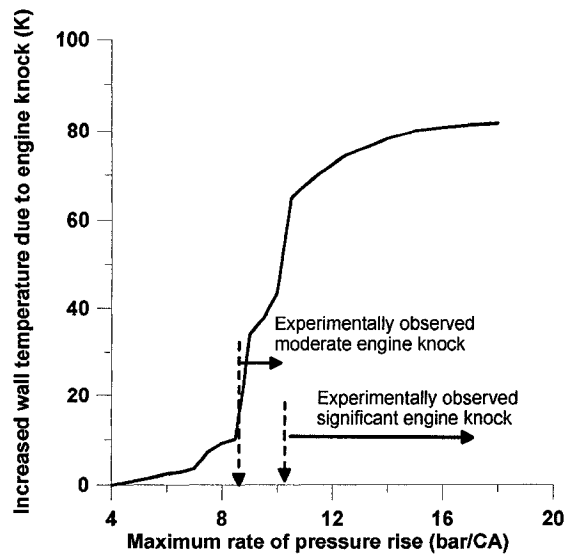


Figure 3-4 : Contribution of engine knock to wall temperature (determined by trial and error based on experimental data)

¹ Based on the idea suggested in this study, one could further develop a realistic wall temperature by optimizing parameters or correlation against the values obtained from experiment or a more detailed model. Actual wall temperature could then be used to find a better correlation for heat transfer sub-modeling (see Section 7.2: Future Work for More Detail).

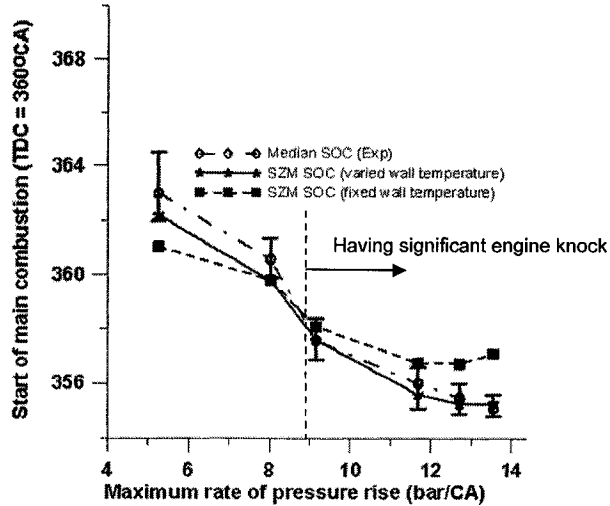


Figure 3-5 : The performance of the model with and without wall temperature correlation (using a methane fuelled HCCI engine)

Table 3-3 : Initial conditions for performance testing of SZM with effective wall correlation

Fuel Exp dP/dCA max (bar/CA)	Methane					
	5.3	8	9.7	11.7	12.7	13.6
Equivalence ratio	0.39	0.37	0.34	0.30	0.36	0.37
Reformer Gas, % RG	0.0	5.6	14.9	15.8	20.1	19.8
Exhaust Recirc., % EGR	22.0	20.3	19.5	8.4	20.5	19.8
T Intake Manifold (K)	413	413	413	413	355	413
P intake manifold (bar)	1.4	1.4	1.4	1.4	1.4	1.4
P exhaust manifold (bar)	1.4	1.4	1.4	1.4	1.4	1.4

The performance of a model with and without considering the effective wall temperature was tested with an engine running at 5 operating conditions in which the wall temperature was expected to be different, i.e., having different IMEP and maximum rate of pressure rise. The conditions of those 5 points are summarized in Table 3-3. Note that the values of maximum rate of pressure rise and IMEP to estimate effective wall temperature were from the experiment. The IVC conditions were estimated from an iterative solver from a multi-zone combustion model. Figure 3-5 shows a comparison of SZM performance with and without variable wall temperatures. The constant wall temperature was set to be 400 K which was the median value of these five cases. It can be seen that the prediction

of SOC is significantly improved by using variable wall temperature for the operating conditions with changing engine knock level and IMEP. (Having said that, the assumption of constant wall temperature is quite accurate for an engine operating at a previously characterized engine load and/or knock level).

3.4. Gas Exchange Sub-Modeling

The governing equations to calculate in-cylinder properties during gas exchange processes are the same as those used during the closed system interval of IVC to EVO (Equations 3.2, 3.4, 3.5 and 3.27). However, since there is mass flow in and out of a combustion chamber, an additional constitutive equation to govern flow is needed for the last term of Equation 3.5. Note that changes in the concentrations of each species (Equation 3.5) are attributed to both chemical reactions and the contribution of such species by the mass flows in and out. However, chemical reactions are generally ignored at low temperature (<500K) to save computational time.

As described in Heywood [72], mass flow through valves can be calculated, using one dimensional isentropic flow through a nozzle, with the calculation depending on whether the flow is choked (when $P_T / P_0 \leq [2/(\gamma + 1)]^{\gamma/(\gamma-1)}$). For a non-choked flow, Equation 3.33 is used while Equation 3.34 is for choked flow. (The derivation and more discussion of Equations 3.27 and 3.28 can be found in [72]).

$$\dot{m} = \frac{C_D A_R P_0}{(RT_0)^{1/2}} \left(\frac{P_T}{P_0} \right)^{1/\gamma} \left\{ \frac{2\gamma}{\gamma-1} \left[1 - \left(\frac{P_T}{P_0} \right)^{(\gamma-1)/\gamma} \right] \right\}^{1/2} \quad (3.33)$$

$$\dot{m} = \frac{C_D A_R P_0}{(RT_0)^{1/2}} \left(\frac{2}{\gamma+1} \right)^{(\gamma+1)/2(\gamma-1)} \quad (3.34)$$

where C_D is the discharge coefficient which is defined as a ratio of effective flow area (A_E) to reference area (A_R). For simplicity, the reference area is given by the valve curtain area (see Equation 3.35).

$$A_R = A_C = \pi D_v L_v \quad (3.35)$$

The discharge coefficient was chosen based on flow regimes that can be divided into three segments: very low lifts, intermediate lifts and high lifts [72]. During low lifts, most of the flow still attaches to valve components, causing C_D to go up. As the separation between flow and valve component is greater during intermediate lifts, C_D decreases. However, further lift increases the minimum flow area while the level of separation remains the same, giving high values of C_D . Finally, as the valve becomes fully lifted, more separation occurs, leading to lower C_D . The pattern of C_D can be found in Figure 3-6.

The flow model was validated using mass flow information and pressure history during the gas exchange process. With the initial conditions at intake valve opened (IVO) known, performance of the flow model is shown in Figure 3-7 and Figure 3-8. The regression analysis shows that one dimensional isentropic flow is accurate in predicting the amount of flow in both methane fuelled and heptane fuelled engines. In addition, an excellent agreement was found between experimental and simulation results of in-cylinder pressure during the intake process (see Figure 3-9). Excellent prediction on the amounts of mass flow and in-cylinder pressure is a referral to accurate IVC conditions. Nevertheless, this conclusion can only be true when the initial conditions (at IVO) provided to the flow sub-model are precise enough. That is not generally the case for a single zone combustion engine model. As shown below, the single zone model significantly over-estimates the expansion pressure.

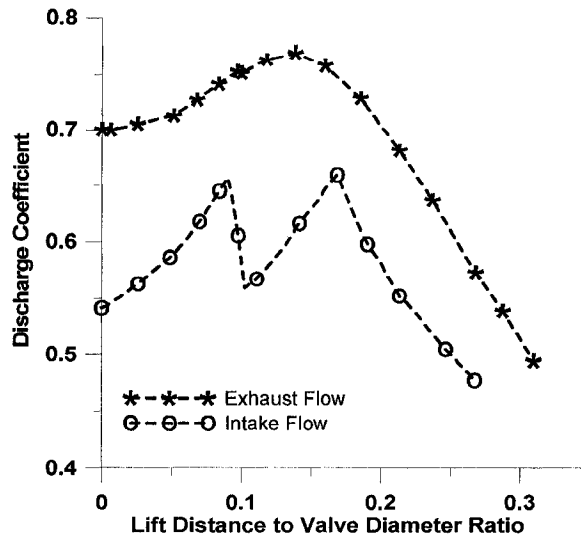


Figure 3-6 : Discharge coefficients for intake and exhaust process (from [72])

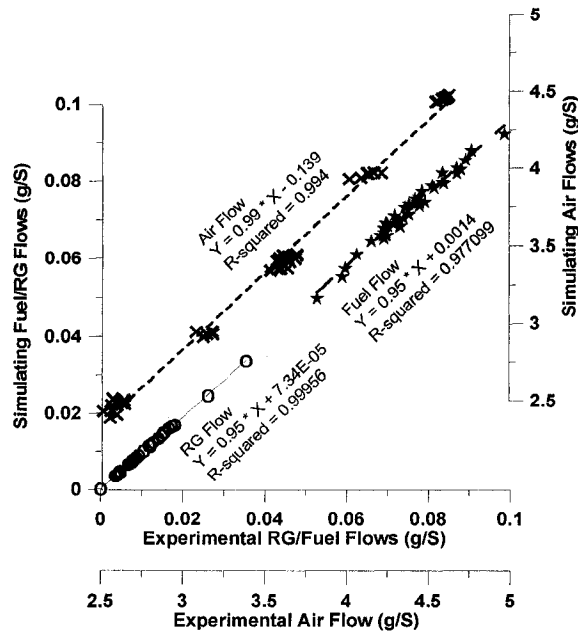


Figure 3-7: Regression analysis of fuel-, RG- and air- mass flows of a methane fuelled HCCI engine

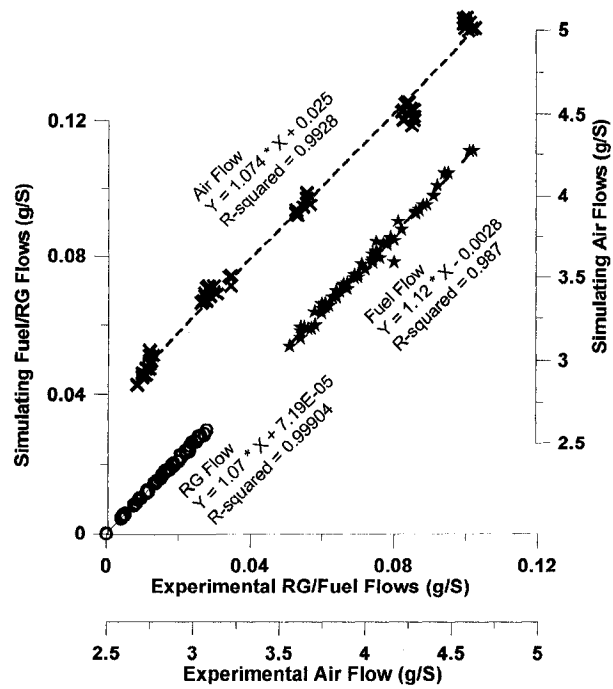


Figure 3-8 : Regression analysis of fuel-, RG- and air- mass flows of a heptane fuelled HCCI engine

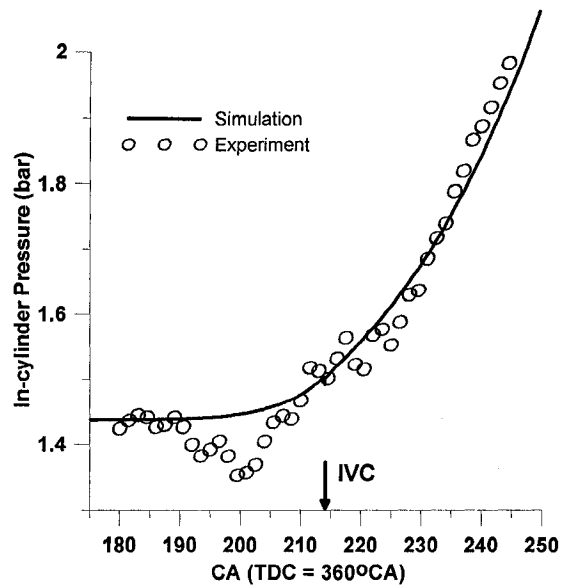


Figure 3-9 : Example of in-cylinder pressure during gas exchanging process

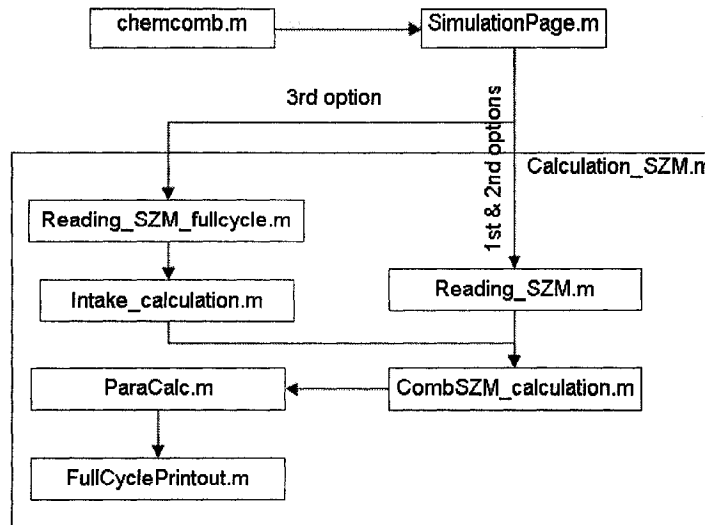


Figure 3-10: Main structure of Single zone calculation in CHEMCOMB (the names in the chart referred to Appendix C)

3.5. CHEMCOMB Single Zone HCCI Model

The theory described above has been applied to program a single zone combustion engine model. The main structure of the single zone model in CHEMCOMB is shown in Figure 3-10. The program allows users to select three options to set initial conditions depending on their objectives and available information. **First** is to arbitrarily set the conditions at intake valve close. This option is suitable to investigate the effects of changing conditions without any interference of different IVC conditions from various operating conditions. **Second** is to specify the mass flow rate for fuel, air and external EGR. This option is suitable when the mass flow data are available. Note that the gas exchange calculation (Section 3.5) is not applied in the first two options. **The final option** is the most engine-like modeling which includes all the calculations described earlier such as gas exchange sub modeling. Ideally, the initial conditions (IVC conditions) as well as boundary conditions (wall temperature) of this option should have been arrived at by iterating a simulation until the results reach steady state, just as what happens in an actual engine. However, the estimation of wall

temperature and the intake valve opened conditions are not very accurate with a single zone model due to the inability to predict the maximum rate of pressure rise and constantly higher expansion pressure/temperature. Therefore, a single zone combustion engine model can only provide a credible solution with specified initial conditions (at IVO) and boundary conditions (wall temperature) obtained from either experiments or another more accurate model, i.e., a multi-zone model as described in Chapter 4.

3.5.1. Required Inputs

The inputs to the CHEMCOMB SZM engine simulation can be summarized into two categories. The first category consists of the general information that all of the three options require. The second category is the set of inputs for mixtures and operating conditions, which are different among the three input options.

The general information includes:

- **Engine specification:** compression ratio, cylinder bore dimensions, length of connecting rods and the valve lift profiles
- **Operating conditions:** engine speed, wall temperature, relative temperature change

Initial mixture conditions:

Initial mixture specifications are different among the three input options. For the 1st and 3rd options, the mixtures are described by standard engine fuel parameter, i.e., equivalence ratio (Φ) together with % RG, while the other option requires only the information of fuel, air and RG flows. The definitions of equivalence ratio and % RG are,

- Equivalence ratio $\equiv \frac{\sum V^+}{\sum V^-} \approx \frac{F/A)_{actual}}{F/A)_{stoich}}$

- % RG $\equiv \frac{m_{RG}}{m_{RG} + m_{fuel}}$

In addition to fuel, RG and air, % external EGR also needs to be specified for all three options and is defined as,

- %EGR $\equiv \frac{m_{EGR}}{m_{EGR} + m_{intake}} \approx \frac{[CO_2]_{intake}}{[CO_2]_{exhaust}}$

Without the flow model, determination of internal residual mass fraction at IVC becomes the key issues for the 1st and 2nd options. In this study, the work of Fox [143] and Cavina [144] was adopted to evaluate percentage of residual trapped at IVC. Based on physical interpretation, internal residual fraction can be found from,

$$x_r = a \times \left(\frac{2}{C}\right)^{0.5} \times \frac{\pi}{360} \times \frac{r_c - 1}{r_c} \times \frac{OF}{N/60} \times \left(\frac{P_{exh}}{P_{int}}\right)^{\frac{k+1}{2k}} \times \left(\frac{\|P_{exh} - P_{int}\|}{P_{exh} \times R \times T_{int}}\right)^{0.5} \quad (3.36)$$

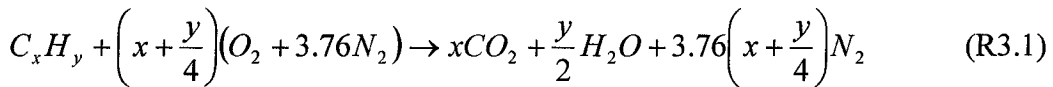
$$+ \frac{1}{C} \times \frac{r_c - 1}{r_c} \times \phi \times \left(\frac{V_{IVO}}{V_d}\right) \times \left(\frac{P_{exh}}{P_{int}}\right)^{1/k}$$

where, $C = \left(1 + \frac{LHV}{c_{v,int} \times T_{int} \times (m_{cyl}/m_{fuel}) \times r_c^{k-1}}\right)^{1/k}$ (3.37)

and $OF = \frac{D_i A_i + D_e A_e}{V_d}$ (3.38)

In order to evaluate the ratio of cylinder mass to the amount of fuel, the following equation (Equation 3.39) is used [144].

$$m_{cyl}/m_{fuel} = 1 + AFR + AFR \times \frac{\%EGR}{1 - \%EGR} + \frac{x_r}{1 - x_r} \times \left(1 + \frac{AFR}{1 - \%EGR}\right) \quad (3.39)$$



```

! Input file for CHEMCOMB model
!
Fuelselection
!
Fuel composition = CH4,0.965/C2H6,0.019/CO2,0.008/N2,0.049
RG compositions = H2,0.75/CO,0.66
% RG           = 5.701
Equivalence ratio = 0.29426
Mixture temperature = 413.15
!
Specification
!
CR           = 19.50
Bore         = 8.26
Stroke       = 11.43
Connecting rod = 25.40
!
Conditions (working conditions)
!
Ns          = 800.0000
Tw          = 470.6700
Treact      = 500.0000
Heat transfer factor (compression) = 2.43287
Heat transfer factor (expansion)   = 2.43287
beta        = 34
!
Initial Conditions
!
IVC pressure (MPa) = 0.1507
IVC temperature (K) = 426.136
%EGR = 0
Exhaust pressure (MPa) = 0.140233
Exhaust temperature (K) = 480
Coolant temperature (C) = 100.316
!
Recorded species
!
Species = H2O
!
Products
!
products = Complete
!
Valve Input File
!
File name = CFRvalveProfile.xls
!
! Note this is the input

```

Figure 3-11 : Example of an input file for a single zone model - option 1 (specifies conditions at IVC)

```

! Input file for CHEMCOMB model
!
Fuelselection
!
Fuel composition = CH4,0.965/C2H6,0.019/CO2,0.008/N2,0.008
RG compositions = H2,0.75/CO,0.25
Fuel mass flow (g/s) = 0.0865
RG mass flow (g/s) = 0.01132
Air mass flow (g/s) = 2.4983
Mixture Temperature (K) = 413.15
!
Specification
!
CR          = 19.50
Bore        = 8.26
Stroke      = 11.43
Connecting rod = 25.40
!
Conditions (working conditions)
!
Ns          = 800.0000
Tw          = 383.1431
Treact      = 500.0000
Heat transfer factor (compression) = 2.008
Heat transfer factor (expansion)   = 2.008
beta        = 34
!
Initial Conditions
!
IVC pressure (MPa)      = 0.1519
%EGR                    = 41.2177
Pressure in exhaust system = 0.141649
Exhaust temperature = 480
Coolant temperature (C) = 100.287
!
Recorded species
!
Species = H2O
!
Products
!
products = Complete
!
Valve Input File
!
File name (in ValveProfile folder) = CFRvalveProfile.xls
!
! Note this is the input

```

Figure 3-12 : Example of an input file for a single zone model - option 2 (specifies the amount of mass flow into an engine)

```

! Input file for CHEMCOMB model
!
Fuelselection
!
Fuel composition = CH4,0.965/C2H6,0.019/CO2,0.008/N2,0.008
RG compositions = H2,0.75/CO,0.25
% RG           = 10.796
Equivalence ratio = 0.57937
!
Specification
!
CR           = 19.50
Bore         = 8.26
Stroke       = 11.43
Connecting rod = 25.40
!
Conditions (working conditions)
!
Ns          = 800.0000
Tw          = 383.1431
Treact      = 500.0000
Heat transfer factor (compression) = 2.008
Heat transfer factor (expansion) = 2.008
beta        = 34
!
Initial Conditions
!
Intake manifold pressure = 0.141
Exhaust manifold pressure = 0.141649
Pressure @ IVO = 0.139
Intake manifold temperature = 413.15
Exhaust temperature = 451.2
%EGR        = 41.2177
Coolant temperature (C) = 100.287
!
Recorded species
!
Species     = H2O
!
Products
!
products = Complete
!
Valve Input File
!
File name (in ValveProfile folder) = CFRvalveProfile.xls
!
! Note this is the input

```

**Figure 3-13 : Example of an input file for a single zone model - option 3
(Full engine cycle)**

The system of equations (3.30 and 3.33) was then solved to obtain the residual mass fraction by the Successive-Over-Relaxation (SOR) method. The residual mass fraction obtained from the system of Equations 3.36 to 3.39 is, however, lower than the value obtained from the one dimensional isentropic flow model. Therefore, a correcting factor of $a=1.3$ is applied.

Finally, the composition of both external and internal residuals is assumed to be the same as the products obtained from complete combustion (see Reaction R 3.1). This assumption is reasonable if the engine is operating with low in-cylinder temperature, i.e., no dissociation, and the engine speed is so low that all active species change to stable molecules (complete combustion products).

Required initial operating conditions:

Beyond specifying the initial mixture composition, the initial operating conditions also need to be specified. The inputs for initial operating conditions are different depending on the input option. For the first option, the required initial conditions are the gas conditions at IVC (IVC temperature and pressure). The model automatically calculates mass from composition, temperature and pressure information. Since mass is already specified in the 2nd option, only information on IVC pressure is required. With the values of mass and IVC pressure known, IVC temperature can be calculated. Instead of conditions at IVC, which is difficult to identify, the last option requires intake manifold conditions which is much simpler to measure. In order to illustrate the input requirements, Figure 3-11 to Figure 3-13 show the examples of input files for the three options in CHEMCOMB.

3.5.2. Solver

The system of ordinary differential equations is solved by the “ode15s” function in MATLAB. This solver is based on the numerical differentiation formulas

(NDFs) with a variable order solver, using the backward differentiation formulas (BDF) [145].

3.6. Model Performance

The SZM model was verified for both methane-fuelled and heptane-fuelled HCCI engines. The specification of the engine and the experimental set-up done by Hosseini [146] can be found in Section 3.6.1. There are a total of 41 cases used for the validation of a methane-fuelled HCCI engine and 61 cases for a heptane-fuelled HCCI engine. The conditions covered the following ranges for critical parameters: $\phi = 0.21-0.57$, %RG = 0%-30% and %EGR = 0%-40%. (The list of operating conditions for all the validating cases can be found in Appendix D). Both methane and heptane engines were operating at 800 rpm with an intake pressure of approximately 1.5 bar. Intake manifold temperature was 413 K for the methane engine and 383 K for the heptane engine.

A comparison of pressure traces from selected cycles of both engines was first demonstrated to show the performance of the model in capturing in-cylinder pressure trace. Then, the linear regression of simulating SOC against experimental SOC was plotted to observe the overall performance of the model in predicting ignition timing. The experimental pressure trace and experimental SOC were selected in such a way that the peak pressure is at the median position in the 100 cycle sample. Such a value was selected, (instead of mean or median values), so that meaningful comparisons could be made between one parameter and the others. That is, all parameters come from the median peak pressure cycle, even though a median IMEP and a median SFC could have been on different cycles. (This has been done in order to be consistent with the validation of a multi zone model in Chapter 4 where multiple parameters are compared).

3.6.1. Experimental Set-up

An CFR engine with bore and stroke of 82.6×114.3 mm was modified to operate in HCCI mode at wide open throttle by Hosseini [146]. A heater was installed at the intake manifold in order to control the intake mixture temperature when needed. A thermocouple and pressure sensor were mounted just before the intake valve to monitor the intake manifold properties. External exhaust was taken right after the exhaust port and recirculated into the heated intake air (before any fuel injection). The amount of external EGR was controlled by a manual butterfly valve.

The engine two gaseous and one liquid fuel injectors in the intake port for investigation of fuel blends. The in-cylinder pressure was measured using a Kistler 6043A water cooled pressure transducer sampled 0.1 CAD resolution. The diagram of the experimental set-up is shown in Figure 3-14 and the engine specifications are in Table 3-4.

Table 3-4 : Engine Specification. (Note the first compression ratio is for a CNG-HCCI engine, and the second is for an n-heptane-HCCI engine).

Engine Parameters (unit)	Values	Engle Parameters (unit)	Values
Compression ratio	19.5/11.5	IVO (CA)	10
Bore (cm)	8.26	IVC (CA)	214
Stroke (cm)	11.4	EVO (CA)	500
Connecting rod (cm)	24	EVC (CA)	735

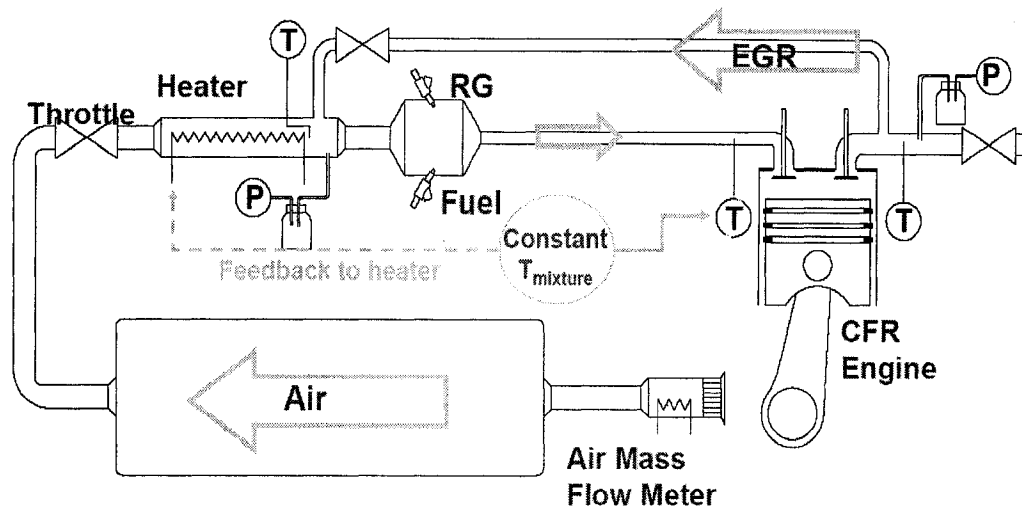


Figure 3-14: Schematic Diagram of an Experimental Set-up [146]

All the experimental data were determined using this engine. As it has two gaseous- and one liquid fuel injectors, switching fuels between heptane and methane or blending either fuel with RG can be simply done. However, as the octane numbers (ON) of the two base fuels are extremely different ($ON_{\text{methane}} \sim 120$ and $ON_{\text{heptane}} \sim 0$), the compression ratios of engines operating with these two fuels cannot be the same in order to generate comparable temperature histories. With motoring pressure traces, the compression ratio of a methane engine was numerically found to be 19 ± 0.5 while the heptane engine had compression ratio of 11.5 ± 0.5 . The tolerance is caused by the uncertainties from heat transfer, blow-by and experimental measurements. Preliminary experimental results, when operating the engines with fuel/air mixtures, determined average compression ratios to be 19.5 (for a methane engine) and 12.0 (for a heptane engine). The slight increase with fuelled operation is expected to be due to less blowby loss at normal operating temperature.

3.6.2. Model Validation Based on Pressure Trace

The example of a comparison of a pressure trace from methane- and heptane-fuelled HCCI engines can be seen in Figure 3-15 and Figure 3-16. It can be seen

that the SZM agrees with experimental data in predicting in-cylinder pressure during compression. However, the pressure history obtained from the SZM becomes in-accurate after ignition takes place. Due to the assumption of having lumped properties in the SZM, the entire mixture burns in one time-step, leading to an extremely short combustion duration and excessively high peak pressure. This is a well-known limitation of single-zone models. Additionally, the SZM gives an over estimation of in-cylinder pressure during expansion compared to the experimental results. The major contribution to this higher expansion pressure is probably due to missing boundary layers. The heat transfer calculation of the SZM is based on normal operation in which boundary layers act as an insulator and this is not properly accounted for during the post-combustion period. The global heat transfer model used in the SZM is more valid for the expansion conditions in the n-heptane-fuelled HCCI engine than for the CNG-fueled engine because of lower peak pressure.

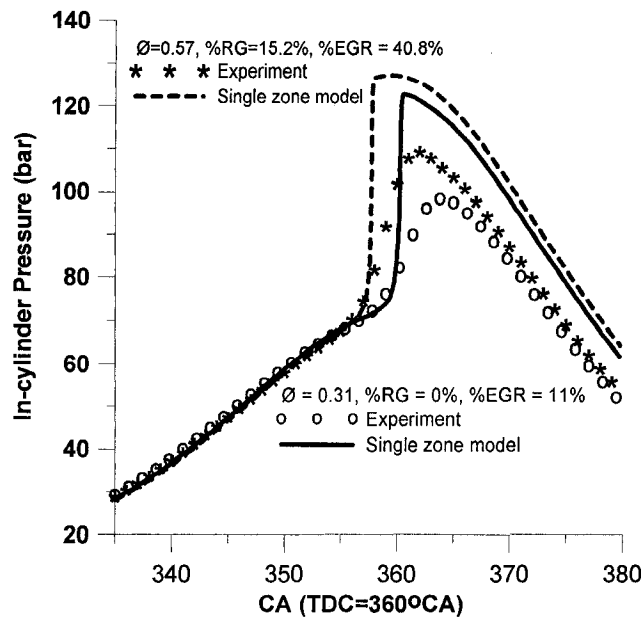


Figure 3-15 : Comparison of pressure histories from a methane-fuelled HCCI engine operating with two different conditions

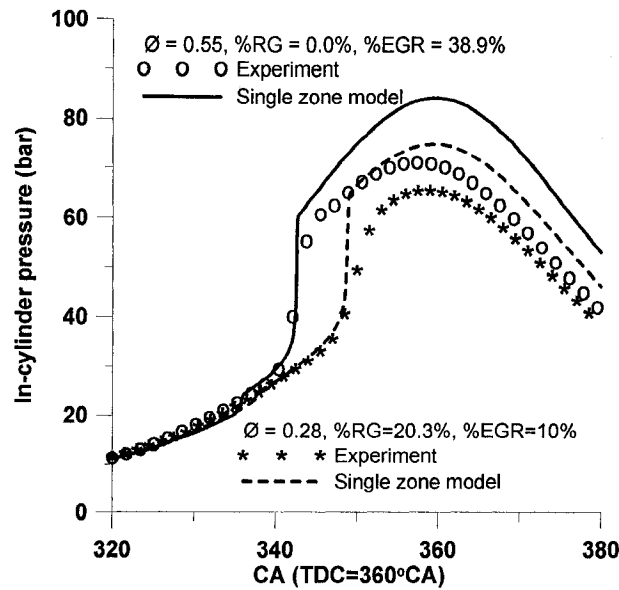


Figure 3-16 : Comparison in pressure histories of an n-heptane-fuelled HCCI engine operating with two different conditions

The over-estimation of combustion rate and in-cylinder peak pressure from a single zone model indicates the incapability of single zone engine models to capture other engine parameters such as maximum in-cylinder pressure, combustion rate, IMEP and peak pressure rise rate (see Figure 3-15). Since SOC timing is the only prediction which can be usefully done with a single zone combustion model, the further analysis of the performance of an SZM will only focus on SOC.

3.6.3. Model Performance in Capturing the Start of Main Combustion

Regression analysis was adopted to measure the overall SZM performance in predicting SOC timing over a range of conditions. Model performance is said to be perfect when the slope of best-fitted linear regression relating those two variables is unity. The best-fit linear regressions for CNG and heptane are plotted in Figure 3-17 and Figure 3-18. There is excellent agreement between the model and experimental data in capturing SOC behavior of both engines as the slopes of the regression lines are close to unity.

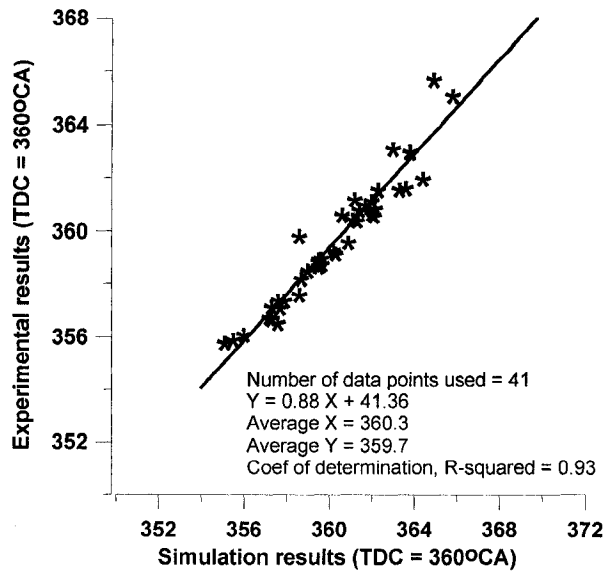


Figure 3-17 : Comparison between simulated and experimental SOC of a CNG HCCI engine through a regression analysis

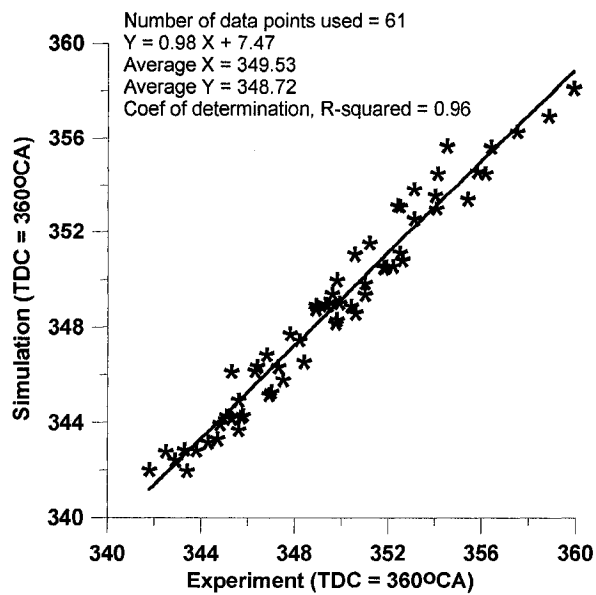


Figure 3-18 : Comparison between simulated and experimental SOC of a heptane HCCI engine through a regression analysis

3.7. Summary

The model developed in this chapter is probably the most detailed single zone combustion model existing as it includes a built-in gas exchange model to predict initial conditions (at intake valve close), imperfectly stirred mixture phenomena and variable wall temperature depending on operating conditions. The model was proven to be accurate to capture the point where ignition occurs over a wide range of operating conditions for both methane- and heptane-fuelled HCCI engines although there is some variation when compared to experimental results.

Although the model is good at predicting SOC, it does not imitate the sequential HCCI combustion process in an actual engine. Hence, all combustion takes place almost instantly, leading to an over-predicted peak pressure and a shortened combustion period. Consequently, high peak pressures together with the absence of boundary layers causes the expansion pressure to be greater than normal. As the SZM gives an overestimation of the peak pressure and expansion pressure, it cannot accurately predict other engine parameters such as IMEP and the maximum rate of pressure rise. Therefore, a model that allows inhomogeneity across a combustion chamber, i.e., a multi-zone model, is needed in order to more accurately describe the start of main combustion.

4 Multi Zone HCCI Model

The previous chapter has shown that attempting to model HCCI combustion with the assumption of uniform properties, (temperature, pressure and concentration), leads to extremely fast combustion rate and short combustion duration. Consequently, peak pressure and temperature are over estimated, as well as expansion pressure in some cases. In actual HCCI engines, the charge near the walls is cooler than in the centre of the cylinder near the end of compression due to the dissipation of heat to the walls. To more accurately estimate combustion behavior, (especially combustion duration), and engine performance parameters, a model where mixture properties vary spatially is needed. Multi zone models commonly consider temperature gradients in the combustion chamber and are widely accepted in terms of predicting burning duration. Likewise there is potential for significant variations in fuel concentration and recirculated exhaust concentration throughout the cylinder and these variations can also affect reaction rates. Hence, combustion models attempting to quantify HCCI combustion effects should be able to respond to the temporal and spatial variation of mixture strength and residual fraction in the charge as well as temperature.

The methodology to calculate a multi-zone combustion model is similar to that of a single-zone combustion model except for the variation of mixture properties across the combustion chamber. To accomplish this, a number of aspects must be considered. Those include zone configuration, zone boundary movements, heat transfer sub modeling, initial condition settings and possibly an improved calculation method to reduce computational load. These aspects of a multi-zone model and the model implementation are discussed in the following sections. Model performance and validation is demonstrated in Section 4.8.

4.1. Main Assumptions of the Model

The model is based on thermodynamic property models for mixed gases, ideal gas theory, specified heat transfer models, detailed chemical kinetics and geometrical constraints provided by the engine. The zone configuration has been designed to allow temperature differences among wall, cylinder head and piston head regions (see Figure 4-1). Within each zone, the gas properties are considered to be lumped and pressure is considered to be uniform for all zones [92] as is normal for pre-knock conditions. For both fuels, the composition is assumed to be frozen for any zones where the temperature is less than 500K, thus reducing computation time. Heat transfer sub-modeling includes convection to walls, convection between zones and gray-gas radiation from gas zones to the wall. The only interactions between zones are heat transfer and work transfer; no mass transfer is considered between zones.

To initiate conditions at intake valve closure, a one-dimensional quasi-steady flow model was used to calculate the gas exchange process. This gave the average values, (temperature, pressure and gas composition), at intake valve closure. Imperfectly stirred mixture effects were included via the virtual enthalpy exchange between hotter internal residual and cooler intake mixture, (as described in Section 4.3). These developments allowed calculation of the initial conditions and the entire cycle without arbitrary adjustments. In addition, a new segregation solution technique (as described in Section 4.5) was used to reduce computational effort by roughly one order of magnitude, making it possible to run multiple simulations on common personal computers.

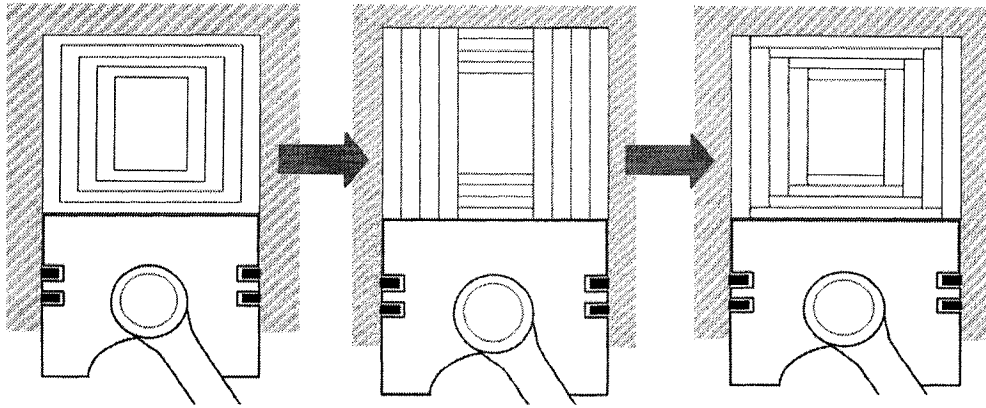


**Figure 4-1 : Development of zone configuration.
(4-Layer configuration at right is used in the multi-zone model)**

4.2. Zone Configuration

The zone configuration has been developed as shown in Figure 4-1. The left configuration has been widely used in other published papers, eg. [90], because of its simplicity and it has computational time advantages compared with the second and third configurations. However, this configuration does not allow for temperature differences between the cylinder wall, piston head and cylinder crown. The second configuration [18] provides a potential to include these temperature differences, but still connects all annular zones to both the piston and cylinder head surfaces. This study introduces a third zone configuration which allows for a more realistic situation with a different boundary temperature for each surface and non-surface zone. This is a very important feature for exploring effects of having non-uniform wall temperature between cylinder wall, piston head and cylinder crown. Further, such an approach might assist in analyzing engines using a hot spot to assist ignition of homogeneous mixtures. Such an engine could be considered as a partial HCCI engine and might provide an alternative way to control HCCI engine combustion timing through a controllable temperature hot spot.

With the zone layout decided, the next step is to justify the number of zones required to describe HCCI engine combustion behavior. A simple single zone

model, (with no cooled boundary layers), makes all the mixtures ignite in one time step, resulting in extremely fast combustion and over-prediction of peak pressure, (see Chapter 3). Figure 4-2 shows the effects of different numbers of layers (N_{Layer}) on the calculated pressure trace and the cycle computation time for a methane HCCI engine where ignition occurred very close to piston top dead centre (TDC). (Note that the total number of zones is equal to $3*N_{layer}+1$). With one layer, the mixtures were almost misfiring because the only zone hot enough to ignite did not lead to consecutive combustion of other zones. Sequential combustion initially occurred when there were 2 layers; however, it still did not match the experimental result. With 3 or more layers the predicted combustion behavior changed only marginally. Therefore, with a consideration of model fidelity and computational time, the optimum number of layers was set at four and the multi-zone model thus had thirteen zones. The zones are chosen to have equal mass so the volume distribution [147, 148] is set by combustion chamber properties as in Figure 4-3.

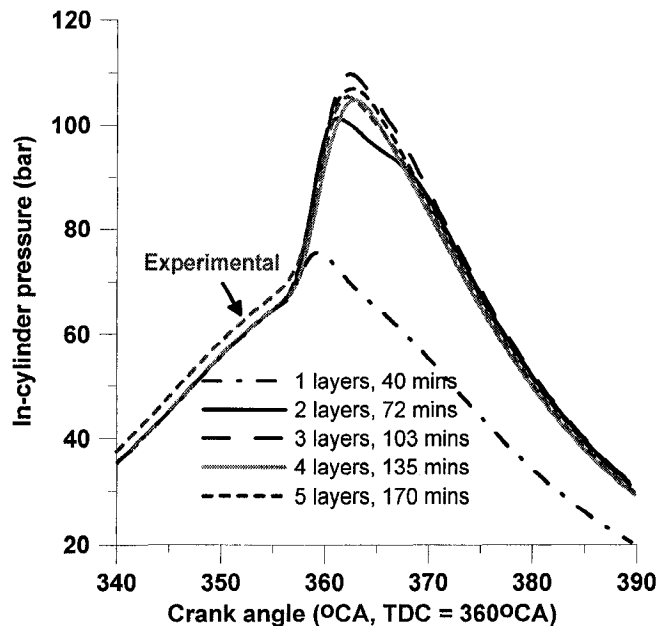


Figure 4-2 : Effects of zone numbers on pressure trace and computation time (Methane HCCI engine)

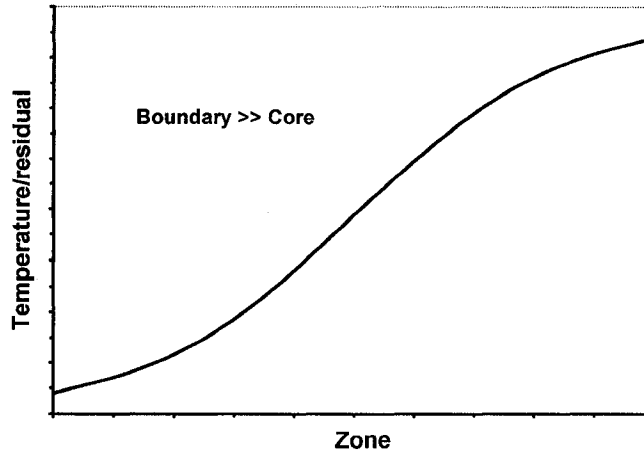


Figure 4-3 : Pattern of in-cylinder temperature and internal residual distribution at IVC. Both residual and temperature are assumed higher at the cylinder 'core' region.

4.3. Inhomogeneity Scheme

Although the 'H' in 'HCCI' refers to 'homogeneous', it has been shown that inhomogeneity of temperature and residual has a significant impact on HCCI combustion behavior [18, 23] and, in fact, is required to give realistic combustion time values. For this study, the IVC temperature and internal residual inhomogeneity are assumed to be S-shaped [147] as shown in Figure 4-3. The physical justification for this pattern is given by the schematic of flow behavior during the intake stroke, (Figure 4-4). Cool mixtures entering into a combustion chamber predominantly move towards the walls and are concentrated near the outer cylinder wall by the centrifugal effect of any swirl. This leads to a higher density of intake mixture (lower internal residual fraction) and hence lower temperature in the boundary layer regions at the time of IVC.

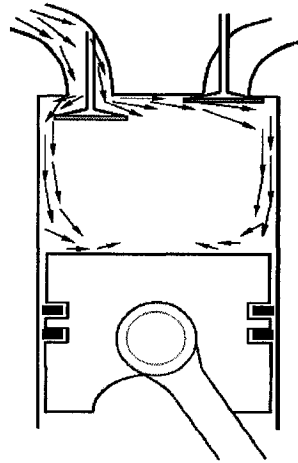


Figure 4-4 : Motion of fluids in cylinder during gas intake process

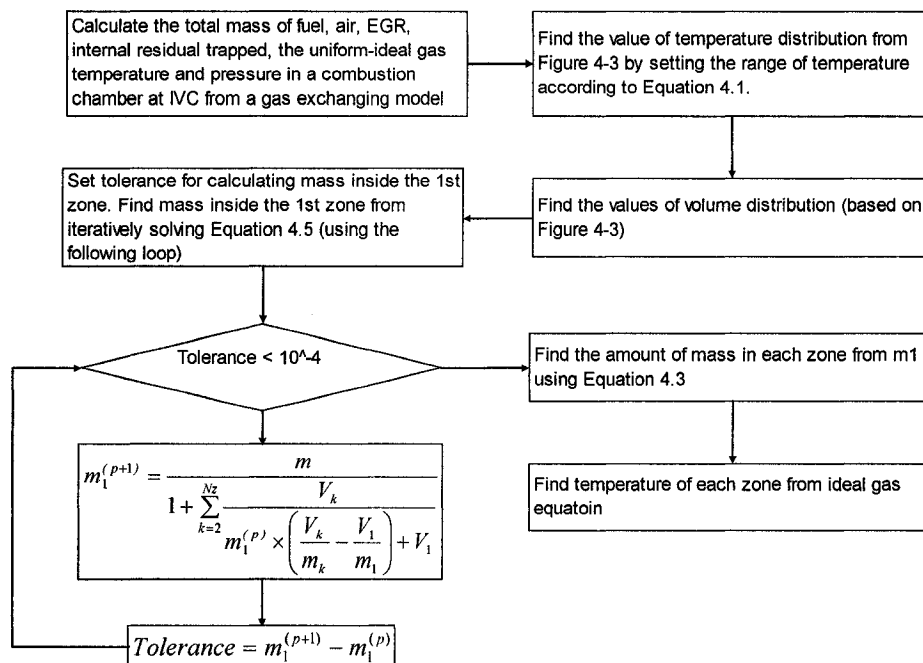


Figure 4-5 : A flow chart for setting Mass and temperature distribution

Assigning temperature and composition inhomogeneity while preserving the intake mass fraction requires a series of procedures as laid out by the process flow diagram in Figure 4-5. First, the average IVC temperature was obtained from the

gas exchange process (refer to Chapter 3, Section 3.8 for calculation). Then, the in-cylinder temperature range was set based on the full value of the temperature difference between internal residual and intake temperatures (see Equation 4.1).

$$\Delta T = \left(\frac{1}{K_T} \right) (T_{residual} - T_{intake}) \quad (4.1)$$

Next, the temperature distribution was needed. To assign a temperature to each zone, the ideal gas equation is rearranged into:

$$\frac{V_k}{m_k} = \frac{R_{ave,k} T_k}{P} \quad (4.2)$$

Assuming that the average gas constant of each zone is equal, the difference between the specific volume of k^{th} zone and the specific volume of the first zone, (the boundary-layer annular zone), can be found from:

$$\frac{V_k}{m_k} - \frac{V_1}{m_1} = \frac{R_{ave}}{P} \times (T_k - T_1) \quad (4.3)$$

where V_k is the volume of the k^{th} zone and is obtained from a normal distribution function of which parameters μ and σ are 0 and 1 respectively, (see Figure 4-6). Note that the core zone (zone 13 in Figure 4-6) is one edge of each of the normal distributions for annular, top and bottom layers. The term $(T_k - T_1)$ is a temperature difference between the k^{th} zone and the first zone and is estimated from the arbitrary temperature distribution curve (Figure 4-3).

The ratio of mass in the k^{th} zone to mass in the first zone can then be estimated from Equation 4.3.

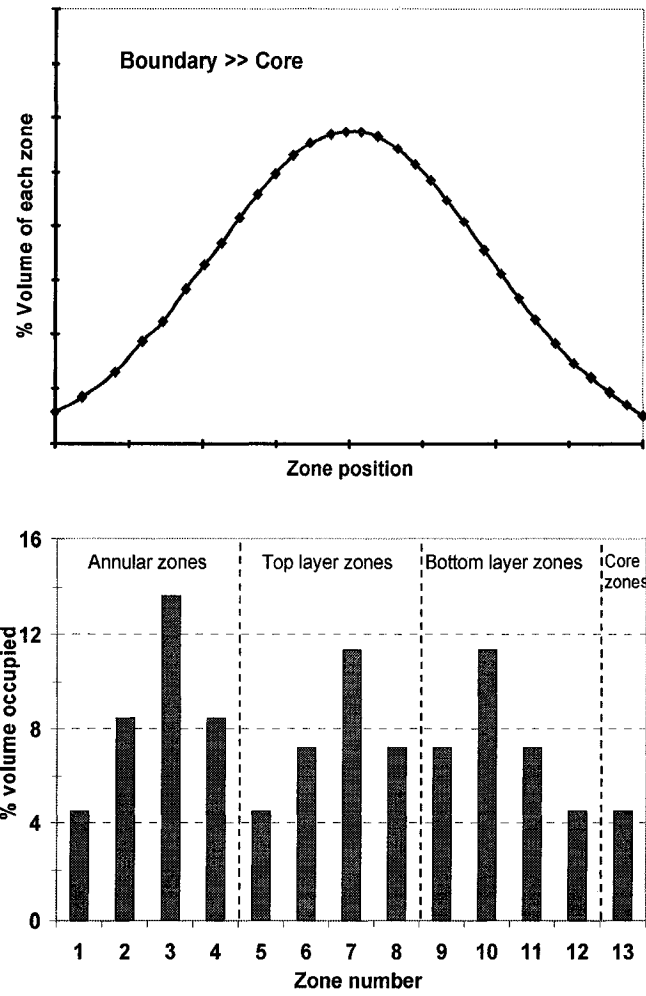


Figure 4-6 : Configuration of volume distribution at IVC

Since the summation of mass in all zones must equal the total intake mass, (Equation 4.4), mass in the first zone can be iteratively solved from Equation 4.5.

$$\sum m_k = m_{cyl} \quad (4.4)$$

$$m_1^{(p+1)} = \frac{m_{cyl}}{1 + \sum_{k=2}^{N_z} \frac{V_k}{m_1^{(p)} \times \left(\frac{V_k}{m_k} - \frac{V_1}{m_1} \right) + V_1}} \quad (4.5)$$

Once mass in each zone is found, the ideal gas equation is used to estimate zone temperature.

Finally, an internal residual distribution needs to be calculated. First, the total residual fraction is calculated from,

$$f = \frac{v_{EVC}}{v_{IVC}} \times \frac{V_{IVC}}{V_{EVC}} \quad (4.6)$$

Based on the residual mass fraction pattern (Figure 4-3), we can estimate the residual fraction of the boundary layer zone (f_{min}) from,

$$m_{res} = \sum_{k=1}^{N_z} f_k m_k = \sum_{k=1}^{N_z} (f_{min} + \Delta f_k) \quad (4.7)$$

where Δf_k is the difference between the residual fraction of the k^{th} zone and the residual fraction of the first zone and is found from the residual fraction distribution pattern (Figure 4-3).

4.4. Transport Properties Calculation

The multi-zone model governing equations require detailed gas properties to calculate heat transfer between zones to zones. The calculation is based on molecular transport characterization of the gas mixtures as described in the CHEMKIN sub-routine in [110]. The calculation of transport properties would not be as important if mixture composition is similar from case to case. However, since the study is intended to investigate the effects of reformer gas that contains 75% H_2 , the significantly different transport properties of H_2 might affect the average mixture properties. Therefore, evaluating transport properties for each case is necessary. The parameters in a transport properties input file are:

- ε / k_B - The Lennard-Jones potential wall depth (in Kelvin),
- σ - The Lennard-Jones collision diameter (in Angstroms),

- μ_D - The dipole moment (in Debye, 1 Debye = $10^{-18} \text{cm}^{3/2} \text{erg}^{1/2}$),
- α - The polarizability (in cubic Angstroms) and
- Z_{rot} - The rotational relaxation collision number at 298 K

Figure 4-7 shows a sample of part of the transport properties input file. For instance, for O₂,

$$\begin{aligned}
 \varepsilon / k_B &= 107.400 \text{ Kelvin} \\
 \sigma &= 3.458 \text{ Angstroms} \\
 \mu &= 0.000 \text{ Debye} \\
 \alpha &= 1.600 \text{ Angstrom}^3 \\
 Z_{rot} &= 3.800
 \end{aligned}$$

To calculate gaseous conductivity for evaluating laminar heat convection between zones, the reduced temperature was calculated from,

$$T^* = \frac{k_B T}{\varepsilon_k} \quad (4.8)$$

T* was then used to evaluate the collision integral ($\Omega^{(1,1)*}$ and $\Omega^{(2,2)*}$), see Equation 4.9 to Equation 4.11. Note that the coefficients for these Equations (4.9 to 4.11) are concluded in Table 4-1.

$$\Omega^{(1,1)*} = a_1 + a_2 T^* + a_3 (T^*)^2 + a_4 (T^*)^3 + a_5 (T^*)^4 \quad (4.9)$$

$$A^* = a_1 + a_2 T^* + a_3 (T^*)^2 \quad (4.10)$$

$$\Omega^{(2,2)*} = A^* \Omega^{(1,1)*} \quad (4.11)$$

O	0	80.000	2.750	0.000	0.000	0.000
O2	1	107.400	3.458	0.000	1.600	3.800
NO2	2	200.000	3.500	0.000	0.000	1.000 ! *
C6H11	3	482.473	5.307	0.000	0.000	0.000

Figure 4-7 : Example of input table for transport property coefficients

Table 4-1 : Coefficients for calculating collision integral and associated parameters [111]

		A1	a2	a3	a4	a5
$T^* < 5$	$\Omega^{(1,1)*}$	2.353E+00	-1.359E+00	5.220E-01	-9.426E-02	6.435E-03
	A^*	1.108E+00	-9.480E-03	1.692E-03		
$5 \leq T^* \leq 10$	$\Omega^{(1,1)*}$	1.266E+00	-1.644E-01	2.295E-02	-1.632E-03	4.583E-05
	A^*	1.087E+00	3.196E-03	-8.929E-05		
$T^* \geq 10$	$\Omega^{(1,1)*}$	8.5264E-01	-1.355E-02	2.616E-04	-2.465E-06	8.654E-09
	A^*	1.106E+00	6.651E-04	-3.409E-06		

Based on the collision integral, the binary diffusion coefficients and a single component viscosities can be obtained from Equation 4.12 and Equation 4.13,

$$D_{jk} = \frac{3}{16} \frac{\sqrt{2\pi k_B^3 T^3 / m_{jk}}}{P \pi \sigma_{jk}^2 \Omega^{(1,1)*}} \quad (4.12)$$

$$\eta_k = \frac{5}{16} \frac{\sqrt{\pi m_k k_B T}}{\pi \sigma_k^2 \Omega^{(2,2)*}} \quad (4.13)$$

Assuming that thermal conductivity of an individual species composed of translational, rotational and vibrational contributions [110], the binary diffusion coefficients (Equation 4.12) and a single component viscosities (Equation 4.13) were used to calculate the contribution from rotation (Equation 4.14), vibration (Equation 4.15) and translation (Equation 4.16).

$$f_{rot} = \frac{\rho D_{kk}}{\eta_k} \left(1 + \frac{2}{\pi} \frac{A}{B} \right) \quad (4.14)$$

$$f_{vib} = \frac{\rho D_{kk}}{\eta_k} \quad (4.15)$$

$$f_{trans} = \frac{5}{2} \left(1 - \frac{2}{\pi} \frac{C_{v,rot}}{C_{v,trans}} \frac{A}{B} \right) \quad (4.16)$$

where parameters A and B and molar heat capacity given in Table 4-2.

Table 4-2 : Related parameters for calculating translational, rotational and vibrational contributions to thermal conductivity of an individual species

Linear molecule	Nonlinear molecule
$A = \frac{5}{2} - \frac{\rho D_{kk}}{\eta_k}$	
$B = Z_{rot} + \frac{2}{\pi} \left(\frac{5}{3} \frac{C_{v,rot}}{R} + \frac{\rho D_{kk}}{\eta_k} \right)$	
$\frac{C_{v,trans}}{R} = \frac{3}{2}$	
$\frac{C_{v,rot}}{R} = 1$	$\frac{C_{v,rot}}{R} = \frac{3}{2}$
$C_{v,vib} = C_v - \frac{5}{2}R$	$C_{v,vib} = C_v - 3R$

Finally, the pure species thermal conductivities are calculated using Equation 4.17 and the average thermal conductivities of mixtures composed with several species are calculated based on combination averaging formula (see Equation 4.18).

$$\lambda_k = \frac{\eta_k}{W_k} (f_{trans} C_{v,trans} + f_{rot} C_{v,rot} + f_{vib} C_{v,vib}) \quad (4.17)$$

$$\lambda = \frac{1}{2} \left(\sum_{k=1}^K X_k \lambda_k + \frac{1}{\sum_{k=1}^K (X_k / \lambda_k)} \right) \quad (4.18)$$

4.5. Calculations for the closed system interval

This section discusses the main calculation that covers the closed system interval from IVC to EVO. It covers the main governing equations, zone-to-zone heat transfer calculation and zone boundary movement.

4.5.1. Governing equations of a full multi zone model

The model equations must govern changes of total volume-, zone volume-, in-cylinder pressure-, mixture composition-, in-cylinder temperature- and total mass. The total volume change was calculated based on the mechanical movement of a piston as discussed in Chapter 3 (see Equation 3.4).

By having the same pressure in each zone, the volume of each zone can be found from the ideal gas relation (see Equation 4.19)

$$\frac{V_k}{m_k R_k T} = \frac{V_{cyl}}{\sum_{k=1}^K m_k R_k T_k} \quad (4.19)$$

where V_{cyl} is the cylinder volume as calculated from the Equation 3.26. From Equation 4.19, the equation to govern the change in volume of each zone can be found from the derivative of V_k which is,

$$\frac{dV_k}{dt} = \frac{dV_{cyl}}{dt} \times \frac{m_k R_k T_k}{\sum_{k=1}^{N_z} m R T} + \frac{(V_{cyl})}{\left(\sum_{k=1}^{N_z} m_k R_k T_k \right)^2} \left\{ \left(\sum_{k=1}^{N_z} m_k R_k T_k \right) \left(m_k R_k \frac{dT_k}{dt} + m_k T_k \frac{dR_k}{dt} \right) \right. \\ \left. - \left(m_k R_k T_k \right) \left(\sum_{k=1}^{N_z} m_k R_k \frac{dT_k}{dt} + \sum_{k=1}^{N_z} m_k T_k \frac{dR_k}{dt} \right) \right\} \quad (4.20)$$

Equation 4.20 can be rearranged into Equation 4.24 through the following steps; (Equation 4.21 to Equation 4.23). Assuming uniform in-cylinder pressure, the ideal gas equation can be written as,

$$PV_{cyl} = \sum_{k=1}^{N_z} m_k R_k T \quad (4.21)$$

Therefore, the first term on the right hand side of Equation 4.20 is,

$$\frac{dV_{cyl}}{dt} \times \frac{m_k R_k T_k}{\sum_{k=1}^{N_z} m_k R_k T_k} = \frac{dV_{cyl}}{dt} \times \frac{m_k R_k T_k}{PV_{cyl}} \quad (4.22)$$

Considering the second term on the right hand side of Equation 4.20, based on Equation 4.21, the coefficient in front of the bracket can be re-written as,

$$\frac{(V_{cyl})}{\left(\sum_{k=1}^{N_z} m_k R_k T_k\right)^2} = \frac{1}{P \left(\sum_{k=1}^{N_z} m_k R_k T_k\right)} \quad (4.23)$$

Substituting Equations 4.22 and 4.23 into Equation 4.20 yields,

$$\frac{dV_k}{dt} = \frac{m_k}{P} \left[\frac{R_k T_k}{V_{cyl}} \times \frac{dV_{cyl}}{dt} + R_k \frac{dT_k}{dt} + T_k \frac{dR_k}{dt} - \frac{R_k T_k}{\sum_{k=1}^{N_z} m_k R_k T_k} \sum_{k=1}^{N_z} \left(m_k R_k \frac{dT_k}{dt} + m_k T_k \frac{dR_k}{dt} \right) \right] \quad (4.24)$$

To trace in-cylinder pressure, a derivative of the ideal gas equation (Equation 4.21) is used, (see Equation 4.25):

$$\frac{dP}{dt} = \frac{1}{V_{cyl}} \times \sum_{k=1}^{N_z} \left(m_k T_k \frac{dR_k}{dt} + m_k R_k \frac{dT_k}{dt} \right) - \frac{1}{V_{cyl}} \times \frac{dV_{cyl}}{dt} \times \sum_{k=1}^{N_z} (m_k R_k T_k) \quad (4.25)$$

The change in mixture composition is calculated with chemical kinetics formulation already discussed in Chapters 2 and 3. For a particular zone, the change in species concentration is,

$$\frac{dY_{k,j}}{dt} = \frac{\dot{\omega}_{k,j} W_j}{\rho_k} + \sum_{n=1}^{N_E} \frac{\dot{m}_n}{m} (Y_j^{cyl} - Y_j^{inlet}) \quad (4.26)$$

The second term on the right hand side of Equation 4.26 is always zero during IVC to EVO as there is no mass transferred across zone boundaries; (ie. neither mass transfer between zones nor blow-by out of the cylinder). The chemical production rate ($\dot{\omega}_{k,j}$) is found as described in Chapter 2.

The equation to govern temperature of each zone was derived from a zero-dimensional energy balance equation with heat transfer and boundary work transfer. For the k^{th} zone, the energy balance can be written as,

$$\frac{dU_k}{dt} = \frac{dQ_k}{dt} - P \frac{dV_k}{dt} \quad (4.27)$$

The internal energy of the k^{th} zone, U_k is calculated as the sum of the internal energies of all species:

$$U_k = \sum_{i=1}^{N_s} m_{k,i} u_{k,i} \quad (4.28)$$

The derivative of Equation 4.28 yields:

$$\frac{dU_k}{dt} = \sum_{i=1}^{N_s} \left(u_i \frac{dm_{k,i}}{dt} + m_{k,i} \frac{du_{k,i}}{dt} \right) \quad (4.29)$$

The rate of change of mass of the i^{th} species, $\frac{dm_{k,i}}{dt}$, is calculating using

$$\frac{dm_{k,i}}{dt} = m_k \times \frac{dY_{k,i}}{dt} \quad (4.30)$$

Considering the last term on the right hand side of Equation 4.27, the rate of change of volume of the k^{th} zone is replaced with Equation 4.24 and the rate of total internal energy is substituted by Equation 4.29. Therefore, the final equation to govern in-cylinder temperature change is,

$$\begin{aligned}
\frac{dT_k}{dt} = & -\sum_{i=1}^{N_s} u_i \frac{dY_i}{dt} - \frac{RT}{V} \times \frac{dV_{cyl}}{dt} - T \frac{dR}{dt} + \frac{RT}{\sum_{k=1}^{N_z} m_k R_k T_k} \\
& \times \sum_{k=1}^{N_z} \left(m_k R_k \frac{dT_k}{dt} + m_k T_k \frac{dR_k}{dt} \right) + \frac{dQ_k}{dt}
\end{aligned} \tag{4.31}$$

Finally, by applying the non-perfectly stirred mixture calculation (as described in Chapter 3), the original energy balance equation is modified to:

$$\begin{aligned}
\frac{dT_k}{dt} = & -\sum_{i=1}^{N_s} u_i \frac{dY_i}{dt} - \frac{RT}{V} \times \frac{dV_{cyl}}{dt} - T \frac{dR}{dt} + \frac{RT}{\sum_{k=1}^{N_z} m_k R_k T_k} \\
& \times \sum_{k=1}^{N_z} \left(m_k R_k \frac{dT_k}{dt} + m_k T_k \frac{dR_k}{dt} \right) + \left(\frac{dQ}{dt} - \tau \times m_{int} \overline{c_{p,int}} (T - T_{int}) \right)
\end{aligned} \tag{4.32}$$

4.5.2. Heat transfer

Figure 4-8 shows a schematic of heat transfer between the multiple zones and the chamber walls. The overall heat transfer can be classified into three main categories: 1) convection to the walls, 2) conduction from zone to zone, and 3) radiation from zones to walls. The total heat transfer for the k^{th} zone can be calculated as,

$$\dot{Q}_k = -\dot{q}_{convection} - \dot{q}_{radiation} + \dot{q}_{conduction} \tag{4.33}$$

General calculation of heat dissipation to the wall is the same as that used in the SZM (as described in Chapter 3). However, instead of using bulk temperature, the temperature at the boundary layers was used to calculate convection to the wall. In addition, the effects of engine knock were added to original convection model during combustion². This is important since an HCCI engine has very fast combustion and often operates at close-to-knock or marginal knock conditions. Engine knock changes the rate of heat loss as the insulating boundary layers are

² The basic Woschni correlation does not include the effects of engine as it was derived from normal operation in an SI engine.

disrupted by the knock pressure waves, leading to an increase in convection. (This was not done in the SZM as there was little variation in combustion rate, i.e., all mixtures burned too fast). The occurrence and severity of engine knock is related to the cylinder pressure rise rate so a knock correcting factor was developed as shown in Figure 4-9. This factor is applied to correct the convection heat transfer for fast combustion / knock effects, i.e., the constant c_2'' in Table 3-1 is multiplied by this factor during combustion. The correlation was developed based on careful analysis of the apparent heat loss for four experimental cases with different peak pressure rise rate in a methane HCCI engine.

Conduction between zones depends on a temperature gradient from zone to zone. To find a temperature gradient, a linear variation of temperature around zone boundaries is assumed. The total conductivity (Equation 4.34) is used to cover absent phenomena such as any turbulence or mass exchange effects [103, 104].

$$\lambda_{total} = \lambda_{lar} + \lambda_{tur} \quad (4.34)$$

The laminar conductivity is calculated from the mixture-averaged properties of ideal gas transport theory [110] (see Section 4.3), while the turbulent conductivity is estimated based on Yang's work [149] as being used in [103, 104]. The equation for evaluating turbulent heat conductivity is,

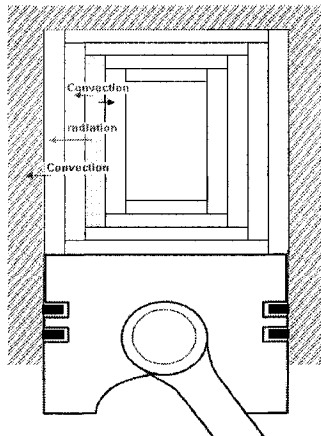


Figure 4-8: Schematic of heat transfer

$$\frac{\lambda_{tur}}{\lambda_{lar}} = \frac{Pr_{lar}}{Pr_{tur}} \times \frac{\mu_{tur}}{\mu_{lar}} \quad (4.35)$$

where $\frac{\mu_{tur}}{\mu_{lar}}$ is the ratio between the turbulent viscosity to the laminar viscosity and is calculated from,

$$\frac{\mu_{tur}}{\mu_{lar}} = \kappa y_n^+ [1 - \exp(-2\alpha\kappa y_n^+)] \quad (4.36)$$

As discussed in Chapter 1, turbulence does not significantly affect HCCI combustion behaviours although it may influence spatial heat transfer inside a cylinder. Therefore, instead of solving a fully integrating calculation of y_n^+ for each zone (which would take a significant amount of computational resources), for simplicity, y_n^+ is kept constant and is estimated from:

$$y_n^+ = \frac{u^*}{\mu_w} \int_0^{bore/2} \rho dy_n \quad (4.37)$$

Note here that the value of κ is 0.41, u^* is 0.06 and the characteristic velocity is assumed to be proportional to piston speed with a constant, v^* .

At this point, the multi-zone combustion model is fully described by the system of differential equations and could be solved by using the MATLAB ode15s solver as described in Section 3.5.2. This is referred to as a fully coupling solver (or sequential solver). The main advantage of that approach is that all the mixture properties can be traced without any adjustment at each time step. In addition, provided that the stiffness of the problem can be handled by the selected ODE solving technique, the results obtained from a sequential solver would ideally be the most accurate possible solution. However, the stiffness of a large system of ordinary differential equations leads to a combination of convergence failures, numerical inaccuracies and very long computation times. The alternative to a

sequential solver is to use a segregation technique, (as developed in the next section). The general principle of segregation techniques is to pre-solve a much smaller set of differential equations for each zone rather than considering all equations in all zones simultaneously.

4.6. Segregation solver

Some form of segregated solution technique is widely used to lower the computational time barrier to HCCI multi dimensional combustion modeling [90]. This section describes a new way to segregate the multi-zone HCCI modeling problem which is relatively simple for the case where a single zone model solution is already available. The flow chart of the segregation is shown in Figure 4-10.

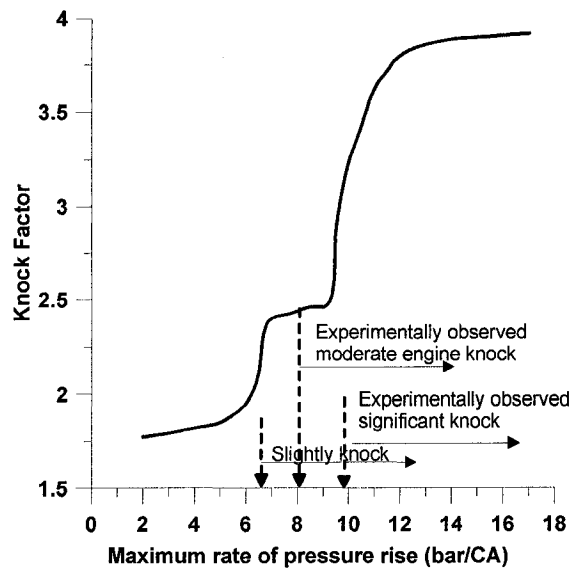


Figure 4-9: Correcting factor to heat transfer modeling for engine knock

4.5.1. Evaluating volume change rate of each zone:

A volume change rate of each zone is solved together with the rate of temperature change in each zone. Based on the differential equations discussed earlier, the system of linear equations to solve the rate of volume change in each zone and pressure change can be found as:

$$f_i = A_i - X_i - B_i X_{Nz+i} = 0, \quad i = 1 \rightarrow Nz \quad (4.38)$$

$$f_i = C_k - X_i + D_k X_k + E_k \sum_{j=1}^{Nz} m_j R_{ave,j} X_j = 0, \quad (4.39)$$

$$i = Nz + 1 \rightarrow 2 \times Nz \quad \text{and} \quad k = i - Nz$$

where f_i is the i^{th} function in the system of equations,

$$A_i = -\frac{1}{\rho_i c_v} \left(\sum_{j=1}^{Ns} u_j \dot{\omega}_j MW_j \right) + \frac{1}{m_i c_v} \times \left(\frac{dQ_i}{dt} - \beta m_{int,i} \bar{c}_{p,int} (T_i - T_{int}) \right) \quad (4.40)$$

$$B_i = T_i \times \frac{\sum_{j=1}^{Ns} x_j R_j}{m_i c_v} \quad (4.41)$$

$$C_k = \frac{m_k R_{ave,k} T_k}{\left(\sum_{j=1}^{Nz} m_j R_{ave,j} T_j \right)} \times \frac{dV}{dt} + \frac{V}{\left(\sum_{j=1}^{Nz} m_j R_{ave,j} T_j \right)} \times \left(m_k T_k \frac{dR_{ave,k}}{dt} \right) \quad (4.42)$$

$$- V \times \frac{m_k R_{ave,k} T_k}{\left(\sum_{j=1}^{Nz} m_j R_{ave,j} T_j \right)^2} \times \sum_{j=1}^{Nz} m_j T_j \frac{dR_{ave,j}}{dt}$$

$$D_k = \frac{Vm_k R_{ave,k}}{\sum_{j=1}^{Nz} m_j R_{ave,j} T_j} \quad \text{and} \quad E_k = -\frac{Vm_k R_{ave,k} T_k}{\left(\sum_{j=1}^{Nz} m_j R_{ave,j} T_j \right)^2} \quad (4.43)$$

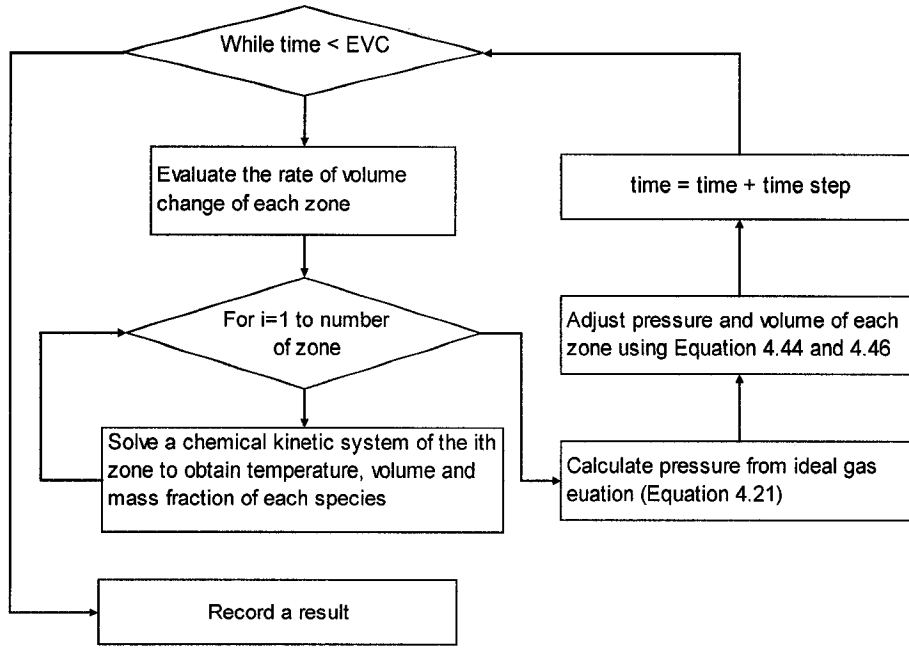


Figure 4-10 : An algorithm for segregating a MZM

The system of equations above was derived from the governing equations of a full multi-zone combustion model, (Equations 4.11, 4.12, and 4.15). The Successive Over Relaxation (SOR) method was adopted to solve the above system of equations. Note that the rates of temperature change (dT_k/dt) are the variables X_1, \dots, X_{Nz} and the rates of volume change (dv_k/dt) are the variables X_{Nz+1}, \dots, X_{2Nz} .

4.5.2. Adjusting pressure and volume of each zone:

Evaluating a single overall pressure and separate, unique volume for each zone explicitly leads to some error because the summation of zone volumes can be slightly different from the current chamber geometrical volume, $V(\theta)$. To prevent this mismatch from accumulating with time, the pressure and volume of each zone calculated by the ODE solver must be slightly adjusted to match the current cylinder volume. We assume that temperature and compositions in each zone are not changed due to the adjustment.

From,

$$P_o V_i^{old} = m_i R_{ave,i} T_i \quad (4.44)$$

and

$$PV_i^{new} = m_i R_{ave,i} T_i = P(V_i^{old} + v_i') \quad (4.45)$$

We can obtain,

$$(P_0 - P)V_i^{old} = Pv_i' \quad (4.46)$$

Summing Equation 4.46 yields,

$$\sum (P_0 - P)V_i^{old} = \sum Pv_i' = P\Delta v \quad (4.47)$$

Note that for Equations 4.44 to 4.47,

- P_0 = In-cylinder pressure obtained at each time step
- P = Adjusted in-cylinder pressure
- V_i^{old} = Volume of the i^{th} zone obtained at each time step
- v_i' = Volume correction of the i^{th} zone
- Δv = Total volume correction

Equation 4.47 is then used to calculate an adjusted pressure. Note that an adjusted volume of each zone can be found by substituting a new pressure into Equation 4.45. Using a segregation solver can substantially reduce computational time. The time reduction varies depending on the stiffness of the system of equations and can be up to roughly one order of magnitude, (see Figure 4-11).

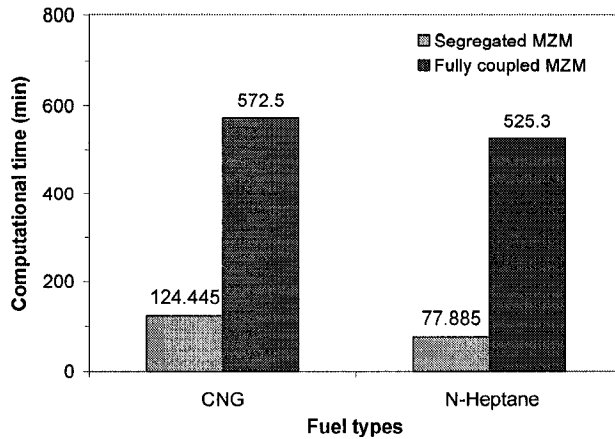


Figure 4-11 : A comparison of required computational time when using fully coupling and segregated solvers (on a 2.2GHz dual-core processor, AMD Opteron PC with 2.6GB RAM)

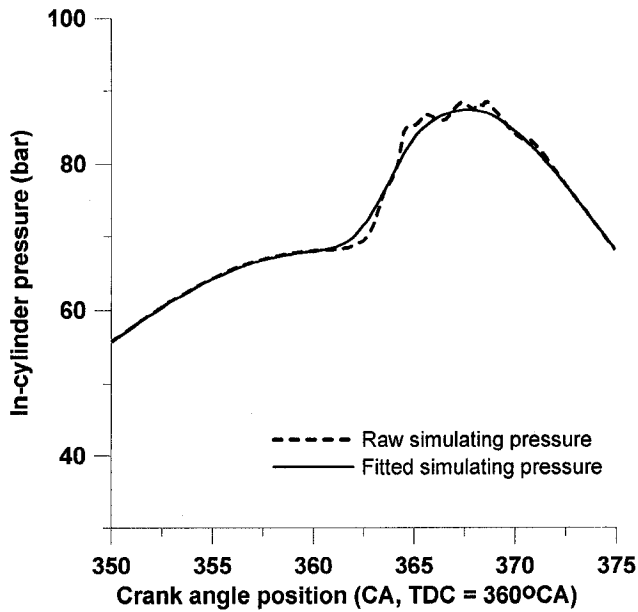


Figure 4-12: Comparison between raw and filtered pressure traces

4.7. Technique to Smooth Pressure Trace

The original pressure trace obtained from the simulation has an oscillatory behavior during the combustion process due to sequential combustion in a series of zones of finite size. The pressure trace is used to calculate a variety of

combustion-related engine parameters, including maximum rate of pressure rise. The pressure oscillations caused by finite zone volume are an undesirable artifact which would interfere with this calculation. To smooth the pressure, those oscillations were treated as high frequency noise and a low-pass signal filtering technique was adopted based on a triangular smoothing technique. The raw pressure trace obtained from the model was first interpolated to 100,000 data points. The smoothing width, (triangle half-width), was set to 800. Figure 4-12 shows a comparison between original and filtered pressure traces. It is notable that the filtered pressure accurately represents the original pressure data but without the noise artifact and is suitable for evaluating the maximum rate of pressure rise.

4.8. CHEMCOMB Multi Zone HCCI Model

The CHEMCOMB package also includes multi-zone combustion model (see the main structure in Figure 4-14), solved by both fully coupling and segregated solvers. Similar to the single zone combustion model (described in Chapter 3), the multi-zone model allows three input options: specifying intake valve closed conditions, specifying mass flow values and automatic operation based on a full engine cycle. The last option also provides an updated wall temperature for the next cycle, using an under-relaxation method to prevent divergence and accelerate convergence (see Equation 4.48).

$$T_{wall}^{(i+1)} = T_{wall}^{(i)} + \omega \times (T_{wall}^{(i+1)} - T_{wall}^{(i)}) \quad (4.48)$$

where ω is the under relaxation coefficient which was generally set to 0.75 . However, if the maximum rate of pressure rise exceeds 10.5 bars/CA at the first iteration, (indicating knock), the relaxation factor is set to 0.2 for the first iteration to prevent a sudden divergence.

The required inputs as well as in-code calculation of each option is the same as the ones used in SZM (explained in Chapter 3). Beyond these inputs, additional inputs are required to describe inhomogeneity. These parameters include:

- a ratio between characteristic velocity and piston speed,
- a ratio between temperature range at IVC and difference between hot residual and cool intakes and
- a number of zones which is specified by the number of layers.

For a multi-zone model solved with a segregation technique, additional information on time-step size must be specified. (Note that time step in this model is referred to as the step at which the properties are adjusted in Figure 4-11). The model allows users to set two different time steps with a factor to change from one step to another. Two time steps must be specified because calculations must be more frequent at higher temperature where changes in zone properties (due to chemical reactions) occur more rapidly. The coarse-to-fine-time-step ratio is arbitrarily set to 6.67. The magnitude of each time step was justified by comparing a segregated result with that time step to an original MZM result with a fine time step. Figure 4-13 shows that the suitable time steps are 2×10^{-4} S for a coarser step size and 3×10^{-5} S for a finer step size and too large time step could lead to divergence. Because it achieves equivalent results to the fully coupled MZM but with much less computational time, the segregated multi-zone model has been used throughout the rest of this study.

To summarize input requirement, Figure 4-15 to Figure 4-17 are the examples of the input files for the three input options. For the segregation solver, step size is the only additional information required. Note that the segregated MZM uses the same MATLAB built-in solver function as the SZM, (ode15s).

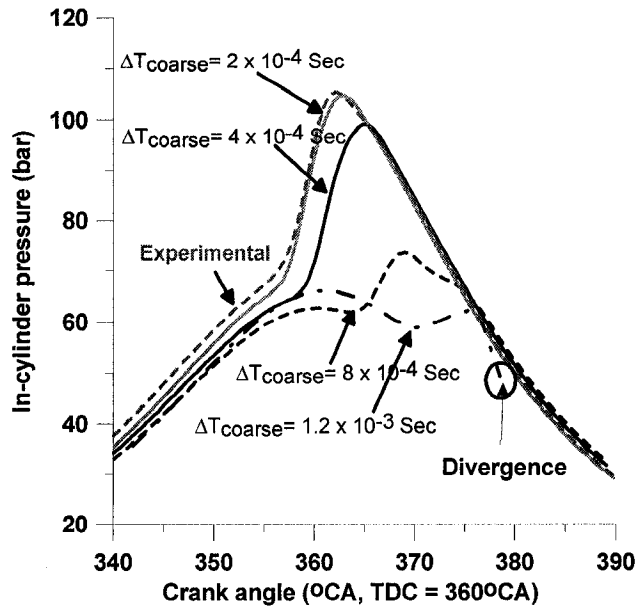


Figure 4-13 : Effects of segregating time step to HCCI pressure trace of a methane engine

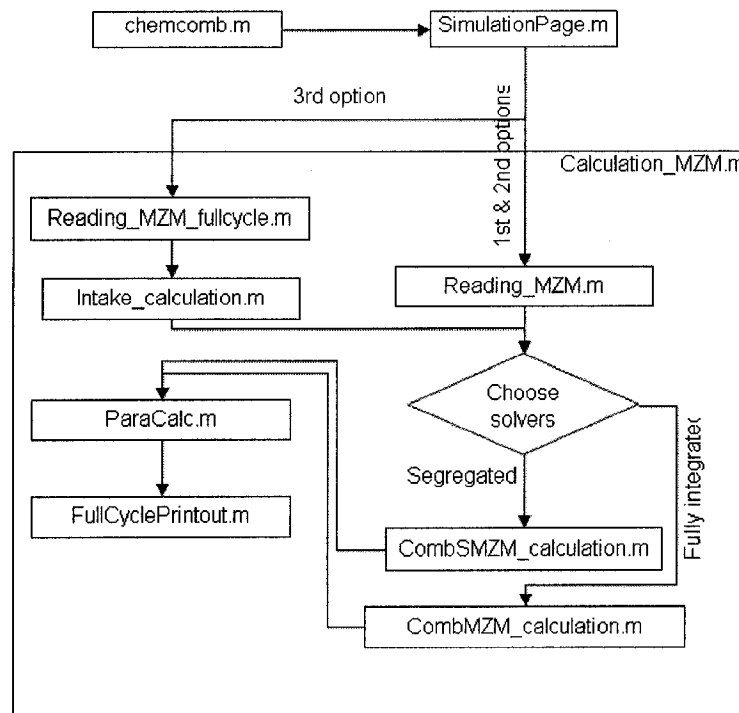


Figure 4-14 : Main structure of Mingle zone calculation in CHEMCOMB (the names in the chart referred to Appendix C)


```

! Input file for CHEMCOMB model
!
Fuelselection
!
Fuel composition = CH4,0.965/C2H6,0.019/CO2,0.008/N2,0.008
RG compositions = H2,0.75/CO,0.25
% RG = 10.796
Equivalence ratio = 0.57937
Mixture temperature = 413.15
!
Specification
!
CR = 19.50
Bore = 8.26
Stroke = 11.43
Connecting rod = 25.40
!
Conditions (working conditions)
!
Ns = 800.0000
Tw (Wall) = 380.895
Tw (Crown) = 380.895
Tw (Piston) = 380.895
Treact = 500.0000
Heat transfer factor (compression) = 2
Heat transfer factor (expansion) = 2
Knock Factor = 2
beta = 31
Characteristic velocity factor = 0.032
!
Time Descretization
!
Coarsing time-step = 0.0002
Refining time-step = 3e-005
Refining factor = 1.035
Coarsing factor = 1.1
!
Initial Conditions
!
IVC pressure (MPa) = 0.1519
IVC temperature (K) = 421.173
%EGR = 41.218
Exhaust pressure (MPa) = 0.142
Exhaust temperature (K) = 505.706
Coolant temperature (C) = 100.287
!
Inhomogeneity
!
Number of layers = 4
Temperature difference = def
% Residual inhomogeneity = 5
Factor to set dT = 2.2
Volume distribution scheme = 3
! (1 = Equal mass distribution, 2 = Equal Volume distribution, and 3 = Normal
distribution)
!
Recorded species
!
Species = H2O
!
Products
!
products = Complete
!
Valve Input File
!
File name (in ValveProfile folder) = CFRvalveProfile.xls
!
! Note this is the input

```

Figure 4-15: Example of an input file for a single zone model option 1 (Specify IVC condition)

```

! Input file for CHEMCOMB model
!
Fuelselection
!
Fuel composition = CH4,0.965/C2H6,0.019/CO2,0.008/N2,0.008
RG compositions = H2,0.75/CO,0.25
Fuel mass flow (g/s) = 0.0865
RG mass flow (g/s) = 0.01132
Air mass flow (g/s) = 2.4983
Mixture Temperature (K) = 413.15
!
Specification
!
CR = 19.50
Bore = 8.26
Stroke = 11.43
Connecting rod = 25.40
!
Conditions (working conditions)
!
Ns = 800.0000
Tw (Wall) = 380.895
Tw (Crown) = 380.895
Tw (Piston) = 380.895
Treact = 500.0000
Heat transfer factor (compression) = 2
Heat transfer factor (expansion) = 2
Knock Factor = 2
beta = 31
Characteristic velocity factor = 0.032
!
Time Descretization
!
Coarsing time-step = 0.0002
Refining time-step = 3e-005
Refining factor = 1.035
Coarsing factor = 1.1
!
!
Initial Conditions
!
IVC pressure (MPa) = 0.1519
%EGR = 41.218
Exhaust pressure (MPa) = 0.142
Exhaust temperature (K) = 505.706
Coolant temperature (C) = 100.287
!
Inhomogeneity
!
Number of layers = 4
Temperature difference = def
% Residual inhomogeneity = 5
Factor to set dT = 2.2
Volume distribution scheme = 3
! (1 = Equal mass distribution, 2 = Equal Volume distribution, and 3 = Normal
distribution)
!
Recorded species
!
Species = H2O
!
Products
!
products = Complete
!
Valve Input File
!
File name (in ValveProfile folder) = CFRvalveProfile.xls
!

```

**Figure 4-16: Example of an input file for a single zone model option 2
(Specify mass flow rate)**

```

! Input file for CHEMCOMB model
!
Fuelselection
!
Fuel composition = CH4,0.965/C2H6,0.019/CO2,0.008/N2,0.010
RG compositions = H2,0.75/CO,0.27
% RG           = 10.796
Equivalence ratio = 0.57937
!
Specification
!
CR           = 19.50
Bore         = 8.26
Stroke       = 11.43
Connecting rod = 25.40
!
Conditions (working conditions)
!
Ns           = 800.0000
Tw (Wall)    = 383.143
Tw (Crown)   = 383.143
Tw (Piston)  = 383.143
Treact       = 500.0000
Heat transfer factor (compression) = 2.05
Heat transfer factor (expansion)   = 2.05
Knock Factor = 1.7
beta         = 34
Characteristic velocity factor = 0.032
!
Time Descretization
!
Coarsing time-step = 5e-005
Refining time-step = 1.5e-005
Refining factor = 1.035
Coarsing factor = 1.1
!
Initial Conditions
!
Intake manifold pressure      = 0.1432
Exhaust manifold pressure    = 0.141649
Pressure @ IVO = 0.138
Intake manifold temperature   = 413.15
Exhaust temperature = 451.2
%EGR           = 41.218
Coolant temperature (C) = 100.287
!
Inhomogeneity
!
Number of layers = 4
Temperature difference = def
% Residual inhomogeneity = 5
Factor to set dT = 2.2
Volume distribution scheme = 3
! (1 = Equal mass distribution, 2 = Equal Volume distribution, and 3 = Normal
distribution)
!
!
Recorded species
!
Species = H2O
!
Products
!
products = Complete
!
Valve Input File
!
File name (in ValveProfile folder) = CFRvalveProfile.xls
!
! Note this is the input

```

Figure 4-17: Example of an input file for a single zone model option 3 (Full engine cycle)

4.9. Model performance

This section investigates the performance of the segregated multi-zone combustion model on both methane and heptane fuelled HCCI engines. For a 400 RPM methane fuelled HCCI engine, the simulation was tested by an engine fuelled with 0.25 to 0.5 equivalence ratio and 0 to 20% of the fuel mass replaced by reformer gas (RG) blending. The amount of external EGR was varied from 0% to 40%. The heptane engine was set to operate at 800 RPM with equivalence ratio 0.21 to 0.55. The list of operating conditions for the validating cases can be found in Appendix D. Note that these tested conditions were chosen based on the availability of valid experimental information for comparison. The specification of the methane fuelled- and heptane fuelled engines are the same as those in Chapter 3.

Model validation based on comparison of cylinder pressure traces and important engine parameters is discussed in Section 4.9.1 and Section 4.9.2. Additionally, the student's t-test has been used to evaluate the difference between mean values obtained from experiment and simulation at a 95% confidence level

4.9.1. Model performance in capturing in-cylinder pressure history

The modeled results were compared with experimental pressure traces drawn from engine tests at the same operating conditions addressed above. Experimental traces were selected from a sample of 100 consecutive cycles after eliminating traces which had knock oscillations in the peak pressure. Of the remaining cycles, the median peak pressure cycle was selected to avoid arguments about cyclic variation, (which is not negligible near the limits of acceptable combustion).

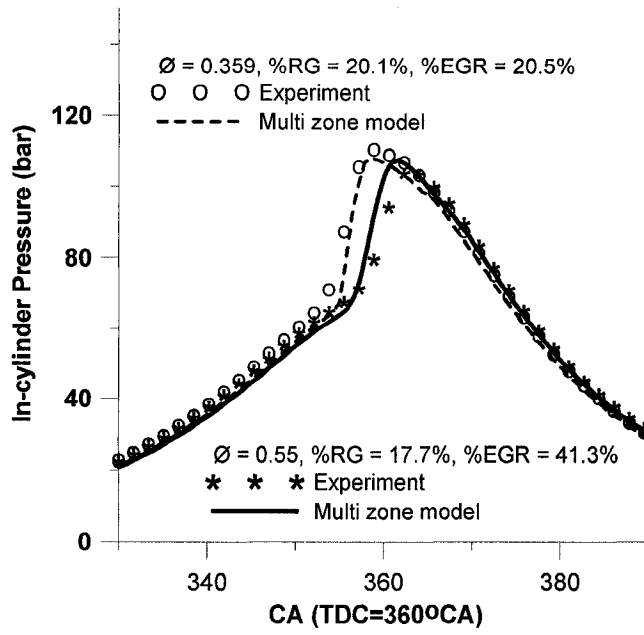


Figure 4-18 : Comparison of pressure histories from a methane fuelled HCCI engine operating with two different conditions

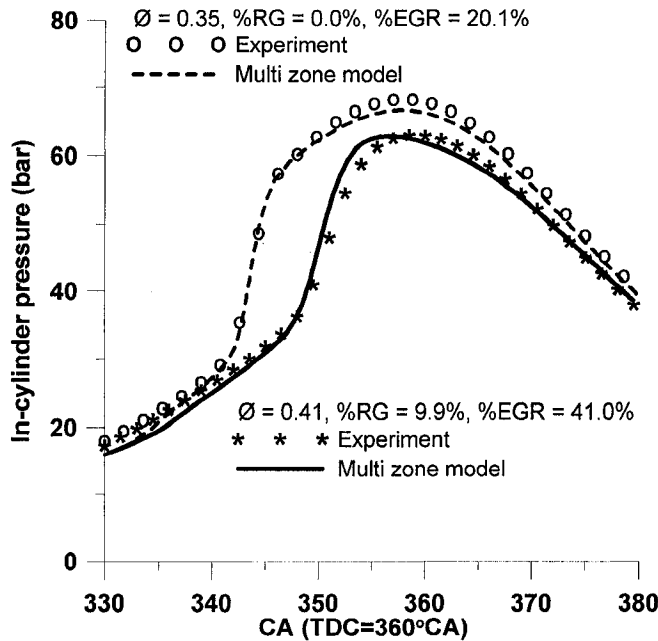


Figure 4-19 : Comparison of pressure histories from n-heptane fuelled HCCI engine operating with two different conditions

Figure 4-18 and Figure 4-19 provide examples of pressure traces for heptane- and methane- fuelled HCCI engines. It can be seen that the multi-zone model accurately captures the in-cylinder pressure development during the compression, combustion and expansion periods over a range of conditions for both engines. In particular, the model can capture the behaviors not available from the SZM, i.e., peak pressure and combustion rate. The improvement over a single zone model is mainly due to the realistic levels of in-homogeneity which give a significant increase in combustion duration and a more accurate distribution of temperatures during the expansion period. Because the model can accurately predict both combustion behavior and engine parameters provides a good confidence in using the model to investigate parameter effects and decide a better technique to control HCCI engines.

While matching a pressure trace is a good test of a combustion model, the real objective is to model combustion behaviors and engine performance with HCCI operation. Therefore, validation of the model on specific parameters is vital. Regression analysis and statistical correlation have been adopted to measure the model's ability to capture experimental trends.

The statistical correlation coefficient is used to quantitatively measure how well the simulation follows experimental trends. The correlation coefficient is calculated from the normalized covariance function (Equation 4.50),

$$R(i, j) = \frac{C(i, j)}{\sqrt{C(i, i)C(j, j)}} \quad (4.50)$$

where $C(i, j)$ is the covariance function of the two sets of data whose elements are indicated by i and j .

Parameters of interest include start of main combustion (SOC), indicated mean effective pressure (IMEP), maximum pressure and the maximum rate of pressure rise ($dP/d\theta_{\max}$). SOC represents combustion timing while IMEP represents the

engine. Peak pressure is a key parameter for engine design. Maximum pressure rise rate is an indicator of knocking tendency.

4.9.2. Model performance in capturing important engine parameters

In this study, SOC was defined as the point where rate of pressure rise is maxima. It is important to note that experimental values presented here were those for the cycle with median peak pressure timing. The values obtained from that specific cycle are used for consistency, i.e., the median IMEP could result from a different cycle from the median peak pressure cycle and it could bias the comparison to base each correlation on a different cycle .

Figure 4-20 and Figure 4-21 indicate the excellent performance of the MZM in predicting SOC of both engines over the range of validating cases. A regression fit slope of 1.0 would be ideal and the fitted slopes are 1.06 (for methane) and 0.97 (for heptane). Some variation between simulating and experimental results can be noticed due to the experimental fluctuation. For example, Figure 4-22 shows that the model accurately predicts the trend of advancing SOC timing when methane is replaced by RG for a HCCI engine. The experimentally obtained values follow the same trend as the model but with significant fluctuations in the measured values.

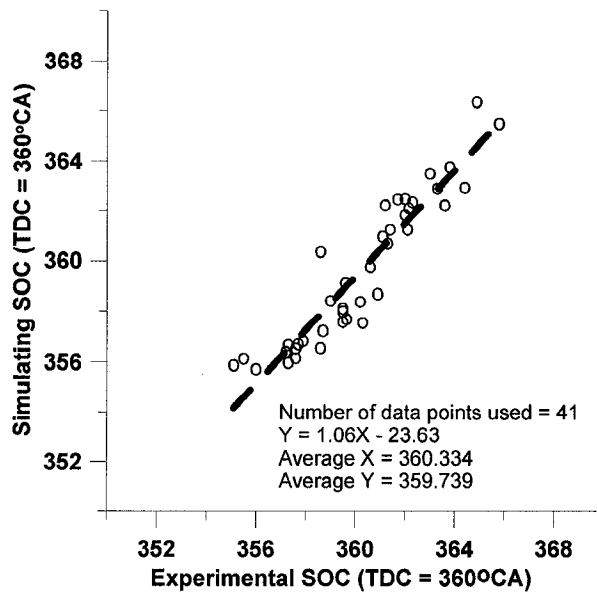


Figure 4-20 : Prediction of the start of main combustion from a CNG engine

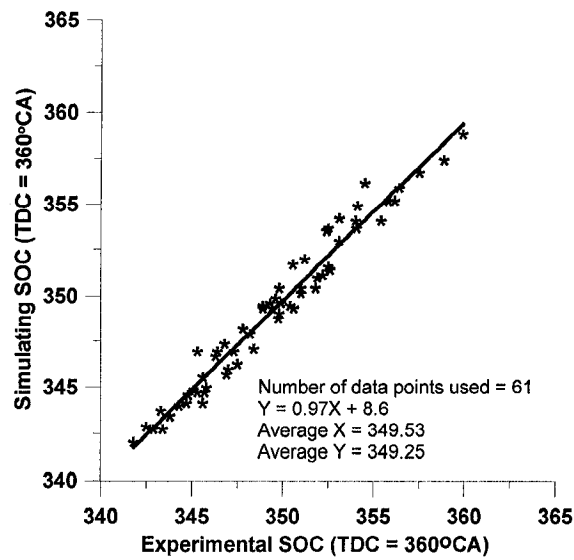


Figure 4-21 : Prediction of the start of main combustion from a heptane engine

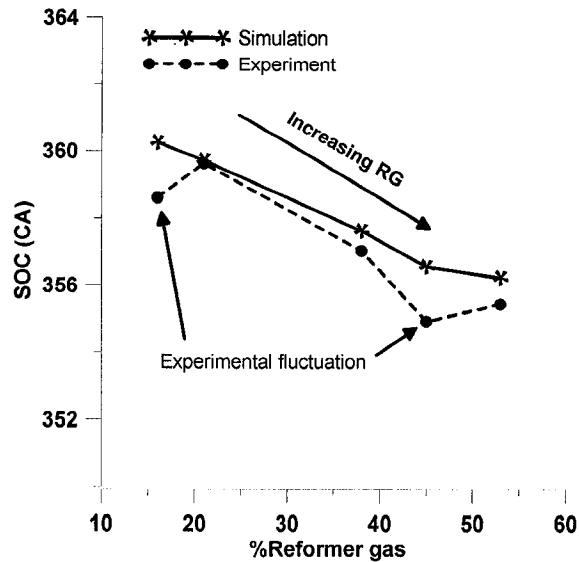


Figure 4-22 : Example of experimental fluctuations captured by a model (The five cases were performed in a 470 rpm CNG-HCCI engine with $\phi \sim 0.37$, %EGR $\sim 5\%$, $T_{int} = 413.15K$ and $P_{int} = 0.92$ bars)

In comparison with SOC prediction, the model provides less accurate but still reasonable results for other engine parameters, e.g. Figure 4-23 and Figure 4-24. There are three main reasons. First, marginal changes in pressure history over compression or expansion periods can greatly influence both IMEP and SFC, i.e., 1% change in expansion pressure could cause 10% difference in IMEP. Second, there are always some experimental fluctuations as discussed earlier. Finally, the experimental uncertainty during combustion is difficult to capture especially when there is no any arbitrary fitting correlation, i.e., Wiebe function, to fit the model to the experiment. With this in mind, the main objective is to produce a model which can capture the result produced by changing a controllable parameter (within a reasonable magnitude). The correlation coefficient was adopted to measure the relationship between experimental and simulating results.

Figure 4-25 and Figure 4-26 show an excellent performance of a model on capturing the trends of pressure related parameters, i.e., peak pressure and maximum rate of pressure rise. The simulation results are more than 90% correlated to the experiment. The agreement between simulations and experiments on integrated parameters, such as IMEP and efficiency, is somewhat lower, (see

Figure 4-27 and Figure 4-28 for the reasons mentioned above. Additionally, prediction of the amount of fuel inducted into a cylinder from 1D isentropic flow may differ from that of a real engine, which further magnifies the uncertainty for efficiency.

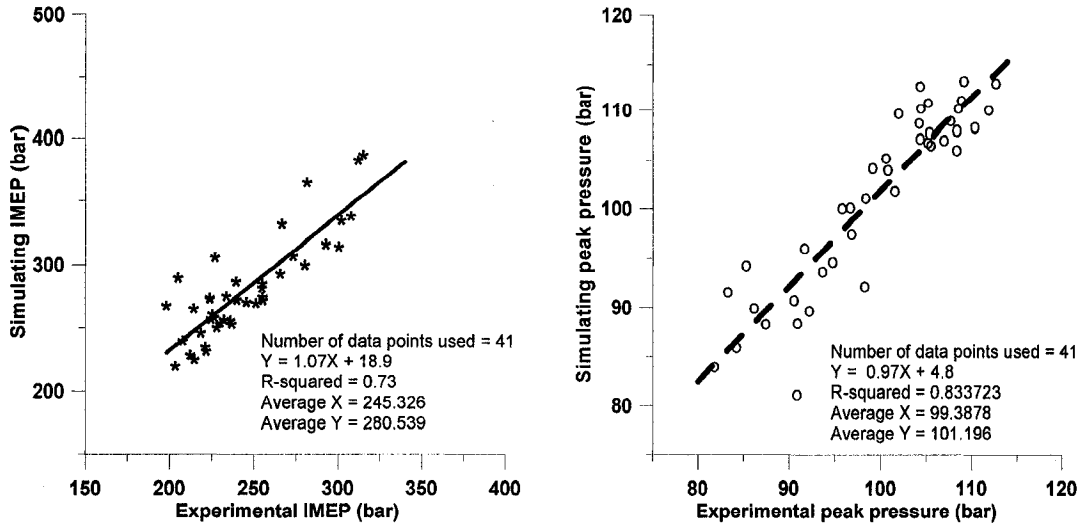


Figure 4-23 : Example of MZM performance on some engine parameters from a CNG engine

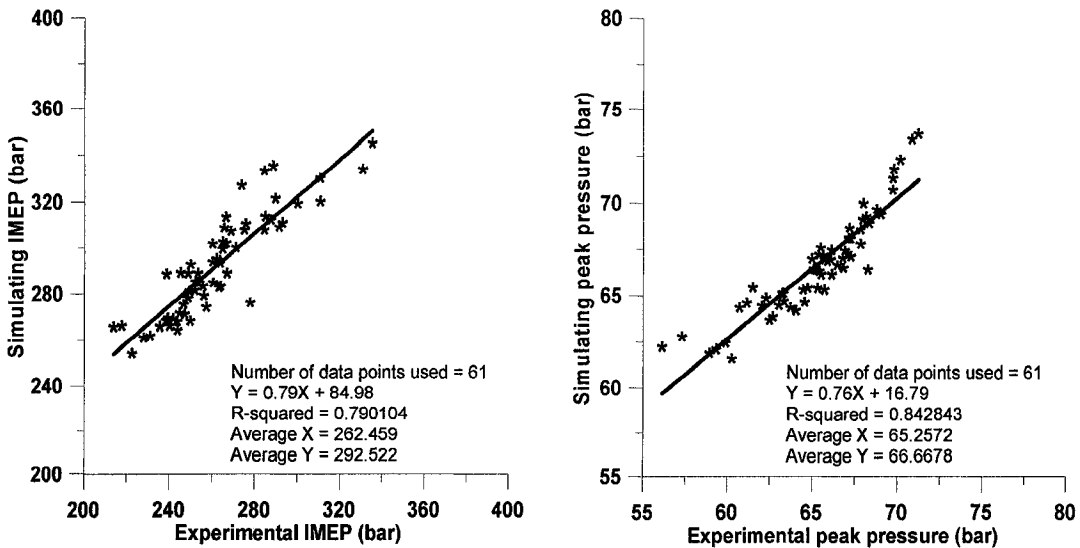


Figure 4-24 : Example of MZM performance on some engine parameters from a heptane engine

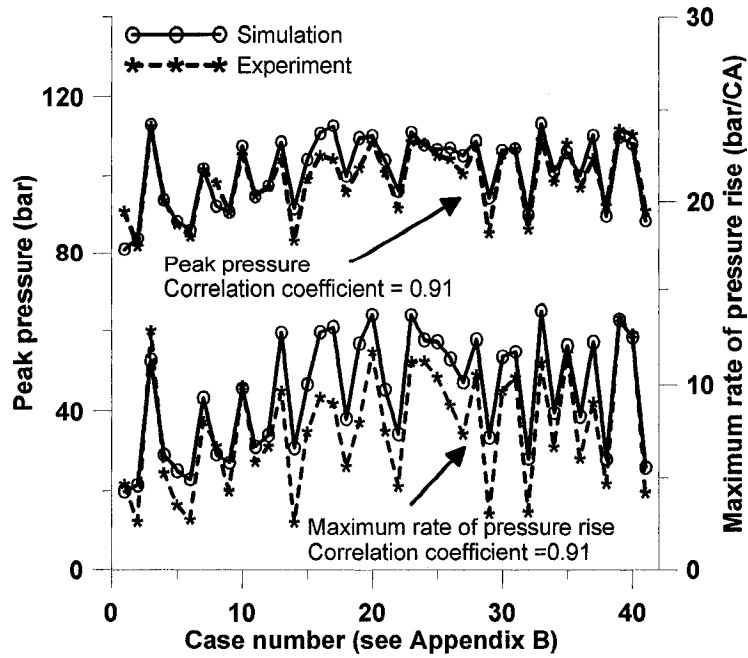


Figure 4-25 : Performance of MZM on capturing the trends of pressure related parameters of a CNG engine

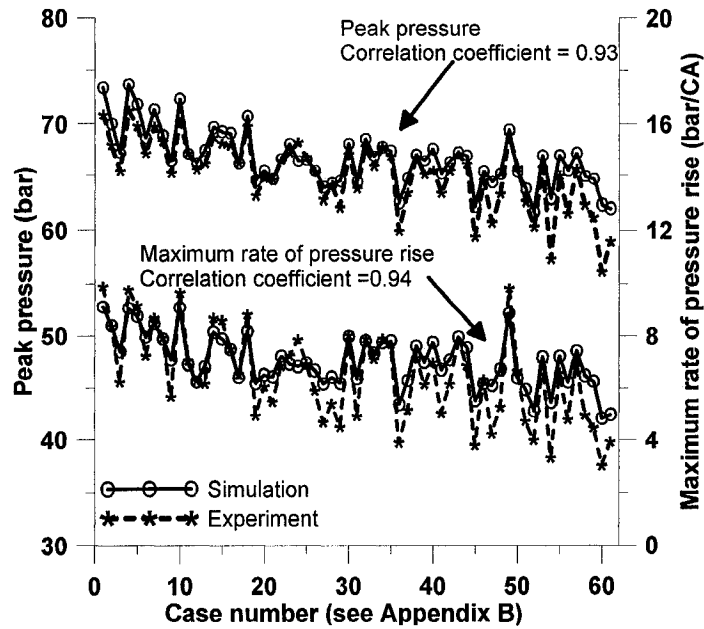


Figure 4-26 : Performance of MZM on capturing the trends of pressure related parameters of a heptane engine

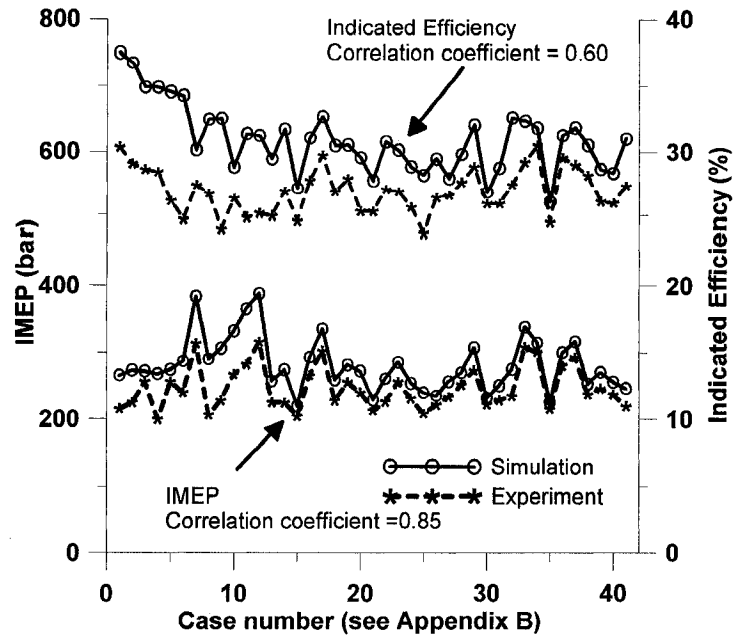


Figure 4-27 : Performance of MZM on capturing the trends of engine performance parameters of a CNG engine

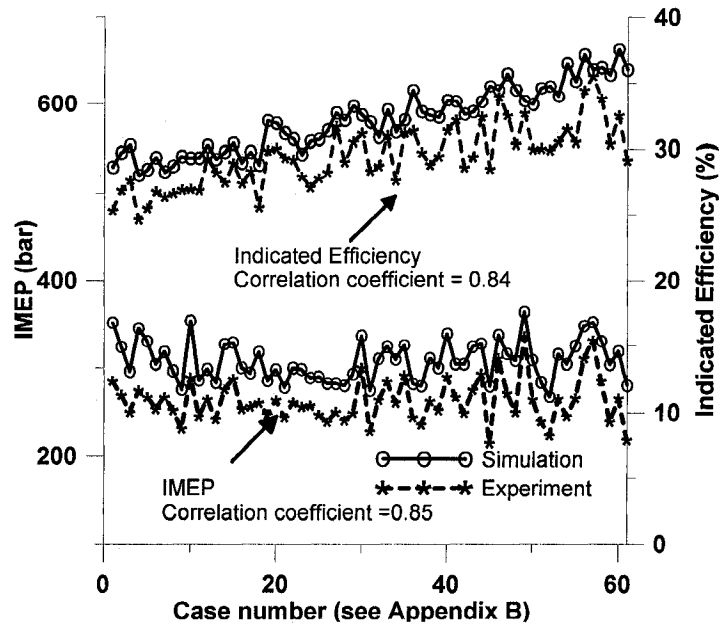


Figure 4-28 : Performance of MZM on capturing the trends of engine performance parameters of a heptane engine

The main purpose of the model, which is to capture the changes of HCCI combustion caused by changes of controllable input parameters, is met as seen from the correlation coefficient values. The enhanced accuracy compared with the SZM is attributing to realistic characterization of the non-homogeneous mixture during combustion. Because it has a realistic combustion period, the MZM calculates a reasonably accurate IMEP value and the trend of IMEP, peak pressure, maximum rate of pressure rise and efficiency is predicted accurately when a variety of input parameters are changed. The novelty of the model is that, because it predicts wall temperature and heat transfer, it can give a reasonable prediction without case-by-case adjustments.

4.10. Summary

As the mixture inside an engine operating with the HCCI technique is not absolutely “homogeneous”, the multi-zone model described here accounts for that inhomogeneity, especially at the end of compression. The major concepts of the multi-zone model developed in this chapter are similar to the models developed by other researchers: mixtures in each zone are assumed to be homogeneous ideal gas with temperature and composition varying from zone to zone while pressure is uniform across the combustion chamber. Beyond these major concepts, several new features have been included in this work. Those features include 1) the method of setting the initial conditions, 2) a new derivation for the model, 3) a modified heat transfer calculation which includes variable wall temperature, grey gas radiation heat transfer and the effects knock and 4) the alternative segregation technique which speeds calculations.

In order to confidently use the model for further investigation on an HCCI engine, the model’s performance was validated with a range of different mixture compositions and operating conditions for both methane and heptane fueled engines. For a methane engine, the range covered equivalence ratio = 0.4 to 0.6, %RG = 0 to 25% and % EGR = 0 to 30%. For a heptane engine the range covered

equivalence ratio = 0.21 – 0.55, %RG = 0% - 30% and %EGR = 0% - 40%. The results of this validation showed that pressure histories obtained from the model are in a good agreement with experimental pressure traces, including a range of characteristic shapes. Consequently, good predictions were obtained for combustion timing, peak pressure, maximum pressure rise rate, IMEP and indicated efficiency. This is a significant development for HCCI modeling and design since it allows researchers to predict the behavior of HCCI combustion engines with some confidence and to study the influence of controllable parameters on HCCI engine performance.

5 The Effects of Changing Mixture Composition Parameters on Heptane- and Methane-HCCI combustion

The earlier chapters have described the development and verification of the models for predicting HCCI engine characteristics over a range of operating conditions without any arbitrary adjustment of key parameters such as initial temperature or mass loss. This chapter focuses on the application of the model to investigate the effects of changing mixture composition by different means.

It is widely recognized that a slight change in a matrix of operating parameters could lead to a significant change in combustion behavior, especially when an engine operates at the edge of a good combustion region. This is primarily because HCCI combustion relies on mixture auto-ignition initiated at certain conditions in which environmental energy exceeds activation energy. Additionally, the auto-ignitibility of mixtures is also varied when the composition of fuel-air-additive-EGR change, (i.e., the activation energy changes). Even though only one parameter in a controllable parameter matrix is altered, a change in combustion behavior results from several factors affecting mixture properties and in-cylinder environment. For example, consider two operations where the mixtures have different Air/Fuel Ratios (AFR). The mixtures have different compression temperature histories (thermodynamic effect) and auto-ignite at different temperatures (chemistry effects). In addition, the richer mixture has higher peak temperature, causing combustion chamber wall temperature to be higher (in-cylinder environment effect).

In this study, the effects on HCCI due to changing operating parameters are classified in three categories: 1) thermodynamic, 2) chemistry and 3) environmental (wall temperature). The intent of this chapter is to identify the most influential effects on HCCI combustion when the mixture composition is adjusted

in four different ways: ϕ , %RG, %external EGR and %internal EGR. The numerical investigation was generally done on the cases that were confirmed by the experiments. However, the control system on the experimental engine is not sufficient enough to provide good operating points in which only external EGR changes in a methane HCCI engine. In addition, the engine does not have a variable valve timing system capable of controlling internal EGR content. Therefore, the investigation on such cases was done without experimental confirmation. However, as the model can predict HCCI combustion over a range of operations that have different external EGR fractions and initial mixture temperatures, the level of confidence is considerably high.

5.1 Measures of In-cylinder Environment, Thermodynamic and Chemistry Properties with Changing Mixtures

As in most aspects of HCCI combustion, there were several properties and parameters that could be chosen to represent the in-cylinder environment, thermodynamic and chemistry effects of changing HCCI mixtures.

- The effective wall temperature was chosen as a good measure of the change in in-cylinder environment because it is sensitive to changes in combustion and it directly influences the conditions for combustion.
- The ratio of specific heats ($k = C_p/C_v$) was chosen to illustrate the thermodynamic property effects because it is a direct consequence of changing mixture composition and has a strong effect on mixture temperature rise during compression. It is important to note that ratio of specific heats is also a function of mixture temperature, which is interrelated to the effects of changing in-cylinder environment and chemistry. Therefore, in order to illustrate the pure effects from thermodynamic property change, the ratio of

specific heat (k) is plotted against mixture temperature, i.e., k is considered at a particular temperature, rather than looking at k history during compression.

- The chemistry effects of changing mixture composition could be characterized by the concentration of a radical species like H_2O_2 or by a measure of the early temperature rise.

In the single-stage auto-ignition process of high octane number fuels such as CNG, a rise in H_2O_2 concentration is an early indicator of pre-flame reactions, preceding the sharp rise of OH radicals that occurs with the actual auto-ignition (see Figure 5-1). An increase in H_2O_2 radical density at a lower temperature would infer that composition changes were affecting the pre-flame reaction chemistry. However, when investigation include both low and high octane number fuels, using the H_2O_2 indicator could be troublesome as different mixture composition changes simultaneously affect temperature and chemistry differently for high octane and low octane fuels. This is primarily because the low octane fuel mixtures exhibit low-temperature cool-flame and pre-flame mechanisms which release a significant amount of heat at low temperature and this heat release contributes significantly to the auto-ignition at a relatively low radical concentration.

Considering this difference in radical contribution to auto-ignition a measure of early temperature rise was judged more appropriate to measure chemistry effects over a range of mixture octane numbers.

- Therefore, the "rate of temperature rise at a specified mixture temperature" ($dT/d\theta @ T$) was chosen to indicate the chemistry effect of mixture changes on HCCI combustion.

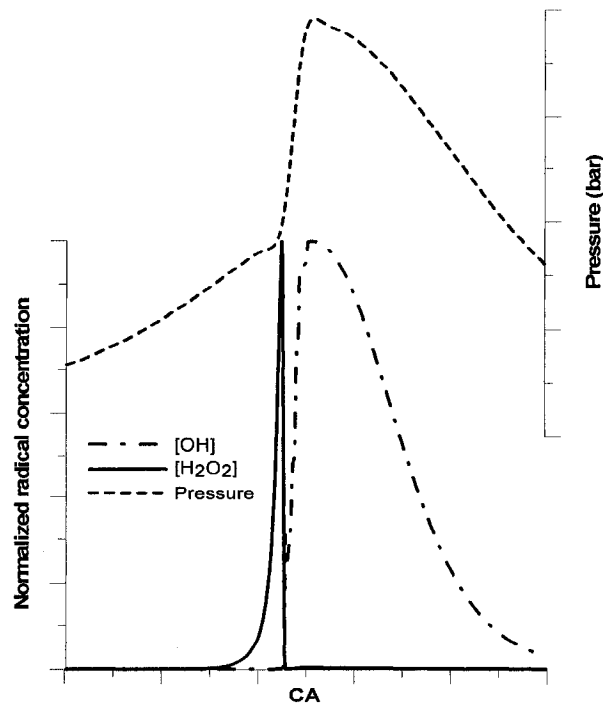


Figure 5-1 : Timing of H_2O_2 and OH concentration changes at the time of CNG ignition

The rate of temperature rise depends on three factors: 1) mixture chemistry, 2) compression rate and 3) heat transfer. To specifically isolate chemistry effects using “ $dT/d\theta @ T$ ”, the tests need to be done on an engine which has the same speed and wall temperature, assuming that heat transfer for a fixed wall-temperature engine is approximately identical. Then, for a given mixture temperature, a faster temperature rise indicates that the pre-flame chemistry has become more exothermic, leading towards earlier auto-ignition, i.e., that the mixture octane number is reduced.

5.2 Equivalence Ratio Effects on HCCI Combustion

Figure 5-2 and Figure 5-3 show both simulations and experimental pressure traces of CNG- and heptane- HCCI engines respectively. As the mixture equivalence ratios are increased, the gross effect is that SOC timing is advanced and pressure is increased for both CNG- and heptane-fuelled engines. However, the advance might be attributed to different factors as changing ϕ progressively

affects all three factors: wall temperatures, thermodynamic properties and mixture chemistry. Having more fuel increases engine power and maximum rate of pressure rise, resulting in hotter engine wall temperature and hotter residual gas temperature. At the same time, it directly changes both thermodynamic and chemical properties of the mixtures.

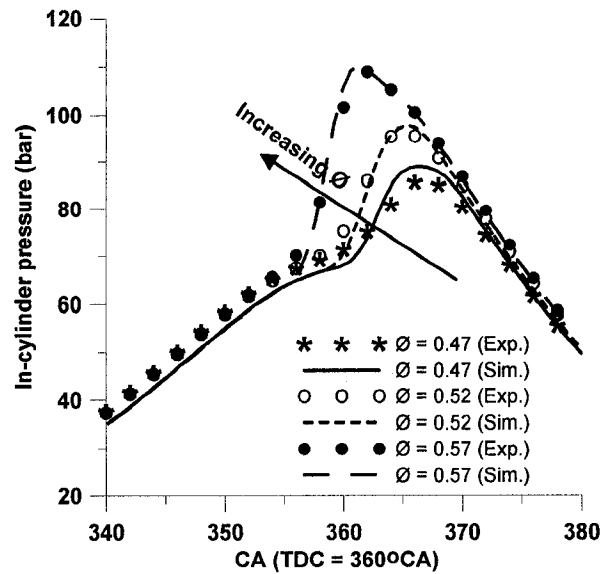


Figure 5-2 : Pressure histories from a CNG engine operating with different ϕ mixtures

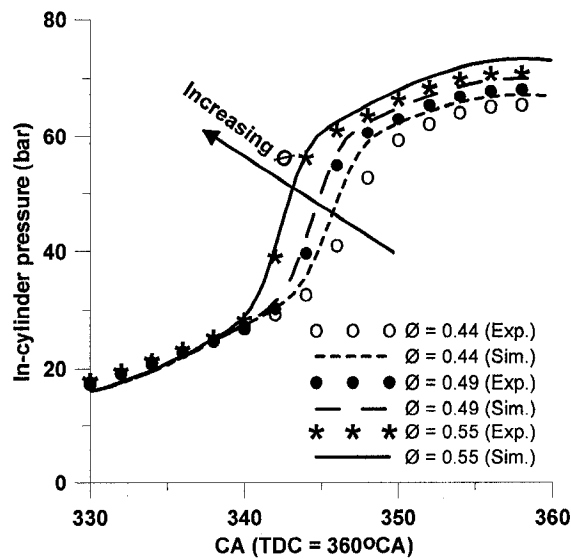


Figure 5-3 : Pressure histories from a heptane engine operating with different ϕ mixtures

Changes in wall- and IVC- temperatures with increasing ϕ have been plotted in Figure 5-4 (for a methane engine) and Figure 5-5 (for a heptane engine). Increasing mixture energy content leads to generally hotter wall temperatures, especially when knock intensity surpasses the intermediate level ($dP/d\theta_{\max} > 8.75\text{-}9$ bar/CA), leading to much higher peak pressure and advancing SOC, (see the CNG case as ϕ changes from 0.52 to 0.57). Nevertheless, IVC temperature is only slightly changed until the knock becomes significant. This is due to a balance between hot internal residual and temperature-controlled intake charge.

While altered in-cylinder environment can already explain the trend direction of advancing SOC timings with increasing ϕ , the contribution due to changes in thermodynamic- and chemical properties of the mixtures must also be investigated.

Figure 5-6 and Figure 5-7 show the effects of ϕ on thermodynamic properties of CNG/air mixtures. The fuel and combustion product molecules (heptane/methane, CO_2 and H_2O) are generally larger than air molecules, so increasing fuel quantity lowers the specific heat ratio during compression and would thus reduce the compression temperature. (Based on an air standard cycle, a 0.005 reduction in k value through the compression can lower compression temperature by more than 20 K depending on initial temperature and engine geometry). Therefore, if only thermodynamic effects were considered, richening the mixtures would tend to retard SOC timing. This is the opposite of the results obtained from both experiment and modeling so it is clear that the thermodynamic effect is dominated by other effects for both CNG and heptane HCCI engines when equivalence ratio, ϕ , is varied.

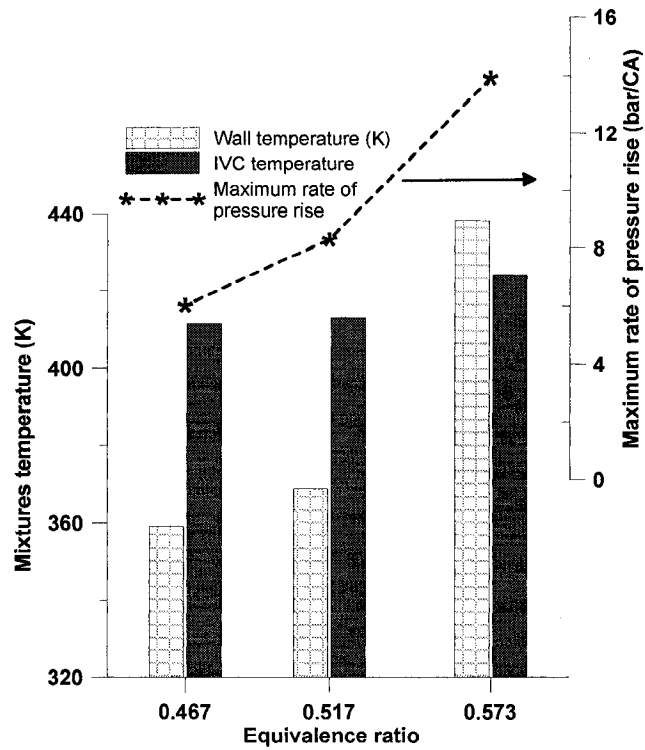


Figure 5-4 : Wall- and IVC- temperatures of a CNG engine with various ϕ mixtures

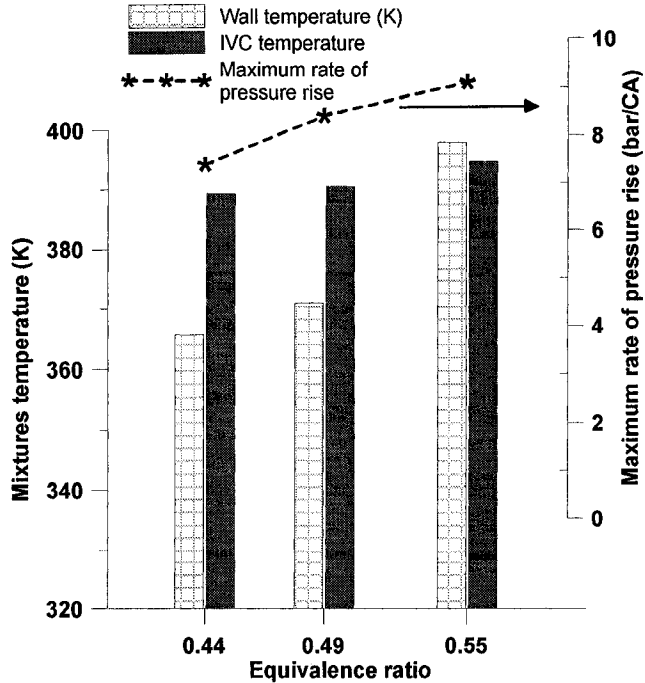


Figure 5-5 : Wall- and IVC- temperatures of a heptane engine with various ϕ mixtures

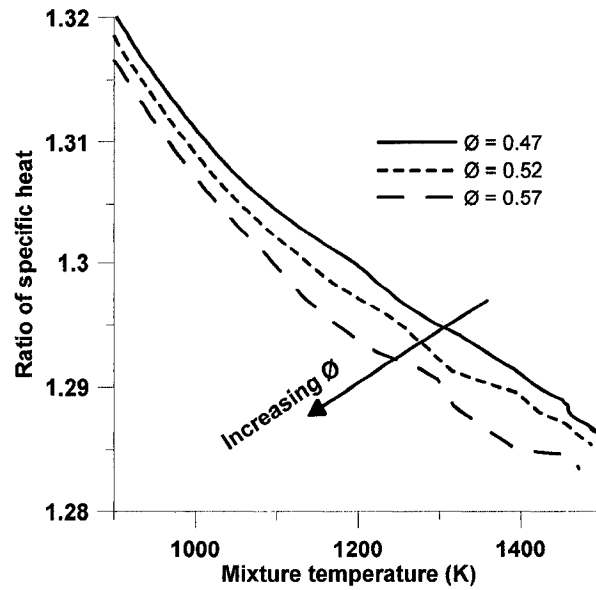


Figure 5-6 : Variation of specific heat ratio, k , in a CNG-fueled engine with different ϕ . (These k values are weighted average of multiple zones with differing composition, leading to apparent oscillations as each zone reacts)

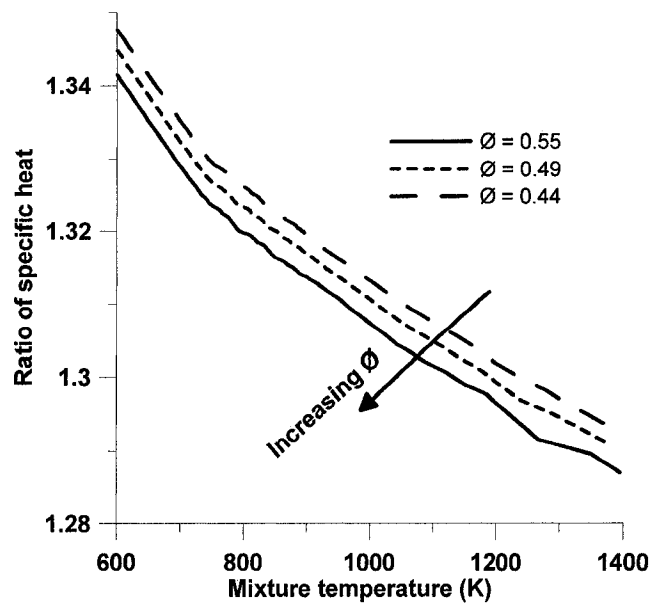


Figure 5-7 : Variation of specific heat ratio, k , in a heptane-fueled engine with different ϕ

Figure 5-8 and Figure 5-9 demonstrate the effects of varying equivalence ratio, ϕ , on mixture chemistry in CNG- and heptane-fuelled engines respectively. Richer mixtures become highly exothermic, i.e., ignite at a lower mixture temperature and their rate of temperature change is higher (at a given temperature) once

ignition occurs. This can be examined systematically by using a given $dT/d\theta$ value, (such as 40K/CA), to define ignition and observing the mixture temperature at which this occurs, (eg., ~1070K for $\phi=0.47$ and ~1050K for $\phi=0.57$ from Figure 5-8). Faster combustion of richer mixtures leads to higher peak pressure, faster pressure rise rate and hotter mixtures, (ultimately causing wall temperature to be greater). However, it is notable that richer CNG mixtures require slightly more energy input, (are more endothermic), as stable molecules decompose to radicals at intermediate temperature, (see the expanded section of Figure 5-8).

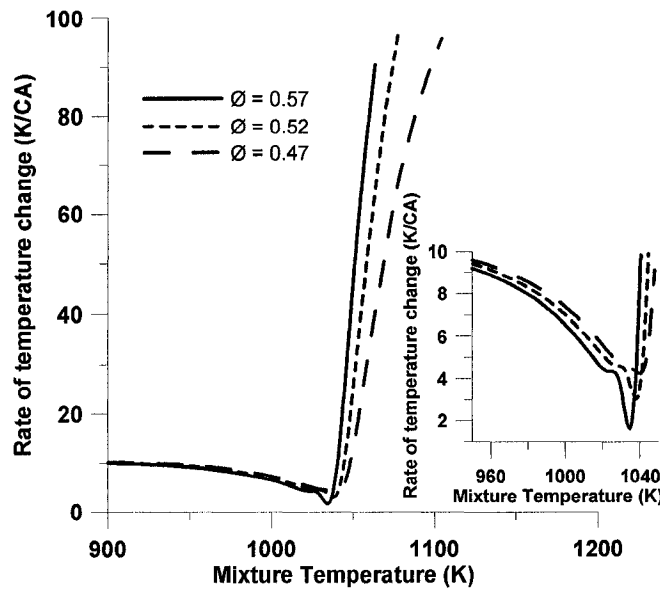


Figure 5-8 : Rate of temperature rise, $dT/dt@T$, for CNG-fueled HCCI with various fuel fractions

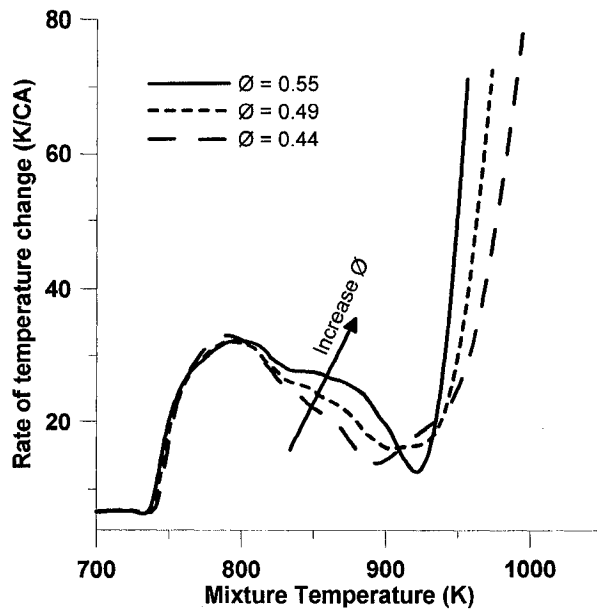


Figure 5-9 : Rate of temperature rise, $dT/dt@T$, for heptane-fueled HCCI with various fuel fractions

Similar effects of earlier main stage auto-ignition and faster combustion were also found in the heptane engine (see Figure 5-9). The differences were that the main stage auto-ignition occurred at a lower temperature (around 950 K) and was preceded by a substantial, exothermic 1st stage reaction starting around 740 K. Increasing mixture equivalence ratio resulted in the later stages of this 1st stage reaction becoming more exothermic which is an indication that chemistry is contributing to the advance of auto-ignition. It can be concluded that although thermodynamic properties of richer mixtures tend to significantly retard SOC, advance SOC of engines can still be found due to 1) higher wall temperature and 2) lower auto-ignition temperature.

5.3 Reformer Gas Effects on HCCI Combustion

Both experiments and simulations showed an advance in SOC timing as more RG replaces high ON methane/air mixtures (see Figure 5-10) and retardation in SOC timing as more RG replaces low ON heptane/air mixtures (see Figure 5-11). The contribution of RG replacement to thermodynamic property changes is very

similar so the reason for opposite combustion behaviour changes must be related to in-cylinder environment or chemistry factors. The effects on in-cylinder environment are considered first.

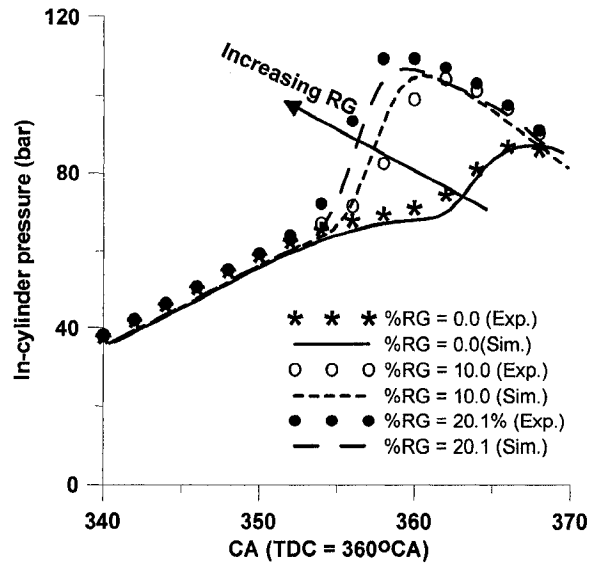


Figure 5-10 : Pressure histories from a CNG engine with RG addition

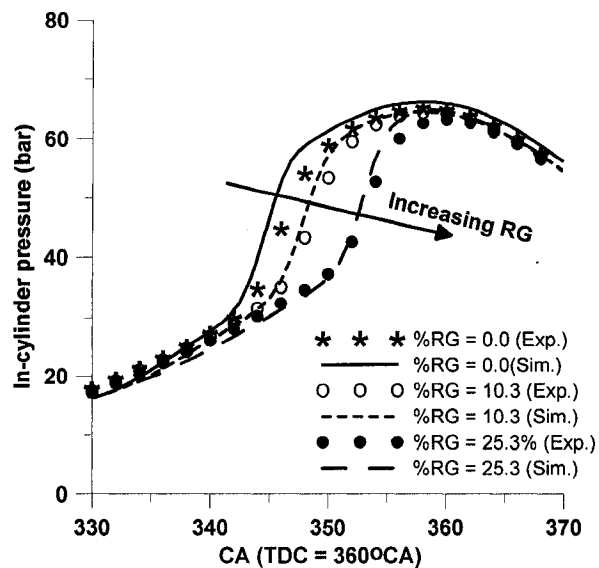


Figure 5-11 : Pressure histories from a heptane engine with RG addition

Figure 5-12 and Figure 5-13 show the IVC mixture temperature, wall temperature and maximum pressure rise rate, (a knock indicator) for the simulated cycles in Figure 5-10 and Figure 5-11. Figure 5-12 indicates significant changes in wall temperature and IVC temperature when CNG-RG/air mixtures were replaced with sufficient RG to causes engine knock, resulting in significant advance in SOC timing. However, with the same level of knock, the in-cylinder environment does not seem to affect pure CNG HCCI as can be seen by comparing the 20% and 30% cases. When the mixtures contained 30% RG, wall temperature was lower, yet SOC happened earlier. The ineffectiveness, (when there is no engine knock), of wall temperature became obvious in a heptane engine (Figure 5-13). At certain operating conditions, the in-cylinder environment, (wall temperature), only changed slightly with additional RG but SOC timing was noticeably altered. This indicates other contributions from RG and after eliminating thermodynamic and in-cylinder environment effects, these must be chemistry effects.

Figure 5-14 shows the effect of RG replacement on thermodynamic properties, (i.e., specific heat ratio). Before the main combustion, the specific heat ratio is slightly greater as RG replaces CNG due to the diatomic molecules (H_2 and CO) which are lighter than the fuel molecules they replace, leading to hotter end-of-compression mixtures. (Based on air standard cycle analysis, a 0.01 change in k can cause just over 20K change in compression temperature depending on initial temperature and engine geometry). The same effects, (rising specific heat ratio, k , and compression temperature), are found when RG replaces n-heptane in the n-heptane-fueled HCCI engine before cool flame, see Figure 5-15. However, instead of advancing ignition timing, the SOC was retarded with increasing RG replacement. Since RG replacement raises the pre-combustion temperature and yet retards ignition timing, the mixture chemistry effects of RG replacement must be examined for the explanation.

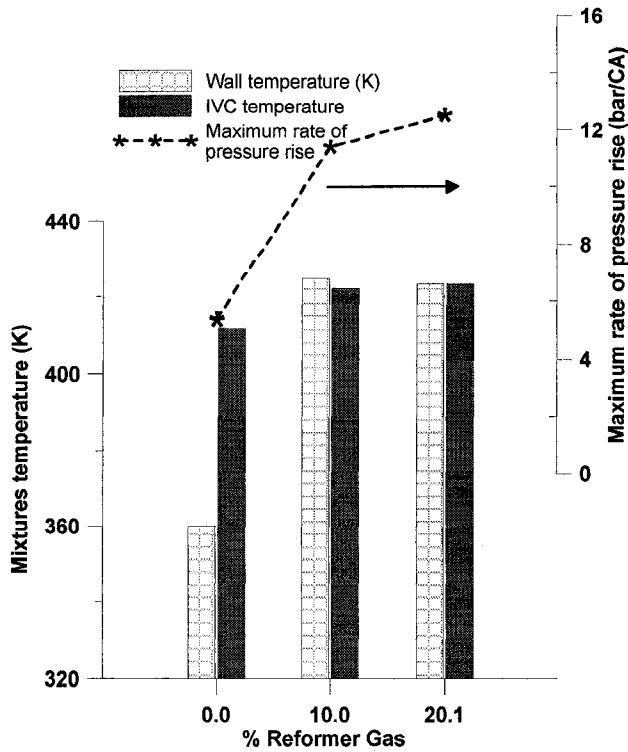


Figure 5-12 : Wall- and IVC- temperatures of a CNG engine with RG addition

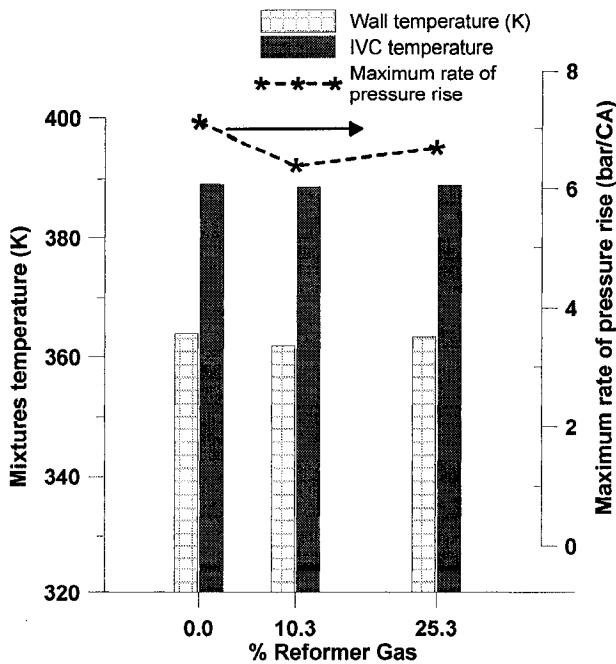


Figure 5-13 : Wall- and IVC- temperatures of a heptane engine with RG addition

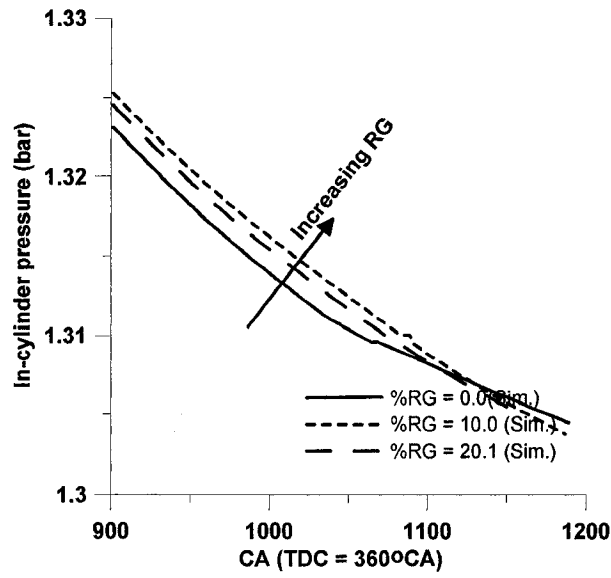


Figure 5-14 : Variation of specific heat ratio, k , in a CNG-fueled engine with varying RG fractions

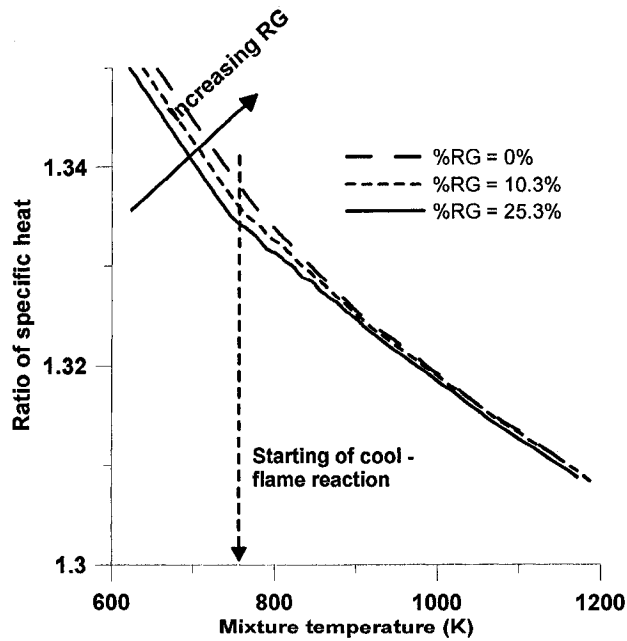


Figure 5-15 : Variation of specific heat ratio, k , in a heptane-fueled engine with varying RG fractions

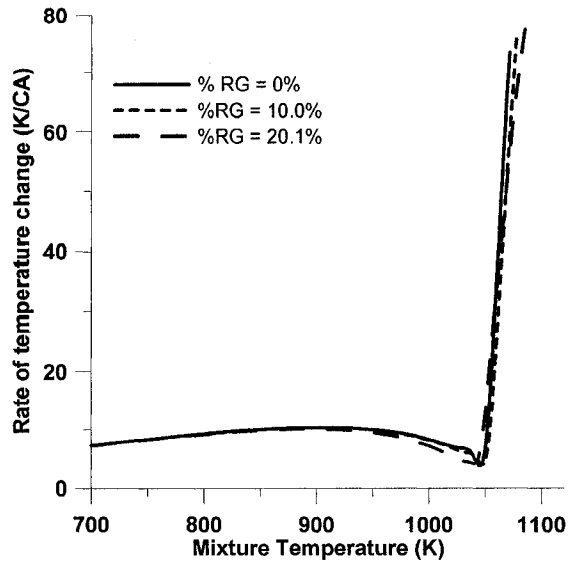


Figure 5-16 : Rate of temperature rise, $dT/dt@T$, for CNG-fueled HCCI with RG addition

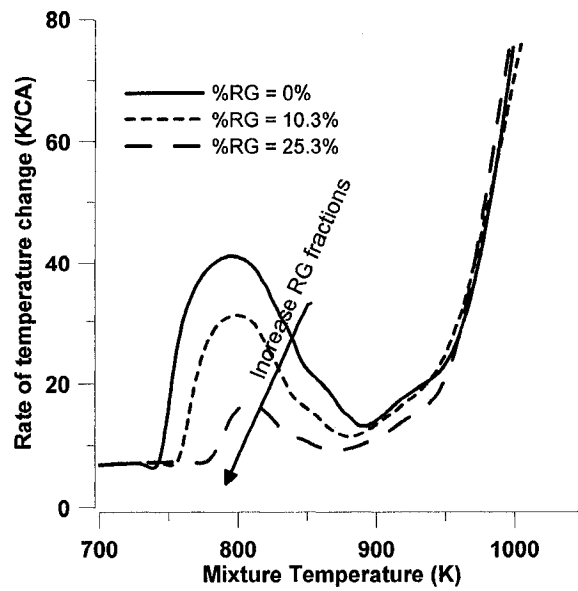


Figure 5-17 : Rate of temperature rise, $dT/dt@T$, for heptane-fueled HCCI with RG addition

Figure 5-16 shows the effects of RG replacement on the "rate of temperature rise at a given temperature" (or $dT/dt@T$) of a CNG engine. The chemistry effects seen were small for this high ON fuel. With RG replacement, the ignition process started at a marginally lower mixture temperature but the temperature rise rate did

not accelerate as fast. This resulted in essentially no change in ignition temperature when defined as “temperature at which $dT/d\theta$ exceeds 40K/CA”.

These results are slightly different from a previous study that has shown a slight effects of chemistry changes when a small amount of RG was first added to pure methane-air-residual mixture until H_2 is saturated [70].

The lack of chemistry effects seen in this study might be because high in-cylinder pressure (as the engine was supercharged) suppressed some relevant reactions. Nevertheless, the main conclusion is unchanged, which is “the result indicates that the RG effect on CNG-fueled combustion is primarily through the thermal route, (which has a continuous tendency to increase with significant amounts of added RG)”.

In contrast, for the low ON heptane mixtures, RG blending interferes with the 1st stage combustion (Figure 5-17), resulting in retardation of SOC timing. In addition, as the peak temperature and the maximum rate of pressure rise are less when the mixtures contain more RG fraction, wall temperature is lower. As a result of cool flame suppression and lower wall temperature, the start of main combustion was progressively retarded for heptane mixtures with more RG.

5.4 External EGR Effects on HCCI Combustion

Given the limitations of a practical HCCI engine experiment, it is usually difficult or impossible to obtain a series of good operating points in which the EGR ratio is the only factor being changed while all other parameters remain fixed. Performing such a study is one of the strengths of a simulation but it must be noted that the investigation in this section is purely numerical without direct experimental confirmation. Figure 5-18 and Figure 5-19 show that SOC timing is progressively retarded as external EGR is added for both CNG and heptane-fuelled HCCI. The reason for SOC retardation has already been explained by Zhao et al [46] as a

combination of dilution, thermodynamic and chemistry effects. However, beyond this explanation, the model used in this study allows examination of the influence of the in-cylinder environment as well.

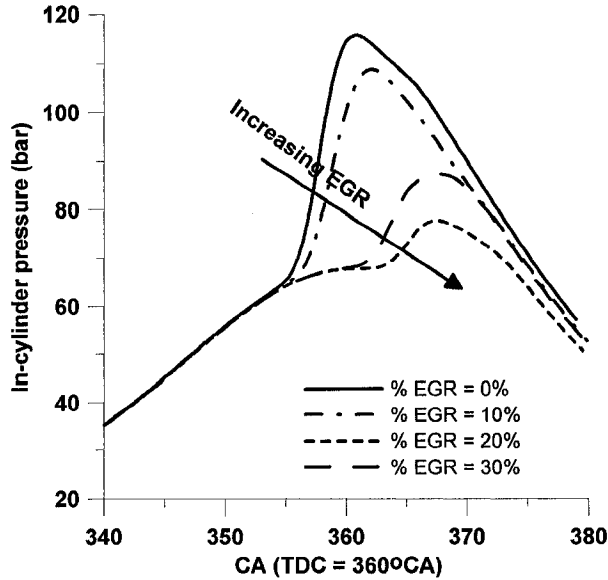


Figure 5-18 : CNG-HCCI pressure traces of an engine operating with different %EGR

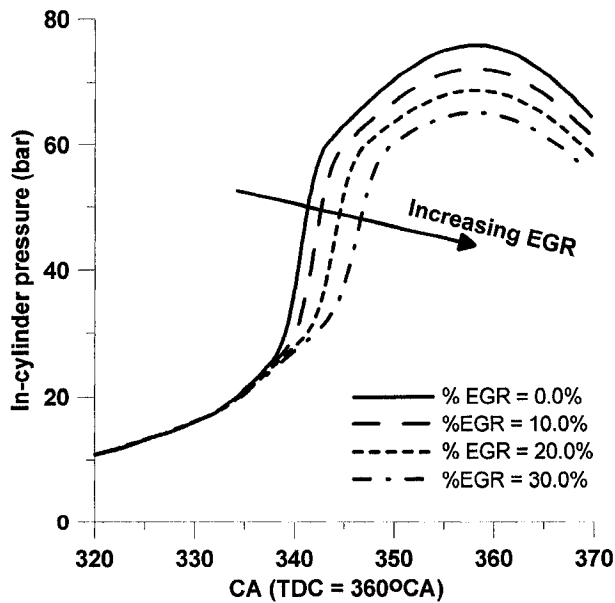


Figure 5-19 : Heptane-HCCI pressure traces of an engine operating with different %EGR

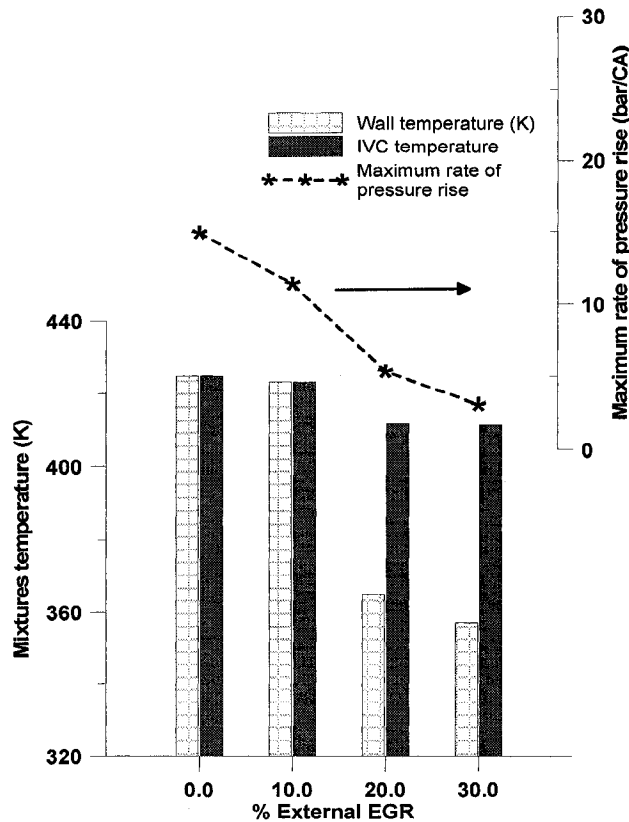


Figure 5-20 : Effects of external EGR to wall- and IVC- temperatures inside a CNG engine

Figure 5-20 illustrates wall and IVC mixture temperatures for a CNG engine operating with varying levels of external EGR. The lower energy density with increased EGR mixtures causes lower combustion temperature leading to cooler wall temperature and cooler pre-compression mixture. The same effects, (lowering wall temperature and IVC temperature), were found in the n-heptane-fueled HCCI engine, (see Figure 5-21).

The following section evaluates the relative contribution of environmental and mixture properties effects for external EGR. Due to the heavier combustion product molecules in EGR, (CO_2 and H_2O), the mixture specific heat ratio is expected to be lower as the fresh charge is diluted with EGR. However, given the overall lean mixture, about 75% of both exhaust and intake charges is nitrogen and the methane molecules in CNG have a similar k effect to CO_2 and H_2O .

Hence, the difference in k due to EGR dilution of CNG-air mixtures is marginal, (between 0.3% - 0.7% depending on mixture equivalence ratio as shown in Figure 5-22).

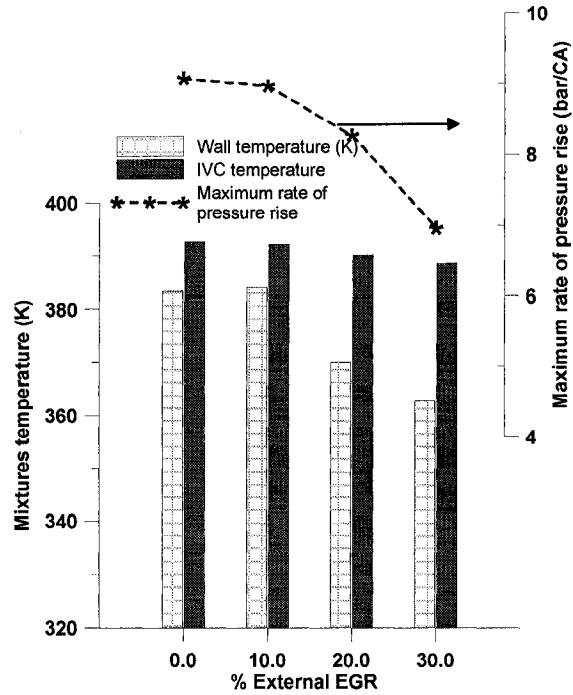


Figure 5-21 : Effects of external EGR on wall- and IVC- temperatures inside a heptane engine

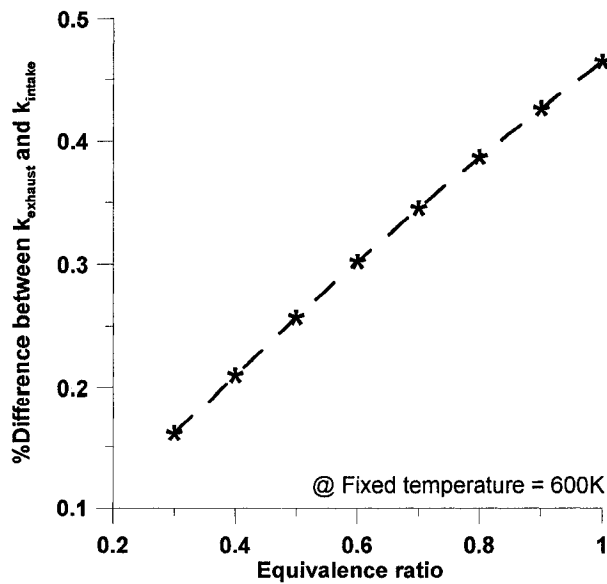


Figure 5-22 : A comparison of ratio of specific heat between fresh charges and exhausts using different ϕ CNG mixtures

Figure 5-23 shows that varying from 0% to 30% EGR fraction produces a negligible change on CNG HCCI compression temperature up to about 1050 K, at which point ignition occurs. The thermodynamic property effect of external EGR on heptane HCCI is somewhat different as shown in Figure 5-24. The combustion product molecules in EGR are significantly smaller than C_7H_{16} so EGR dilution provides a modest rise in specific heat ratio $k = C_p/C_v$ during compression. The higher k value leads to higher compression temperature which should advance ignition timing. However, SOC timing of heptane was retarded by adding external EGR, indicating that the thermodynamic property change effect was dominated by other effects, (i.e., wall temperature as discussed earlier and/or chemistry as discussed in the following section).

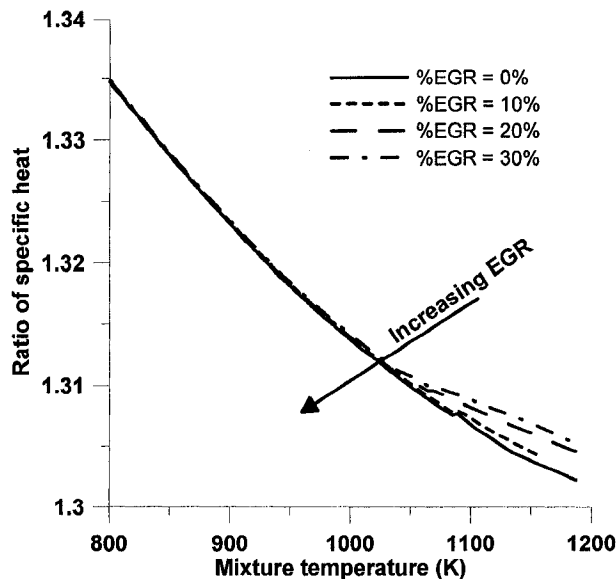


Figure 5-23 : Thermodynamic (k) effects of external EGR addition to CNG HCCI

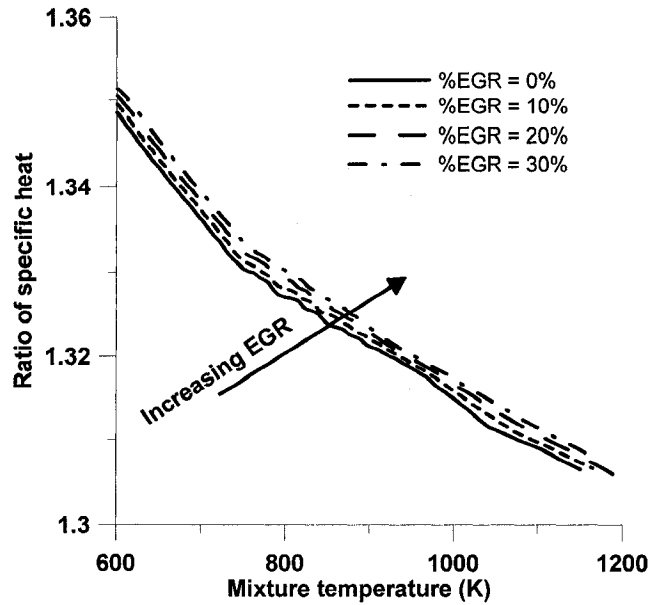


Figure 5-24 : Thermodynamic (k) effects of external EGR addition to heptane HCCI

Figure 5-25 shows the chemistry effects of external EGR for CNG-HCCI combustion chemistry and Figure 5-26 shows the same effects for heptane-HCCI combustion. For both cases, the energy release rate of the high-temperature, post-ignition reaction is significantly slower with added external EGR dilution. A quantitative way of measuring this effect is to note the mixture temperature at which $dT/d\theta$ exceeds 40 K/CA (autoignition temperature). For the CNG case, 30% EGR raises the autoignition temperature by 20K and for the heptane case 30% EGR raises the autoignition temperature by 50K. In the heptane case, EGR also reduces the low-temperature, 1st stage combustion rate (see Figure 5-26).

When comparing these results with the previous equivalence ratio results, it is clear that diluting mixtures with EGR has stronger effects on HCCI combustion than comparable dilution with excess air (Section 5.2).

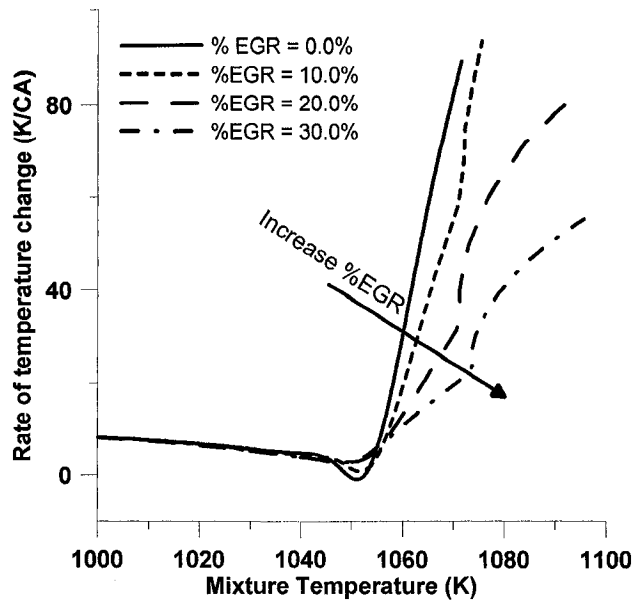


Figure 5-25 : Rate of temperature rise for CNG-fueled HCCI with various EGR fractions

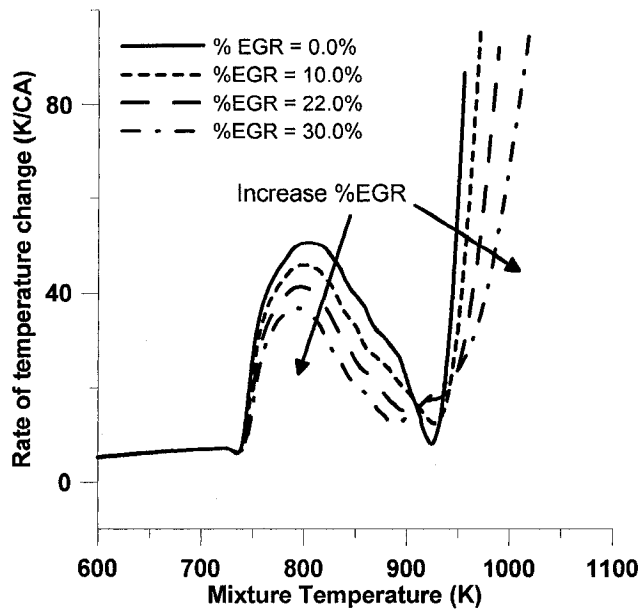


Figure 5-26 : Rate of temperature rise for heptane-fueled HCCI with various EGR fractions

5.5 Internal EGR Effects on HCCI Combustion

As part of this modeling study, the amount of internal EGR was manipulated using the technique of exhaust valve re-opening [150] and the gas exchange model. The exhaust re-breathing technique can provide a wider range of internal EGR fraction than using VVT. The lifting profiles of both intake and exhaust valves are shown in Figure 5-27. Clearly, hot residual in the mixtures of an engine with profile C is the greatest, followed by profiles B and C respectively. Again, this part of the study was purely numerical since the experimental engine did not have suitable valve actuation to provide an experimental validation.

Figure 5-28 and Figure 5-29 show that increasing content of internal residual has the same effect on both CNG-HCCI and heptane-HCCI engines, i.e. SOC was slightly advanced as the amount of internal residual increased. Despite the advancing SOC timing, the engines operated with lower peak pressure and slightly slower combustion (slower rate of pressure rise).

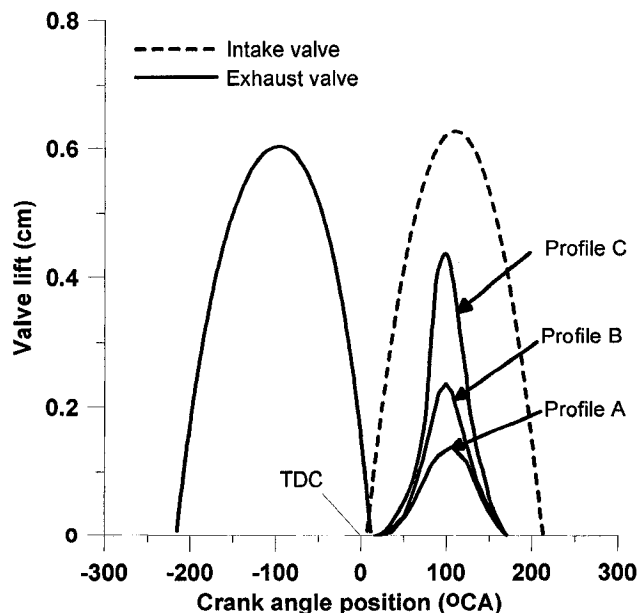


Figure 5-27 : Intake and Exhaust valve profiles

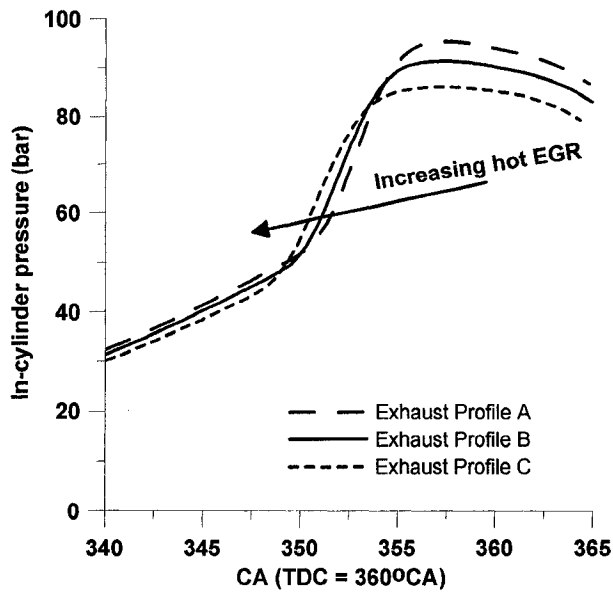


Figure 5-28 : Pressure traces of a methane HCCI engine operating with different hot EGR levels

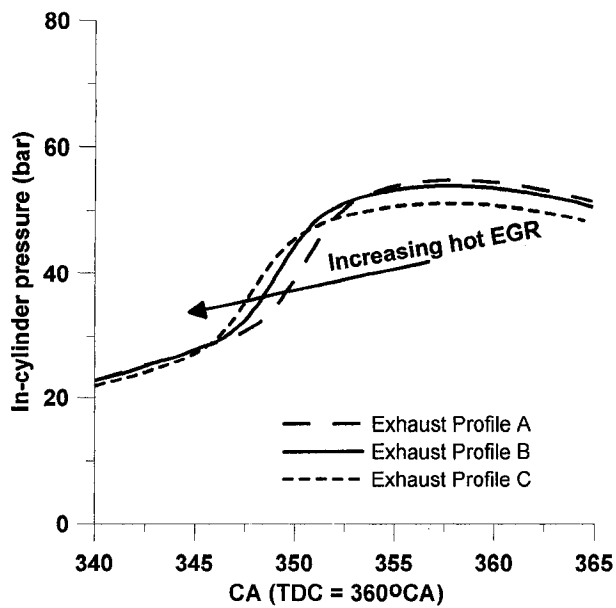


Figure 5-29 : Pressure traces of a methane HCCI engine operating with different hot EGR levels

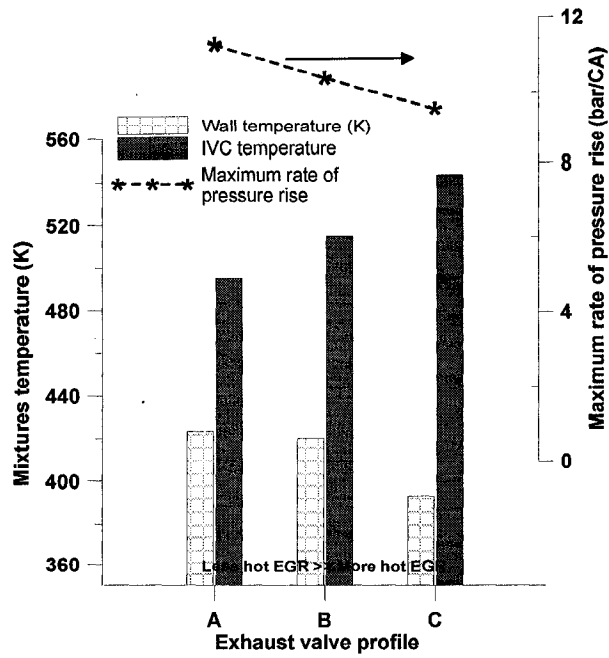


Figure 5-30 : Effects of external EGR to wall- and IVC- temperatures inside a heptane engine

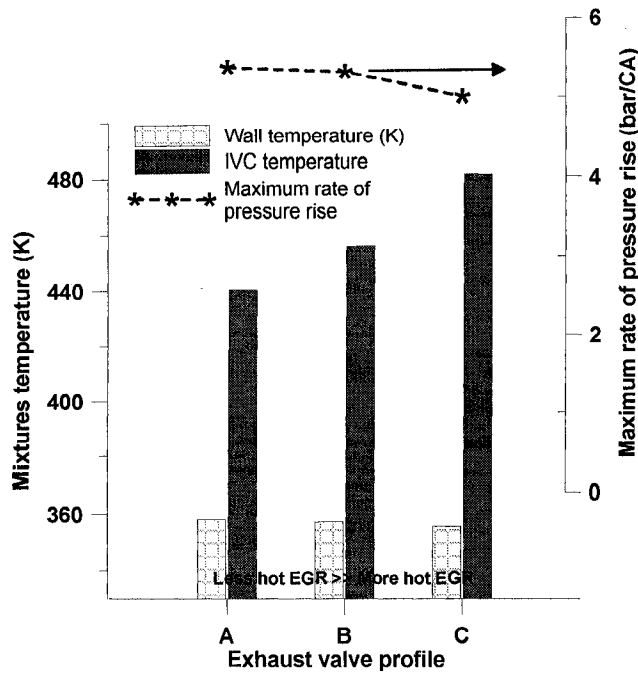


Figure 5-31 : Effects of external EGR to wall- and IVC- temperatures inside a heptane engine

This uniform advance of SOC with increasing hot EGR was examined in light of the three controlling factors: in-cylinder environment, (IVC temperature and wall temperature), thermodynamic property effects and chemistry effects. (The effect of radicals recycled with the retained EGR was neglected in this study since the engines were operating at low speed, allowing active radicals to react and form complete products before the start of the next cycle. In addition, the mixture temperature is low, encouraging formation of stable molecules before compression).

Figure 5-30 and Figure 5-31 show significant changes in IVC temperature for both engines when the exhaust valve closing time varied. With temperature being the dominant parameter for HCCI combustion, increasing IVC temperature irresistibly advances SOC. Aside from this temperature effect with internally retained EGR, other changes in mixture properties are the same as those associated with external EGR. Thus, thermodynamic changes have only marginal effects on HCCI combustion timing while chemical changes tend to retard SOC and reduce main combustion rate, particularly for low octane fuels. The higher IVC closing temperature dominates over any thermodynamic effects while the added dilution slows and moderates the main combustion period, resulting in lowered peak pressure and pressure rise rate.

5.6 Engine control at different operating modes

The previous sections focused on the effects of controlled mixture composition changes for a specific working condition in order to understand the mechanisms that change HCCI combustion behavior. This section demonstrates the effects of the three controllable parameters (ϕ , %RG and %EGR) on indicated mean effective pressure (imep), indicated efficiency, peak pressure and maximum pressure rise rate. Note that internal EGR has not been investigated at this time as it is difficult to obtain specified hot EGR fractions by changing exhaust valve breathing profiles and this requires further investigation. The effects of changing

mixture compositions were investigated for four different engine operating conditions,

- Low speed with natural aspiration,
- High speed with super charging,
- Low speed with natural aspiration and
- High speed with super charging.

Note that engine speed affects combustion behaviors of conventional engines (both SI and CI) in terms of allowable time for 1) complete combustion by flame front traveling across the chamber or by fuel injection and mixing and 2) heat loss to the wall. In an HCCI engine, there is no flame front travel or mixing during combustion and total combustion is relatively rapid. However, the auto-ignition process requires a period of time for chemical reactions and is very sensitive to wall temperature so speed can affect ignition timing. Also, engine knock results when combustion raises the cylinder pressure too rapidly. For the fast combustion of HCCI engines, higher engine speeds can be an advantage in avoiding knock. In this section, moderate engine knock is defined as the point where $dP/d\theta$ exceeds 8.5bar/CA while strong engine knock is defined as the point where $dP/d\theta$ exceeds 10.5bar/CA.

Figure 5-32 to Figure 5-34 shows the effects of three controllable variables (ϕ , %RG and % external EGR) on engine parameters. In general, high engine speed operation provides a shorter time period during the compression stroke, resulting in retarded SOC timing and sometimes misfiring. Boosting intake pressure not only enhances engine IMEP but also increases IVC temperature, resulting in advance SOC timing.

IMEP varies with energy content, as can be seen by comparing IMEP for mixtures with different ϕ and EGR. Figure 5-32 shows that IMEP increases with increasing energy content as ϕ is raised and Figure 5-34 shows the IMEP decreasing with decreasing energy content as % External EGR is raised. This confirms that ϕ and

EGR adjustment can be used to control engine load to meet varying operating demands. However, it also shows that attempting to use ϕ and EGR to optimize combustion timing and efficiency at a specified speed/load condition will become complex since multiple parameters would need to be adjusted to keep IMEP constant.

In general, engine efficiency depends on several factors related to mixture composition and operating conditions. The efficiency trends shown in Figure 5-32 to Figure 5-34 with ϕ , %RG and %EGR are sometimes inconsistent between fuel types, engine speeds and engine load levels. The reason is that optimum engine efficiency has a great deal to do with combustion phasing. A careful comparison of efficiency trends and SOC timing trends shows that efficiency tends to increase as the start of combustion moves closer to TDC, i.e., the optimum peak pressure timing is slightly after TDC. This emphasizes the importance of finding a good method to control HCCI combustion timing at any specified speed and load operating condition.

Beyond the direct efficiency concerns, excessively advanced SOC timing could cause a severe engine knock unless the mixtures are sufficiently diluted. When an engine knock occurs, changes in peak pressure seem to be marginal when operating conditions are similar. However, early ignition causing engine knock can lead to a significant drop in IMEP due to 1) greater negative compression work and 2) more heat loss from hotter in-cylinder mixtures. The effects of different SOC timing on IMEP can be seen by examining the case of a supercharged CNG engine operating at different engine speeds (Figure 5-32 b). Figure 5-35 shows the pressure traces of the two cases. Although combustion in a low speed engine is more complete, leading to higher peak pressure, the earlier and faster combustion results in more negative compression work, higher heat loss, lower pressure during expansion and consequently lower IMEP and efficiency for the low speed engine. This is a classic case showing the importance of ignition timing control for optimum engine output and efficiency with varying engine speed and load.

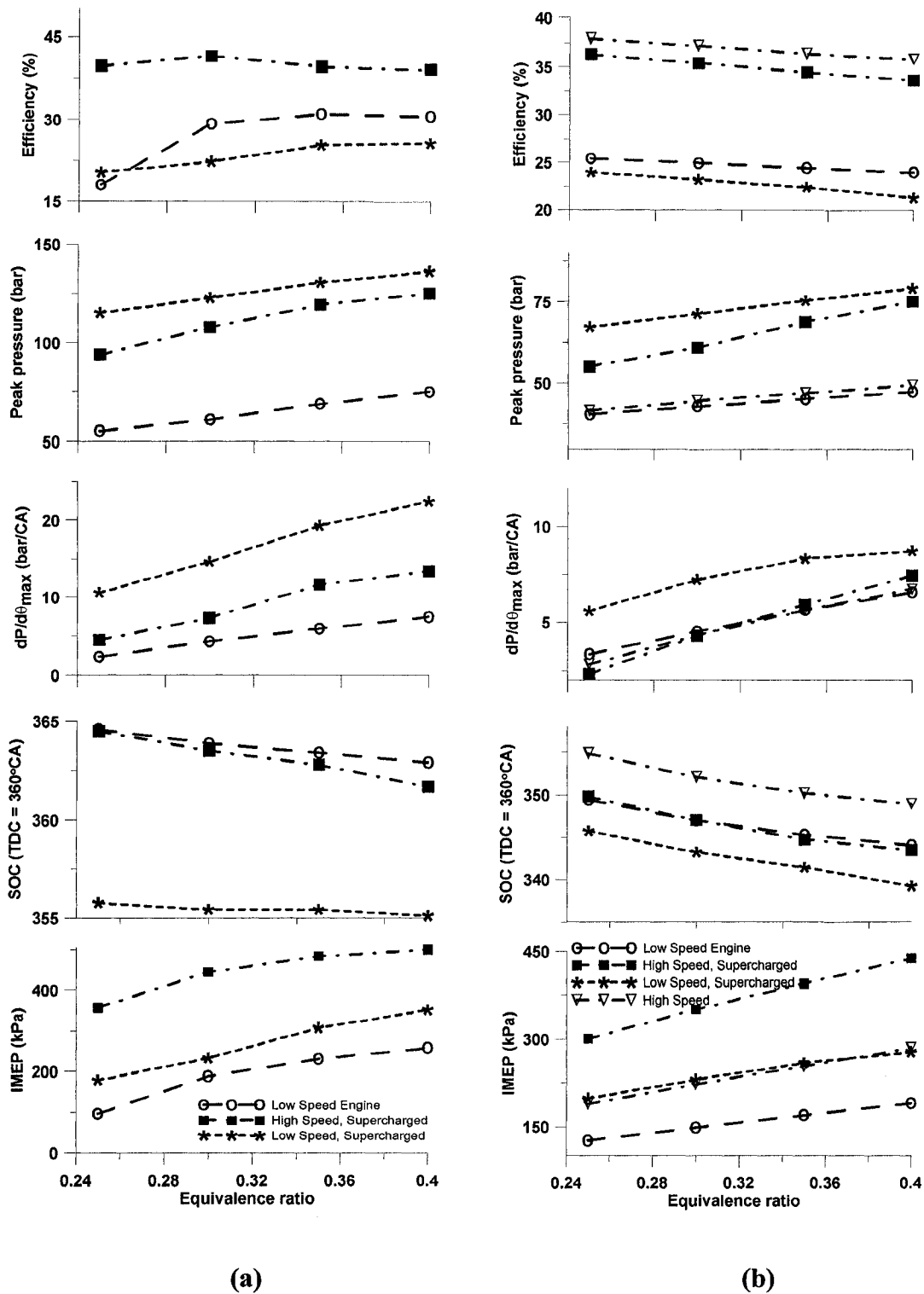


Figure 5-32 : Effects of changing equivalent ratio under different operating modes in a heptane engine, (a) methane HCCI engine and (b) heptane HCCI engine

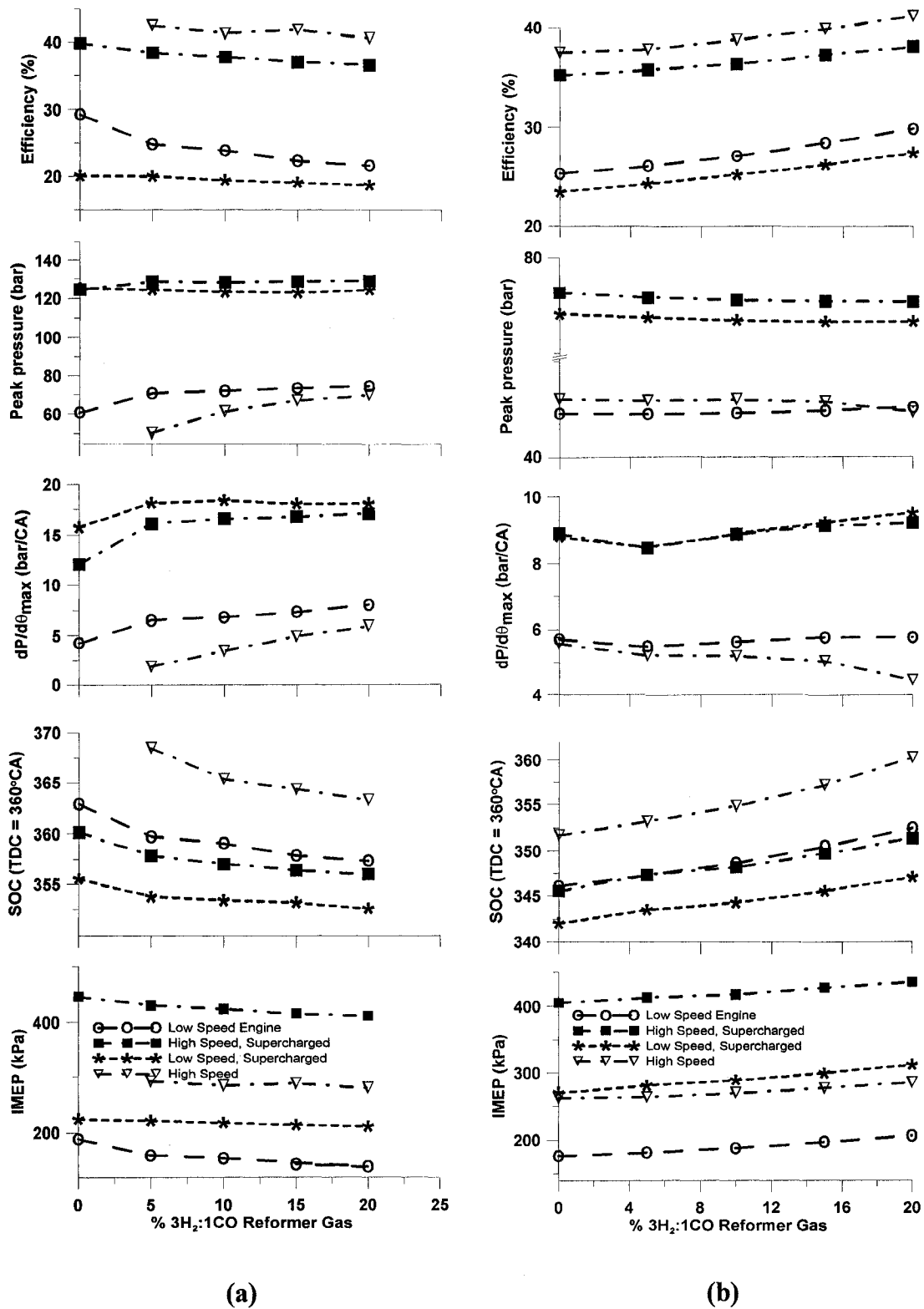


Figure 5-33 : Effects of changing 3H₂-1CO RG under different operating, (a) methane HCCI engine and (b) heptane HCCI engine

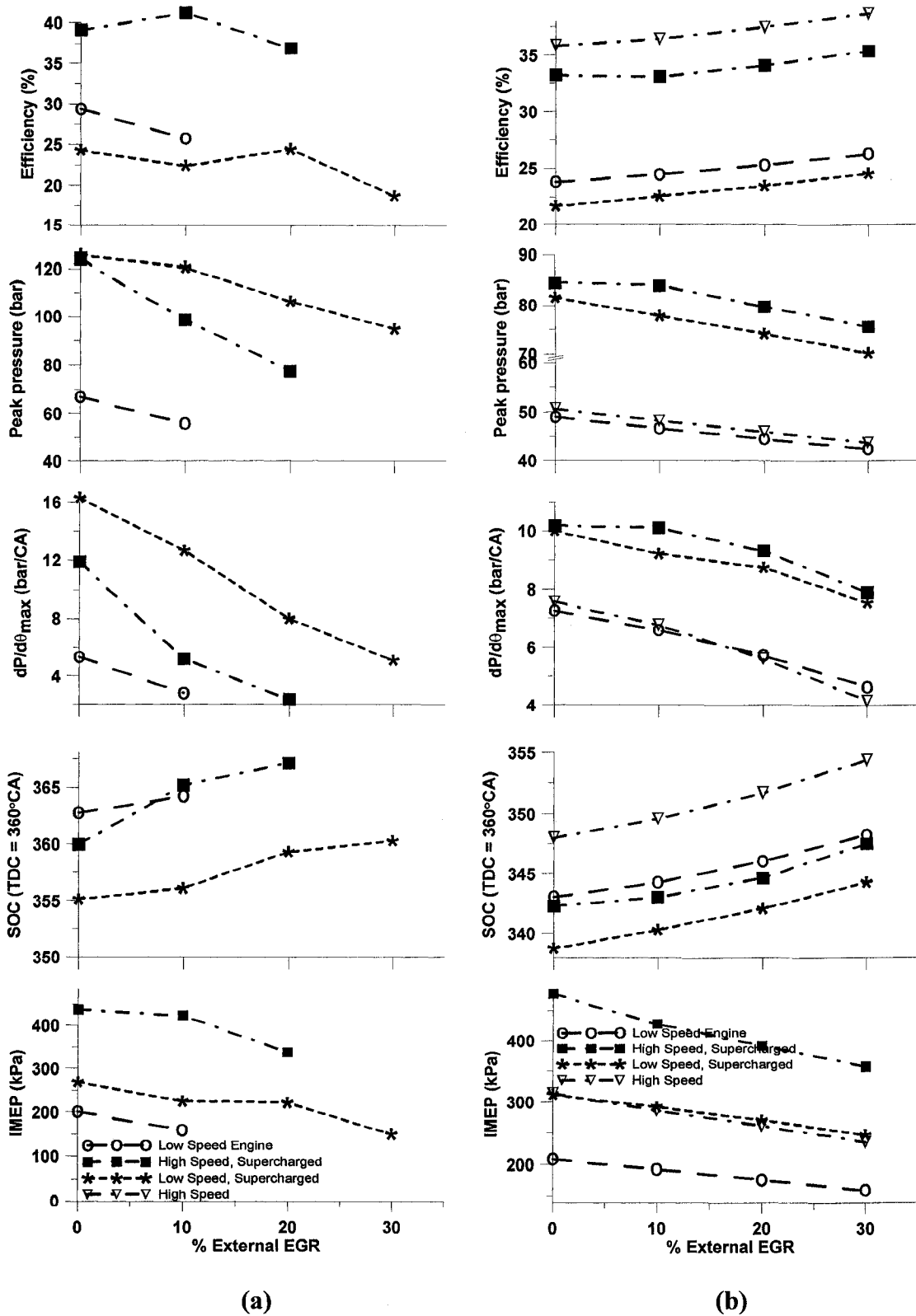


Figure 5-34 : Effects of changing % external EGR under different operating, (a) methane HCCI engine and (b) heptane HCCI engine

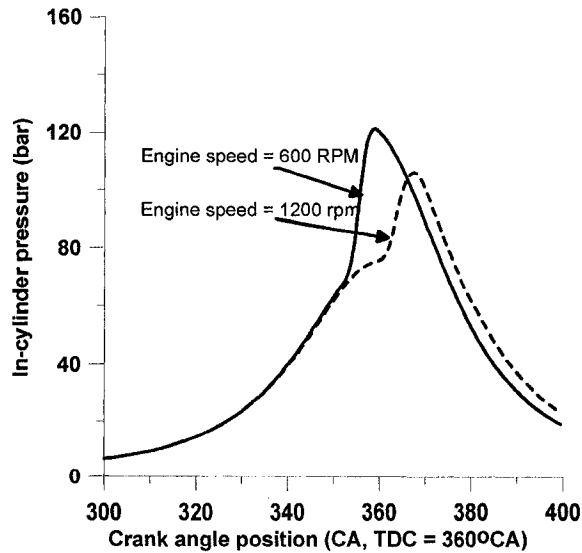


Figure 5-35 : Pressure histories of a supercharged CNG engine operating at two different speeds

Analysis of Figure 5-32 to Figure 5-34 shows that only varying RG can preserve the level of IMEP while adjusting ignition timing to significantly improve combustion characteristics since RG blending can alter mixture properties without significantly changing mixture energy contents. By providing almost constant IMEP while significantly changing HCCI combustion characteristics, varying RG fractions could probably be the most suitable control mechanism for HCCI engines. While different engine loads are achieved by changing ϕ or intake pressure, RG blend fraction can be varied to control ignition timing. Detailed consideration of these control techniques is provided in the following section.

5.7 Control perspective

To practically run an engine over a range of loads and speeds, it is necessary to have control methods which can adjust engine IMEP and ignition timing independently and which work over the practical speed range. Although varying ϕ can slightly alter HCCI combustion characteristics, it is not feasible as an ignition timing controller because slightly adjusting ϕ results in

- 1) a significant variation in IMEP which could cause either excessive or insufficient powers for engine applications and
- 2) a rapid change in combustion rate which could lead to engine knock.

As a result, the practical use of ϕ variation is to adjust the engine power output while the HCCI engine operates at nominally open throttle conditions for optimum efficiency. Therefore other mechanisms, such as altering %EGR (both hot and cold), or %RG must be introduced to control SOC timing to obtain good combustion quality.

External EGR has some feasibility for control due to the capability to significantly change HCCI combustion characteristics using cold EGR. However, adjusting the amount of external EGR also significantly changes IMEP, requiring simultaneous adjustments of other parameters in order to retain an engine load requirement. Further, implementing a combustion timing control system based on EGR flow rate between exhaust and intake is complicated since:

1. the level of exhaust pressure needs to always be significantly greater than intake pressure and this has pumping loss efficiency considerations,
2. the temporal response of the external EGR system becomes a critical factor in combustion timing control and is inherently too slow to achieve cycle by cycle control.

Despite these draw-backs, external EGR is usually applied to dilute the mixture under certain conditions, especially to broaden the high torque side of the operating range, (ie diluting high ϕ mixtures to moderate combustion rate).

Internal EGR, (which was not specifically simulated in this study), provides an attractive path towards controlling the HCCI engine due to the capability for rapid control through variable valve timing (VVT) systems. VVT systems using solenoid-operated valves have the potential for cycle-by-cycle control of hot EGR

which, as shown earlier, can directly affect ignition timing. However, while it has more effect on ignition timing than external EGR, internal EGR still suffers from basic drawbacks:

- 1) Adjusting internal EGR on a cycle-by-cycle basis requires very fast valve control systems with high associated costs,
- 2) Varying internal EGR also affects IMEP, requiring other parameters to be correspondingly adjusted and
- 3) Hot EGR significantly lowers volumetric efficiency so the maximum amount of hot EGR being used is limited by engine power output requirement.

Because of its rapid response capability, internal EGR adjustment is likely to be part of any practical HCCI control system, particularly during transient operations. However, the drawbacks limit its practicality for controlling ignition timing over a broad range of operating conditions.

Dual fuel blending using two fuels with different octane number provides another feasible method to control SOC timing of HCCI engines. The capability to adjust combustion behaviors without significant change in power output and to control HCCI combustion on cycle-to-cycle basis makes dual fuel blending attractive. However, the cost and complexity of an additional fuel system, (including both on-engine equipment and fuel delivery and storage infrastructure), provides a significant obstacle.

Reformer gas (RG) blending overcomes part of the difficulty associated with dual fuel blending systems by requiring only one fuel supply infrastructure and fuel storage system. The RG is produced on site from the base fuel. This involves an energy cost and adds significant equipment costs to the engine, (reformer and second fuel injection system). While these costs provide a barrier, they need to be considered in light of the greater control capability offered and the probability that the overall cost will be lower than a fast VVT system. The results of this study

show that RG blending provides a means of HCCI ignition timing control which does not interfere with engine load and is usable over a range of speed and load conditions.

5.8 Summary

Changes in HCCI combustion characteristics can be attributed to three main factors: changes of in-cylinder environment, mixture thermodynamic properties and mixture chemistry. When mixture compositions change, these three factors affect HCCI combustion at different levels of significance depending on the approach used and engine operating conditions. The following conclusions were found in this chapter:

- When mixtures energy content (ϕ) is changed, the in-cylinder environmental factor is dominant for high-octane fuel (methane) HCCI combustion. For low-octane fuel (heptane) HCCI combustion, interference with the 1st stage combustion process dominates change in combustion behaviors.
- When reformer gas (RG) blending is applied to high-octane (methane) HCCI combustion, the timing is advanced. A combination of changing thermodynamic properties and in-cylinder environment is mainly responsible for changes in combustion. For heptane HCCI combustion, blending with RG delays ignition timing by chemistry effects: primarily interference with the first stage combustion.
- Varying external EGR fractions has negligible effects on compression mixture thermodynamic properties as the major composition of both fresh mixtures and exhausts is nitrogen gas. Chemistry and environmental effects, on the other hand, are significantly affected by external EGR, which reduces maximum pressure rise rate and maximum temperature. Consequently, wall temperature of an engine operating with greater EGR fraction is cooler. As a result of changes in mixtures' chemistry (dilution and radical production) and

in-cylinder environment, SOC is significantly retarded by added external EGR.

- Internal or hot EGR residuals provide the same effects on HCCI combustion as external EGR. The dilution effects caused combustion to be slower and peak pressure to be lower. However, the additional heating effect overrides all other effects on ignition timing, leading to advanced SOC with added internal EGR.
- In a low speed engine, longer compression time provides time for mixture reactions, resulting in earlier ignition timing and faster combustion.
- Increasing intake manifold pressure raises initial temperature and therefore advances the start of combustion. In addition, with generally greater pressure throughout the cycle, IMEP is higher in an engine with elevated intake pressure.
- Because it can control auto-ignition timing without directly changing IMEP, RG blending has some potential as a means of HCCI timing control. This offers the capability to optimize combustion phasing, (thus efficiency), and to broaden the HCCI engine operating range.

6 Summary and Future Work

6.1. Summary of Model Development

Chemistry based HCCI engine models were developed in order to evaluate the most effective way to control HCCI engines fuelled with heptane and methane base fuels. These fuels represent two extremes of auto-ignitable fuels. Before engine modeling, the basic calculations of chemical kinetics and shock tube auto-ignition were reviewed. For mechanism selection, well-known mechanisms were first adopted, (GRI mech was used to model methane combustion while heptane combustion was modeled by a mechanism from Chalmers University). The conclusions from using those mechanisms are:

- Both models can give a good agreement with shock tube experimental data.
- GRI mech can model methane/air/EGR combustion in an HCCI engine.
- Although the Chalmers mechanism can be used to model pure heptane/air combustion, it cannot capture quantitative changes in combustion behaviors when parts of the heptane/air mixtures are replaced with reformer gas.

As the mechanism from Chalmers could only qualitatively capture the effects of heptane/RG combustion, further development on this mechanism was required, which could be done by adjusting Arrhenius coefficients of the influential reactions. In order to select the influential parameters, the auto-ignition process of heptane from Chalmers mechanism was investigated. This examination led the following observations:

- H₂O and CO production produce most of the energy during 1st stage combustion.
- CO₂ production accounts for most of the heat release for the main combustion.
- Radicals produced by the 1st stage combustion, particularly H₂O₂ and HO₂, are the key initiators of the exothermic 2nd stage reactions.

Analysis of the heptane auto-ignition process, together with sensitivity analysis, provided the list of reactions to be parametrically optimized. A model that coupled genetic algorithm optimization to shock tube ignition delay data and single zone HCCI combustion modeling was developed to systematically evaluate the most suitable parameters. With an optimum set of parameters, the Chalmers Mechanism was able to handle a wider range of conditions, especially when a significant amount of reformer gas replaces heptane/air/EGR mixtures. The improved and validated mechanisms were used to model combustion in an HCCI internal combustion engine.

The first engine model developed in this study was a single zone combustion model, based on a simplified assumption of having uniform properties across the combustion chamber. An important feature of any HCCI combustion model is the way that initial conditions are set. The developed model provides three options for users: 1) directly specify IVC conditions, 2) specify mass flow rates of fuel, air and RG and 3) specify the intake manifold conditions. For the final option, initial conditions (average in-cylinder properties at intake valve close) are obtained from a one dimensional isentropic flow model of the cylinder and intake. The single zone model proved the operation of the chemical kinetic models by accurately predicting ignition timing over a wide range of compositions and operating conditions. However, like all single zone models, it over-predicts the combustion rate, pressure rise rate and peak pressure since it simplifies the real combustion chamber with a uniform, lumped parameter model. To study combustion behavior beyond ignition, as well as actual engine performance, a less simplified model is required.

A more sophisticated multi-zone combustion model was also developed. The model allows for the spatial in-homogeneity of temperature and composition, which actually occurs and develops during compression in a real engine. Several novel features have been introduced into the model, such as 1) calculation to set up spatial distribution at IVC, 2) the inclusion of radiation heat transfer, 3)

modification of convection heat transfer to include changing wall temperature (heat transfer to the wall) and turbulence effects (heat transfer between zones) and 4) a new segregation solver. The validation of the multi-zone model shows an excellent prediction of SOC without arbitrary adjustments. The model was also proven capable of capturing the changing trend of other engine parameters (IMEP, peak pressure, maximum rate of pressure rise and engine efficiency) with reasonable magnitude.

6.2. Summary of Model Application

The capability to predict a full in-cylinder pressure cycle without any arbitrary adjustment of IVC properties and to predict wall temperature allows the fully developed multi-zone model to:

1. Investigate the integrated effects, (including changing in-cylinder environment, mixture thermodynamic properties and mixture chemical properties), on HCCI combustion when varying mixture compositions. Note that variation in mixture compositions has been done through adjusting: equivalence ratio (ϕ), RG fractions, %cold EGR and % hot EGR.
2. Observe the effects of changing mixture composition on HCCI engine operation at different operating modes (high/low speeds with supercharged/natural aspirated intakes).

It was found that the ranking of factors affecting HCCI combustion, (ie. in-cylinder environment, mixture thermodynamics and mixture chemistry), varied depending on the values of mixture control variables (ϕ , %RG, %external EGR and %internal EGR) and the base fuel octane rating. Changing in-cylinder environment provides the greatest effect on HCCI combustion characteristic when the amount of high octane fuel contents (ϕ) changes. Mixture chemistry and mixture thermodynamics changes are more responsible for combustion behavior when the mixture fuel blend is altered by RG blending additives. (In this study,

the RG used was a simulated RG consisting only of light gases: 75% H_2 -25% CO). The predominance of thermal or chemical effects depends on the base fuel auto-ignition properties. With external EGR, the various effects are balanced so that changing the level of external EGR mostly affects early ignition temperature rise through diluted mixture strength, (a chemistry effect). However, with internal EGR, the in-cylinder environment effects of higher pre-compression temperature override all others, thus advancing SOC with increasing internal EGR level.

Over a range of engine speed and intake pressure, changing SOC timing has generally less impact on IMEP than changing the mixture energy content, (unless SOC happens much too early or late). With this in mind, it can be concluded that varying the RG blend fraction while maintaining similar mixture energy content could provide a good means to control HCCI combustion without significantly affecting other parameters (such as engine speed and IMEP). The advantage of varying RG blend fraction as a fast timing control is that, unlike varying ϕ or EGR, it can control timing at a fixed operating point without needing to simultaneously control of several parameters.

Provided that technologies of on-board dual fuel systems are affordable and supporting infrastructures are extensive, simplicity and ability to control HCCI combustion on cycle basis prospers the use of RG as HCCI controller. Having said that, the potentially-achieved fuel economy has not been yet considered and further analysis on optimum fuel economy at particular load and speed is strongly recommended.

6.3. Future Work

The work presented in this thesis has 1) laid out the basis of chemical kinetic calculation, 2) presented the Genetic Algorithm technique for chemical kinetic mechanism optimization and 3) developed the HCCI engine models (both SZM and MZM) to the point where it can be used without any case-by-case adjustments, which allows researchers to conduct further study HCCI combustion

and/or preliminary design an HCCI engine. Preliminary application has shown that such modeling work is very vital to HCCI development since various combinations of controllable parameters can lead to complex and significant changes in HCCI combustion.

6.3.1 Application to HCCI Engine Control Optimization

The first continuation of this work would be the application of the model to find an optimum operating condition of an engine with specified control mechanism, i.e., filling the map presented in Figure 6-1. For a developed engine, such an operating map would include operating region boundaries, control parameter settings and the resultant fuel consumption for each operating point. Since the models were developed in MATLAB, finding optimum operation for each point can be simply done by coupling the model (preferably MZM) to direct-search or any optimization toolboxes provided by MATLAB. In addition, the model can be used to pre-test any control mechanism prototypes, (either closed-loop or open-loop control) by linking the model to the control algorithms which might be developed using MATLAB SIMULINK.

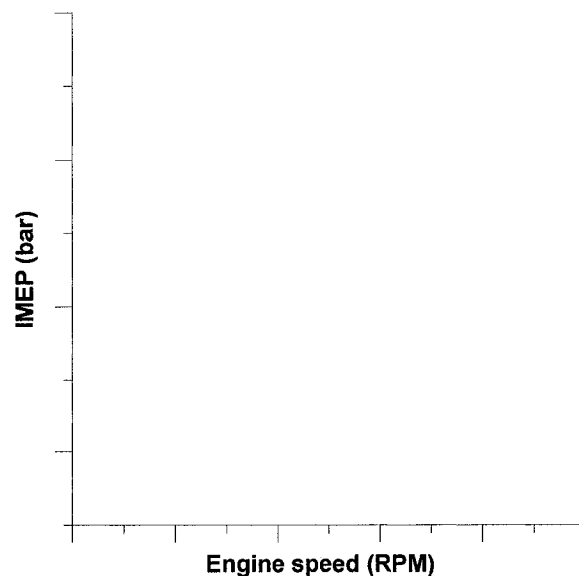


Figure 6-1 : The example of performance map that can be filled in by the developed models

6.3.2 Improvement of Model

Several improvements can still be done to the model itself. First is the wall temperature (T_w) and engine heat transfer prediction (\dot{Q}_w). Since the model was currently using the inherit correlation with some modification (based on the data from a specific engine) to predict T_w and \dot{Q}_w , pre-validation on these two calculations might be required before using the model to do actual study on other engines than a CFR engine. The development of the general correlations can be done using finite element together with experimental T_w measurements. Another improvement that can be done on the current model is to model flows through valve (during gas exchanging process) with a more detail computational fluid dynamic (3D). Since there are some 3D CFD packages available for MATLAB, combining 3D CFD to the developed HCCI models should be relatively easier and more effective than coupling two commercialized packages (one for CFD and the other for HCCI combustion). Improving chemical kinetic mechanism is another interesting field that can directly be done using the package developed in this thesis.

6.3.3 Incorporation of Additional Combustion Models

Finally, the model can be extended to simulate other types of engines (such as a diesel engine) by including another set of governing equations for injection and combustion. Those equations can be based on CFD or simplified correlation. The advantage of including HCCI and diesel within one engine model is that a dual-mode engine can be more confidently optimized when both operating modes are simulated within the same software.

REFERENCES

1. Atkins M and Koch C.(2003). *A well-to-wheel comparison of several powertrain technologies*. SAE Paper, 2003-01-0081.
2. Iida N.(1994). *Combustion analysis of methanol-fueled Active Thermo-Atmosphere Combustion (ATAC) engine using a spectroscopic observation*. SAE Paper, 940684.
3. Goto K, et al.(2004). *Analysis of the Characteristics of HCCI Combustion and ATAC Combustion Using the Same Test Engine*. SAE Paper, 2004-32-0097.
4. Iijima A, Yoshida K, and Shoji H.(2005). *A Comparative Study of HCCI and ATAC Combustion Characteristics Based on Experimentation and Simulations - Influence of the Fuel Octane Number and Internal EGR on Combustion*. SAE Paper, 2005-01-3732.
5. Onishi S, et al.(1979). *Active Thermo-Atmosphere Combustion (ATAC)-a new combustion process for internal combustion engines*. SAE Paper, 790501.
6. Cao L, et al.(2006). *Investigation into the Effect of Injection Timing on Stoichiometric and Lean CAI Operations in a 4-Stroke GDI Engine*. SAE Paper, 2006-01-0417.
7. Milovanovic N and Chen R.(2001). *A Review of Experimental and Simulation Studies on Controlled Auto-Ignition Combustion*. SAE Paper, 2001-01-1890.
8. Shimazaki N, Akagawa H, and Tsujimura K.(1999). *An experimental study of premixed lean diesel combustion process*. SAE Paper, 1999-01-0181.
9. Najt P M and Foster D E.(1983). *Compression-ignited homogeneous charge combustion*. SAE Paper, 830264.
10. Kimura S, et al.(2001). *Ultra-clean combustion technology combining a low-temperature and premixed combustion concept for meeting future emission standards*. SAE Paper, 2001-01-0200.
11. Kimura S, et al.(1999). *New combustion concept for ultra-clean and high-efficiency small DI diesel engines*. SAE Paper, 1999-01-3681.
12. Johansson B.(2007). *Homogeneous charge compression ignition: the future of IC engines?* International Journal of Vehicle Design, 44(1/2): p. 1-19.
13. Kuzuyama H, et al.(2007). *A Study on Natural Gas Fueled Homogeneous Charge Compression Ignition Engine Expanding the Operating Range and Combustion Mode Switching*. SAE Paper, 2007-01-0176.
14. Iida M, et al.(2003). *Characteristics of Homogeneous Charge compression Ignition (HCCI) Engine Operation for Variations in Compression Ratio, Speed, and Intake Temperature While Using n-Butane as a Fuel*. Transaction of the ASME, 125: p. 472-478.
15. Stone R.(1999). *Introduction to Internal Combustion Engines*. 3rd ed: SAE, Inc. 641.

16. Koopmans L, et al.(2004). *Location of the First Auto-Ignition Sites for Two HCCI Systems in a Direct Injection Engine*. SAE Paper, 2004-01-0564.
17. Ogink R.(2004).Computer Modeling of HCCI Combustion,PhD thesis,Division of Thermo and Fluid Dynamics,Chalmers University of Technology.
18. Kongsereparp P, Kashani B, and Checkel M D.(2005). *A stand-alone multi-zone model for combustion in HCCI engines*. in *Fall Technical Conference of the ASME Internal Combustion Engine Division*. Ottawa, Canada.
19. Babajimopoulos A, Assanis D N, and Fiveland S B.(2002). *An approach for modelling the effects of gas exchange processes on HCCI combustion and its application in evaluating variable valve timing control strategies*. SAE Paper, 2002-01-2829.
20. Babajimopoulos A, Lavoie G A, and Assanis D N.(2003). *Modelling HCCI combustion with high levels of residual gas fraction~A comparison of two VVA strategies*. SAE Paper, 2003-01-03220.
21. Kong S-C, et al.(2001). *Modeling and experiments of HCCI engine combustion using detailed chemical kinetics with multidimensional CFD*. SAE Paper, 2001-01-1026.
22. Flowers D L.(2001).Combustion in Homogenous Charge Compression Ignition Engines: Experiments and Detailed Chemical Kinetic Simulations,PhD ThesisUniversity of California.
23. Amano T, Morimoto S S, and Kawabata Y.(2001). *Modeling of the effect of Air/Fuel ratio and Temperature Distribution on HCCI Engines*. SAE Paper, 2001-01-1024.
24. Koopmans L, et al.(2003). *Demonstrating a SI-HCCI-SI mode change on a Volvo 5- cylinder electronic valve control engine*. SAE Paper, 2003-01-0753.
25. Iida M, et al.(2003). *Characteristics of Homogeneous Charge Compression Ignition (HCCI) Engine Operation for Variations in Compression Ratio, Speed, and Intake Temperature While Using n-Butane as a Fuel*. *Journal of Engineering for Gas Turbines and Power*, 125(2): p. 472-478.
26. Flynn P F, et al.(1999). *Diesel combustion: An integrated view combining laser diagnostics, chemical kinetics, and empirical validation*. SAE Paper, 1999-01-0509.
27. Lavy J, et al.(2000). *Innovative ultra-low nox controlled auto-ignition combustion process for gasoline engines: the 4-space project*. SAE Paper, 2000-01-1837.
28. Milovanovic N, et al.(2005). *SI-HCCI-SI Mode Transition at Different Engine Operating Conditions*. SAE Paper, 2005-01-0156.
29. Olsson J-O, et al.(2002). *Compression Ratio Influence on Maximum Load of a Natural Gas Fueled HCCI Engine*. SAE Paper, 2002-01-0111.

30. Zhao H, Peng Z, and Ladommatos N.(2001). *Understanding of controlled autoignition combustion in a four-stroke gasoline engine*. Proc Instn Mech Engrs, 215(D): p. 1297-1310.
31. Haraldsson G, et al.(2002). *HCCI Combustion Phasing in a Multi Cylinder Engine Using Variable Compression Ratio*. SAE Paper, 2002-01-2858.
32. Flowers D, et al.(2000). *HCCI in a CFR Engine: Experiments and Detailed Kinetic Modeling*. SAE Paper, 2000-01-0328.
33. Thring R H.(1989). *Homogeneous Charge Compression Ignition (HCCI) engines*. SAE Paper, 892068.
34. Persson H, et al.(2004). *The effect of intake temperature on HCCI operation using negative valve overlap*. SAE Paper, 2004-01-0944.
35. Flowers D, et al.(2001). *Operation of a four-cylinder 1.9 l propane-fueled homogeneous charge compression ignition engine: Basic operating*. SAE Paper, 2001-01-1895.
36. Iida M, et al.(2001). *The effect of intake air temperature, compression ratio and coolant temperature on the start of heat release in an HCCI (homogeneous charge compression ignition) engine*. SAE Paper, 2001-01-1880.
37. Haraldsson G, et al.(2004). *HCCI closed-loop combustion control using fast thermal management*. SAE Paper, 2004-01-0943.
38. Flowers D, et al.(2001). *Detailed Chemical Kinetic Simulation of Natural Gas HCCI Combustion: Gas Composition Effects and Investigation of Control Strategies*. Journal of Engineering for Gas Turbines and Power, 123.
39. Yang J, Culp T, and Kenney T.(2002). *Development of a gasoline engine system using HCCI technology~The concept and the test results*. SAE Paper, 2002-01-2832.
40. Stanglmaier R H and Roberts C E.(1999). *Homogeneous charge compression ignition (HCCI): Benefits, compromises, and future engine applications*. SAE Paper, 1999-01-3682.
41. Sun R, Thomas R, and Gray C L.(2004). *An HCCI engine: Power plant for a hybrid vehicle*. SAE Paper, 2004-01-0933.
42. Olsson J-O, Tunestål P, and Johansson B.(2004). *Boosting for high load HCCI*. SAE Paper, 2004-01-0940.
43. Olsson J-O, et al.(2001). *A turbocharged dual-fuel HCCI engine*. SAE Paper, 2001-01-1896.
44. Christensen M and Johansson B.(2000). *Supercharged homogeneous charge compression ignition (HCCI) with exhaust gas recirculation and pilot fuel*. SAE Paper, 2000-01-1835.
45. Olsson J-O, et al.(2003). *The effect of cooled EGR on emissions and performance of a turbocharged HCCI engine*. SAE Paper, 2003-01-0743.
46. Zhao H, et al.(2001). *Understanding the effects of recycled burnt gases on the controlled autoignition (CAI) combustion in four-stroke gasoline engines*. SAE Paper, 2001-01-3607.

47. Oakley A, et al.(2001). *Experimental Studies on Controlled Auto-ignition (CAI) Combustion of Gasoline in a 4-Stroke Engine*. SAE Paper, 2001-01-1030.
48. Zhao H, et al.(2002). *Performance and analysis of a 4-stroke multi-cylinder gasoline engine with CAI combustion*. SAE Paper, 2002-01-0420.
49. Girard J W, et al.(2002). *An Investigation of the Effect of Fuel-Air Mixedness on the Emissions from an HCCI Engine*. SAE Paper, 2002-01-1758.
50. Law D, et al.(2000). *Controlled Combustion in an IC-Engine with a Fully Variable Valve Train*. SAE Paper, 2000-01-0251.
51. Hiraya K, et al.(2002). *A study on gasoline-fueled compression ignition engine~A trial of operation region expansion*. SAE Paper, 2002-01-0416.
52. Kalghatgi G T and Head R A.(2004). *The available and required autoignition quality of gasoline-like fuels in HCCI engines at high temperatures*. SAE Paper, 2004-01-1969.
53. Risberg P, Kalghatgi G, and Ångstrom H-E.(2003). *Auto-ignition Quality of Gasoline-Like Fuels in HCCI Engines*. SAE Paper, 2003-01-3215.
54. Oyama K, Urushihara T, and Nakano T.(2004). *The effect of fuel properties on low and high temperature heat release and resulting performance of an HCCI engine*. SAE Paper, 2004-01-0553.
55. Arthur D M.(2005).Using Hydrigen to Extend EGR limit of SI Engines,M.Sc.,Mechanical Engineering,University of Alberta.
56. Atkins M J.(2004).Experimental Examination of the Effects of Fuel Octane and Diluent on HCCI Combustion,M.Sc. Thesis,Mechanical Engineering,University of Alberta.
57. Atkins M J and Koch C R.(2005). *The effect of fuel octane and diluent on homogeneous charge compression ignition combustion*. Proc. IMechE. Part D: J. Automobile Engineering, 219: p. 665-675.
58. Yao M, et al.(2004). *The Effect of PRF Fuel Octane Number on HCCI Operation*. SAE Paper, 2004-01-2992.
59. Aroonsrisopon T, et al.(2002). *Comparison of HCCI operating ranges for combinations of intake temperature, engine speed and fuel composition*. SAE Paper, 2002-01-1924.
60. Aroonsrisopon T, et al.(2002). *An Investigation Into the Effect of Fuel Composition on HCCI Combustion Characteristics*. SAE Paper, 2002-01-2830.
61. Wagner U, et al.(2003). *An experimental study of homogeneous charge compression ignition (HCCI) with various compression ratios, intake air temperatures and fuels with port and direct fuel injection*. SAE Paper, 2003-01-2293.
62. Strandh P, et al.(2004). *Cycle-to-cycle control of a dual-fuel HCCI engine*. SAE Paper, 2004-01-0941.
63. Shudo T, Ono Y, and Takahashi T.(2002). *Influence of hydrogen and carbon monoxide on HCCI combustion of dimethyl ether*. SAE Paper, 2002-01-2828.

64. Zheng Z, et al.(2004). *Experimental Study on HCCI Combustion of Dimethyl Ether(DME)/Methanol Dual Fuel*. SAE Paper, 2004-01-2993.
65. Iida C Z and Konno M.(2005). *Ignition mechanisms of HCCI combustion process fuelled with methane/DME composite fuel*. SAE Paper, 2005-01-0182.
66. Tominaga R, et al.(2004). *Effects of heterogeneous EGR on the natural gas-fueled HCCI engine using experiments, CFD and detailed kinetics*. SAE Paper, 2004-01-0945.
67. Hosseini V and Checkel M D.(2006). *Reformer gas enrichment of natural gas homogeneous charge compression ignition (HCCI) combustion*. in *Combustion Institute/ Canadian Section, Spring meeting*. Waterloo.
68. Jamal Y and Wyszynski M L.(1994). *On-board generation of hydrogen-rich gaseous fuels—a review*. *International Journal of Hydrogen Energy*, 19(7): p. 557-572.
69. Hosseini V and Checkel M D.(2005). *Alternative mode combustion study: HCCI fueled with heptane and spark ignition fueled with reformer gas*. in *ASME Internal Combustion Engine Division 2005 Fall Technical Conference*. Ottawa, Canada: ASME.
70. Kongsereparp P and Checkel M D.(2007). *Investigating the Effects of Reformed Fuel Blending in a Methane- or n-Heptane-HCCI Engine Using a Multi-Zone Model*. SAE Paper, 2007-01-0205.
71. Zheng J, et al.(2004). *Some observations on the effects of EGR, oxygen concentration, and engine speed on the homogeneous charge combustion of n-heptane*. SAE Paper, 2004-01-1905.
72. Heywood J B.(1988). *Internal Combustion Engine Fundamentals*: McGraw-Hill, Inc. 930 Pages.
73. Shaver G M.(2005). *Physics-based modeling and control of residual-affected HCCI engines using variable valve actuation*, Department of mechanical engineering, Stanford University.
74. Livengood C J and Wu C P.(1955). *Correlation of autoignition phenomena in internal combustion engines and rapid compression machines*. in *Proceedings of Fifth International Symposium on Combustion*.
75. Checkel M D and Dale J D.(1986). *Testing a third derivative knock indicator on a production engine*. SAE Paper, 861216.
76. Checkel M D and Dale J D.(1986). *Computerized knock detection from engine pressure records*. SAE Paper, 860028.
77. Woschni G.(1967). *Universally applicable equation for the instantaneous heat transfer coefficient in the internal combustion engine*. SAE Paper, 670931.
78. Nakano M, et al.(2000). *Effects of exhaust gas recirculation in homogeneous charge compression ignition engines*. *International Journal of Engine Research*, 1(3).
79. Zeng W, Xie M, and Jia M.(2007). *Numerical investigation on the application of catalytic combustion to HCCI engines*. *Chemical Engineering Journal*, 127(1-3): p. 81-93.

80. Dec J E and Sjöberg M.(2003). *A Parametric Study of HCCI Combustion – the Sources of Emissions at Low Loads and the Effects of GDI Fuel Injection*. SAE Paper, 2003-01-0752.
81. Gnanam G, et al.(2005). *HCCI Combustion With Internal Fuel Reforming, Varied Levels of EGR and Charge Preheat - A Computational Study*. SAE Paper, 2005-01-0140.
82. Goldsborough S, Scott S, and Blarigan P V.(1999). *A Numerical Study of a Free Piston IC Engine Operating on Homogeneous Charge Compression Ignition Combustion*. SAE Paper, 1999-01-0619.
83. Fiveland S B and Assanis D N.(2000). *A four-stroke homogeneous charge compression ignition engine simulation for combustion and performance studies*. SAE Paper, 2000-01-0332.
84. Christensen M, et al.(1998). *Supercharged homogeneous charge compression ignition*. SAE Paper, 980787.
85. Dec J E.(2002). *A computational study of the effects of low fuel loading and EGR on heat release rates and combustion limits in HCCI engines*. SAE Paper, 2002-01-1309.
86. Fiveland S B and Assanis D N.(2001). *Development of a Two-Zone HCCI Combustion Model Accounting for Boundary Layer Effects*. SAE Paper, 2001-01-1028.
87. Eng J A, Leppard W R, and Sloane T M.(2003). *The Effect of Di-Tertiary Butyl Peroxide (DTBP) Addition to Gasoline on HCCI Combustion*. SAE Paper, 2003-01-1028.
88. Kongsereparp P and Checkel M D.(2007). *Novel Method of Setting Initial Conditions for Multi-zone HCCI Combustion Modeling*. SAE Paper, 2007-01-0674.
89. Aceves S M, et al.(2000). *A Multi-Zone Model for Prediction of HCCI Combustion and Emissions*. SAE Paper, 2000-01-0327.
90. Aceves S M, et al.(2001). *A Decoupled Model of Detailed Fluid Mechanics Followed by Detailed Chemical Kinetics for Prediction of Iso-Octane HCCI Combustion*. SAE Paper, 2001-01-3612.
91. Noda T and Foster D E.(2001). *A Numerical Study of Control Combustion Duration of Hydrogen-Fueled HCCI by Using Multi-Zone Chemical Kinetics Simulation*. SAE Paper, 2001-01-0250.
92. Easley W, Agarwal A, and Lavoie G.(2001). *Modeling of HCCI Combustion and Emissions Using Detailed Chemistry*. SAE Paper, 2001-01-1029.
93. Bhawe A, et al.(2004). *Modelling a dual-fuelled, multi-cylinder HCCI engine using a PDF-based engine cycle simulator*. SAE Paper, 2004-01-0561.
94. Kraft M, et al.(2000). *Investigation of combustion emissions in a homogeneous charge compression injection engine: Measurements and a new computational model*. Proceedings of the Combustion Institute, 28: p. 1195-1201.

95. Iwashiro Y, et al.(2002). *Fuel Consumption Improvement and Operation Range Expansion in HCCI by Direct Water Injection*. SAE Paper, 2002-01-0105.
96. Iida S, Kusaka J, and Daisho Y.(2003). *Numerical Study on Iso-Octane Homogeneous Charge Compression Ignition*. SAE Paper, 2003-01-1820.
97. Kong S-C, et al.(2003). *Modelling the effects of geometry-generated turbulence on HCCI engine combustion*. SAE Paper, 2003-01-1088.
98. Li G, et al.(2003). *CFD simulation of HCCI combustion in a 2-stroke DI gasoline engine*. SAE Paper, 2003-01-1855.
99. Chang K, et al.(2006). *Analysis of Load and Speed Transitions in an HCCI Engine Using 1-D Cycle Simulation and Thermal Networks*. SAE Paper, 2006-01-1087.
100. Christensen M and Johansson B.(2002). *The effect of in-cylinder flow and turbulence on HCCI operation*. SAE Paper, 2002-01-2864.
101. Flowers D, et al.(2003). *Effect of mixing on hydrocarbon and carbon monoxide emissions prediction for isooctane HCCI engine combustion using a multi-zone detailed kinetics solver*. SAE Paper, 2003-01-1821.
102. Yu R X, et al.(2007). *Effect of Turbulence on HCCI Combustion*. SAE Paper, 2007-01-0183.
103. Komninou N P, Hountalas D T, and Kouremenos D A.(2004). *Development of a new multi-zone model for the description of physical processes in HCCI engines*. SAE Paper, 2004-01-0562.
104. Komninou N P, Hountalas D T, and Kouremenos D A.(2005). *Description of In-Cylinder Combustion Processes in HCCI Engines Using a Multi-Zone Model*. SAE Paper, 2005-01-0171.
105. Smith G P, et al.(http://www.me.berkeley.edu/gri_mech/, (last visited in November 2006). *GRI-mech3.0 data*.
106. Golovichev V.(last visited in February 2007).Semi-reduced n-Heptane autoignition mechanisms.<http://www.tfd.chalmers.se/~valeri/MECH.html>.
107. Montgomery C, et al.(2006). *Selecting the optimum quasi-steady-state-species for reduced chemical kinetic mechanisms using a genetic algorithm*. *Combustion and Flame*, 144: p. 37-52.
108. Elliot L, et al.(2004). *A Novel Approach to the Optimization of Reaction Rate Parameters for Methane Combustion Using Multi-Objective Genetic Algorithms*. *Journal of Engineering for Gas Turbines and Power*, 126: p. 455 - 464.
109. Elliott L, et al.(2005). *The use of ignition delay time in genetic algorithms optimization of chemical kinetics reaction mechanisms*. *Engineering Applications of Artificial Intelligence*, 18: p. 825 - 831.
110. Kee R J, et al.(2000). *CHEMKIN Collection, Release 3.6*, Reaction Design, Inc.: San Diego, CA.
111. Gardiner W C and Burcat A.(1984). *Combustion chemistry*. New York: Springer-Verlag, c1984.
112. Turns S R.(2000). *An Introduction to Combustion*. 2nd ed: McGraw Hill.

113. Checkel D M.(2004). *An Introduction to Internal Combustion Engine, MEC E 541 course notes*, Mechanical Engineering Department, University of Alberta: Edmonton, Canada.
114. Stewart P H, Larson C W, and Golden D M.(1989). *Pressure and Temperature-Dependence of Reactions Proceeding Via α -Bound Complex .2. Application to $2\text{ch}_3\text{-C}_2\text{h}_5+\text{H}$* . Combustion and Flame, 75(1): p. 25-31.
115. Troe J.(1983). *Theory of Thermal Unimolecular Reactions in the Fall-Off Range .1. Strong Collision Rate Constants*. Berichte Der Bunsen-Gesellschaft-Physical Chemistry Chemical Physics, 87(2): p. 161-169.
116. Golovichev V.(<http://www.tfd.chalmers.se/~valeri/MECH.html>, (last visited in February 2007). *Semi-reduced n-Heptane autoignition mechanisms*. Chalmers Institute of Technology, Sweden.
117. Djuricic Z M.(2004).*Chemical Kinetics of Nitrogen Fixation in Hydrocarbon Flame Fronts*,Chemical and Fuels Engineering,University of Utah.
118. Morsy M H.(2006). *Ignition control of methane fueled homogeneous charge compression ignition engines using additives*. Fuel, 86: p. 533-540.
119. Zhu J, Zhang D, and King K D.(2001). *Reforming of CH₄ by partial oxidation: thermodynamic and kinetic analyses*. Fuel, 80: p. 899-905.
120. Huang J and Bushe W K.(2006). *Experimental and kinetic study of autoignition in methane/ethane/air and methane/propane/air mixtures under engine-relevant conditions*. Combustion and Flame, 144(1): p. 74-88.
121. Huang J, et al.(2006). *Shock initiated ignition in homogeneous methane-hydrogen-air mixtures at high pressure*. International Journal of Chemical Kinetics, 38(4): p. 221-233.
122. Huang J, et al.(2004). *Shock-tube study of methane ignition under engine-relevant conditions: experiments and modeling*. Combustion and Flame, 136(1-2): p. 25-42.
123. Patel A, Kong S-C, and Reitz R D.(2004). *Development and validation of a reduced reaction mechanism for HCCI engine simulations*. SAE Paper, 2004-01-0558.
124. Chong E K P and Zak S H.(2002). *An Introduction to Optimization, 2nd Edition*. 2nd ed. New York: Wiley, c2001. 476.
125. Milstein J.(1981). *The inverse problem: estimation of kinetic parameters*, in *Modelling of Chemical Reaction Systems*, K.H. Ezbart, P. Deuflhard, and W. Jager, Editors. 1981, Springer: Berlin.
126. Frenklach M, Wang H, and Rabinowitz J.(1992). *Optimisation and analysis of large chemical kinetic mechanisms using the solution mapping method-combustion of methane*. Progress in Energy and Combustion Science, 18(47-73).
127. Chu J Z, et al.(2003). *Constrained optimization of combustion in a simulated coal-fired boiler using artificial neural network model and information analysis*. Fuel, 82(6): p. 693-703.
128. Elliott L, et al.(2004). *A Novel Approach to the Optimization of Reaction Rate Parameters for Methane Combustion Using Multi-Objective Genetic*

- Algorithms*. Journal of Engineering for Gas Turbines and Power, 126: p. 455 - 464.
129. Elliott L, et al.(2005). *Reaction mechanism reduction and optimization using genetic algorithms*. Industrial & Engineering Chemistry Research, 44(4): p. 658-667.
 130. Wade A S, et al.(2004). *Optimization of the arrhenius parameters in a pseudo-detailed mechanism for jet fuel thermal oxidation using genetic and simplex algorithms*. Energy & Fuels, 18(6): p. 1896-1908.
 131. Matlab.(2002). *Genetic Algorithm and Direct Search tool box User's Guide*. Natick, MA: The Math Works, Inc.
 132. Ciezki H and Adomeit G.(1993). *Shock-Tube Investigation of Self-Ignition of n-Heptane Air Mixtures Under Engine Relevant Conditions*. Combustion and Flame, 93(4): p. 421-433.
 133. Kirchen P.(2004). Thermokinetic Modeling of the HCCI Cycle: Predicting the Ignition Timing, Master thesis, Department of Mechanical Engineering, University of Alberta.
 134. Ramos J I.(1989). *Internal Combustion Engine Modeling*. New York: Hemisphere Publishing Corporation.
 135. Hottel H C and Sarofim A F.(1967). *Radiative Transfer*. New York: McGraw-Hill.
 136. Leckner B.(1972). *Spectral and Total Emissivity of Water Vapor and Carbon Dioxide*. Combustion and Flame, 19: p. 33-48.
 137. Wilhelmsson C, et al.(2005). *Combustion Chamber Wall Temperature Measurement and Modelling During Transient HCCI Operation*. SAE Paper, 2005-01-3731.
 138. Chang J, et al.(2004). *New Heat Transfer Correlation for an HCCI Engine Derived from Measurements of Instantaneous Surface Heat Flux*. SAE Paper, 2004-01-2996.
 139. Wu H W and Chiu C P.(1988). *A study on the integration model of heat transfer in an engine fin*. Heat and Mass Transfer, 24: p. 363-369.
 140. Jafari A and Hannani S K.(2006). *Effect of fuel and engine operational characteristics on the heat loss from combustion chamber*. INTERNATIONAL COMMUNICATIONS IN HEAT AND MASS TRANSFER, 33(1): p. 122-134.
 141. Fischer G.(2000). Expertenmodell zur Berechnung der Reibungsverluste von Otto-motoren, PhD thesis Technische Universitaet Darmstadt.
 142. Shaw B T and Hedrick J K.(2002). *Coldstart engine combustion modelling to control hydrocarbon emissions*. in *15th Triennial World Congress*. Barcelona, Spain.
 143. Fox J W, Cheng W K, and Heywood J B.(1993). *A model for predicting residual gas fraction in spark-ignition engines*. SAE Paper, 931025.
 144. Cavina N, Siviero C, and Suglia R.(2004). *Residual Gas Fraction Estimation: Application to a GDI Engine With Variable Valve Timing and EGR*. SAE Paper, 2004-01-2943.
 145. Matlab.(2002). *Solvers for Explicit and Linearly Implicit ODEs*, Matlab version 7.0.0 (R14).

146. Hosseini V and Checkel M D.(2007). *Effect of Reformer Gas on HCCI Combustion- Part I: High Octane Fuels*. SAE Paper, 2007-01-0208.
147. Ogink R.(2002). Gasoline HCCI Modeling: An Engine Cycle Simulation Code with a Detailed-Chemistry, Multi-Zone Combustion Model, Licentiate in Engineering Thesis Chalmers University of Technology.
148. Ogink R.(2003). *Applications and Results of a User-Defined, Detailed-Chemistry HCCI combustion Model in the AVL BOOST Cycle Simulation Code*. in *International User Meeting 2003, AVL*. Graz, Austria.
149. Yang J and Martin J K.(1989). *Approximate Solution - One-Dimensional Energy Equation for Transient, Compressible, Low Mach Number Turbulent Boundary Layer Flows*. Journal of Heat Transfer, 111: p. 619-624.
150. Chiang C J and Stefanopoulou A G.(2007). *Stability analysis in homogeneous charge compression ignition (HCCI) engines with high dilution*. Ieee Transactions on Control Systems Technology, 15(2): p. 209-219.

APPENDIX A

CGS/ SI conversion of related parameters

measuring	CGS unit	SI equivalent
pressure	barye (ba)	0.1 pascal (Pa)
heat energy	calorie (cal)	4.1868 joule (J)
force	dyne (dyn)	10^{-5} newton (N)
work, energy	erg	10^{-7} joule (J)
acceleration	galileo (Gal)	0.01 meter per second squared ($m \cdot s^{-2}$)
heat transmission	langley	41.84 kilojoules per square meter ($kJ \cdot m^{-2}$)
dynamic viscosity	poise (P)	0.1 pascal second (Pa·s)
kinematic viscosity	stokes (St)	10^{-4} square meters per second ($m^2 \cdot s^{-1}$)
electric dipole moment	debye (D)	3.33564×10^{-30} coulomb meter (C·m)

APPENDIX B

Calculation of Some Important Properties

The detail of the following calculation can be found in [110]. However, for referencing purposes and completeness, the calculation was concluded in this section.

B.1. Conversion of units regarding mole, mass and concentration

- Mass fraction to mole fraction:

$$X_k = \frac{Y_k}{W_k \sum_{j=1}^K \left(\frac{Y_j}{W_j} \right)} = \frac{Y_k \bar{W}}{W_k} \quad (\text{A.1})$$

- Mass fraction to molar concentration

$$[X_k] = \frac{P(Y_k/W_k)}{R \sum_{j=1}^K (Y_j T_j / W_j)} \quad (\text{A.2})$$

- Mole fraction to mass fraction

$$Y_k = \frac{X_k W_k}{\sum_{j=1}^K (X_j W_j)} \quad (\text{A.3})$$

- Mole fraction to molar concentration

$$[X_k] = X_k \frac{P}{R \sum_{k=1}^{N_s} X_k T_k} \quad (\text{A.4})$$

- Molar concentration to mass fraction

$$Y_k = \frac{[X_k]W_k}{\sum_{j=1}^K [X_j]W_j} \quad (\text{A.5})$$

- Molar concentration to mole fraction

B.2. Mixture Average Properties

- Average molecular weight

$$\bar{W} = \frac{1}{\sum_{k=1}^K (Y_k/W_k)} = \sum_{k=1}^K (X_k W_k) = \sum_{k=1}^K ([X_k] W_k) / \sum_{k=1}^K [X_k] \quad (\text{A.6})$$

- Average specific heat constant at constant pressure

$$\bar{C}_p = \sum C X \quad (\text{A.7})$$

APPENDIX C

Table of subroutines

No.	Name	Description	Called in
1	AssistingTool.fig	A user interphase for "Assisting Tool" option in CHEMCOMB.	-
2	AssistingTool.m	A function for AssistingTool.fig, an interphase for "Assiting Tool" option of CHEMCOMB.	chemcomb.m
4	CalcMotorParaAna.m	Calculate motoring pressure trace for parameter calculation.	ParaCalc.m
5	Calculation_IgDelay.m	Calculate ignition delay in shock tube, being called by	SimulationPage.m
6	Calculation_MZM.m	A main function of a multi-zone HCCI combustion model	SimulationPage.m
7	Calculation_SZM.m	A main function of a single-zone HCCI combustion model	SimulationPage.m
8	chemcomb.fig	A main menu to select calculation options	-
9	chemcomb.m	A function for chemcomb.fig, the main menu of CHEMCOMB	-
10	col_integral_function.m	Calculate collision integral	HeatTransMZM.m
11	CombMZM_calculation.m	Calculate in-cylinder properties during close system (IVC to EVO), using a fully coupled MZM	Calculation_MZM.m
12	CombSMZM_calculation.m	Calculate in-cylinder properties during close system (IVC to EVO), using segregated MZM	Calculation_MZM.m
13	CombSZM_calculation.m	Calculate in-cylinder properties during close system (IVC to EVO), using SZM	Calculation_SZM.m
14	component_reading.m	Read and separate component of reactants and products into variables used in the calculation.	Reading_IgDelay.m Reading_SZM.m Reading_SZM_fullcycle.m Reading_MZM.m Reading_SMZM_fullcycle.m
15	dP_calculation.m	Evaluate the in-cylinder pressure rise rate for segregated MZM	CombSMZM_calculation.m
16	energycontent_order.m	Specify the order of fuel species in a mechanism (for calculating total energy input)	Calculation_SZM.m Calculation_MZM.m
17	EnthalFormation.m	Calculate enthalpy formation of each reaction	Calculation_SZM.m Calculation_MZM.m
18	equilibrium_constant.m	Calculate equilibrium constants	kin_calculation.m
19	ExpAnaCalculation.m	Calculate experimental engine parameters from pressure traces.	AssistingTool.m
20	Exhaust_calculation.m	Calculate exhaust gas exchanging process	Calculation_SZM.m Calculation_MZM.m

No.	Name	Description	Called in
21	FullCyclePrintout.m	Print out the results to .xls and .dat files (for both SZM and MZM).	Calculation_SZM.m Calculation_MZM.m
22	GA_CalCombine.m	A main function to calculate the GA-SZM-Ignition delay coupled model.	SimulationPage.m
23	GA_CalcIgDelayForGA.m	Calculate ignition delay model for GA fitness function	GA_CombineFitnessFnc.m
24	GA_Calculation.m	Perform genetic algorithm optimization of GA-SZM-Ignition delay coupled model and print out the results.	GA_CalCombine.m
25	GA_CalSZMForGA.m	Calculate SZM model for GA fitness function.	GA_CalCombine.m
26	GA_CombineFitnessFnc.m	Set-up a fitness function for GA-SZM-Ignition delay coupled model.	GA_CalCombine.m
27	gas_thcond_calculation.m	Calculate gaseous conductivity for heat transfer between zones.	HeatTransMZM.m
28	heating_value.m	Calculate heating value of fuels.	ParaCalc.m
29	HeatTrans_MZM.m	Calculate heat transfer for the MZM.	ODE_MZM.m
30	HeatTrans_SZM.m	Calculate heat transfer for the SZM.	ODE_SZM.m ODE_SZM_frozen.m
31	HR_SZM.m	Calculate combustion parameter and heat release history.	ParaCalc.m
32	input_component_interpreter.m	Read mixture components and mole numbers of each component.	component_reading.m
33	Intake_calculation.m	Calculate in-cylinder properties during intake gas exchanging process.	Calculation_SZM.m Calculation_MZM.m
34	kin_calculation.m	Calculate (both reverse and forward) reaction rate constants.	ODE_SZM.m ODE_IgDelay.m ODE_MZM.m ODE_sMZM.m
35	MassflowCal.m	Record in-cylinder properties during flow-through-intake period.	Intake_calculation.m
36	MassflowCalExh.m	Record in-cylinder properties during flow-through-exhaust period.	Exhaust_calculation.m
37	molecular.m	Calculate molecular weight and ideal gas constant (on mass basis) of each species.	Reading_IgDelay.m Reading_SZM.m Reading_SZM_fullcycle.m Reading_MZM.m Reading_SMZM_fullcycle.m
38	MZMInhomoAssign.m	Calculate in-cylinder inhomogeneity at intake valve closure.	Calculation_MZM.m
39	MZMRecordData.m	Store a result of each calculating interval to one set of results for a multi zone model (fully coupled).	CombMZM_calculation.m

No.	Name	Description	Called in
40	ODE_exhaust.m	Set-up a system of ODE for in-cylinder properties during exhaust gas exchanging process.	Exhaust_calculation.m
41	ODE_IgDelay.m	Set-up a system of ODE for zero dimensional shock-tube calculation.	Calculation_IgDelay.m
42	ODE_intake.m	Set-up a system of ODE for in-cylinder properties during intake gas exchanging process.	Intake_calculation.m
43	ODE_MZM.m	Set-up a system of ODE for multi zone combustion modeling during non-perfectly stirred mixture period (early after IVC), using fully coupled solver.	CombMZM_calculation.m
44	ODE_MZM2.m	Set-up a system of ODE for multi zone combustion modeling when the mixtures in each zone are perfectly stirred, using fully coupled solver.	CombMZM_calculation.m
45	ODE_sMZM.m	Set-up a system of ODE for multi zone combustion modeling during close system (segregated solver).	CombSMZM_calculation.m
46	ODE_sMZM_frozen.m	Set-up a system of ODE for single zone combustion modeling during close system (froze chemistry).	Comb.SMZM_calculation.m
47	ODE_SZM.m	Set-up a system of ODE for single zone combustion modeling during close system (chemical kinetic calculation activated).	CombSZM_calculation.m
48	ODE_SZM_forzen.m	Set-up a system of ODE for single zone combustion modeling during close system (frozen chemistry).	CombSZM_calculation.m
49	order_indicator_sing.m	Specify the position of a particular species in a property array for SZM calculation.	component_reading.m
50	order_indicator_multi.m	Specify the position of a particular species in a property array for MZM heat transfer calculation.	HeatTransMZM.m
51	ParaCalc.m	Analyze combustion and engine parameters.	Calculation_SZM.m Calculation_MZM.m
52	pressure_gradient.m	Calculate rates of pressure change (bar/CA)	ExpAnaCalculation.m
53	q_generator.m	Calculate reaction rate of production.	ODE_SZM.m ODE_MZM.m ODE_MZM2.m ODE_sMZM.m
54	reaction_indication.m	Define the zone where temperature exceeds the reaction active temperature for a segregated multi zone model.	CombSMZM_calculation.m

No.	Name	Description	Called in
55	reading.m	Read a chemical kinetic mechanism file in the folder "Data_files\Fuel".	Reading_IgDelay.m Reading_SZM.m Reading_SZM_fullcycle.m Reading_MZM.m, Reading_SMZM_fullcycle.m
56	Reading_IgDelay.m	Define all parameters from shock-tube ignition delay input data obtained from ReadingIgDealyFile.m.	Calculation_IgDelay.m GA_CalCombine.m
57	Reading_MZM.m	Define all parameters from a 1st or 2nd option MZM input data obtained from ReadingInputFileMZMIVC.m or ReadingInputFileMZMmassflow.m respectively.	Calculation_MZM.m
58	Reading_SMZM_fullcycle.m	Define all parameters from a 3rd option MZM input data obtained from ReadingInputFileMZMFull.m.	Calculation_MZM.m
59	Reading_SZM.m	Define all parameters from input data a SZM input file (.txt) of the 1st (specifying IVC conditions) and 2nd (specifying mass flow rates) input options.	Calculation_SZM.m GA_CalCombine.m
60	Reading_SZM_fullcycle.m	Define all parameters from the input data obtained from ReadingInputFileSZMFullCycle.m.	Calculation_SZM.m
61	ReadingAlgor.m	Read a section of input text files.	ReadingInputFileMZMFull.m ReadingInputFileMZMIVC.m ReadingInputFileSZMFullCycle.m ReadingInputFileSZMIVC.m ReadingInputFileSZMmassflow.m
62	ReadingGA.m	Read a GA-SZM-Ignition Delay coupled input file in the folder "...input\GA".	SimulationPage.m
63	ReadingDelayFile.m	Prepare input data for a shock tube ignition delay model from an shock tube ignition delay input file (.txt) in the folder "...input\IgDelay".	SimulationPage.m
64	ReadingInputFile.m	Open input file (s).	SimulationPage.m
65	ReadingInputFileMZMFull.m	Prepare input data for a multi-zone model (3rd option - fully coupled) from a MZM input file (.txt) in the folder "...input\MZMFullCycle".	SimulationPage.m
66	ReadingInputFileMZMIVC.m	Prepare input data for a multi-zone model (1st option - specifying IVC conditions) from a 1st option MZM input file in the folders "...input\MZMIVC" or "...input\SMZMIVC".	SimulationPage.m

No.	Name	Description	Called in
67	ReadingInputFileSZMFullCycle.m	Prepare input data for a single zone model (3rd option - full engine cycle calculation) from a SZM input file (.txt) in the folder "...\\input\\SZMFullCycle".	SimulationPage.m
68	ReadingInputFileSZMIVC.m	Prepare input data for a single zone model option 1 (specifying IVC conditions) from a 1st option SZM input file in the folder "...\\input\\SZMIVC".	SimulationPage.m
69	ReadingInputFileSZMmassflow.m	Prepare input data for a single zone model option 2 (specifying mass flows of fuel, RG and air) from a 2nd option SZM input file in the folder "...\\input\\SZMmassflow".	SimulationPage.m
70	ReadReact.m	Prepare reaction data for an output file.	SpecDetailPrintOut.m
71	ref_molmolecule.m	Read "ref_molecularweight.txt" file in the "...\\Data_files\\fuel" folder to set the reference of C, H, O and N molecular weight.	molecular.m
72	ResidMassFracCal.m	Calculate residual mass fraction.	Reading_SZM.m
73	Sens_CallgDelay.m	Calculate sensitivity of Arrhenius coefficients to ignition delay in shock tube, using zero-dimensional shock tube model.	AssistingTool.m
74	Sens_CalSZM.m	Calculate sensitivity of Arrhenius coefficients to SOC timing of an HCCI engine using single zone model.	AssistingTool.m
75	SimulationPage.fig	A user interphase to call Ignition Delay, SZM, MZM and Genetic algorithm optimization.	chemcomb.m
76	SimulationPage.m	A function for SimulationPage.fig	-
77	SMZMRecord.m	Store a result of each calculating interval to one set of results for a segregated multi zone model.	CombSMZM_calculation.m
78	SpeciesDetail.m	Calculate the rate of production/destruction of interesting species.	Calculation_SZM.m Calculation_MZM.m
79	SpeciesDetailPrintOut.m	Print out the detail of species to an output file.	Calculation_SZM.m Calculation_MZM.m
80	SZMRecordData.m	Store a result of each calculating interval to one set of results for a single zone model.	CombSZM_calculation.m
81	thermo_data.m	Calculate thermodynamic properties from NASA coefficients	ODE_SZM.m ODE_MZM.m ODE_MZM2.m ODE_sMZM.m

No.	Name	Description	Called in
83	transport_reading.m	Read the data from a transport phenomena file in the folder "...\\Data_files\\Transport" for transport phenomena calculation.	Reading_SZM.m Reading_SZM_fullcycle.m Reading_MZM.m Reading_MZM_fullcycle.m
84	troefactor_calibration.m	Calculate the pressure dependent factor using Troe parameters.	kin_calculation.m
85	volume_fn.m	Calculate volume and rate of volume change at any CA position.	Reading_SZM.m Reading_SZM_fullcycle.m Reading_MZM.m Reading_MZM_fullcycle.m CombMZM_calculation.m CombSZM_calculation.m CombSMZM_calculation.m
86	y_forming.m	Form a full variable vector (temperature, pressure zone volume and mass fraction in every zone) from the result obtained from ODE solver during the time when mixtures in each zone are NOT perfectly stirred.	CombMZM_calculation.m CombSMZM_calculation.m
87	y_forming2.m	Form a full variable vector (temperature, pressure zone volume and mass fraction in every zone) from the result obtained from ODE solver during the time when mixtures in each zone are perfectly stirred.	CombMZM_calculation.m CombSMZM_calculation.m
88	y_instant_forming.m	Prepare a variable vector (temperature, pressure, zone volume and mass fraction of species in the zone where temperature is greater than inactive temperature) to calculate in-cylinder properties during the time when mixtures in each zone are NOT perfectly stirred	CombMZM_calculation.m CombSMZM_calculation.m
89	y_instant_forming2.m	Prepare a variable vector (temperature, pressure, zone volume and mass fraction of species in the zone where temperature is greater than inactive temperature) to calculate in-cylinder properties during the time when mixtures in each zone are perfectly stirred	CombMZM_calculation.m CombSMZM_calculation.m
90	zone_geometry.m	Calculate the geometry of each zone for multi-zone combustion modeling.	CombMZM_calculation.m CombSMZM_calculation.m

APPENDIX D

Detail of Mixture Conditions Used to Validate Model Performance

Table D- 1 : Mixture Conditions Used to Test Performance of CNG HCCI engine Modeling

Case No.	Phi	%RG	%EGR	Case No.	Phi	%RG	%EGR
1	0.55	17.7	41.3	22	0.36	10.4	20.3
2	0.57	15.2	40.8	23	0.35	10.0	21.3
3	0.52	15.8	41.1	24	0.33	10.0	20.0
4	0.47	15.2	43.0	25	0.35	15.0	21.2
5	0.55	15.3	42.6	26	0.34	14.9	19.5
6	0.46	19.7	44.0	27	0.37	19.8	19.8
7	0.44	20.7	43.5	28	0.36	20.1	20.5
8	0.47	30.7	42.5	29	0.32	0.0	10.6
9	0.48	0.0	32.0	30	0.31	0.0	11.0
10	0.45	0.0	30.1	31	0.29	0.0	10.0
11	0.47	5.1	30.0	32	0.29	5.9	11.6
12	0.39	4.9	30.2	33	0.31	9.8	10.7
13	0.39	9.6	31.6	34	0.30	15.8	8.4
14	0.45	0.0	20.7	35	0.30	0.0	0.0
15	0.39	0.0	22.0	36	0.27	0.0	0.0
16	0.36	0.0	22.0	37	0.29	5.7	0.0
17	0.34	0.0	22.0	38	0.28	4.5	0.0
18	0.39	5.1	21.7	39	0.26	5.1	0.0
19	0.37	5.6	20.3	40	0.27	10.0	0.0
20	0.34	5.5	22.2	41	0.27	0.0	0.0
21	0.38	9.8	19.8				

Table D- 2 : Mixture Conditions Used to Test Performance of CNG HCCI engine Modeling

Case No.	Phi	%RG	%EGR	Case No.	Phi	%RG	%EGR
1	0.55	0	38.9	32	0.35	0	20.1
2	0.49	0	39.8	33	0.32	0	20.8
3	0.44	0	39.9	34	0.34	10.5	21.9
4	0.49	5.4	40.2	35	0.31	10.3	21.6
5	0.45	5.1	40.7	36	0.3	14.9	20.6
6	0.43	10	41	37	0.34	20.4	20.3
7	0.41	9.9	41	38	0.31	25.3	21.1
8	0.48	15.1	41.2	39	0.28	24.9	21.6
9	0.46	15.4	41.7	40	0.33	5.5	9.9
10	0.41	15	41.5	41	0.29	4.9	9.4
11	0.46	20.3	40.3	42	0.28	11.5	9.3
12	0.38	20	41.5	43	0.28	11.5	9.3
13	0.45	25.3	40.8	44	0.27	13.7	10
14	0.41	25.3	41.4	45	0.3	15.4	11
15	0.44	30.3	42.1	46	0.26	15.1	10.7
16	0.4	30.8	42.4	47	0.29	20.2	10.9
17	0.49	0	31.3	48	0.28	20.3	10
18	0.46	0	31.1	49	0.28	25.6	10.4
19	0.41	0	31.3	50	0.25	25.6	11.4
20	0.48	4.9	31.5	51	0.23	25.8	9.7
21	0.44	5.3	32	52	0.21	30.9	0
22	0.4	5.5	32.8	53	0.23	30.5	0
23	0.41	15.9	32.3	54	0.25	30.2	0
24	0.35	14.9	32.5	55	0.25	25.9	0
25	0.39	21.3	31.6	56	0.23	20.1	0
26	0.36	20.3	31.2	57	0.25	20.2	0
27	0.43	25.5	30.3	58	0.27	15.3	0
28	0.38	30.3	29.6	59	0.27	10.6	0
29	0.35	30.4	28.8	60	0.28	5.4	0
30	0.32	30.1	28.9	61	0.26	5.1	0
31	0.38	0	19.8				